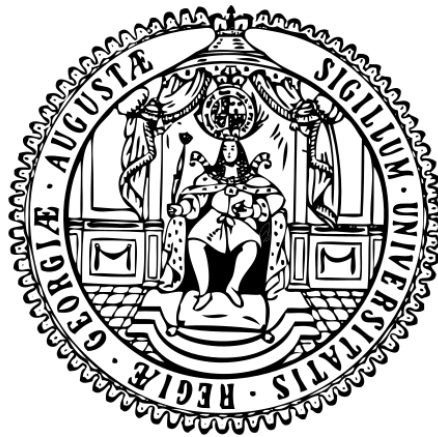


Effects of acute and long-term tachypacing on atrial engineered human myocardium

Doctoral thesis

In partial fulfilment of the requirements for the degree

“Doctor rerum naturalium“ (Dr. rer. nat.)



in the Molecular Medicine Study Programme
at the Georg-August University Göttingen

Submitted by

Tony Jean Stanis Rubio

Born in

Alès, France

Göttingen, 2023

Members of thesis committee

Prof. Dr. med. Niels Voigt (reviewer)

Institute of Pharmacology and Toxicology
University Medical Centre Göttingen
Robert-Koch-Straße-40, Göttingen, Germany

Prof. Bernd Wollnik (reviewer)

Institute of Human Genetics
University Medical Centre Göttingen
Heinrich-Düker-Weg 12, 37073 Göttingen, Germany

Prof. Dr. Henning Urlaub

Max-Planck-Institute for Biophysical Chemistry
Bioanalytical Mass Spectrometry Group
Am Fassberg 11, 37077 Göttingen, Germany

Extended members of the examination board

Prof. Dr. Sarah Köster

Institute for X-Ray Physics

Georg-August-University Göttingen

Friedrich-Hund-Platz 1, 37077 Göttingen, Germany

Prof. Dr. mult. Thomas Meyer

Institute for Molecular Psychocardiology

University Medical Centre Göttingen

Waldweg 33, 37075 Göttingen, Germany

Prof. Dr. Katrin Streckfuß-Bömeke

Institute for Pharmacology and Toxicology

Julius-Maximilians-University Würzburg

Versbacher Straße, 97078 Würzburg, Germany

Date of disputation

Date of disputation: _____

Affidavit

I hereby declare that the work presented in this thesis titled “Effects of acute and long-term tachypacing on atrial engineered human myocardium” has been written independently with no other source and aids than quoted.

Tony Jean Stanis Rubio

Göttingen, 2023

Acknowledgements

First, I would like to express my gratitude towards Pr. Niels Voigt for welcoming me in his team and for the opportunity he gave me with this thesis. Also, I'm truly grateful for his patience, his trust and the great scientific discussions that made this whole project possible.

Next, I would like to thank all the members of my thesis committee and especially Pr. Bernd Wollnik and Pr. Henning Urlaub for their helpful comments and suggestions during our meetings, but also Pr. Sarah Kester, Pr. Thomas Meyer, and Pr. Katrin Streckfuß-Bömeke for reviewing this work.

I'm also extremely grateful for all the help, the support and the good working atmosphere made possible by all the past and present members of the Voigt lab and the institute of pharmacology and toxicology. I would like to particularly thank Fiona, Lena, Robin and Yannic for all their immense help and hard work which also made this thesis possible, but also the constant support and motivation from Aiste, Fleur, Funsho, Julius, Lena, Lea, Luisa, Marie, Melanie, Philipp, Vanessa and Will. Immense thanks also goes to Stefanie Kestel and Ines Müller for their excellent technical support, but also for their patience and all the assistance they provided me.

Special thanks to Pr. Jean-Yves Le Guennec for his dedication on the master « Médecine expérimentale et régénératrice » but also for his understanding, but also to Dr. Marie Demion, Dr. Hamid Moha ou Maati and Pr. Michel Vignes for sharing their interest on the cardiology field and for introducing us to the wonderful world of the electrophysiology.

It goes without saying that I am extremely grateful for the lab experience I had the opportunity to live in the group of Dr. Fabien Brette under the wise supervision of the Dr. Alice Recalde. Special cheer also goes to Dr. Caroline Cros and to my former lab mates Matthieu and Kylian who made this experience such an unforgettable one.

My study time in Montpellier was such an enriching experience thanks to the amazing friendships I made along this crazy journey. Particular thanks to the WC family and to Charlène, Florence, Lucile, Manon, Mathilde, Jacques, Jérémy, Maxime and Paul, but of course also to Maurizio and Sarah. Immense cheers to each and every one of you for all the wonderful moments we spent together, and for all the good memories at Tonton's: cheers!

To everyone belonging to the Alès' team: thank you for being by my side for such a long time, thank you for your friendship and thank you for being who you are.

To Judith, it is difficult to express how grateful I am for these three years that just passed. Thank you for the moments we spent together, thank you for your help, your motivation and your understanding during the good and the difficult times. Thank you for all your support and for introducing me into your wonderful family.

Finally, I would like to thank my family for their help, their patience and their love. None of this could have been possible without you and I'm eternally grateful for the chance I had to be supported as such and for believing in me.

To all the persons I did not mention and supported me during this journey, please be ensure my deepest gratitude.

List of publications

Kyryachenko S, Georges A, Yu M, Barrandou T, Guo L, Bruneval P, **Rubio T**, Gronwald J, Baraki H, Kutschka I, Aras KK, Efimov IR, Norris RA, Voigt N, Bouatia-Naji N (2021): Chromatin Accessibility of Human Mitral Valves and Functional Assessment of MVP Risk Loci. *Circ Res* 128, E84–E101

Peris-Yagüe V, **Rubio T**, Fakuade FE, Voigt N, Luther S, Majumder R (2022): A Mathematical Model for Electrical Activity in Pig Atrial Tissue. *Front Physiol* 13, 250

Seibertz F, Sutanto H, Dülk R, Pronto JRD, Springer R, Rapedius M, Liutkute A, Ritter M, Jung P, Stelzer L, Hüsgen L, Klopp M, **Rubio T**, Fakuade FE, Mason FE, Hartmann N, Pabel S, Streckfuß-Bömeke K, Cyganek L, Sossalla S, Heijman J, Voigt N (2023): Electrophysiological and calcium-handling development during long-term culture of human induced pluripotent stem cell-derived cardiomyocytes. *Basic Res. Cardiol.* *Accepted for publication.*

Statement of conjoint work

The voltage-clamp measurements were performed by Robin Springer, MD student, during his medical thesis under my supervision.

The optical action potentials were recorded by Melanie Ritter, MD student.

Fiona Popp, MD student, helped with the measurements of the action potentials of the crimson engineered human myocardium during her MD thesis under my supervision.

The optical pacer was built by Yannic Döring, PhD student, during his master thesis under my supervision.

The illumination protocols were performed by Runzh Shi, PhD student in the group of Pr. Tobias Brüggemann.

Dr. Feresteh Haghighi performed the PCR experiments.

Table of contents

1	Introduction	1
1.1	Normal electrophysiology of the heart	1
1.1.1	Cardiac action potential	1
1.1.2	The different cardiac action potentials	9
1.1.3	Cardiac excitation-contraction coupling	11
1.2	Atrial fibrillation	13
1.2.1	General characterisation	13
1.2.2	Important definitions in the context of atrial fibrillation: substrate, trigger, re-entry, and rotor	14
1.2.3	Symptoms of atrial fibrillation	15
1.2.4	Molecular mechanisms associated with the development of atrial fibrillation	16
1.3	Different models to study human atrial fibrillation	20
1.3.1	Human models	20
1.3.2	Cellular models	22
1.3.3	Organoid models	24
1.4	Experimental protocols to induce atrial fibrillation	25
1.4.1	Tachypacing	25
1.5	Channelrhodopsin and optogenetics	26
1.5.1	History and definitions	26
1.5.2	Mechanism of action	29
1.5.3	Utilisation of the channelrhodopsins	29
1.6	Hypotheses and aims of the project	33
2	Material and methods	35
2.1	Human experiments	35
2.1.1	Patient data	35
2.1.2	Sample collection for biochemical investigation	35
2.1.3	Sample collection and preparation for electrophysiological measurements	35
2.1.4	Electrophysiological measurements	36
2.1.5	Data analysis	37
2.2	Cellular experiments	37
2.2.1	Cell line generation	37
2.2.2	Fibroblasts primary cultures expansion and maintenance	38
2.2.3	Coverslip preparation	39
2.2.4	Voltage-clamp recordings	40

2.2.5	Optical action potential recordings	42
2.2.6	Automated voltage-clamp measurements of I _{Ca,L}	43
2.2.7	Electrical tachypacing of cardiomyocytes derived from induced pluripotent stem cells	44
2.3	Engineered human myocardium experiments	45
2.3.1	Engineered human myocardium preparation	45
2.3.2	Electrical and optical tachypacing	47
2.3.3	Electrophysiological measurements	47
2.3.4	Data analysis	48
2.4	Light pacer	48
2.5	Light sensitive engineered human myocardium experiments	49
2.5.1	Virus-based engineered human myocardium generation	49
2.5.2	Optogenetic stimulation of engineered human myocardium	51
2.5.3	Acute and long-term force measurements in response to light pulses in atrial engineered human myocardium	51
2.6	Quantitative polymerase chain reaction assays	52
2.7	Statistical analysis	53
3	Results	54
3.1	Characterisation of atrial fibrillation in human myocardium	54
3.1.1	Patients suffering from chronic atrial fibrillation show impaired action potential parameters	54
3.1.2	Patients suffering from chronic atrial fibrillation have an impaired response to a muscarinic receptor agonist	56
3.2	Induced pluripotent stem cells as a model to study electrical remodelling associated with atrial fibrillation	60
3.2.1	Elaboration of atrial cardiomyocytes derived from an induced pluripotent stem cell line to study atrial fibrillation	60
3.2.2	Atrial and ventricular cardiomyocytes derived from induced pluripotent stem cells show distinct electrophysiological profile	62
3.3	Electrical tachypacing in induced pluripotent stem cells	65
3.3.1	Electrical tachypacing of atrial induced pluripotent stem cells induces electrical remodelling	65
3.3.2	Calcium pacing medium privation prevents electrical remodelling in atrial induced pluripotent stem cells	68
3.4	Atrial fibrillation in an engineered human myocardium model	70
3.4.1	Atrial and ventricular engineered human myocardium show distinct atrial and ventricular electrophysiological profiles	70
3.4.2	24-hour electrical tachypacing induces electrical remodelling in atrial engineered human myocardium	73

3.5	Optogenetic tools to study long-term atrial tachypacing in atrial engineered human myocardium: the adeno-associated-virus-channelrhodopsin-2 approach	75
3.5.1	Successful introduction of channelrhodopsin-2 into atrial cardiomyocytes derived from induced pluripotent stem cells using an adeno-associated-virus-2 vector	76
3.5.2	Atrial engineered human myocardium generated with atrial cardiomyocytes derived from pluripotent stem cells transfected with an adeno-associated-virus-2 carrying a channelrhodopsin-2 are light sensitive, but long-term introduction of the virus impairs electrophysiology of the tissues	78
3.5.3	Optical tachypacing of atrial engineered human myocardium generated with atrial induced pluripotent stem cells transfected with an adeno-associated-virus-2 carrying a channelrhodopsin-2 induces electrical remodelling	80
3.6	Optogenetic tools to study long-term atrial tachypacing in atrial engineered human myocardium: the chrimson approach	81
3.6.1	Chrimson atrial engineered human myocardium show distinct atrial electrophysiological specificity	82
3.6.2	Chrimson atrial engineered human myocardium is light sensitive	84
3.6.3	24-hour optical pacing induces electrical remodelling in atrial chrimson engineered human myocardium	85
3.6.4	7-day optical pacing extends the spectrum of electrical remodelling in atrial chrimson engineered human myocardium	87
4	Discussion	91
4.1	Induced pluripotent stem cells serve as a model to study electrical remodelling associated with atrial fibrillation	91
4.1.1	Addition of retinoic acid during induced pluripotent stem cell differentiation promotes atrial differentiation	92
4.1.2	Atrial cardiomyocytes derived from induced pluripotent stem cells show distinct electrophysiological profile compared to ventricular cardiomyocytes derived from induced pluripotent stem cells	92
4.1.3	Atrial engineered human myocardium shows distinct atrial electrophysiological phenotype	93
4.2	Hallmarks of electrical remodelling associated with atrial fibrillation	93
4.2.1	Action potential shortening and resting membrane potential hyperpolarisation are classical hallmarks of electrical remodelling	94
4.2.2	Impaired response to an M2-receptor agonist is another hallmark of atrial fibrillation	94
4.3	Electrical tachypacing induces electrical remodelling in atrial induced pluripotent stem cells	95

4.3.1	Electrical tachypacing induces atrial fibrillation-like electrical remodelling	95
4.3.2	Calcium is a major key player of electrical remodelling	97
4.3.3	Electrical tachypacing on atrial engineered human myocardium induces atrial fibrillation-like electrical remodelling	97
4.4	Acute optical tachypacing induces electrical remodelling in atrial engineered human myocardium	98
4.4.1	Atrial cardiomyocytes derived from induced pluripotent stem cells transfected with an adeno-associated-virus-2 carrying a channelrhodopsin-2 show light sensitivity	99
4.4.2	Atrial cardiomyocytes derived from induced pluripotent stem cells transfected with an adeno-associated-virus-2 carrying a channelrhodopsin-2 can be used for generating light sensitive tissues but long-term introduction of the virus impairs the normal electrophysiology of the cells	100
4.4.3	24-hour optical tachypacing of atrial engineered human myocardium generated with atrial cardiomyocytes derived from induced pluripotent stem cells transfected with an adeno-associated-virus-2 carrying a channelrhodopsin-2 induces atrial fibrillation-like electrical remodelling	101
4.5	Long-term optical tachypacing extends the electrical remodelling observed after acute optical tachypacing	102
4.5.1	Atrial chrimson engineered human myocardium show atrial electrophysiological specificity and are light sensitive	103
4.5.2	24-hour optical pacing of atrial chrimson engineered human myocardium results in atrial fibrillation-like electrical remodelling	104
4.5.3	Long-term pacing of atrial chrimson engineered human myocardium unravels time specific character of electrical remodelling	105
5	Limitations	107
6	Summary and outlook	109
7	References	114

List of figures

Figure 1: Schematic action potential with the different phases.	2
Figure 2: Schematic representation of the different cardiac action potentials and the kinetics of activation of the major ion channels involved in the generation of the action potentials.	11
Figure 3: Schematic representation of the molecular mechanisms involved in the excitation-contraction mechanism.	12
Figure 4: Schematic representation of re-entry and rotors.	15
Figure 5: Amount of publications including the word "Optogenetic" in title or abstract since 2002.	28
Figure 6: Human action potential.	55
Figure 7: Effects of M2-receptor agonist carbachol perfusion on the human atrial action potential.	56
Figure 8: Induced pluripotent stem cell differentiation protocol.	60
Figure 9: Comparison of the mRNA expression levels of L-type Ca^{2+} channels and inward rectifier K^{+} channels in atrial and ventricular cardiomyocytes derived from induced pluripotent stem cells, and atrial and ventricular patient biopsies.	61
Figure 10: Optical action potential measurements in atrial and ventricular cardiomyocytes derived from induced pluripotent stem cells.	62
Figure 11: $I_{\text{Ca,L}}$ measurement in atrial and ventricular cardiomyocytes derived from induced pluripotent stem cells.	63
Figure 12: Basal inward-rectifier and carbachol induced K^{+} current measurement in atrial and ventricular cardiomyocytes derived from induced pluripotent stem cells.	64
Figure 13: Tachypacing-induced remodelling of action potentials in cardiomyocytes derived from induced pluripotent stem cells.	65
Figure 14: Tachypacing-induced development of agonist independent constitutive $I_{\text{K,ACh}}$ activity.	66
Figure 15: Tachypacing-induced remodelling of $I_{\text{Ca,L}}$ in atrial cardiomyocytes derived from induced pluripotent stem cells.	67
Figure 16: Electrical tachypacing in low- Ca^{2+} medium prevents the electrical remodelling-induced action potential shortening.	68
Figure 17: Electrical tachypacing in low- Ca^{2+} medium prevents the electrical tachypacing-induced $I_{\text{K,ACh}}$ remodelling and the apparition of a constitutive $I_{\text{K,ACh}}$.	69
Figure 18: Engineered human myocardium generation protocol.	70
Figure 19: Electrophysiological characterisation of atrial and ventricular engineered human myocardium.	71

Figure 20: Action potential measurements in response to vagal agonist carbachol in atrial and ventricular engineered human myocardium.	72
Figure 21: Electrical remodelling of atrial engineered human myocardium induced by 24-hour electrical tachypacing.	73
Figure 22: Effects of M2-receptor agonist carbachol on electrically paced atrial engineered human myocardium.	74
Figure 23: Plasmid construction of the adeno-associated-virus carrying the channelrhodopsin-2.	75
Figure 24: Functional assessment of light sensitivity in atrial cardiomyocytes derived from induced pluripotent stem cells transfected with an adeno-associated-virus-2 carrying a channelrhodopsin-2.	76
Figure 25: Flow cytometry analysis of atrial derived pluripotent stem cells transfected with an adeno-associated-virus-2 carrying channelrhodopsin-2.	77
Figure 26: Functional assessment of light sensitivity in atrial engineered human myocardium generated using atrial cardiomyocytes derived from induced pluripotent stem cells transfected with an adeno-associated-virus-2 carrying a channelrhodopsin-2.	78
Figure 27: Long-term electrophysiological effects of the introduction of a channelrhodopsin-2 using an adeno-associated-virus-2 vector.	79
Figure 28: Self-constructed pacer for the optical pacing of atrial engineered human myocardium expressing the channelrhodopsin-2.	80
Figure 29: Electrical remodelling of atrial engineered human myocardium generated with atrial induced pluripotent stem cells transfected with an adeno-associated-virus-2 carrying a channelrhodopsin-2 induced by 24-hour electrical tachypacing.	81
Figure 30: Electrophysiological characterisation of atrial and ventricular chrimson engineered human myocardium.	82
Figure 31: Action potential measurements in response to M2-receptor agonist carbachol in atrial chrimson engineered human myocardium.	83
Figure 32: Functional assessment of light sensitivity in chrimson atrial engineered human myocardium.	84
Figure 33: Electrical remodelling of atrial chrimson engineered human myocardium induced by 24-hour optical tachypacing.	85
Figure 34: Effects of M2-receptor agonist carbachol on 24-hour optically paced atrial engineered human myocardium.	86
Figure 35: mRNA levels of L-Type Ca^{2+} channels, inward-rectifier K^{+} channels, muscarinic receptors and adenosine receptors in atrial	

engineered human myocardium subjected to 24-hour optical tachypacing.	87
Figure 36: Continuous optical long-term pacing for 7 days at 1 Hz.	88
Figure 37: Electrical remodelling of atrial engineered human myocardium induced by 7-day optical tachypacing.	89
Figure 38: Effects of M2-receptor agonist carbachol on atrial engineered human myocardium optically paced for 7 days.	90

List of tables

Table 1: Ion channel involved in phase 0 of the cardiac action potential.	3
Table 2: Ion channels involved in phase 1 of the action potential.	5
Table 3: Ion channels involved in phase 2 of the cardiac action potential.	6
Table 4: Ion channels involved in phase 3 of the cardiac action potential.	8
Table 5: Ion channel involved in phase 4 of the cardiac action potential.	9
Table 6: Advantages and disadvantages of the utilisation of the human model for the study of atrial fibrillation.	21
Table 7: Advantages and disadvantages of the utilisation of iPSC model for the study of atrial fibrillation.	24
Table 8: Advantages and disadvantages of the utilisation of the engineered human myocardium model for the study of atrial fibrillation.	25
Table 9: Biophysical characteristics of channelrhodopsin-1 and channelrhodopsin-2 and chrimson and a few of their variants used in research.	32
Table 10: Transport solution composition.	36
Table 11: Fibroblast culture media compositions.	39
Table 12: Cardiomyocyte medium composition.	40
Table 13: Composition of bath and pipette solutions used for voltage-clamp recordings.	41
Table 14: Composition of Tyrode's solution used for optical action potential recordings.	43
Table 15: Composition of the solutions used with the automated patch-clamp system.	44
Table 16: Induced pluripotent stem cell pacing medium composition.	45
Table 17: Engineered human myocardium medium composition.	46
Table 18: Sharp-microelectrode Tyrode's modified solution.	47
Table 19: Tyrode's solution used for light sensitivity assessment in atrial cardiomyocytes derived from induced pluripotent stem cells transfected with an adeno-associated-virus-2 carrying a channelrhodopsin-2.	50
Table 20: Primers used for quantitative polymerase chain reaction assays.	53
Table 21: Clinical characteristics of patients used for sharp-microelectrode experiments.	59

Abbreviations

[I] _{ext}	Ion concentration in the external compartment
[I] _{int}	Ion concentration in the internal compartment
AAV-2	Adeno-associated-virus-2
AAV2-ChR2	Adeno-associated-virus-2 carrying a channelrhodopsin-2
AAV2-ChR2 atrial EHM	Engineered human myocardium generated using atrial cardiomyocytes derived from induced pluripotent stem cell and transfected with an adeno-associated-virus-2 carrying a channelrhodopsin-2
ACE	Angiotensin-converting enzyme
AF	Atrial fibrillation
AP	Action potential
APD	Action potential duration
ATP	Adenosine triphosphate
Atrial iPSC	Atrial cardiomyocyte derived from induced pluripotent stem cells
BHK	Baby hamster kidney
Ca ²⁺	Calcium
CAMKII	Calcium/Calmodulin kinase II
CAMKII δ	Calcium/Calmodulin kinase II δ
cAMP	Cyclic adenosine monophosphate
ChEF	Chop1 and Chop2 chimera fused by the loop between helices E and F
ChIEF	Variant of ChEF with a mutation on the isoleucine 170
CHF	Congestive heart failure
ChR1	Channelrhodopsin-1

ChR2	Channelrhodopsin-2
Chop1	Channelopsin 1
Chop2	Channelopsin 2
CICR	Calcium-induced calcium-release
Cl ⁻	Chloride
DAD	Delayed afterdepolarisation
EAD	Early afterdepolarisation
EC	Excitation-contraction
ECG	Electrocardiogram
ECGI	Electrographic imaging
E _{DF}	Driving force
EHM	Engineered human myocardium
E _{ion}	Equilibrium potential of the ion i
E _m	Membrane potential
E _{qK}	Equilibrium potential of the potassium channels
ERP	Effective refractory period
F	Faraday's constant
FGF	Fibroblast growth factor
G	Conductance
G _{ion}	Membrane conductance for the ion
HCN	Hyperpolarisation-activated Cyclic Nucleotide-gated
HEK	Human embryonic kidney
HF	Heart failure
I _{Ca,L}	L-type calcium current
I _{Ca,T}	T-type calcium current
IGF	Insulin-like growth factor
I _h	Proton current
i _{ion}	Conductance of the ion i
I _{K,ACh}	Acetylcholine-dependant inward rectifier current
I _{K1}	Inward rectifier potassium current

$I_{Kir,fb}$	Barium-sensitive inward rectifier fibroblast current
I_{Kur}	Ultra-rapid potassium current
$I_{Kv,fb}$	Tetraethylammonium-sensitive voltage-gated fibroblast current
I_{Na}	Sodium current
$I_{Na,late}$	Late component of the sodium current
$I_{Na,peak}$	Peak current of the sodium current
I_{NCX}	Sodium-calcium exchanger current
IMDM	Iscove's modified Dulbecco's medium
iPSC	Induced pluripotent stem cell
I_{to}	Transient outward potassium current
$I_{to,f}$	Fast variant of the transient outward potassium current
$I_{to,s}$	Slow variant of the transient outward potassium current
K^+	Potassium
K2P	Two-pore-domain potassium channel
KO ^{-/-}	Knockout
LTCC	L-type calcium-channel
LVEF	Left ventricular ejection fraction
MCU	Mitochondrial calcium uniporter
MEA	Multi electrode array
MOPS	3-(N-Morpholino)propanesulfonic acid, 4-Morpholinepropanesulfonic acid
mRNA	Messenger ribonucleic acid
Na^+	Sodium
NCX	Sodium-calcium exchanger
NFAT	Nuclear factor of activated T-cells
N_{ion}	Number of ion channels
PKA	Protein kinase A
PKC	Protein kinase C
P_o	Probability of opening

R	Ideal gas constant
RA	Retinoic acid
ROS	Reactive oxygen species
RPMI	Roswell Park Memorial Institute medium
RSB	Retinal Schiff base
RyR2	Ryanodine receptor 2
SERCA	Sarcoplasmic reticulum calcium ATPase
SR	Sinus rhythm
SRet	Sarcoplasmic reticulum
T	Temperature
TGF β	Transforming growth factor β
VEGF	Vascular endothelial growth factor
Ventricular iPSC	Ventricular cardiomyocyte derived from induced pluripotent stem cells
VSD	Voltage sensing domain
Z	Charge of the ion
γ_{ion}	Unitary conductance of the ion [i]

Abstract

Atrial fibrillation is the most common supraventricular arrhythmia and is associated with molecular remodelling that promotes the maintenance and worsening of the disease. Although extensive research has been performed to develop treatments to hamper the progression of atrial fibrillation, many attempts showed disappointing results when transferred to clinics. One reason could be that the results obtained in the study models do not cross the transferability gap and the observed results could not be applicable to human pathophysiology. However, the exclusive utilisation of human tissue comes with a certain number of limitations, including the poor availability of the material. One solution could come from the huge progress made in the development of induced pluripotent stem cells (iPSC), and their utilisation for 3D *in vitro* modelling. Unlike human materials, they are readily available, and unlike animal models, the results obtained can better be transferred to human pathophysiology. Therefore, we hypothesised that atrial cardiomyocytes derived from iPSC could be used to study mechanisms associated with acute and long-term electrical remodelling in atrial fibrillation.

In the first part, we investigated whether atrial cardiomyocytes derived from induced pluripotent stem cells (atrial iPSC) could be a suitable model for studying acute (24 hours) electrical remodelling associated with atrial fibrillation. Results showed that 3 Hz electrically paced (tachypaced) atrial iPSC showed electrical remodelling characterised by a reduction of the action potential duration at 90% repolarisation (APD₉₀), a decreased L-type Ca²⁺ current (I_{Ca,L}), an impaired activation of the acetylcholine-activated inward-rectifier K⁺ current (I_{K,ACh}) and the development of a constitutively active and agonist independent I_{K,ACh}. The I_{K,ACh} impairment was associated with a significantly reduced expression of Kir3.4.

In the second part, we evaluated the effects of acute electrical tachypacing on atrial engineered human myocardium (EHM). We showed that electrical tachypacing for 24 hours was associated with a significant reduction of the APD₉₀ and an impaired response to the M2-receptor agonist, carbachol.

In the last part, we investigated the effects of long-term optical tachypacing on atrial EHM. This was permitted by the utilisation of an atrial iPSC line expressing the fast variant of the channelrhodopsin chrimson. The acute optical tachypacing of chrimson atrial EHM showed the same electrical remodelling observed in the electrically tachypaced atrial EHM, characterised by a significant reduction of the APD₉₀ and an altered response to the M2-receptor agonist carbachol. Additionally, long-term optical tachypacing (7 days) of chrimson atrial EHM resulted in a hyperpolarisation of the resting membrane potential, an increase in the action potential amplitude, and the maximum upstroke velocity.

Altogether, this thesis shows that atrial iPSC and atrial EHM models can be used as experimental tools to investigate the electrical remodelling associated with acute and long-term atrial fibrillation, thus giving an outlook on the possibilities of using novel genome editing technologies for the elaboration of study models.

1 Introduction

1.1 Normal electrophysiology of the heart

1.1.1 Cardiac action potential

The term action potential (AP) refers to the changes in the membrane potential during a cycle of membrane depolarisation-repolarisation framed by a period of membrane potential equilibrium, called resting membrane potential (RMP). The cardiac AP can be seen as the macroscopic manifestation of the activation and inactivation of the ion channels present at the membrane of a cardiac cell over time.

AP properties can vary a lot depending on the specie (Clauss et al. 2019; Schüttler et al. 2020), the cell population considered (Cyganek et al. 2018) or even the layer of the organ we are considering (Liu et al. 1993). Furthermore, the capacity of an excitable cell to generate an AP does exist outside of the cardiac system (namely in the neural system). Finally, excitable cells are also very susceptible to variations caused by their environment (temperature, oxygen concentration, pH, ion concentration, pressure).

A classic cardiac AP can be decomposed into five phases going from 0 to 4, each associated with the participation of specific ion channels. A schematic human AP is drawn in **Figure 1**, and the different phases that compose it are described below. Biophysical concepts underlying the generation of an action potential are described in the **Supplemental content 1**.

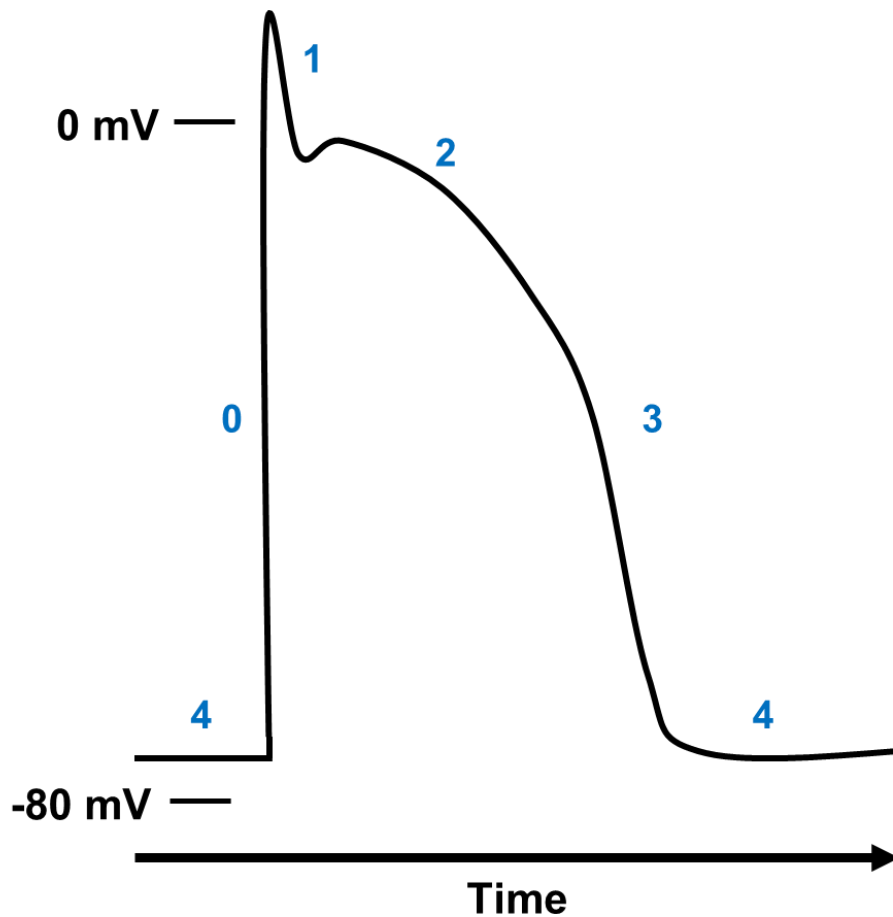


Figure 1: Schematic action potential with the different phases. The different action potential phases are numbered as follows: phase (0) is the upstroke, (1) is the early repolarisation phase, (2) is the plateau phase, (3) is the late repolarisation phase, (4) is the resting phase. mV: millivolts.

Phase 0

The phase 0 corresponds to the AP's fast depolarisation phase (or upstroke). The principal ion channels involved in this phase are the voltage-dependant sodium channels, carrying the I_{Na} current (Marban et al. 1998). Following an activation pre-pulse (slow depolarisation for nodal cells or electrical pre-pulse), the membrane potential reaches the activation potential of the voltage-gated sodium channels, thereby causing their activation and their opening. The resulting current is a massive inward depolarising current that rapidly shifts the membrane potential to a positive voltage in a few milliseconds.

At the molecular level, 10 genes have been found to encode for the α -subunits (Goldin et al. 2000). The principal isoform of the α -subunit at the cardiac level is the NaV_{1.5} (encoded by the gene SNCA5).

Many mutations have already been described and associated with the development of arrhythmia. Amongst them, the one concerning the permeability pore and the selectivity filter seems to be the most frequent, where over 70 mutations only on these two components of the channel have already been described (Jiang et al. 2020). Most of them are responsible for the development of arrhythmia, particularly a form of congenital long QT syndrome (LQT3) called Brugada's syndrome (Baroudi et al. 2001; Baroudi et al. 2002).

In the context of atrial fibrillation (AF), inhibition of the late component of the I_{Na} has been investigated as a potential therapeutic target because of its arrhythmogenic potential (Burashnikov 2017; Chu et al. 2020; Ton et al. 2021). However, a recent study in a lone AF goat model could not show any potential therapeutic effects on the utilisation of the I_{Na} inhibitor ranolazine for restoring sinus rhythm (Opačić et al. 2021).

Gene	α -subunit	Current	Agonist	Antagonist	References
SCNA1	NaV1.5	I_{Na}	Acotinide, Sea anemone toxin	Flecainide, Quinidine, Amiodarone, TTX	Isom et al. 1992; Isom et al. 1995; Morgan et al. 2000; Maier et al. 2003; Abriel 2007; Jiang et al. 2020

Table 1: Ion channel involved in phase 0 of the cardiac action potential.

Phase 1

The phase 1 refers to the early repolarisation of the AP. During this phase, sodium channels are inactivated with only its late tail current subsisting. The transient outward potassium channel (I_{to}) quickly activates to engage the early repolarisation of the membrane. This fast activation is responsible for the “notch”, observable in the AP.

I_{to} is a complex current whose electrophysiological characteristics depend on the α -subunit heterodimeric construction. Two different I_{to} have been observed and characterised namely $I_{to,f}$ (fast) and $I_{to,s}$ (slow). Each current is the resulting from the heterodimeric constructions of the α -subunit, and the combination is defining the resulting current: $Kv_{4.2}$ and/or $Kv_{4.3}$ α -subunits assembly will result in $I_{to,f}$ whereas $Kv_{1.4}$ and/or $Kv_{1.7}$ α -subunits assembly will result in $I_{to,s}$ (Oudit et al., 2001). Their names were given according to their recovery kinetics from inactivation. While they both have comparable activation and inactivation speeds (2-10 and 25-80 ms for their activation and inactivation, respectively), their recovery time from inactivation varies a lot (80-200 ms and 1-2s for the fast and slow forms respectively). Finally, it has been shown that the $I_{to,f}$ current density, was larger in comparison with $I_{to,s}$ and that these functional heterogeneities were coupled with an expressional heterogeneity throughout the heart. Interestingly, fast isoforms are rather expressed in short AP regions and the slow forms in the long AP regions (the fast form is mostly expressed in the left epicardial region, the right ventricle, and the base of the heart, while the slow form in the septum, left ventricular endocardium and the apex of the heart). This particularity gives I_{to} a modulatory and coordinating role for the ventricle repolarisation and contraction, ensuring the correct direction of the repolarisation wave.

For all these reasons, mutations affecting I_{to} can result in arrhythmogenic events by generating alternans (Ni et al. 2019) or early after depolarisations (EAD) which facilitate the initiation and the maintenance of AF (Zhao et al. 2012). Recently, the inhibition of I_{to} has been shown to be a promising possibility for treating J-wave syndrome patients (Ye et al. 2022). The study showed that in patient-derived iPSC, the utilisation of acetatin, a powerful I_{to} blocker, was able to restore the AP notch, alleviating the arrhythmogenic potential of a mutation on the KCND3 gene.

The second major player of phase 1 of the AP is the ultra-rapid outward current I_{Kur} . First, it is important to note that I_{Kur} is functionally expressed only in the atria. In the AP, I_{Kur} also plays a role in the generation of the notch. However, the role of I_{Kur} is more complex as it indirectly regulates the activity of all outward currents because it regulates the AP plateau's height. Studies have shown the inhibition

of I_{Kur} resulted in an elevation of the plateau in a dose-dependent manner (Loose et al. 2014). Although I_{Kur} plays a role as repolarising current, its inhibition has been shown not to necessarily prolong AP duration, with its effects also depending on the patient's rhythm status (Loose et al. 2014). In sinus rhythm patients, it has been proposed that the inhibition of I_{Kur} was associated with an elevation of the plateau phase and an augmentation of the availability of the I_{Kr} channel, thus fastening the repolarisation (Gintant 2000). However, because AF is associated with the impairment of several currents involved in the AP (including $I_{Ca,L}$: van Wagoner et al., 1999; $I_{to,f}$: van Wagoner et al., 1997; Workman et al., 2001 and I_{K1} : Dobrev et al., 2002), inhibition of I_{Kur} in AF showed different results i.e. AP prolongation (Wettwer et al. 2004).

Because of its central role regarding the AP shape, mutations in the α -subunit Kv1.5 has been linked with several forms of lone AF (Olson et al. 2006; Parvez and Darbar 2010; Christophersen et al. 2013). Furthermore, because of its atrial specificity, the inhibition of I_{Kur} represents a great therapeutic target in the context of AF and is under large investigation for developing clinical approaches featuring this channel (Gunaga et al. 2017; Borrego et al. 2021).

Gene	α -subunit	Organisation	Current	Agonist	Antagonist	References
KCND2 KCND3	Kv4.2 Kv4.3	$I_{to,f}$ Kv4.2 and/or Kv4.3	I_{to}	NS5806	Acetatin 4-AP	Yang et al. 2004; Lundby et al. 2008; Ravn et al. 2008; Calloe et al. 2011; Nielsen et al. 2013
KCNA4 KCNA7	Kv1.4 Kv1.7	$I_{to,s}$ Kv1.7 and/or Kv1.4				
KCNA5 KCNC1	Kv1.5 Kv3.1	-	I_{Kur}		AVE0118, 4-AP, MK-0448, Vernakalant	Wettwer et al. 2004; Christ et al. 2008; Loose et al. 2014; Lévy et al. 2021

Table 2: Ion channels involved in phase 1 of the action potential.

Phase 2

The phase 2 of the cardiac AP corresponds to the plateau phase and is the longest phase of the cardiac AP. It involves calcium (Ca^{2+}) related channels ($I_{\text{Ca,L}}$, I_{NCX}) and is associated with several electrophysiological and physiological mechanisms.

$I_{\text{Ca,L}}$ is the most prominent current of this phase. It is not only responsible for an inward depolarising current but also participates in cell contraction via its participation in the Ca^{2+} -induced Ca^{2+} -release (CICR) mechanism, which is initiated in the microdomains it forms with the Ca^{2+} -activated ryanodine receptor, situated on the sarcoplasmic reticulum (SRet) membrane. $I_{\text{Ca,L}}$ is generated by the L-type Ca^{2+} -channel (LTCC), a Ca^{2+} channel belonging to the voltage-gated family of Ca^{2+} channels, formed by the assembly of Cav1.2 α -subunits. A gain of function mutation on the CACNA1C gene encoding for the Cav1.2 protein is associated with long-QT syndrome (Wemhöner et al. 2015; Mellor et al. 2019).

Gene	α -subunit	Current	Agonist	Antagonist	Reference
CACNA1C	Cav1.2	$I_{\text{Ca,L}}$	BayY5959	Nifedipine, verapamil, dihydropyridine, aconitine	Satin et al. 2011; Ortner and Striessnig 2016; Wu et al. 2017

Table 3: Ion channels involved in phase 2 of the cardiac action potential.

Phase 3

Phase 3 of the AP directly follows the plateau phase. It corresponds to the slow repolarisation phase and is mediated by the activity of repolarising potassium currents.

The main channels involved in this phase are the delayed rectifier potassium currents I_{Kr} , I_{Ks} , the potassium current activated by acetylcholine ($I_{\text{K,ACh}}$, in atria only) and the inward rectifier current I_{K1} in a smaller proportion.

The rapid component of the delayed rectifier K^+ channels (I_{Kr}) starts the slow repolarisation phase of the action potential. The cardiac I_{Kr} channel is encoded

by the human ether-a-go-go-related gene (hERG or $K_v11.1$) and is named rapid in opposition to the slow component of the delayed rectifier K^+ channels. It is more present in ventricular than in atrial tissues of humans (Pond et al. 2000). I_{kr} is an outward repolarising current, whose activation starts below the isoelectric line until it reaches a maximum between -30 and -40mV (Hancox et al., 1998). It is important to note that its denomination refers to its activation kinetic and does not presume the current profile: although I_{kr} is activated earlier than I_{ks} , its intensity builds up gradually, so that I_{kr} reaches its maximum intensity after I_{ks} (Imredy et al. 2008). It is a major player of the slow repolarisation phase and is particularly under scrutiny during drug development phases, as its inhibition is arrhythmogenic and can result in the development of ventricular fibrillation or torsade-de-pointes in the ventricle (Hancox et al. 2008; Calderone et al. 2010; Parikh et al. 2017; Sharifi et al. 2017) and drug-induced long QT syndrome (Witchel 2011). Finally, the loss of function of the gene encoding for the $K_v11.1$ protein has been associated with a long QT syndrome (LQT2), characterised by a prolongation of the AP (Gu et al. 2021).

The second member of the delayed rectifier K^+ -channels is I_{ks} , carrying the slow component. I_{ks} is encoded by the *KCNQ1* gene and the K_vLQT1 protein constitutes the α -subunit of the channel. Although it is accepted that I_{ks} participate in the repolarisation of the AP, controversies remain regarding its actual contribution in the AP repolarisation reserve (Liu and Antzelevitch 1995; Bosch et al. 1998; Varró et al. 2000; Lengyel et al. 2001; Jost et al. 2005). Nevertheless, mutations of the gene encoding for the K_vLQT1 protein can also lead to a form of long QT syndrome (long QT syndrome type 1; Schwartz et al., 2021), and there is evidence showing that drug-induced long QT syndrome can also be caused by the inhibition of I_{ks} (Veerman et al. 2013), demonstrating that I_{ks} plays an important role in the late repolarisation of the AP in human.

Another specific current is the G-protein-activated K^+ -current ($I_{K,ACh}$) current. In a physiological context, this channel is activated by the vagal nerve-released neurotransmitter acetylcholine and acts in favour of the para-sympathetic balance (Heijman et al. 2018). $I_{K,ACh}$ is the result of a heterotetrameric construction of GIRK1 and GIRK4 subunits (Krapivinsky et al. 1995; Corey et al. 1998). $I_{K,ACh}$ also

participates in cardiac automaticity, but its exact role remains unclear (Mesirca et al. 2013). $I_{K,ACh}$ quickly became an interesting target in the context of atrial fibrillation, as it was shown that its activity was altered and was associated with electrical remodelling increasing the propensity for atrial fibrillation development (Hashimoto et al., 2006; Kovoov et al., 2001).

Gene	α -subunit	Current	Agonist	Antagonists	References
KCNH2	Kv11.1 (HERG)	I_{Kr}		Dofetilide, KCB-328	
KCNQ1	KVLQT1	I_{Ks}	DIDS, L-364,373-R-L3), mefenamic acid	Chromanol 29B, L-735,821	Salata et al. 1998; Banyasz et al. 2005; Yang et al. 2013; Printemps et al. 2019
KCNJ3 KCNJ5	Kir3.1 Kir3.4	$I_{K,ACh}$	Acetylcholine, carbachol, adenosine	Tertiapin	

Table 4: Ion channels involved in phase 3 of the cardiac action potential.

Phase 4

Phase 4 of the AP is associated with the RMP phase. During this phase, most of the Ca^{2+} and Na^{+} voltage-gated channels are closed, because of the very low membrane potential. The membrane potential can be associated with the equilibrium potential of the potassium channels (E_{qK}) located at ± -80 mV, and is mediated by the activity of the inward rectifying potassium current (I_{K1}).

Gene	Protein	Organisation	Current	Agonist	Antagonist	Reference
KCNJ2	Kir2.1 Kir2.2 Kir2.3	Homo/hetero tetramers	I_{K1}	Zacopride, tetramisole	PA-6	Hoeker et al. 2017; Jebran et al. 2022; Liu et al. 2022

Table 5: Ion channel involved in phase 4 of the cardiac action potential.

1.1.2 The different cardiac action potentials

Because ion channel expression is heterogeneous throughout the different cardiac compartments, the AP shape and duration is also different, depending on at the considered location (Liu et al. 1993; Liu and Antzelevitch 1995; Bryant et al. 1998). Furthermore, within the same tissue variability exists. On the following paragraph, we will describe the main characteristics associated with the different cardiac AP.

Sinus node action potential

The sinus node AP is unique because of the presence of the I_f current that is responsible for the automaticity of the nodal cells. This current is unique, because of the singular biophysical properties associated with its functioning. I_f is carried by a heterodimeric construction of isomers belonging to the hyperpolarisation-activated cyclic nucleotide-gated (HCN) family, and its activation is placed under the control of a regulatory subunit, part of the MinK family (MinK-related peptide 1, MirP1; Weisbrod et al., 2016; H. Yu et al., 2001). Unlike other cardiac depolarising currents (particularly sodium currents), this current is carried through a channel whose activation is mediated by hyperpolarisation of the membrane and is permeable to cations (Na^+ and K^+).

The I_f current is not strictly specific to the nodal cells, but is also expressed in the other cell types participating in the conduction system of the cardiac tissue (DiFrancesco 1981; Baruscotti et al. 2010). I_h (the current resulting in the expression of HCN channels) is also found in the central nervous system (Berger et al. 2003), pancreatic β -cells (El-Kholy et al. 2007), the enteric nervous system (Wang et al. 2012) or even in the portal vein (Greenwood and Prestwich 2002) however, its physiological role in these specific tissues is not always clear.

In terms of the action potential duration (APD), sinus node cells show a short APD compared to the ventricular APD, ranging around 150 ms in humans (Verkerk et al., 2009).

Ventricular action potential

The ventricular AP also has its specifics. The ventricle is the contractile chamber of the heart, and its AP is characterised by a long plateau phase above the isoelectric line. The ventricular AP is longer (from 350 to 500 ms) than the atrial AP (Kang et al. 2016; Nánási et al. 2021; Koncz et al. 2022).

This difference in APD is due to the different expression and function of ion channels involved in the AP (Cyganek et al., 2018; X. Zhang et al., 2017).

Atrial action potential

The atrial AP is characterised by a more triangular shape and a more depolarised RMP (Wang et al. 1998). Its plateau is classically described under the isoelectric line, and because of the expression of I_{Kur} channels, the plateau phase is less prominent (Loose et al. 2014). Finally, its duration is shorter in comparison to the ventricular AP (250-400 ms; Colman et al., 2018; Fakuade et al., 2021).

The atrial AP is different from the ventricular one, mainly because of the presence of atrial-specific currents (namely I_{Kur} , and $I_{K,Ach}$, both described above).

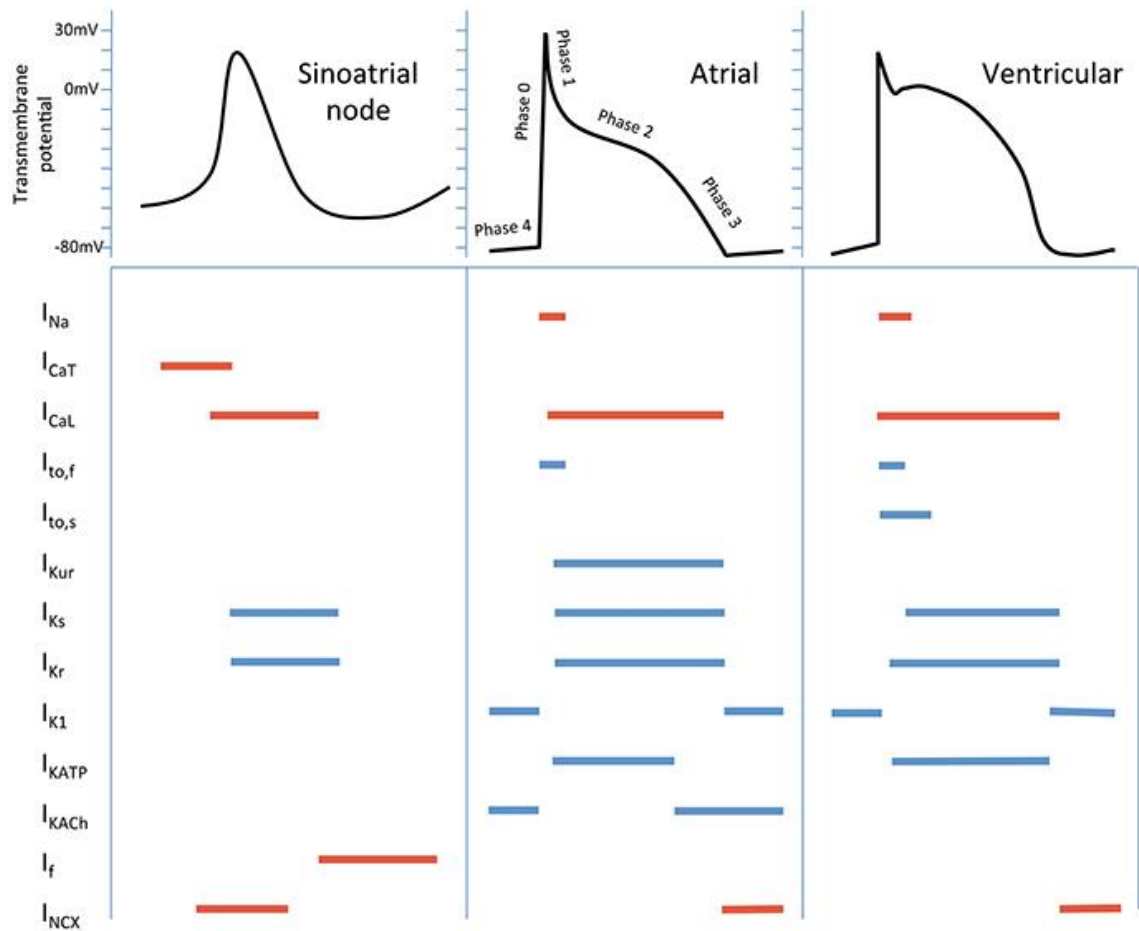


Figure 2: Schematic representation of the different cardiac action potentials and the kinetics of activation of the major ion channels involved in the generation of the action potentials. Blue represents an outward current, red represents an inward current. From Lane and Tinker 2017, with permission.

1.1.3 Cardiac excitation-contraction coupling

The term excitation-contraction coupling describes the sequence of events leading to the contraction of a cardiac cell following its excitation, its membrane depolarisation, and the generation of an AP.

Cell contraction is a phenomenon mediated by Ca^{2+} , mostly originating from the SRet. During the plateau phase of the AP, the Ca^{2+} influx generated by the activation of the L-type Ca^{2+} current activates the ryanodine receptor-2, located at the SRet membrane, leading to a massive unloading of Ca^{2+} into the cell, this is the CICR phenomenon (Bers 2002). This Ca^{2+} will eventually bind to contractile protein of the cell (namely the contraction inhibitory protein troponin C which has

its inhibition relieved upon Ca^{2+} binding) and trigger the contraction of the cell via ATP hydrolysis at the myosin protein's heads (Cooper 2000).

Relaxation occurs through the activation of several mechanisms, all participating in the reduction of intracellular Ca^{2+} . At the cell membrane, the $\text{Na}^+/\text{Ca}^{2+}$ -exchanger (NCX) and the Ca^{2+} -ATPases are mobilised to extrude Ca^{2+} out of the cytosol. Inside the cell, the sarcoplasmic reticulum Ca^{2+} -ATPase (SERCA) and the mitochondrial Ca^{2+} -uniporter (MCU) initiate Ca^{2+} reuptake in their respective compartments. Because of the diminution of the Ca^{2+} concentration, the inhibitory role of troponin C is relieved, and the contractile proteins are ready for the next cycle (Bers 2002).

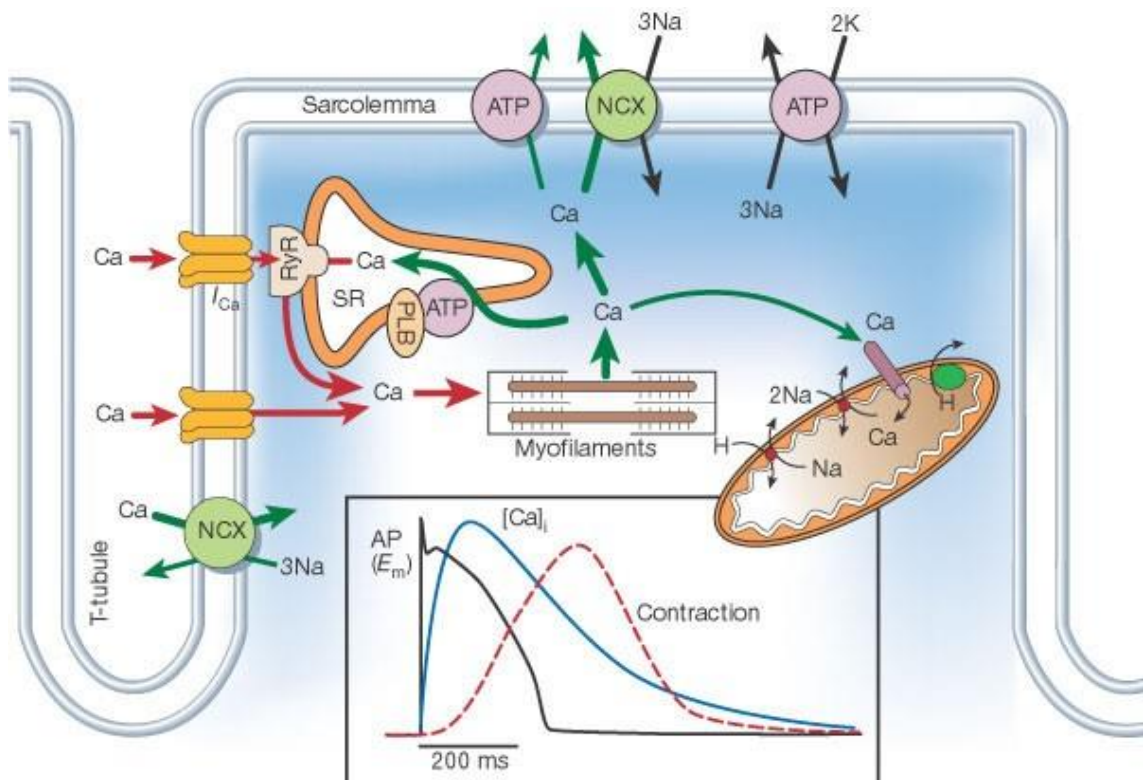


Figure 3: Schematic representation of the molecular mechanisms involved in the excitation-contraction mechanism. From Bers 2002, with permission.

1.2 Atrial fibrillation

1.2.1 General characterisation

With a prevalence of 1 to 2%, atrial fibrillation is the most common supraventricular arrhythmia in the western world (Hindricks et al. 2021). Current estimations state that over 9 million people were affected in 2010 and are projected to reach over 14 million people in 2060 in Europe alone (Hindricks et al. 2021).

AF is characterised by a loss of the coordinated atrial depolarisation in favour of the apparition of several ectopic depolarisation foci throughout the atria. Because of this loss of electrical coordination, AF is associated with an impairment of the contractile function of the atria and several other comorbidities (Allessie et al. 2002; Yeh et al. 2008; Sossalla et al. 2010). On top of the existing so-called “lone AF”, characterising AF as a direct consequence of a genetic mutation (Parvez and Darbar 2010; Christophersen et al. 2013; Olesen et al. 2013), AF is also a multifactorial disease whose development and maintenance is influenced by many factors (Goette et al. 1996; Bosch et al. 1999; Allessie et al. 2002; Nattel et al. 2008). Furthermore, AF can also be the end point of several other pathologies or part of larger syndromes (Lubitz et al. 2010; Qiao et al. 2016; Melillo et al. 2020). Also, AF has been shown to be a risk factor of its own promotion and maintenance (Wijffels et al., 1995).

Atrial fibrillation evolution is classified in three different stages depending on the duration of the episode and the attempts made to restore to SR. The first stage is called paroxysmal AF and is referring to the early development phase of the disease. AF is considered as paroxysmal until a duration of seven days. When the episode persists longer, the patient disease is qualified as persistent, but the conversion to sinus rhythm (SR) is still possible. When the conversion is no longer achievable and no further attempt are made, the patient’s disease is qualified as permanent (Hindricks et al. 2021).

At the clinical level, many factors can influence the development of AF. They can be separated into two distinct groups: non-modifiable factors (including age or

genetic predisposition), and modifiable factors (including individual behaviour and consequences of lifestyle such as hypertension, diabetes mellitus, smoking, alcohol consumption, obesity, sedentarily or psychological stress or psychosocial factors, Hindricks et al., 2021). AF itself is associated with an increase in the mortality risk, however dying from AF itself is extremely rare (Freeman et al. 2015). Life threatening risks associated with the development of AF are mainly due to the apparition of comorbidities associated with the development of the pathology or the risk factors associated with developing AF.

1.2.2 Important definitions in the context of atrial fibrillation: substrate, trigger, re-entry, and rotor

The pathophysiological description of AF is classically associated with notions of substrates and trigger events (Rivard et al. 2007; Mulla et al. 2019; Klapper-Goldstein et al. 2020).

The substrate can refer to left atrial dilatation, fibrosis, atrial contractile dysfunction, or electromechanical disturbances. It includes all the factors that can constitute the terrain, thereby favouring the initiation or the maintenance of an arrhythmogenic event. The AF substrate development and extent is intimately linked to the extent of the disease and the AF state of the patient (Rivard et al. 2007), and its development is also influenced by the non-modifiable and modifiable factors mentioned above.

Trigger events refer to ectopic activity that can lead to the generation of an arrhythmic episode that can perpetuate and evolve in presence of a developed substrate. Ectopic beats constitute the majority of the trigger events, but others do exist, such as sympathetic/para-sympathetic imbalance (Voigt et al. 2012; Heijman et al. 2018).

Two major arrhythmogenic phenomena are also intricately linked to AF and arrhythmia: re-entry, and rotors.

A re-entry is a self-sustained arrhythmia propagating in a closed-loop circuit. Re-entry based arrhythmias are part of the impulse conduction group of arrhythmias and are to be distinguished from the impulse generated arrhythmia.

Their origin can be various and can include electrolyte abnormalities or channelopathies, mechanical stress (Timmermann et al. 2017), fibrosis or genetic background (Aguilar & Nattel, 2016; Senst & Zeltser, 2019; Wit & Cranefield, 1978).

A rotor characterises a wave singularity whose reverberations radiate at high speed around a central core in a spiral way. Rotors are to be differentiated from the classical re-entries mainly because of the nature of their cores. Functionally in a re-entry, the core acts as an inert obstacle from which the depolarisation wave spirals around. However, in a rotor the core constitutes the area from where the disorganisation initiates because of its high instability (Krummen et al., 2015; Nattel et al., 2017).

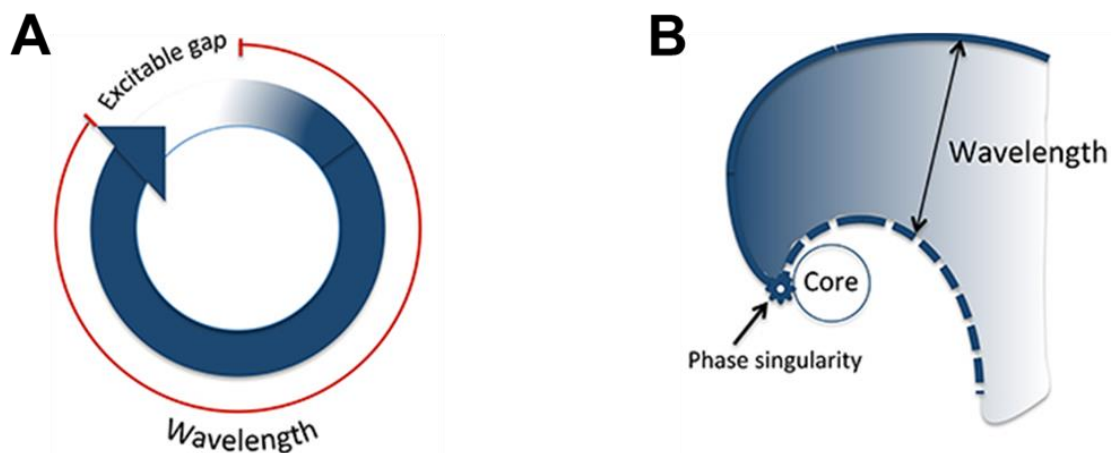


Figure 4: Schematic representation of re-entry and rotors. A, Classical anatomical re-entry, B, rotor re-entry. From Lane und Tinker 2017, with permission.

1.2.3 Symptoms of atrial fibrillation

Although 50 to 80% of AF patients are asymptomatic (Zöller et al. 2013), some symptoms can occur with the intensity varying between patients due to the severity and the evolution of the disease. Symptoms classically include breath shortening, fatigue, chest discomfort, palpitation, dizziness or even anxiety during AF episodes (Hindricks et al. 2021). Management of these symptoms is organised in concertation between the physician and the patient, according to the patient's perception of the disease. The therapeutic approach and treatments are described in the **Supplemental content 3**.

1.2.4 Molecular mechanisms associated with the development of atrial fibrillation

Molecular mechanisms associated with the development of atrial fibrillation can be separated into three different groups according to the nature of their associated remodelling. In the following part, we will mainly focus on structural and electrical remodelling. The remodelling associated with Ca^{2+} handling is described in the **Supplemental content 2**.

Structural remodelling

Structural remodelling is a slow process at the centre of the development and maintenance of atrial fibrillation. It occurs in the left atria, particularly in the posterior wall. In opposition to the electrical remodelling that starts when the first arrhythmia occurs, structural remodelling is a slow-going process that is hardly reversible when installed (Allessie et al. 2002).

At the macroscopic level, atrial dilatation is the most significant hallmark of the structural remodelling associated with atrial fibrillation (Ausma et al. 1997). At the microscopic level, structural changes include a wide range of elements, including cellular hypertrophy, myolysis, cellular dedifferentiation (Allessie et al. 2002), fibrosis, apoptosis, mitochondria, and sarcoplasmic disruption (Ausma et al. 1997) or connexin organisation disruption (Akar et al., 2004, 2007; Kostin et al., 2002).

Atrial dilatation can be the result of all the microscopic events happening in the atria but also the consequence of modifiable (hypertension, obstructive sleep apnoea, obesity, valvular heart disease, congestive heart failure, ischemia, inflammation) or non-modifiable factors (age or genetics) that can lead to the increase of atrial pressure or volume overload, ultimately leading to atrial dilatation (Verheule et al. 2003; Xi et al. 2009). Furthermore, atrial dilatation has been shown to increase the dispersion of the atrial effective refractory period (Satoh & Zipes, 1996), or increase anisotropy in the atria (Wong et al. 2012), both of which increase the susceptibility to arrhythmogenic events of AF induction (which is the reason why it can be considered to be a substrate).

A difficult aspect of the structural remodelling and its main microscopic feature, fibrosis, is that it can be the end point of many different conditions such as cardiomyopathies, mitral valve diseases, myocarditis or even senescence (Melillo et al. 2020; Pelliccia et al. 2022; Suresh et al. 2022; Zhang et al. 2022). This non-specific aspect adds to the difficulty of efficiently preventing or treating the apparition and the evolution of this substrate.

An example of the contribution of fundamental research to the elaboration of therapeutic approaches to specifically target the development of this substrate was the development of angiotensin-converting enzyme (ACE) inhibitors. Fibrosis has been shown to be highly associated with the increase of the angiotensin-renin system during AF, possibly because of an impairment of the ACE/ACE2 balance (Pan et al., 2007). Therefore, treatments using ACE inhibitors have shown interesting results and reduced the amount of fibrosis (Goette et al. 2000) in AF models, and are now regularly used in clinical treatment (Hindricks et al. 2021)

Electrical remodelling

Electrical remodelling refers to the changes in cardiac electrophysiology that favour the initiation or maintenance of arrhythmogenic events. At the macroscopic level, electrical remodelling is characterised by the apparition of several ectopic depolarisation foci throughout the atria, overtaking the coordinated and organised depolarisation and wavefront originating from the sinus node. This remodelling creates chaotic and uncoordinated depolarisation and contraction of the atria (Hindricks et al. 2021). At the molecular level, many alterations can be described especially at the ion channel level, where several ion channels participating in the action potential generation have been shown to be altered by electrical remodelling (Bosch et al. 1999; Allessie et al. 2002). The electrical remodelling can be investigated using electrophysiology techniques. The techniques used to investigate electrical remodelling are described in the **Supplemental content 6**.

Inward currents

In the context of AF, several inward currents have been shown to have a modified function. We can cite the I_{Na} , $I_{Ca,L}$ or the I_{NCX} .

First, with regards to the sodium channels, the late component has been shown to be particularly prone to remodelling. On top of the CaMKII regulation, inherited forms of AF presenting mutations on Nav1.5 α -subunit have also been reported (Darbar et al. 2008; Ellinor et al. 2008; Makiyama et al. 2008; Olesen et al. 2012). Furthermore, their description shows that the late component of I_{Na} carries arrhythmogenic effects via its participation in the APD, and its increase can favour the occurrence of EADs, while prolonging the opening of the arrhythmogenic window current (Benito et al. 2008; Ellinor et al. 2008; Zimmer and Surber 2008). However, although familial cases of arrhythmia characterised by mutations on the SCN5A gene have been described, especially in the case of long QT or even Brugada syndrome (Baroudi et al. 2001; Antzelevitch and Nof 2008; Benito et al. 2008; Wilde and Amin 2018), the direct link between AF and sodium ion channel activity is poorly studied. Nevertheless, a study from Sossalla et al. showed evidence that in atrial myocardium from patients suffering from AF, although peak I_{Na} was reduced, $I_{Na,late}$ was significantly increased (Sossalla et al. 2010). In this study, they attributed the decrease of $I_{Na,peak}$ to a decreased expression of Nav1.5 as shown previously (Yue et al. 1999), and the increase of $I_{Na,late}$ to an increased expression of Nav1.1 (Xi et al. 2009). However, it can also be caused by the enhanced activity of the CAMKII activity (Wagner et al. 2006). Finally, the increase in I_{Na} can lead to an increased intracellular Ca^{2+} concentration because of the reverse activity of the NCX channels (Sossalla et al. 2008). The consecutive Ca^{2+} influx can furthermore promote the activity of the CAMKII and create a positive feedback loop.

The second major contributor of the electrical remodelling associated with atrial fibrillation is the $I_{Ca,L}$. The Ca^{2+} current has been shown to be decreased in the context of AF, and the impairment of the Ca^{2+} currents and the Ca^{2+} handling is associated with a specific type of remodelling.

Regarding I_{NCX} , it has been shown that its expression and its activity were highly enhanced in AF (Voigt et al. 2012). The higher activity can cause massive

activation of the exchanger, resulting in a more sustained current during the plateau phase, and even causes DADs following Ca^{2+} leaks from the sarcoplasmic reticulum.

Furthermore, CAMKII has been shown to positively regulate NCX activity through phosphorylation and increasing its activity in the context of Ca^{2+} overload, which is related to AF (Heijman et al. 2014; Mesubi et al. 2021).

Outward currents

Several outward currents are prone to remodelling in the context of atrial fibrillation. On top of the activity of the channel placed under the control of the CAMKII (Voigt et al. 2012), other currents are prone to remodelling.

The major one concerns the activity of the $I_{K,ACh}$, and the apparition of an agonist independent constitutively active $I_{K,ACh}$. In a physiological context, this current results from the liberation of the neurotransmitter acetylcholine (ACh) following a para-sympathetic stimulation resulting in an APD abbreviation and cell membrane hyperpolarisation (Heijman et al. 2018). However, during AF, it has been shown to be constitutively active (Dobrev et al. 2005). The reasons for its enhanced activity are a reduction in the inhibition of the channel by the conventional protein kinase C (PKC) isoform, for example $\text{PKC}\alpha$ (Voigt, Friedrich, et al., 2007), and the activation by other PKC isoforms (for example $\text{PKC}\epsilon$, Makary et al., 2011), thus resulting in an increased opening probability of the Kir3.1 α -subunit constituting the channel (Voigt N. et al. 2007).

I_{K1} has also been shown to be altered in AF. I_{K1} is a background current responsible for the RMP (Reilly and Eckhardt 2021). However, when its activity increases, it can also be responsible for APD abbreviation (Zhang et al. 2005). Furthermore, its activity has been shown to be increased in the context of AF. This enhanced activity has been documented as being the result of an increased expression of Kir2.1 mRNA (Dobrev et al. 2005; Gaborit et al. 2005), which could be attributed to reduced levels of miR-1 (Girmatsion et al. 2009), or miR-26 (Wang et al. 2011; Luo et al. 2013), but also an increased opening probability attributed to its phosphorylation status (Dobrev et al. 2005).

Overall, these changes in ion channel function lead to a reduction of the effective refractory period (ERP), thus increasing the excitability of the cell, thereby potentiating arrhythmogenicity (Bosch et al. 1999; Nattel et al. 2008).

1.3 Different models to study human atrial fibrillation

Considering the complexities of AF, choosing an appropriate model is quite challenging and requires selecting specific models for specific scientific questions. Here, we will brush a non-exhaustive picture of the most used models developed to study AF and try to highlight the advantages and disadvantages associated with each model, followed by a candid discussion of the models directly related to our model. Other models commonly used are described in the **Supplemental content 4**.

1.3.1 Human models

The study of AF in humans can be done in several ways. Observational studies are less constraining to set up because of the limitations in terms of technical requirements and patient consent/ethical approval. They classically consist of the repeated measurement of physiological and/or electrophysiological parameters using *in vivo* electrophysiology techniques (for example, electrocardiogram (ECG) or the Torso) to assess the correlations between the apparition a disease and an external factor (way of living, environmental) or an internal parameters (blood sugar value, ECG parameters, hormone, or protein level).

Interventional studies are more complicated for obvious reasons. The first reason is the legal approval of the study (in terms of law and ethics). Clinical trials (for example, for the test of a new antiarrhythmic drug) are made after an excessively long pre-clinical phase to ensure the absence of side effects/teratogenic contraindications that could lead to the withdrawal of the pharmacological agent from the market, thereby engaging the structures in major health care responsibility and financial risks. For this reason, many studies never reach the point of commercial use.

Another way to perform interventional studies using the human model is via the use of surgical residuals and their utilisation by fundamental and/or clinical researchers. Such material can be obtained in many circumstances (for example, during heart transplantation, valve replacement, open heart surgery or biopsies). In these cases, legal and ethical requirements are not as complex and such material can be used for research purposes. Working on human material has the advantage that obtained results can be used directly to understand the pathophysiology of the disease, and fewer precautions need to be taken for their interpretation. However, the requirements are still extremely high, a close collaboration between the surgical department and the research institute must be organised. Human material can be very fragile and coordinated storage and transportation methods need to be discussed beforehand otherwise, the material will not be usable. Also, human material rarely comes from healthy donors and precautions need to be taken. Furthermore, interventions are limited because there are no genetic interventions possible on these tissues and long-term *in vivo* interventional studies are extremely difficult or even impossible to organise (in the context of AF, it is not possible to induce AF in patients for research purposes for obvious reasons).

Advantages	Disadvantages
Translationalability	Organisation requirements are extremely important
	Availability
	<i>In vivo</i> experiments
	Genetic interventions

Table 6: Advantages and disadvantages of the utilisation of the human model for the study of atrial fibrillation.

1.3.2 Cellular models

Cellular models vary and their utilisation depends on the research question addressed. Hence, a wide range of models, including expression models (HEK, CHO, HELA), exist (Fuller et al. 1992; Haraguchi et al. 2015; Pandit et al. 2021). Furthermore, iPSC are widely used, and although standardised models exist, this technology also opens the possibility of developing patient-specific cell lines, offering a plethora of potential study models.

Expression models were originally reserved for answering fundamental questions, as they are used for the characterisation or understanding of mechanisms (for example, the expression of a mutated ion channel in an expression model to study its biophysical properties).

Non-primary cell cultures are often used because of their relatively easy handling and the possibilities they offer in terms of genetic investigations, as well as physiological and electrophysiological investigations.

The utilisation of iPSC is remarkably interesting as it is extremely versatile in terms of possibilities. Moreover, modern differentiation techniques allowed the development of patient-specific iPSC lines, allowing the utilisation of rare patient-specific cells lines. The patient-specific generation of iPSC lines is not only used for the study of cardiac arrhythmia but also as a common approach to study drug interactions or establishing specific therapies in the context of personalised medicine (Huang et al. 2022; Jing et al. 2022; Kaneko 2022; Zhou et al. 2022). Furthermore, the dramatic fall in the costs associated with the utilisation of genome editing technologies, in particular CRISPR/Cas, opened the field of possibilities associated with this model even more.

The major concern associated with the utilisation of the cellular model is its 2D aspect. Although research can be done while integrating different cell types in co-cultures to mimic a physiological environment as much as possible, the 2D component can represent an important limiting factor in many ways and is often cited as one of the major limitations associated with the utilisation of cellular models. This particularly applies in the context of AF as it is known that the interactions of the cardiomyocytes with their environment are a key factor of the

remodelling associated with the development and the maintenance of the disease. Furthermore, iPSC lines are often criticised for their immature profile (electrophysiologically as well as physiologically), likewise the fact that standardised iPSC cell line can express proteins of interest in a different manner (Cyganek et al., 2018; Huang et al., 2022; Zhou et al., 2022). Therefore, it is imperative to carefully choose the iPSC line (and the ion channel or protein expression levels in this cell line) according to the scientific question, ensuring the protocols' pertinence and the results.

Despite all of this, the cellular model is still widely accepted as a good model to study AF, and it remains one of the most used models thanks to all its advantages.

Advantages	Disadvantages
Availability (iPSC, HEK, HELA, Oocytes)	Translationalability (immaturity)
Genetic intervention	Two-dimensional model
Translationalability (++ when patient specific cell line, +/- otherwise)	

Table 7: Advantages and disadvantages of the utilisation of iPSC model for the study of atrial fibrillation.

1.3.3 Organoid models

Engineered human myocardium model

The engineered human myocardium (EHM) model was introduced by Zimmermann et al. in early 2000 (Zimmermann et al. 2000). The EHM model is a remarkably interesting model because of the very versatile experimentation protocols it allows before, during and after the preparation of the tissues. Because they are prepared using iPSC lines, the model allows a lot of variability in terms of type of cells to be used, including genetically modified cell lines. Similarly, fibroblasts used for tissue preparation can also be modified. The EHM model is powerful because of its 3D structure that allows a more precise representation of normal physiology. Furthermore, it is possible to apply rapid pacing protocols to try to induce AF and study the effect of nutrient deprivation, hypoxia, and many other protocols.

Finally, possibilities for utilising such models are endless, and the direction it takes, using them as platform for personalised medicine, or even as therapeutic strategy in the context of heart failure (Jebran et al. 2022), shows the exciting future of the model.

One limiting factor associated with the utilisation of this model comes from its strength and the utilisation of iPSC. As described earlier, iPSC are often criticised for their immaturity, and it is particularly important to carefully select the cell lines according to the needs of the study/the project beforehand. Another limiting factor comes from the material and maintenance costs associated with the use of such a model, and the fact that it requires a lot of technical skills and that mistakes can

end up being expensive. However, it is important to put these costs into perspective with the number of outputs we can obtain from such a model, and the liberty of approaches it grants.

Advantages	Disadvantages
Genetic interventions	Immaturity and variability associated with the utilisation of iPSC
<i>In vivo</i> experiments	Maintenance and generation costs
Availability	Demands a lot of technical skills
Versatility of the model	

Table 8: Advantages and disadvantages of the utilisation of the engineered human myocardium model for the study of atrial fibrillation.

1.4 Experimental protocols to induce atrial fibrillation

Only the tachypacing method will be described hereafter, but other methods do exist. The other principle *in vivo* methods (mitral valve regurgitation and congestive heart failure model) are described in the **Supplement content 5**.

1.4.1 Tachypacing

Tachypacing methods to induce AF are widely accepted by the scientific community (Wijffels et al. 1995; Power et al. 1998; Lemoine et al. 2021). They involve the application of a protocol of high-frequency electrical stimulation pulses towards the heart (or specifically towards the atria or the ventricles), to subject the heart to a high depolarisation rate to mimic an episode of tachycardia and to recreate the different substrates observed in human AF.

Initially developed using an electrical defibrillating device in a goat model (Wijffels et al. 1995), the technique evolved and is now commonly used and accepted to study AF remodelling. Modern approaches utilising optogenetic tools instead of electrical pulses have recently shown great promise and are now used in *in vitro* models (Lemoine et al. 2020). The pacing rate varies according to the specie of the model used but is classically several times higher than the physiological depolarisation rate of the normal heart of the model used (Morillo et al. 1995; Wijffels et al. 1995; Power et al. 1998; Mulla et al. 2019; Murphy et al.

2022). Hence, inducibility of AF in response to stimulation bursts (high frequency short stimulation) is classically assessed after a protocol of electrical tachypacing. Furthermore, Wijffels et al. showed that only 24 hours were sufficient to trigger AF episodes in a goat model, and that the longer the protocol lasted, the longer the episodes could last. Several other parameters showed to be pointing towards an AF-like remodelling after applying a tachypacing protocol: wavelength size and ERP were shortened but the conduction velocity was shown to be not altered (Li et al. 1999). A recent study by Citerni et al. showed that 4 weeks of atrial tachypacing in a swine model was sufficient to induce significant functional deterioration of the atria characterised by a significant reduction of the left ventricular ejection fraction (LVEF), an increase in the end-systolic and -diastolic volumes, mitral valve regurgitation and increase in fibrotic extracellular matrix in both atrial and ventricular compartments (Citerni et al. 2020).

A great advantage of this method is that it is easily applicable to a very wide range of *in vivo* models, including the mammalian model, but also 2D cellular or monolayers and 3D organoid models for *in vitro* experimentations using pacing devices (Lemme et al., 2020; Lemoine et al., 2020, 2021).

Finally, the consequences of the tachypacing protocol have been shown to be reversible. However, the reversibility depends on the extent of the underlying structural remodelling, and it seems that structural and electrical remodelling chances to recover after a tachypacing protocol are not the same. In a dog model of rapid atrial tachypacing, although susceptibility to AF was abolished 7-14 days after the pacing protocol, ultrastructural changes and structural changes remained (Everett IV et al. 2000).

1.5 Channelrhodopsin and optogenetics

1.5.1 History and definitions

Channelrhodopsins are members of the light-gated ion channel family, a group of ion channels whose activity is regulated by electromagnetic radiation (Ernst et al. 2014). The first functional and structural characterisation of a channelrhodopsin (Chr-1) was done in 2003 by Nagel et al. In this study, they not

only demonstrated for the first time that an ion channel initially found in green alga (*Chlamydomonas reinhardtii*, channelrhodopsin-1) responded to light pulses by generating a photocurrent, but they also determined the structure of the channel. They also postulated the potential use of such proteins, enumerating foreseeable possibilities for an experimenter to control the membrane potential of a cell using simple light flashes (Nagel et al. 2003). Later on, the same group characterised another member of the Channelrhodopsin family (channelrhodopsin-2, ChR2), showing that the functional expression of the channel is not only possible in non-mammalian expression model (Oocyte), but also in a mammalian expression system (HEK and BHK cells), thus unravelling new doors and possibilities for the research community (Nagel et al. 2003).

Shortly after, Nagel and Deisseroth showed, for the first time, that a channelrhodopsin could be inserted into rat neuronal cell population using a lentivirus to control their membrane potential via flashlight pulses. The same study also demonstrated the spatial and temporal possibilities of using such techniques, as the light stimulation at very high frequency (up to 20 Hz) still resulted in a response from the cells (with an action potential. Sequel to this, the term “optogenetics” was introduced in 2006 by Deisseroth et al. to refer to an approach utilising genetic engineering and optical technologies to control or monitor biological functions (Deisseroth et al., 2006). This moment started the era of optogenetic techniques, quickly capturing the scientific community's interest upon realisation of the possibilities these new tools could offer (**Figure 5**).

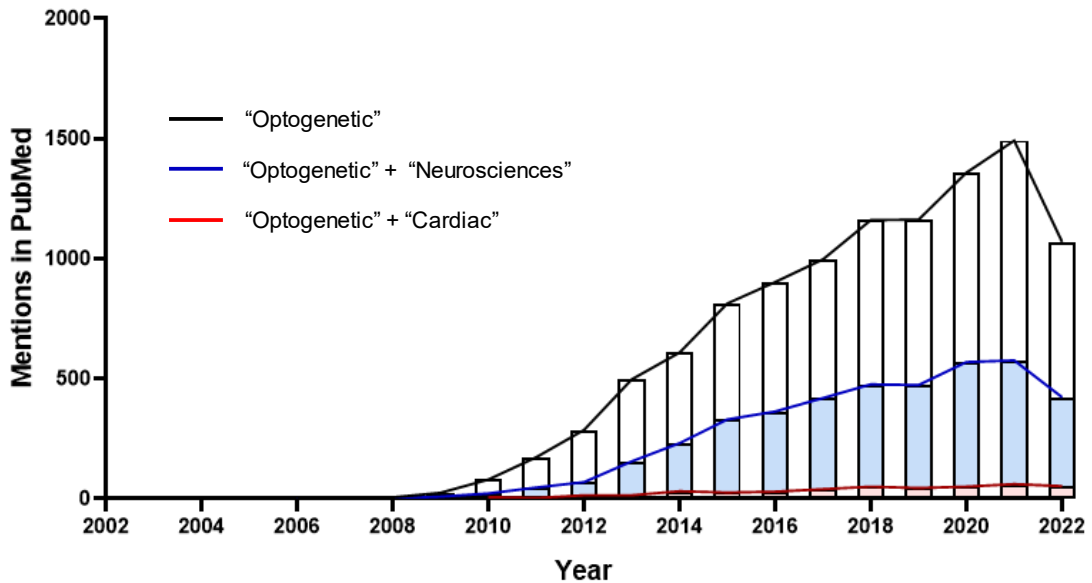


Figure 5: Amount of publications including the word "Optogenetic" in title or abstract since 2002.

Optogenetics has been used in many study models (2D, 3D, isolated cells) and living organs or organisms. As transfection methods developed and became more accessible and precise, the target and control of small cell populations within an organ became possible, ushering in optogenetic-based tools that decorticate molecular pathways came to light (Airan et al. 2009). However, despite the very rapidly growing interest in the neurology field the possibilities that these new tools offered were largely unexplored in the cardiovascular research field until 2010, where Brüggmann et al., and Arrenberg et al., showed the possibilities of the use of such technology for controlling cardiomyocyte excitability in adult mouse hearts and in pacemaker cells of the developing zebrafish heart respectively (Arrenberg et al., 2010; Brüggmann et al., 2010; Entcheva, 2013). This new information brought new light on the powerful potential of optogenetic tools in cardiac research, including its possible therapeutic use, especially as a new alternative to current cardioversion methods (Brüggmann et al. 2018; Sasse et al. 2019; Richter and Brüggmann 2020; Nyns et al. 2022).

1.5.2 Mechanism of action

Microbial and animal rhodopsins are multidomain proteins composed by two major domains. The first domain is called the opsin, or apoprotein. It is a G-protein-coupled receptor constituted by seven transmembrane α -helices forming a binding pocket for its ligand, the retinal. Each transmembrane helix has their C-terminus located on the inside of the cell with their N-terminus region on the outside. Helices are named A to G for type 1 channelrhodopsin and TM1 to TM7 for type 2 channelrhodopsin (Ernst et al. 2014). Helices A, B, C and G constitute the pore (Kato et al. 2012). Helix F is responsible for opening/closing the channel (Vonck 2000). Functional channelrhodopsin functions as a dimer and dimerisation is made on helices C and D (Kato et al., 2012; Müller et al., 2011).

The second domain is the photosensitive domain. It presents a chromophore and is called retinal (Govorunova et al. 2017). The retinal is an aldehyde of vitamin A that is derived from β -carotene, and that is covalently linked to the ϵ -amino group of a lysine on helix G or TM7 via retinal Schiff base (RSB) linkage. When illuminated at a specific wavelength (depending on the nature of the retinal), retinal undergoes isomerisation from all-trans to 13-cis and initiates the so called “photocycle”, leading to a change of conformation of the protein and channel opening (Ernst et al. 2014).

1.5.3 Utilisation of the channelrhodopsins

Previously limited to the described channelrhodopsins ChR1 and ChR2, a wide range of channelrhodopsins are now used for research and even treatment purposes. Also, understanding of the molecular mechanisms associated with the functioning of the channelrhodopsin led to the development of modified channelrhodopsins.

Since ChR1 and ChR2 were the first to be described, they were the first to have their structure experimentally modified. The first modifications targeted their opsins and were called chimeric channelopsins. The first so-called chimeric constructions were Chop1 and Chop2 channelopsins and they comprise the ChR1 and ChR2, without their retinal group. Interestingly, it has been shown that

heterologous expression of Chop2 was able to form a functional channelrhodopsin while incorporating endogenous all-trans-retinal (in human, Nagel et al. 2003).

Directed mutagenesis was also investigated for the improvement of the channelrhodopsins. The main limitation with the utilisation of ChR1 is its insufficient depolarisation potential (because of limited proton permeability in physiological conditions), while the principal limitation associated with the utilisation of ChR2 is its fast inactivation and desensitisation (Nagel et al. 2003; Lin et al. 2009). To curate and improve ChR2, ChEF and ChIEF mutant channelrhodopsins were generated. These mutant channels present recombined mutations of Chop1 and Chop2 proteins. ChEF presents mutations around the retinal-binding pocket regions E and F, whereas ChIEF is a further mutated version of ChEF, presenting a mutation on the isoleucine 170. ChEF exhibited the same inactivation properties of ChR1 but its permeability was increased. ChIEF on the other hand, showed improved kinetics with reduced desensitisation potential. Finally, both ChEF and ChIEF demonstrated better responses, showing precise activation responses to stimulations of up to 25 and 50 Hz for ChEF and ChIEF respectively (Lin et al. 2009).

Over the years, a lot of research has been performed to identify new types of optogenetic channels, with several hundreds of different channelrhodopsins now known. This feat is courtesy of the massive apport of marine biology and plant study as well as the multiplication of new variants of already described channelrhodopsins.

The channelrhodopsin chrimson is one of the channelrhodopsins discovered thanks to transversal research. Initially discovered in algae, it has the particularity to have its opsin sensitive to red-shifted lights (Klapoetke et al. 2014; Mager et al. 2018). Initially applied for neuronal experiments, it has received great interest from other fields, including cardiac research. An advantage of the red-shifted channelrhodopsin is its penetration potential. It is known that red light can penetrate deeper in tissues, thus allowing more versatility for clinical or therapeutical approaches. Furthermore, red light has been shown to be able to

penetrate through the skull (Lin et al., 2013), thus being an interesting candidate for developing resynchronisation therapies using optogenetic technologies.

Name of the protein	Origin	Peak excitation wavelength	Ion permeability	First description	Kinetic properties	References
Channelrhodopsin-2	<i>Chlamydomonas reinhardtii</i>	460 nm	$P_{Ca}/P_{Na}= 0.117$; $P_K/P_{Na}=0.427$; $P_H/P_{Na}=1.062 \cdot 10^6$	(Nagel et al. 2003)	$T_{on}: 2.12 \pm 0.13$ ms, $T_{off}: 13.39 \pm 1.059$ ms	(Mager et al., 2018)
ChIEF	ChEF mutated on isoleucin 170	460 nm		(Lin et al. 2009)	$T_{on}: 2.73 \pm 0.19$ ms, $T_{off}: 9.77 \pm 0.66$ ms	
ChEF	Chop1 + Chop2 + mutation on the E-F binding pocket site	470 nm	$P_{Ca}/P_{Na}= 0.149$; $P_K/P_{Na}=0.673$; $P_H/P_{Na}=0.877 \cdot 10^6$	(Lin et al. 2009)	$T_{on}: 2.921 \pm 0.15$ ms, $T_{off}: 26.31 \pm 1.28$ ms	
Channelrhodopsin-1	<i>Chlamydomonas reinhardtii</i>	500 nm	H ⁺	(Nagel et al. 2002)		
Chrimson	<i>Chlamydomonas noctigama</i>	590 nm	$P_{Ca}/P_{Na}= 0.29 \pm 0.2$; $P_K/P_{Na}=0.62 \pm 0.04$; $P_H/P_{Na} \sim 10^6$	(Klapoetke et al. 2014)	$T_{off}: 24.6 \pm 0.9$ ms	(Mager et al., 2018)
ChrimsonR	Chrimson variant	590 nm		(Mager et al., 2018)	$T_{off}: 15.8 \pm 0.4$ ms	
Chrimson-vf	Chrimson variant	590 nm		(Mager et al., 2018)	$T_{off}: 2.7 \pm 0.3$ ms	
Chrimson-f	Chrimson variant	625 nm	$P_K/P_{Na}=0.63 \pm 0.11$; $P_H/P_{Na} \sim 10^6$	(Mager et al., 2018)	$T_{off}: 5.7 \pm 0.5$ ms	

Table 9: Biophysical characteristics of channelrhodopsin-1 and channelrhodopsin-2 and chrimson and a few of their variants used in research.

1.6 Hypotheses and aims of the project

The study of AF electrical remodelling is a challenging task. Although extremely convenient because of the experimental possibilities they offer, animal models for the study of AF often face poor transferability and applicability of the results obtained in human pathophysiology. Likewise, only working with human material to ensure the applicability comes with a certain number of limitations, including poor availability and the extremely limited extent of feasible interventional protocols. One opportunity comes together with the huge progresses that have been done in the development of iPSC, and their utilisation for 3D *in vitro* modelling. Unlike human material, iPSC are extremely available and many interventional protocols, including genome modification, are feasible, and unlike animal models, because they are derived from human cells, the applicability of the results to human disease is much better.

For all these reasons, we hypothesise that atrial cardiomyocytes derived from induced pluripotent stem cells (atrial iPSC) and atrial EHM models can be used to understand acute and long-term electrical remodelling associated with AF.

The first aim of this work will be to develop an atrial-specific iPSC line and show that this model can be used to study acute electrical remodelling associated with AF. To do so, we will develop a cell differentiation protocol to generate atrial iPSC and, using electrophysiological tools, characterise them. To assess whether we can use these cells as a model to investigate acute electrical remodelling, we will take advantage of the classically used *in vivo* tachypacing methods and electrophysiologically assess whether such protocol can induce the development of AF-like electrical remodelling in our cells. Because the exploration of electrical remodelling can be limited in a 2D model, we will take advantage of the fast-growing development of organoid models and try to propose a 3D alternative to the cellular model.

The second aim of this project is therefore to develop a 3D organoid-based *in vitro* model for the study of acute electrical remodelling. First, we will develop an atrial EHM model using the cells previously mentioned. To investigate whether electrical remodelling can be induced in this model, we will repeat the pacing

methods on our 3D model and investigate the effects of such a protocol using the sharp-microelectrode technique.

The last aim will consist in the study of long-term electrical remodelling. Using the EHM model, we will try to address this point using electrical and optogenetic-based stimulation approaches. The electrical remodelling will be observed using the sharp-microelectrode technique.

2 Material and methods

2.1 Human experiments

2.1.1 Patient data

Patient data was collected and analysed *a posteriori*. Written informed consent was obtained from all patients included in this study. Experimental protocols were approved by the ethics committee of the University Medical Centre Göttingen (No. 4/11/18).

2.1.2 Sample collection for biochemical investigation

Right atrial appendages and myocardial tissues of hypertrophied left ventricle were collected from patients undergoing open heart surgeries and snap frozen directly after collection.

2.1.3 Sample collection and preparation for electrophysiological measurements

Samples were collected directly at the surgery theatre, from patients undergoing open heart surgeries. The right atrial appendage was, immediately after the excision, stored in transport solution at 4°C, which was prepared according to an already published protocol (Voigt et al. 2013), adjusted to pH 7.0 (**Table 10**), and brought back to the institute within 10 minutes following the tissue collection.

Trabecular muscles were then isolated and carefully excised from the right atrial appendage and placed in a custom-built recording chamber under continuous perfusion of heated (37°C) and carbonated (5% CO₂, 95% O₂) Tyrode's solution (**Table 18**). Tissue was left for at least 45 minutes for wash-out and accommodation before the beginning of the recordings.

Molecule	Concentration (in mmol/L)
2,3-butanedione monoxime	30
Glucose	20
KCl	10
KH ₂ PO ₄	1.2
MgSO ₄	5
MOPS	5
NaCl	100
Taurine	50

Table 10: Transport solution composition.

2.1.4 Electrophysiological measurements

Tissues were electrically stimulated with a 1 ms monophasic pulse using a custom-made electrode (FHC, USA). The pulse amplitude was pre-defined as 30% higher than the value required to trigger an action potential. After successful tissue impalement, and after reaching steady state activity, the tissue was then subjected to a train of electrical stimulation at increasing frequencies (0.25 Hz, 0.5 Hz, 1 Hz, 2 Hz, 3 Hz, 4 Hz and 5 Hz). Membrane potential signals were amplified using a Sec-05-X amplifier (npi, Germany), digitised using LabChart PowerLab, and acquired and saved with LabChart Pro 9 software (both: ADInstruments, New Zealand).

After successfully recording action potentials at different stimulation frequencies, a protocol to measure the ERP was applied to the tissue. Briefly, a train of 10 stimuli at fixed frequencies was applied to the tissue, followed by an 11th stimulation at a time interval decreasing after each stimulation cycle. The cycle was repeated until the 11th pulse failed to trigger an action potential.

10 µmol/L carbachol (CCh) were perfused to assess response of the tissues to the M2-receptor agonist. CCh stock solution was diluted in distilled water, and working solution was prepared in Tyrode's solution (**Table 18**). After reaching a steady state, the perfusion solution was switched from Tyrode's solution to Tyrode's containing CCh. 5 ml of solution containing the drug were then perfused

to the recording chamber, followed by another 15 ml of Tyrode's solution corresponding in the death volume of the perfusion system. After this moment, the drug was in the recording chamber, and adequate stimulation protocols were run to measure the "drug condition".

2.1.5 Data analysis

Analysis was performed using LabChart pro 7 (ADInstruments, New Zealand) and GraphPad Prism 9. The average value of 10 consecutive and stable action potentials was calculated in LabChart Pro 7. The following parameters were measured: resting membrane potential (RMP), maximum upstroke velocity (dV/dt_{max}), action potential amplitude (APA) and the action potential duration at 20, 50 and 90% of repolarisation (APD₂₀, APD₅₀ and APD₉₀ respectively).

Statistical analysis was performed using the statistical tool of GraphPad Prism 10 (GraphPad Software Inc., USA). Details of the test conditions are specified for each experiment.

2.2 Cellular experiments

2.2.1 Cell line generation

Both stem cell lines UMGi014-C clone 14 (isWT1.14) and RUCDRi002-A-46 clone 1 (TC-1133-CAG-Chrimson-YFP.1TC1133_CAG-Chrimson-YFP) were differentiated and cultured in our lab according to an already published protocol (Cyganek et al. 2018). Briefly, the stem cells were cultured in feeder-free medium until confluency was reached (StemFlex™ Basal medium, gibco for isWT1.14 cell line; StemMACS™ iPS-Brew XF, Mitenyi Biotec B.V & Co. KG for the TC113-chrimson modified cell line). After this point, mesoderm induction was initiated adding 4 µmol/L CHIR99021 (Sigma-Aldrich) to the culture medium. After 2 days, cardiac differentiation was started adding 5 µmol/L IWP2 (Wnt Antagonist II, Merck) to the medium. The next day, atrial specific differentiation was started, adding 1 µmol/L retinoic acid (Sigma Aldrich) to the culture medium already containing 5 µmol/L IWP2 for the next two following days. After this differentiation step, the first contractions could be observed, and the culture medium was changed for a cardiomyocyte culture medium for the following week. Next, a

lactate selection procedure was initiated to increase the purity of the cell batch using selection medium and after 7 days, culture medium was switched back to the cardiomyocyte culture medium. Finally, 7 days were given to the cells to recover. After this period, 28 days after the initial mesoderm induction, the cells were ready to be used for different purposes for instance for EHM generation or plated on glass coverslips for cellular experiments.

2.2.2 Fibroblasts primary cultures expansion and maintenance

The fibroblasts were obtained from an intern facility at the Medical University of Göttingen. We collected them at intermediate passage number (around 20) and expanded them until passage 26 before renewing the cell culture batch. Maintenance and recovery media compositions are described in **Table 11**. Maintenance was done until confluency, while replacing the maintenance medium every second day.

When confluency was reached, fibroblasts were incubated at 37°C with TrypLE™ Express Enzym 1x (Thermofischer, Cat.#12604013, 4°C) to start dissociation. After 5 to 10 minutes, the cell isolation procedure was stopped using a volume of cardiomyocyte recovery medium (**Table 12**) corresponding to two times the amount of TrypLE™ and centrifuged at 100 g, 4°C for 10 minutes. The supernatant was removed, and the fibroblasts were resuspended in human fibroblasts recovery medium and reseeded at low density in T-175 culture flasks. Two days after reseeded, the medium was removed and replaced by the human foreskin maintenance medium and changed every second day until utilisation or confluency was reached again.

Human foreskin fibroblasts (HFF) maintenance medium	Human foreskin fibroblasts (HFF) recovery medium	Distributor, product reference, storage conditions
500 ml DMEM	500 ml DMEM	Gibco, Cat.#41966029, 4°C
88 ml fetal bovine serum (FBS) (15%)	88 ml fetal bovine serum (FBS) (15%)	Gibco, Cat.#16140071, -20°C
5.9 ml 100X penicillin/streptomycin (1%)	5.9 ml 100X penicillin/streptomycin (1%)	Gibco, Cat.#15140122, -20°C
-	FGF (0.1%)	<i>Peprotech</i> , Cat. #AF-100-18B, -20 °C

Table 11: Fibroblast culture media compositions.

2.2.3 Coverslip preparation

Compositions of the media used for coverslip preparation are described in detail in **Table 12**.

In a 6-well plate or a flask, atrial or ventricular cardiomyocytes derived from induced pluripotent stem cells (atrial and ventricular iPSC) were first washed two times with pre-warmed PBS solution without calcium and magnesium ($\text{Ca}^{2+}/\text{Mg}^{2+}$). Next, cells were incubated for 15-20 minutes at 37°C with room temperature Accutase digestion mix solution (1.5 ml per well for 6 wells, 5 ml per flask when using flasks; Innovative Cell Technologies, Inc.). At the end of the digestion process, cells looked “ball-shaped” and detached from the bottom of the plate or the flask. After this step, digestion was stopped using a volume of cardiomyocyte recovery medium corresponding to twice the volume of Accutase digestion mix. Cells were carefully transferred in a 50 ml Falcon tube and centrifuged at 100 g, 4°C for 10 minutes. Supernatant was removed and cells were resuspended in the desired volume of cardiomyocyte recovery medium, and counted using a Neubauer chamber (Neubauer improved, Paul Marienfeld GmbH & Co.KG).

The cells were counted in the external corners of the chamber, and the exact cell number was determined using the formula:

$$Total\ cell\ count = \left(\frac{average\ amount\ of\ cells\ per\ side}{4} \right) * d * 10^4 * V$$

Where d is the dilution factor and V is the resuspension volume (in ml).

According to the cell number and the desired cellularity, cells were transferred on glass coverslips (Menzel-Gläser Coverslips, ThermoScientific) previously coated with 1:60 Matrigel[®] solution (Corning[®]) and disposed in the well of a 6-well or a 24-well plate and incubated 1 hour at 37°C to allow cell attachment. Finally, wells were filled with cardiomyocyte recovery medium (3 ml per well with a 6-well plate, 1 ml per well for a 24-well plate). 2 days later, the medium was removed and replaced with cardiomyocyte culture medium. Medium was then changed every second day until utilisation.

Cardiomyocyte culture medium	Cardiomyocyte recovery medium	Distributor, storage
49 ml RPMI1640 with Glutamax	49 ml RPMI1640 with Glutamax	Invitrogen, Cat 61870-010, 4°C
1 ml (2%) B27 plus insulin	1 ml (2%) B27 plus insulin	Invitrogen, Cat 17504-044, -20°C
-	25 µmol/L (0.02%) Rock inhibitor	Stemolecule Y27632), Cat 04-0012-10, -20°C

Table 12: Cardiomyocyte medium composition.

2.2.4 Voltage-clamp recordings

The composition of the bath solution and the pipette solution is described in detail in **Table 13**.

A minimum of 7 days after performing the cell plating protocol was let to the cells before they were used for voltage-clamp measurements.

Inward rectifier K⁺ currents were recorded using the whole-cell ruptured patch configuration of the patch-clamp method. Membrane currents were acquired and analysed using the Axopatch 200B amplifier and the pClamp-Software (V10.7 Molecular Devices). Myocytes were continuously perfused with bath solution adjusted at pH=7.4 at 22-24°C. Borosilicate glass microelectrodes had tip resistances from 3 to 5 MΩ when filled with pipette solution (**Table 13**) adjusted at pH 7.4, the seal resistance was between 4–8 GΩ. Series resistance and cell capacitance were compensated prior to the measurement.

The basal inward rectifier potassium current was measured by applying a ramp pulse protocol from –100 to +40 mV at 0.5 Hz. The agonist-inducible I_{K,ACh} was stimulated with 2 μmol/L carbachol and the agonist-independent constitutive I_{K,ACh} current was unmasked using 100 nmol/L of the selective I_{K,ACh} blocker tertiapin, perfused in a bath solution containing 0.1 g/L bovine serum albumin. I_{K1} was identified as Ba²⁺(1 mmol/L)-sensitive current as previously described (Dobrev et al. 2005; Voigt et al. 2007; Voigt et al. 2010).

Molecule	Bath solution concentration (in mmol/L)	Pipette solution concentration (in mmol/L)
NaCl	120	10
KCl	20	40
MgCl ₂	1	-
CaCl ₂	2	-
Glucose	10	-
HEPES	10	10
K-aspartate	-	100
Mg-ATP	-	5
EGTA	-	2
GTP-Tris	-	0.1

Table 13: Composition of bath and pipette solutions used for voltage-clamp recordings.

2.2.5 Optical action potential recordings

The composition of the Tyrode's solution used for optical action potential recordings is described in detail in **Table 13**.

A minimum of 7 days after performing the cell plating protocol was let to the cells before they were used for optical action potential measurements.

Optical action potentials in atrial and ventricular iPSC were recorded as previously described (Seibertz et al. 2020; Peper et al. 2021).

Prior to the measurement of optical action potentials, cells were incubated with 0.1X VoltageFluor2.1Cl (Fluovolt, Thermo Scientific; 20 minutes loading). Coverslips were then transferred to a heated recording chamber filled with Tyrode's solution at pH = 7.35, 37°C and allowed to adjust to the solution for at least 10 mins in the dark before starting the recordings. An external pacing device (MyoPacer Field Stimulator, IonOptix) was used to electrically stimulate the cells at 1 Hz using a 3-5 ms bipolar pulse set with a voltage 30% above the stimulation threshold to ensure the capture of spontaneous beating activity during the measurements.

Optical action potential signals from an isolated and masked cardiomyocyte were acquired using an epifluorescence microscope ($\lambda_{Ex}=470$ nm, $\lambda_{Em}=535$ nm), optimised for high-speed signal capture thanks to the utilisation of a photomultiplier (Cairn Research), digitised (Axon Digidata 1550B, Axon Instruments), saved and analysed using Clampfit 10.7 software. Analysis was performed *a posteriori* on the average of 3 stable action potentials recorded from a single cell.

2 $\mu\text{mol/L}$ CCh was perfused to the cells to investigate the response to the M2-receptor agonist. CCh was prepared in Tyrode's solution described in **Table 14**.

Molecule	Concentration (in mmol/L)
NaCl	140
KCl	4
MgCl ₂	1
CaCl ₂	2
Glucose	10
HEPES	10

Table 14: Composition of Tyrode's solution used for optical action potential recordings.

2.2.6 Automated voltage-clamp measurements of $I_{Ca,L}$

The compositions of the solutions used for the automated measurements of $I_{Ca,L}$ are described in detail in **Table 15**.

An automated patch-clamp system was used for the recording of $I_{Ca,L}$ (SyncroPatch 384, Nanion Technologies GmbH), and thin borosilicate glass 384-well planar chips (1xS-type NPC-384T) were used for all experiments. All solutions used were purchased from Nanion Technologies GmbH.

Briefly, the chips were first loaded with 30 μ l of solution 1, and 20 μ l of cell suspension was added to each well. The pipette solution (internal solution, solution 3) was filled on the internal side of the chip. Next, a negative pressure (150-250 mbar) was exerted to reach the whole-cell configuration. 40 μ l of solution 1 was temporarily added to promote giga seal formation. When a giga-seal was reached, the solution 1 was rapidly moved and replaced with bath solution (solution 4). L-type Ca^{2+} currents ($I_{Ca,L}$) were measured at 0.5 Hz using a voltage-step protocol with a holding potential of -80 mV and a 100 ms ramp pulse to -40 mV followed by a 100 ms test-pulse to +10 mV. The current-voltage (I-V) relationship and activation curve was measured by altering the test pulse from -40 mV by 10 mV every sweep including a final pulse of 60 mV. Experiments were performed at room temperature.

The integrated $I_{Ca,L}$, representing an estimation of Ca^{2+} entering the cell is calculated per litre total cell volume, and was estimated through a capacitance to a volume relationship of 4.57 pF/pL.

PatchControl 384 (Nanon Technologies GmbH) software digitised and acquired the data, and recordings were excluded if they included a seal resistance of $<250\text{ M}\Omega$, a peak current of $<50\text{ pA}$, or an R_{series} of $>20\text{ M}\Omega$ at 10 mV.

Molecule	Solution 1	Seal helping solution (solution 2, in mmol/L)	Internal solution (solution 3, in mmol/L)	Bath solution (solution 4, in mmol/L)
NaCl	140	130	10	140
KCl	4	4	-	4
MgCl ₂	-	1	-	1
CaCl ₂	-	10	-	2
Glucose	5	5	-	5
HEPES	10	10	10	10
EGTA	-	-	10	-
CsCl	-	-	10	-
CsF	-	-	110	-

Table 15: Composition of the solutions used with the automated patch-clamp system.

2.2.7 Electrical tachypacing of cardiomyocytes derived from induced pluripotent stem cells

For the electrical tachypacing of the cardiomyocytes, the glass coverslips containing the cardiomyocytes were gently transferred to a 6-well plate filled with 6 ml cardiomyocyte pacing medium with normal or low Ca^{2+} concentration (**Table 16**), and the pacing plate (C-Dish, IonOptix) was carefully positioned on top of the well, while ensuring not to place it directly on the cell coverslip.

The voltage and the duration of the pulse was adjusted according to their responsiveness to the pulses, and to ensure the overpowering of the

spontaneous beating rate during the pacing period (typically 20-25 V, 5 ms biphasic pulse).

Cardiomyocyte culture medium (low Ca ²⁺ : 0.42 mmol/L)	Cardiomyocyte pacing medium (high Ca ²⁺ : 1.79 mmol/L)	Distributor
49 mL RPMI1640, GlutaMAX	-	Thermo Fisher Scientific
1 mL B27 plus insulin	1 mL B27 plus insulin	Thermo Fisher Scientific
-	49 mL Medium 199, GlutaMAX	Thermo Fisher Scientific

Table 16: Induced pluripotent stem cell pacing medium composition.

2.3 Engineered human myocardium experiments

2.3.1 Engineered human myocardium preparation

The media composition used for the preparation of EHM is described in detail in **Table 17**.

EHM tissues were prepared according to an already described and published protocol (Tiburcy et al. 2017; Tiburcy et al. 2020). iPS derived cardiomyocytes differentiation and maintenance were described above. Fibroblasts provenance and maintenance were also discussed above.

Briefly, a mixture of iPSC derived cardiomyocytes (25%), human fibroblasts (31%), 2X RPMI (14%), NaOH (0.27%), 2% Serum-free maturation medium that contains SFBM (IMDM+GlutaMAX, 1% 100X MEM-NEAA, 1% 100X penicillin/streptomycin, 0.05% L-ascorbic acid + 4% B27 minus insulin, 0.01% IGF-1 + 0.1% VEGF + 0.1% FGF) + 0.1% TGFβ and collagen (27%) was moulded in a custom-made 48-wells plate and incubated at 37°C, 5% O₂. After 1 hour, the wells were filled with serum-free maturation medium containing TGF-β1, and the medium was replaced once a day during the two first days after the casting procedure. After this time, the serum-free maturation medium containing TGF-β1 was replaced by serum-free maturation medium without TGF-β1 and changed

every other day for 30 days until the tissue reached maturation. Experiments were performed between d30 and d40 after EHM casting.

Serum-free base medium (SFBM)	Serum-free maturation medium (SFMM)	Serum-free maturation medium + TGF- β 1	Distributor, product reference, storage conditions
500 ml IMDM + GlutaMAX	-	-	Gibco, Cat. #21056-023, 4 °C
5.1 mL 100X MEM-NEAA (1%)	-	-	<i>Invitrogen</i> , Cat. #11140035, 4 °C
5.1 mL 100X penicillin/streptomycin (1%)	-	-	Gibco, Cat. #15140122, -20 °C
-	SFBM 47.8 ml	SFBM 47.8 ml	-
-	50 μ L IGF-1 (1:1000)	50 μ L IGF-1 (1:1000)	<i>Peptotech</i> , Cat. #AF-100-11, -20 °C
-	50 μ L VEGF (1:1000)	50 μ L VEGF (1:1000)	<i>Peptotech</i> , Cat. #AF-100-20, -20 °C
-	50 μ L FGF (1:1000)	50 μ L FGF (1:1000)	<i>Peptotech</i> , Cat. #AF-100-18B, -20 °C
-	-	50 μ L TGF- β 1 (1:1000)	<i>Peptotech</i> , Cat. #AF 100-21C, -20 °C

Table 17: Engineered human myocardium medium composition.

2.3.2 Electrical and optical tachypacing

After their complete maturation (28 days after casting), tissues were carefully transferred to a custom-made Teflon holder, and placed into a 6-well plate filled with 8 ml of SFMM without TGF- β 1 (**Table 17**).

The pacing plate (C-Dish, IonOptix) was carefully placed on top of the Teflon holder and the EHM, and the pacer started according to the desired protocol.

The voltage and the duration of the pulse was adjusted according to their responsiveness to the pulses, and to ensure the overpowering of the spontaneous beating rate during the pacing period (typically 20-25 V, 5 ms biphasic pulse).

2.3.3 Electrophysiological measurements

Electrophysiological measurements were performed in a custom-built recording chamber perfused with heated (37°C) and carbonated (5% CO₂, 95% O₂) Tyrode's modified solution (**Table 18**). Perfusion was continuous throughout the duration of each experiment.

Molecule	Concentration (in mmol/L)
NaCl	126.7
KCl	5.4
MgCl ₂	1.1
CaCl ₂	1.8
NaHPO ₄	0.42
NaHCO ₃	22
Glucose	5.5

Table 18: Sharp-microelectrode Tyrode's modified solution.

For performing an experiment, the tissue was carefully positioned and stabilised in the centre of the chamber, and at least 30 minutes were allowed for accommodation before the start of each electrophysiological investigation.

Borosilicate glass capillaries (Hilgenberg, Germany) were pulled using a horizontal pipette puller (Zeitz, Germany). Electrical resistance was 30-60 M Ω . Pipettes were backfilled with a 3 M KCl solution. The signal was amplified using a Sec-05-X (npi, Germany) amplifier, digitised using LabChart PowerLab, and acquired and saved using the LabChart Pro 7 software (both: ADInstruments, New Zealand).

The tissue was electrically stimulated using a custom-made electrode (FHC, USA). The stimulation pulse was a 1 ms monophasic pulse. The pulse amplitude was pre-defined as 30% higher than the value necessary to trigger an action potential and to overpower the spontaneous activity of the tissue. After successful tissue impalement, and after reaching a steady state, spontaneous action potentials were recorded. The tissue was then subjected to a train of electrical stimulations at increasing frequencies (1 Hz, 2 Hz and 3 Hz).

2.3.4 Data analysis

Analysis was performed using LabChart pro and GraphPad Prism 7 (GraphPad Software Inc., USA). The average values of 10 consecutive action potentials were calculated in LabChart Pro. The following parameters were measured: resting membrane potential (RMP), action potential maximum upstroke velocity (dV/dt_{max}), action potential amplitude (APA) and the action potential duration at 20, 50 and 90% of repolarisation (respectively APD₂₀, APD₅₀ and APD₉₀).

Statistical analysis was performed using the statistical tool of GraphPad Prism 10. Details of the test conditions are specified for each experiment.

2.4 Light pacer

The light pacing device was custom-built and adjusted to the purpose of the experiment and the experimental model used. Briefly, LEDs were mounted on a breadboard encased in a 3D-printed case, and connected to a trigger box, to control the illumination parameters.

For the optical pacing of atrial EHM generated using atrial EHM generated using atrial iPSC transfected with an adeno-associated-virus-2 carrying a channelrhodopsin-2, blue LEDs (455 nm) were used. For the optical pacing of atrial EHM generated using atrial iPSC modified to express the fast variant of the channelrhodopsin chrimson, red LEDs were used (625 nm).

2.5 Light sensitive engineered human myocardium experiments

2.5.1 Virus-based engineered human myocardium generation

Virus transduction

Freshly differentiated iPSC-derived atrial cardiomyocytes were transduced using an adeno-associated virus carrying a channelrhodopsin coupled with a fluorescent reporter mCherry protein. The plasmid of the virus was chosen according to a previous publication from Lapp et al. , that showed adequate light sensitivity in cells (Lapp et al. 2017).

The whole sequence of the plasmid can be found in the **Supplemental content 7**.

Briefly, freshly prepared and warmed-up cardiomyocyte culture medium (**Table 12**) was added to the desired well, and virus at a concentration of 10^5 gene copies per cell was added to the cells. Even distribution was ensured while carefully doing infinite (∞) sign-shape movements with the plate. The procedure was done on Friday afternoons. Medium was changed with fresh cardiomyocyte culture medium on the following Monday. After this time, cells were treated like normal iPSC cardiomyocyte in culture and followed the regular maintenance plan, so that their medium was changed every second day.

Cell light sensitivity assessment

Three days after the virus introduction, cells were isolated from the culture plate/well and replated on small glass coverslips for cell sensitivity assessment, using the plating protocol described above. Cells were plated at the density of

20.000 cells/coverlip. At least three days were let to the cells plated on glass coverslips before being used, to ensure full recovery from the isolation procedure.

The coverslip was then transferred in a measuring chamber heated at 37°C (RC-24E, Warner Instruments, USA) sealed with a glass coverslip and filled with preheated Tyrode's solution, pH=7.4 (**Table 19**).

Molecule	Concentration (in mmol/L)
NaCl	140
KCl	4
MgCl ₂	1
CaCl ₂	2
Glucose	10
HEPES	10

Table 19: Tyrode's solution used for light sensitivity assessment in atrial cardiomyocytes derived from induced pluripotent stem cells transfected with an adeno-associated-virus-2 carrying a channelrhodopsin-2.

For the illumination protocol, cells were let in the dark in the heating chamber for accommodation for a few minutes. Under the microscope, when a cell was found, a series of light pulses using 455 nm LEDs were applied to it and the cell response was recorded live in a TIF format at 60 images per second for future video reassembly. Light intensity and pulse duration were defined using a Myopacer (Ionoptix, USA).

After the data acquisition, force spectra were analysed using the "MYOCYTER" plugin of ImageJ (Grune et al. 2019).

Cell quantification assays

To quantify virus transduction, flow cytometry cell counting was performed using a BD Accuri C6 plus Flow Cytometer (BD Biosciences, USA). First, cells were isolated using the protocol described in chapter 2.2.3. Next, FACS tubes containing $5 \cdot 10^5$ cells resuspended in 500 μ l PBS without Ca²⁺ and Mg²⁺ were prepared. Prior to the experiment, 5 μ l of 7-aminoactinomycin D (7-DD) was added to each tube and left to incubate for 10 minutes at room temperature in the

dark. On completion of incubation, aliquots containing the cells were mounted on the cell sorting system and acquisition was started with the protocol running at an acquisition speed of 20.000 events per second. Cell type discrimination was based on the 625 nm emission wavelength of the AAV-2 transfected cells, expressing the fluorochrome mCherry. FlowJo™ v10.8.1 software was used for the data analysis.

2.5.2 Optogenetic stimulation of engineered human myocardium

For optical pacing, selected EHM were transferred with their maturation stretchers on a Teflon mould in a 6-well plate filled with serum-free maturation medium (**Table 17**). The optical pacing plate with the correct set of LEDs (455 nm for AAV2-ChR2 and 625 nm for chrimson) was positioned above the 6-well plate, and the light signal parameters were chosen using an external trigger box. Light pulses of 188 $\mu\text{W}/\text{mm}^2$ intensity, were delivered to the tissues at 1 Hz or 3 Hz, for a duration of 1 day or 7 days.

The entire system was placed in an incubator at 37°C and 5% CO₂.

2.5.3 Acute and long-term force measurements in response to light pulses in atrial engineered human myocardium

For the acute and long-term force measurements in response to light pulses, EHM were first carefully removed from their maturation stretchers, and mounted on a custom-made modular bioreactor described previously (Kensah et al. 2011).

Briefly, the bioreactor consists of a central cultivation chamber connected to a rostral linear motor and caudally to an inductive displacement transducer. The EHM was mounted inside the cultivation chamber and connected to both modules. The cultivation chamber was filled with 37°C pre-warmed sterile serum-free maturation medium (**Table 17**, replaced every two days) and the entire bioreactor was stored in an incubator at 37°C with 5% CO₂ for the whole measurement period. The custom-made LED optical stimulator (described above) was placed underneath the transparent cultivation chamber to deliver defined light pulses (1 Hz, 118 $\mu\text{W}/\text{mm}^2$ intensity, 5 ms).

The experiment was monitored live, and every hour, a recording fragment of 10 minutes was automatically saved. Each recording fragment data was analysed using LabChart 10.

2.6 Quantitative polymerase chain reaction assays

Primer sequences are listed in **Table 20**.

Total RNA was isolated from iPSC, EHM and native human tissue samples using TRIzol (Thermo Fisher Scientific, Waltham, MA, USA, #15596018) via phenol-chloroform extraction. Remaining genomic DNA was removed using RNase-free DNase I (Thermo Fisher Scientific, Waltham, MA, USA, #EN0521).

1 µg DNase-treated RNA was transcribed into complementary DNA (cDNA) using a RevertAid First Strand cDNA synthesis kit (Thermo Fisher Scientific, Waltham, MA, USA, #K1622) and random hexamer primers. Quantitative real-time reverse transcriptase polymerase chain reaction (qPCR) was performed using SsoAdvanced™ Universal SYBR Green supermix (Bio-Rad, California, USA, #1725271). Therefore, 25 ng cDNA was used as template per reaction. Fluorescence detection was performed as follows: 10 minutes incubation at 95°C, followed by 40 cycles at 95°C for 15 seconds and 60°C for 1 minute. After 40 cycles, the melt curve analysis was done to ensure amplicon specificity. For relative quantification, expression levels of all target genes were normalised to the housekeeping gene (GAPDH). Relative gene expression levels were calculated using the $\Delta\Delta Cq$ method. It consisted in the subtraction ΔCq of the samples paced at 3 Hz from the average of ΔCq of samples paced at 1 Hz.

Gene	Forward primer	Reverse primer
<i>GAPDH</i>	GGAAGGTGAAGGTCGGAG TCA	GTCATTGATGGCAACAATATCCA CT
<i>CACNA1C</i>	AATCGCCTATGGACTCCTC TT	GCGCCTTCACATCAAATCCG
<i>KCNJ2</i>	GTGCGAACCAACCGCTACA	CCAGCGAATGTCCACACAC
<i>KCNJ3</i>	TCGGCTATGGCTACCGATA CA	GTGCTCGCTGAACATGAGG
<i>KCNJ5</i>	GCGCTTCAACTTGCTCGTC	GCCACTGAGGTTTTCAACACA
<i>ADORA1</i>	CCACAGACCTACTTCCACA CC	TACCGGAGAGGGATCTTGACC
<i>CHRM2</i>	ACACCCTCTACACTGTGAT TGG	GTCCGCTTGACTGGGTAGG

Table 20: Primers used for quantitative polymerase chain reaction assays.

2.7 Statistical analysis

Data is presented as mean \pm SEM unless otherwise specified.

Continuous and unpaired data sets with a sample size of $n \geq 20$ were assumed to be normally distributed in virtue to the central limit theorem and were tested using the unpaired t-test. Normality was tested for the data with sample size between $n = 10-20$, and non-normally distributed unpaired data was compared using the Mann-Whitney-U test. For unpaired data sets with unequal variances (using the F-test), Welch's *t*-test was used.

Paired data sets with normal distribution were compared using paired *t*-test, and correction was applicated in case of multiple comparison. Non-normally distributed data sets were compared using the Wilcoxon match-pairs signed rank test.

3 Results

3.1 Characterisation of atrial fibrillation in human myocardium

3.1.1 Patients suffering from chronic atrial fibrillation show impaired action potential parameters

The recording of action potentials (AP) in trabecular muscle from patients suffering from chronic atrial fibrillation (cAF) showed a very distinct profile in comparison with the AP recorded in sinus rhythm (SR) patients (**Figure 6**). The first visual impression showed a triangulation of the AP in favour to a loss of the plateau phase. Although the analysis of the action potential amplitude (APA) and the maximum upstroke velocity (dV/dt_{max}) did not show any significant differences (SR vs cAF respectively for APA and dV/dt_{max} : 93.20 ± 1.33 mV vs 95.40 ± 2.23 mV; 186.4 ± 5.4 V/s vs 178.2 ± 9.45 V/s, $n=128/29$ vs $40/9$, mean \pm SEM, Welch's t -test, $P>0.05$), action potential duration at 90% repolarisation (APD_{90}) was significantly shorter in cAF patients (SR vs cAF: 403.1 ± 5.48 ms vs 312.3 ± 9.75 ms, $P<0.001$ with unpaired Welch's t -test), and the RMP significantly hyperpolarised (SR vs cAF: -71.94 ± 0.46 mV vs -74.27 ± 0.72 mV, $P<0.05$ using Student's t -test). Furthermore, the evaluation of the restitution curves showed that the APD was independent from stimulation frequency, and the maximum slope was lower in cAF (0.936 vs 0.466 for SR and cAF respectively). To conclude, the measurement of the effective refractory period showed a significantly reduced duration in the cAF group (SR vs cAF: 300.31 ± 10.96 ms vs 227.6 ± 10.24 ms, $P<0.001$ with unpaired Mann-Whitney's test)

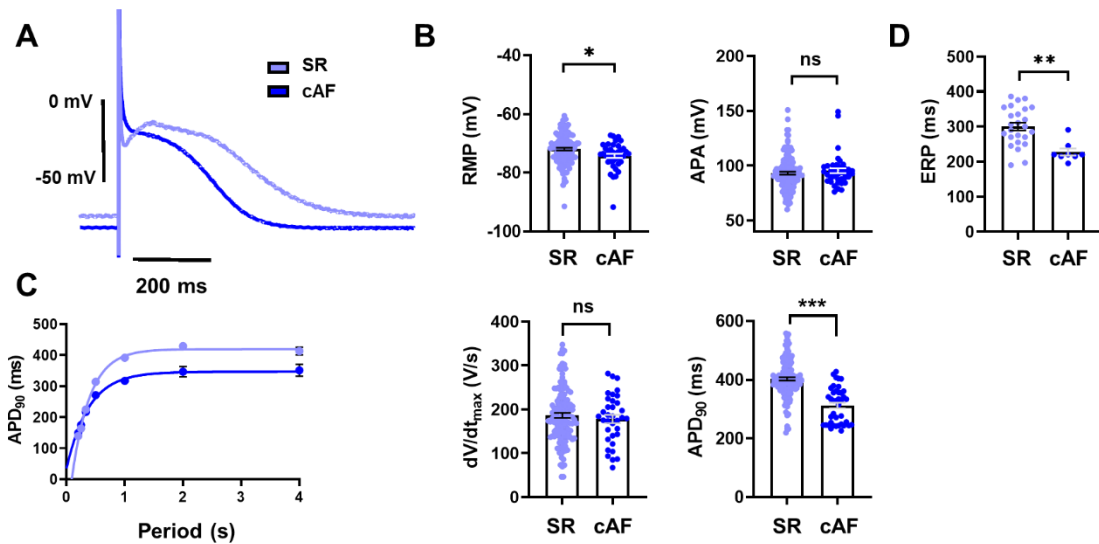


Figure 6: Human action potential. **A**, Representative action potential elicited at 1 Hz measured in sinus rhythm (SR, light blue, $n=128/29$) and chronic atrial fibrillation (cAF, dark blue, $n=40/9$) patients and **(B)** the quantification of resting membrane potential (RMP), action potential amplitude (APA), maximum upstroke velocity (dV/dt_{max}) and action potential repolarisation duration at 90% repolarisation (APD₉₀). **C**, Restitution curves. **D**, Quantification of the effective refractory period (ERP). Data shown as mean \pm SEM. *** $P<0.01$, using Welch's t -test. n/N =number (n) of recordings from N patients.

3.1.2 Patients suffering from chronic atrial fibrillation have an impaired response to a muscarinic receptor agonist

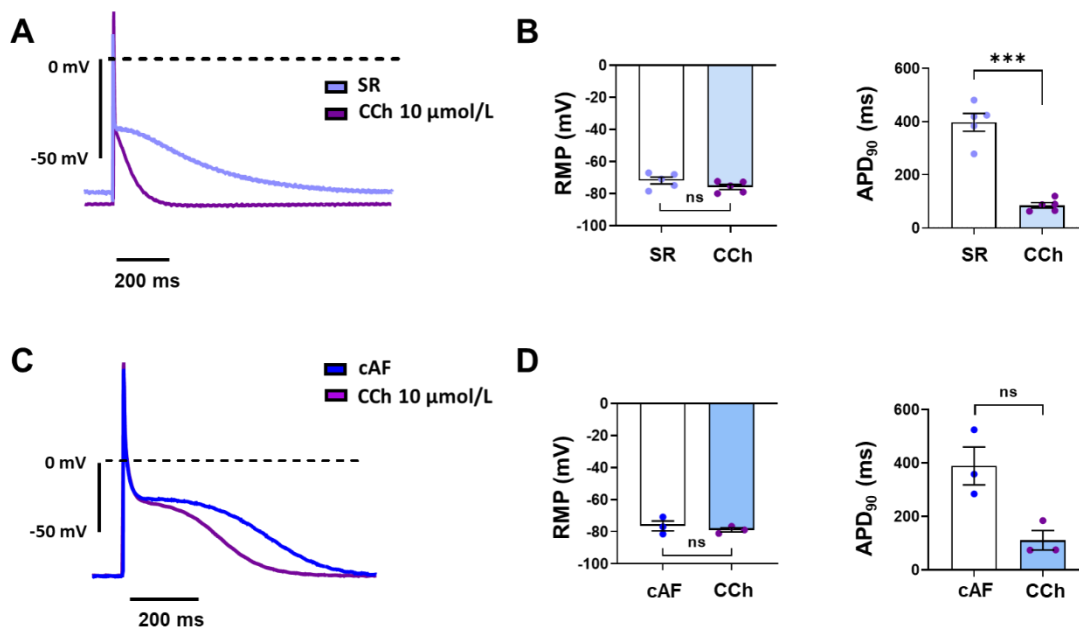


Figure 7: Effects of M2-receptor agonist carbachol perfusion on the human atrial action potential. Representative action potential elicited at 1 Hz from a patient in sinus rhythm (SR, **A**, n=5/5) or suffering from chronic atrial fibrillation (cAF, **C**, n=3/3) before (for SR: light blue trace, **A**; and for cAF: dark blue trace, **B**) and after the perfusion of 10 μmol/L carbachol (CCh, purple traces). (**B**, **D**) Quantification of the effects of the perfusion of CCh on the resting membrane potential (RMP) and the action potential duration at 90 repolarisation (APD₉₀). Data shown as mean±SEM. ***P<0.001 using paired Student's *t*-test. n/N=number (n) of recordings from N patients.

The response of the muscarinic-2 receptor (M2-receptor) to the pharmacological agent carbachol (CCh) or its natural agonist acetylcholine (ACh) is expected to be impaired in patients suffering from AF (Dobrev et al. 2005; Voigt N. et al. 2007). To confirm this hypothesis, we perfused 10 μmol/L CCh to tissues during the AP measurement (**Figure 7**). Perfusion of CCh resulted in a dramatic reduction of the APD in SR tissues (control vs CCh: 397.5±33.51 ms vs 84.97±10.26 ms, n=5/5 respectively P<0.001 using paired Student's *t*-test) accompanied with a slight hyperpolarisation of the RMP (SR vs cAF: -71.9±2.14 mV vs -75.88±1.58 mV respectively, P>0.05 using paired Student's *t*-test). However, effects on the APD₉₀ or on the RMP were absent in tissues from cAF patients (for the APD₉₀ and the RMP, control vs CCh: 388.8±70.92 ms vs 110.8±36.63 ms,

n=3/3, and -76.39 ± 3.09 vs -78.85 ± 1.27 , both $P > 0.05$ using Wilcoxon's rank test), thus relating the hypothesis of an impaired response of the muscarinic receptor upon activation in cAF patients.

		SR	cAF
General	Patients, n	29	9
	Sex, male/female	24/5	8/1
	Age, y	66.1±9.5	70.1±8.6
	Body mass index, kg/m ²	29.1±4.1	29.6±3.2
Intervention	CAD, n	26	7
	MVD/AVD, n	5	3
	Intervention CAD+MVD/AVD, n	2	1
	Intervention time, minutes	255.3±57.6	273.8±84.9
	ECC time, minutes	123.8±59.9	139.5±40.6
Anamnesis	Hypertension, n	26	8
	Diabetes, n	17	4
	Hyperlipidaemia, n	18	3
	NYHA (I/II/III), n	0/5/4	1/2/2
	Stroke, n	0	0
	TIA, n	1	0
CC	Creatinine, µmol/L	0.9±0.2	1.3±0.4
Echocardiography	LAD, mm	42.9±7	45.3±4.9
	LVEDD, mm	50.2±8.8	54.8±8.1
	IVSd, mm	12.8±2.7	13.1±2.2
	LVPWd, mm	12.1±1.8	11.8±1.47
	LVEF, %	57.4±12.3	45.7±10.2
	Diastolic dysfunction, Grade I/II/III	5/4/0	2/3/2
Medication	Digitalis, n	1	0
	ACE inhibitors, n	5	4
	AT1 blockers, n	5	2
	Dihydropyridines, n	5	3
	Diuretics, n	10	5
	Nitrates, n	6	0
	Lipid-lowering drugs, n	17	6

Table 21: Clinical characteristics of patients used for sharp-microelectrode experiments. SR, Sinus rhythm; cAF, chronic atrial fibrillation; CAD, coronary artery disease; MVD/AVD, mitral/aortic valve disease; ECC, extracorporeal circulation; NYHA, New York Heart Association Functional Classification; TIA, transient ischemic attack; CC, clinical chemistry; LAD, left atrial diameter; LVEDD, left ventricular end-diastolic diameter; IVSd, interventricular septum thickness at end-diastole; LVPWd, left ventricular posterior wall thickness at end-diastole; LVEF, left ventricular ejection fraction; ACE, angiotensin-converting enzyme; AT, angiotensin receptor. Data shown as mean±SEM.

3.2 Induced pluripotent stem cells as a model to study electrical remodelling associated with atrial fibrillation

3.2.1 Elaboration of atrial cardiomyocytes derived from an induced pluripotent stem cell line to study atrial fibrillation

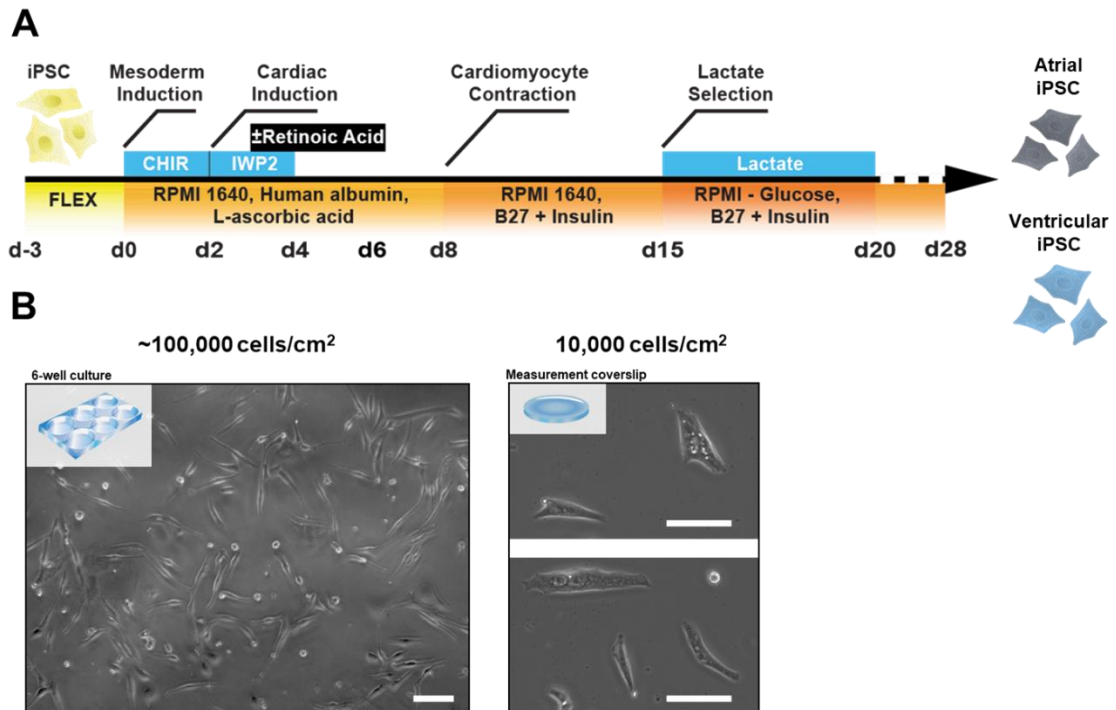


Figure 8: Induced pluripotent stem cell differentiation protocol. **A**, Schematic model of the induced pluripotent stem cell (iPSC) cardiomyocyte differentiation protocols used in this study. Application of 1 $\mu\text{mol/L}$ retinoic acid on day (d) 3 to day 6 induces an atrial specific subtype in the resulting iPSC derived cardiomyocytes. Modified from Seibertz et al. Basic Res Cardiol, in revisions. **B**, Photomicrograph of atrial cardiomyocyte derived from induced pluripotent stem cells employed in this study in dense 6 well plating (left) and sparsely plated monolayers on 10 mm glass coverslips (right) for live single cell measurements. Scale bar = 50 μm .

A major limitation in the study of AF using human tissue is the limitation of freedom to the experimenter (mainly in terms of interventional studies) as it is associated with many requirements and imperatives that do not always depend on the experimenter only. Therefore, a study model is preferable, with the utilisation of iPSC being the most interesting for our purposes because of its large versatility. Hence, we generated atrial and ventricular cardiomyocytes derived from induced pluripotent stem cells (atrial and ventricular iPSC) using the protocol

described in **Figure 8**, and plated them onto small glass coverslips at a density of 10.000 cells/cm². The measurement of their spontaneous beating frequency showed a higher rate in atrial iPSC than in ventricular iPSC (atrial vs ventricular iPSC (Melanie Ritter MD thesis, not shown here). Moreover, the mRNA expression levels of key ion channels involved in the cardiac AP were measured and showed similar expression profiles in our iPSC lines in comparison with native human material (**Figure 9**).

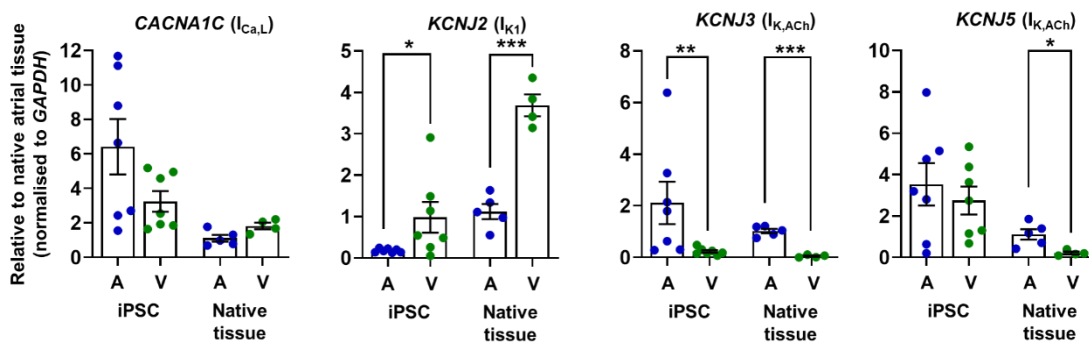


Figure 9: Comparison of the mRNA expression levels of L-type Ca²⁺ channels and inward rectifier K⁺ channels in atrial and ventricular cardiomyocytes derived from induced pluripotent stem cells, and atrial and ventricular patient biopsies. Comparison of the mRNA expression levels of L-type calcium (Ca²⁺) channels (I_{Ca,L}) and inward rectifier K⁺ channels (I_{K1}, I_{K,ACh}) in atrial (A) and ventricular (V) cardiomyocytes derived from induced pluripotent stem cells (iPSC), and atrial (A) and ventricular (V) patient biopsies. Results from 7 atrial and 7 ventricular differentiations as well as 5 atrial and 4 ventricular patient biopsies. Data shown as mean±SEM normalised to atrial patient biopsies. *P<0.05, **P<0.01 and *** P<0.001 using Mann-Whitney U test.

3.2.2 Atrial and ventricular cardiomyocytes derived from induced pluripotent stem cells show distinct electrophysiological profile

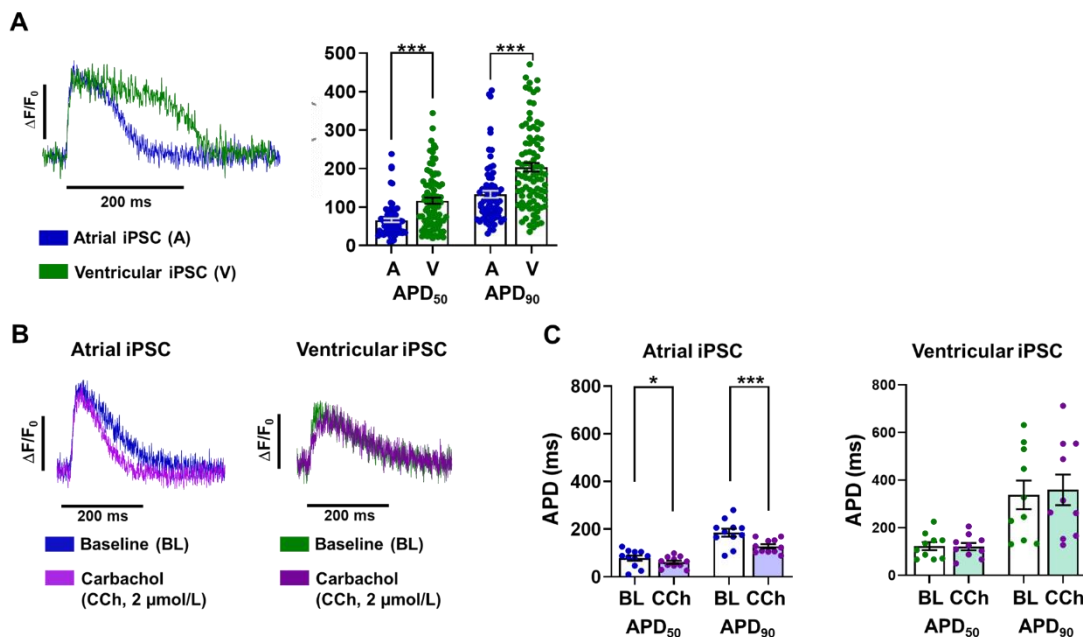


Figure 10: Optical action potential measurements in atrial and ventricular cardiomyocytes derived from induced pluripotent stem cells. **A**, Representative action potentials in atrial (blue trace, $n=74/4$) and ventricular (green trace, $n=89/3$) cardiomyocytes derived from induced pluripotent stem cells (atrial and ventricular iPSC) elicited at 1 Hz and analysis of their action potential duration at 50 and 90% repolarisation (respectively APD₅₀ and APD₉₀). **B**, Representative action potentials measured optically in atrial ($n=11/2$) and ventricular iPSC ($n=10/2$) at 1 Hz stimulation before (baseline, BL) and after the perfusion of the M2-receptor agonist carbachol (CCh, 2 $\mu\text{mol/L}$, purple traces), and **(C)** corresponding quantification of their APD₅₀ and APD₉₀. Data shown as mean \pm SEM. For atrial vs ventricular, *** $P<0.001$ using Welch's t -test. For baseline vs carbachol, * $P<0.05$, *** <0.001 using paired Student's t -test. n/N =number (n) of cell from N batches. Adapted from the MD thesis of Melanie Ritter with permission.

To continue our investigation, we needed to assess the quality of our cells and the efficacy of our differentiation protocol. We performed optical AP measurements in both atrial and ventricular iPSC using optical dye techniques (**Figure 10**). We observed that ventricular iPSC had a longer plateau phase, but also that APD₅₀ and APD₉₀ were significantly longer in ventricular iPSC (ventricular vs atrial: for the APD₅₀ 116.4 ± 7.82 ms, $n=89/3$, vs 65.46 ± 4.96 ms, $n=74/4$, $P<0.001$ using Welch's t -test; for the APD₉₀, 203.6 ± 11.33 ms vs

133±9.17 ms, $P < 0.001$ using Welch's t -test). Furthermore, the perfusion of 2 $\mu\text{mol/L}$ M2-receptor agonist CCh only resulted in an effect in atrial cells (control vs CCh, for the APD_{50} : 78.84±11 ms vs 61.6±7.03 ms, $n=11/2$, $P < 0.05$ using paired Student's t -test and for the APD_{90} : 185.5±16.52 ms vs 128.1±8.59 ms, $P < 0.001$ using paired Student's t -test) whereas perfusion in ventricular iPSC did not result in any changes of the APD (control vs CCh, for the APD_{50} : 122.9±16.75 ms vs 121±15.09 ms, $n=10/2$, and for the APD_{90} : 338.3±60.21 ms vs 359.5±64.18 ms, both $P > 0.05$ using paired Student's t -test). Altogether, the results were suggesting an atrial specificity of our atrial iPSC.

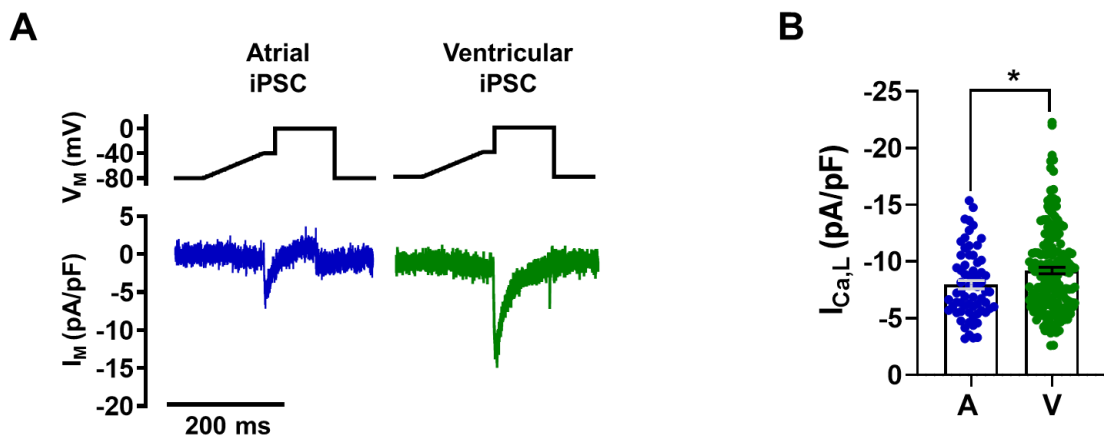


Figure 11: $I_{Ca,L}$ measurement in atrial and ventricular cardiomyocytes derived from induced pluripotent stem cells. **A**, Voltage-clamp protocol (0.5 Hz, top) and representative membrane current (I_M) trace (bottom) of L-type Ca^{2+} current ($I_{Ca,L}$) in atrial (blue) or ventricular (green) cardiomyocytes derived from induced pluripotent stem cells (atrial and ventricular iPSC). **B**, Corresponding quantification of peak $I_{Ca,L}$ (atrial: $n=66/2$, ventricular: $n=176/2$). Data shown as mean±SEM. * $P < 0.05$, ** $P < 0.01$ and *** $P < 0.001$ using Welch's t -test. n/N =number (n) of cell from N batches. Adapted from Seibert et al. 2022.

We continued the electrophysiological characterisation with the measurement of the L-type Ca^{2+} current ($I_{Ca,L}$) using automated patch-clamp (**Figure 11**). The results showed a significantly larger current density in our ventricular cell line

(respectively for atrial and ventricular iPSC: -7.95 ± 0.37 pA/pF, $n=66/2$ vs -9.19 ± 0.29 pA/pF, $n=176/2$, $P < 0.05$ using unpaired Student's *t*-test).

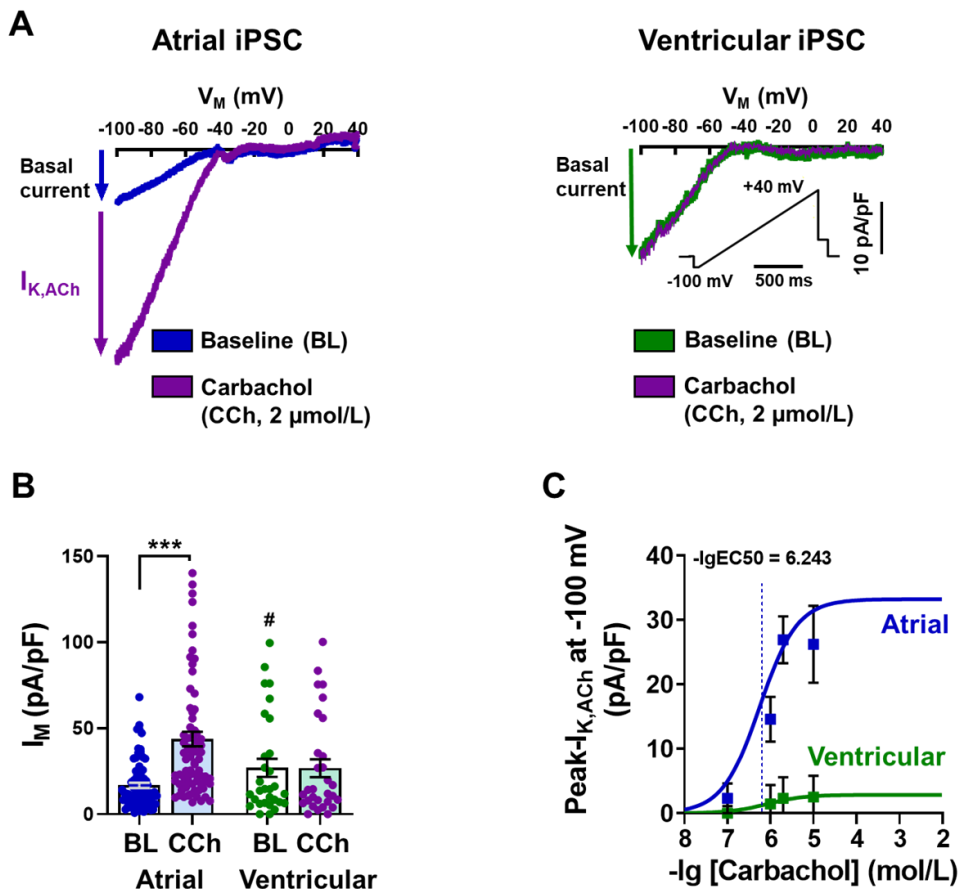


Figure 12: Basal inward-rectifier and carbachol induced K⁺ current measurement in atrial and ventricular cardiomyocytes derived from induced pluripotent stem cells. **A**, Representative voltage-clamp recordings of basal inward-rectifier K⁺ current (I_{K1}) and Carbachol (CCh)-activated $I_{K,ACh}$ in isolated atrial and ventricular cardiomyocytes derived from induced pluripotent stem cells (atrial and ventricular iPSC). Inset indicates depolarising ramp-pulse protocol. **B**, Quantification of total inward-rectifier K⁺ currents before (baseline, BL, I_{K1}) and after application of CCh in atrial ($n=77/6$) and ventricular ($n=31/4$) iPSC at -100 mV. **C**, Concentration-response curves for CCh-mediated activation of $I_{K,ACh}$ defined as CCh-dependent increase of inward-rectifier-K⁺-current amplitude at -100 mV in atrial ($n=7-77/6$) and ventricular ($n=143/1$) iPSC. Data shown as mean \pm SEM. *** $P < 0.001$ using paired Student's *t*-test with Bonferroni multiple comparison procedure. # $P < 0.05$ vs. atrial BL using Welch's *t*-test with Bonferroni multiple comparison procedure. n/N =number (n) of cell from N batches. Adapted from the MD thesis of Robin Springer with permission.

Regarding the potassium currents (**Figure 12**), the current density measurement of the basal inward-rectifier K⁺-current I_{K1} was shown to be significantly smaller at -100 mV in atrial compared to ventricular iPSC (respectively for atrial vs ventricular iPSC: 16.75 ± 1.56 pA/pF, $n=77/6$ vs 26.9 ± 5.23 pA/pF, $n=31/4$, $P < 0.05$ using Welch's *t*-test with Bonferroni multiple comparison procedure). Furthermore, the perfusion of 2 $\mu\text{mol/L}$ CCh only resulted in an inward current ($I_{K,ACh}$) in atrial iPSC (for basal vs CCh condition respectively: 16.75 ± 1.56 pA/pF vs 43.69 ± 4.29 pA/pF, $P < 0.001$ using paired Student's *t*-test with Bonferroni multiple comparison procedure), where no effect could be observed in ventricular iPSC (for basal vs CCh condition respectively: 26.9 ± 5.23 pA/pF vs 26.75 ± 5.23 pA/pF, $P > 0.05$ using paired Student's *t*-test with Bonferroni multiple comparison procedure). Finally, concentration-response curves showed that the CCh effect was dose dependent.

3.3 Electrical tachypacing in induced pluripotent stem cells

3.3.1 Electrical tachypacing of atrial induced pluripotent stem cells induces electrical remodelling

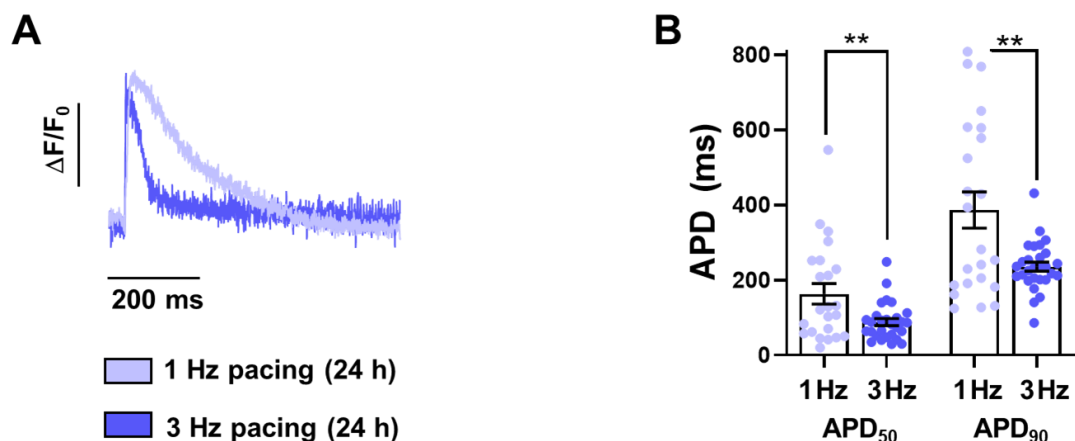
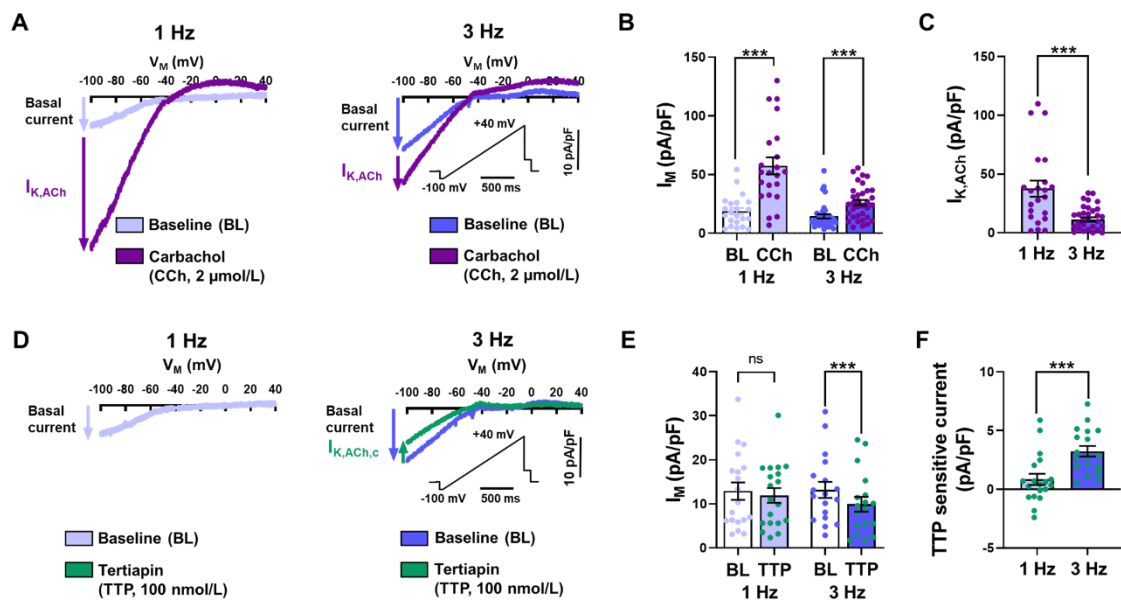


Figure 13: Tachypacing-induced remodelling of action potentials in cardiomyocytes derived from induced pluripotent stem cells. **A**, Representative action potentials elicited at 1 Hz in atrial cardiomyocytes derived from induced pluripotent stem cells (atrial iPSC) after 24-hour electrical pacing at 1 Hz (light blue) and 3 Hz (dark blue). **B**, Quantification of the action potential duration at 50 and 90% repolarisation (APD₅₀ and APD₉₀ respectively; 1 Hz: $n=23/3$, 3 Hz: $n=28/3$). Data are shown as mean \pm SEM. ** $P < 0.01$ using Welch's *t*-test. n/N =number (n) of atrial iPSC from N batches. Adapted from the MD thesis of Melanie Ritter with permission.

To induce electrical remodelling in our study model, we decided to use the electrical tachypacing method originally described by Wijffels et al. (1995), which is now an accepted method to study electrical remodelling caused by atrial fibrillation in different study models, including 2D cellular models. Atrial iPSC plated on glass coverslips were electrically paced for 24 hours and their AP were measured using optical dyes (**Figure 13**). Results show that the electrical pacing induced a reduction of both APD₅₀ (for 1 Hz vs 3 Hz pacing groups respectively: 163±27.26 ms, n=23/3 vs 88.2±9.42 ms, n=28/3, P<0.01 using Welch's *t*-test) and APD₉₀ (for 1 Hz vs 3 Hz groups respectively: 386.5±48.31 ms vs 235.8±12.2 ms, P<0.01 using Welch's *t*-test) in the group paced at 3 Hz compared to 1 Hz pacing.



Interestingly, the measurement of $I_{K,ACh}$ in paced atrial iPSC (**Figure 14**) showed that the current density resulting in the application of CCh was significantly lower in 3 Hz paced cells (1 Hz vs 3 Hz respectively: 37.54 ± 6.87 pA/pF, $n=22/4$ vs 11.33 ± 1.9 pA/pF, $n=34/4$, $p < 0.05$ using Welch's *t*-test), suggesting an impairment of the $I_{K,ACh}$. Interestingly, the perfusion of the $I_{K,ACh}$ selective blocker tertiapin (TTP) unravelled the presence of an agonist independent and constitutively active $I_{K,ACh}$ current, that could at least partially explain the AP shortening observed.

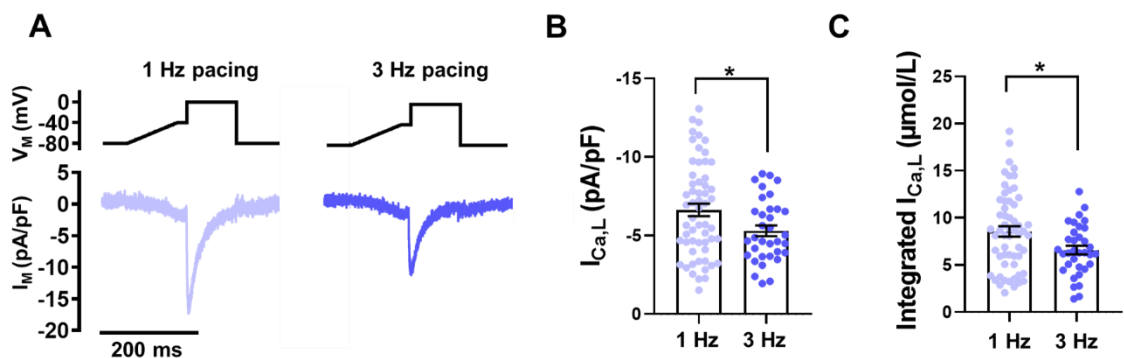


Figure 15: Tachypacing-induced remodelling of $I_{Ca,L}$ in atrial cardiomyocytes derived from induced pluripotent stem cells. **A**, Voltage-clamp protocol (top) and representative membrane current (I_M) recording (bottom) of $I_{Ca,L}$ measured in atrial cardiomyocytes derived from induced pluripotent stem (atrial iPSC) cells after 24-hour pacing at 1 Hz (light blue, $n=23/4$) and 3 Hz (dark blue, $n=28/4$). **B**, Quantification of peak $I_{Ca,L}$. **C**, Integrated $I_{Ca,L}$ expressed as estimated cytosolic Ca^{2+} influx. Data shown as mean \pm SEM. * $P < 0.05$ and using Welch's *t*-test. n/N =number (n) of atrial iPSC from N batches. Adapted from the MD thesis of Lea Stelzer with permission.

Following electrical tachypacing, the L-type Ca^{2+} current was also measured (**Figure 15**). Atrial iPSC, electrically paced at 3 Hz, showed a significant reduction in their current density in comparison with cells paced at 1 Hz (1 Hz vs 3 Hz respectively: -6.63 ± 0.39 pA/pF, $n=58/4$ vs -5.3 ± 0.34 pA/pF, $n=34/4$; $P < 0.05$ using Welch's *t*-test). Furthermore, the measurement of the integrated Ca^{2+} current representing the total Ca^{2+} influx was shown to be significantly reduced, indicating a mechanism to prevent the cell from Ca^{2+} overload during high frequency beating rates.

3.3.2 Calcium pacing medium privation prevents electrical remodelling in atrial induced pluripotent stem cells

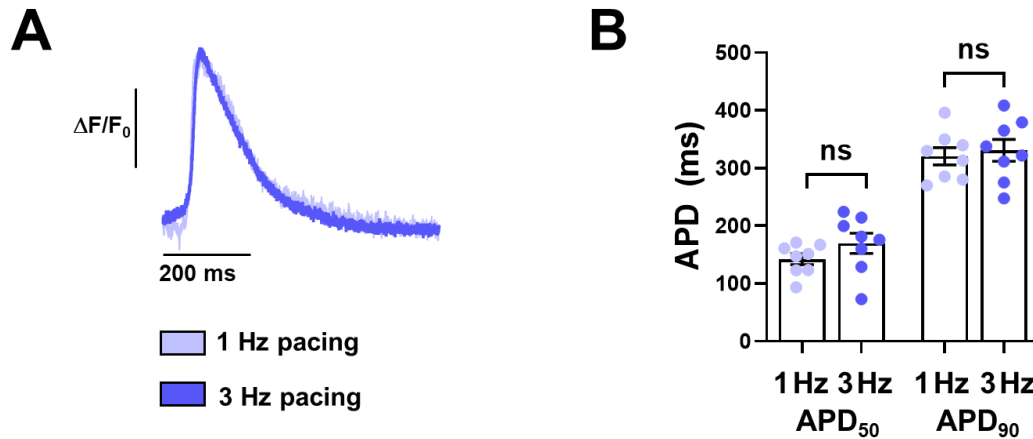


Figure 16: Electrical tachypacing in low- Ca^{2+} medium prevents the electrical remodelling-induced action potential shortening. **A**, Representative optical action potential measured in atrial cardiomyocytes derived from induced pluripotent stem cells (atrial iPSC) after 24 hours of electrical pacing at 1 Hz (light blue, $n=8/1$) or 3 Hz (dark blue, $n=8/1$) in low Ca^{2+} medium and **B**, quantification of their action potential duration at 50 and 90% repolarisation (APD₅₀ and APD₉₀ respectively). n/N =number (n) of atrial iPSC from N batches. Adapted from the MD thesis of Melanie Ritter with permission.

Following this last observation, we assumed that Ca^{2+} overload could play a role in electrical remodelling of the atrial iPSC. To confront this hypothesis, we repeated the experiments in low Ca^{2+} conditions (**Figure 16**). The measurement of the optical action potentials showed no significant changes neither on APD₅₀ (for 1 Hz vs 3 Hz respectively: 142.3 ± 9.47 ms, $n=8/1$ vs 169.8 ± 17.52 ms, $n=8/1$, $P > 0.05$ using Mann-Whitney's test) nor APD₉₀ (for 1 Hz vs 3 Hz respectively: 320.5 ± 14.9 ms vs 330.9 ± 18.93 ms, $P > 0.05$ using unpaired Student's t -test).

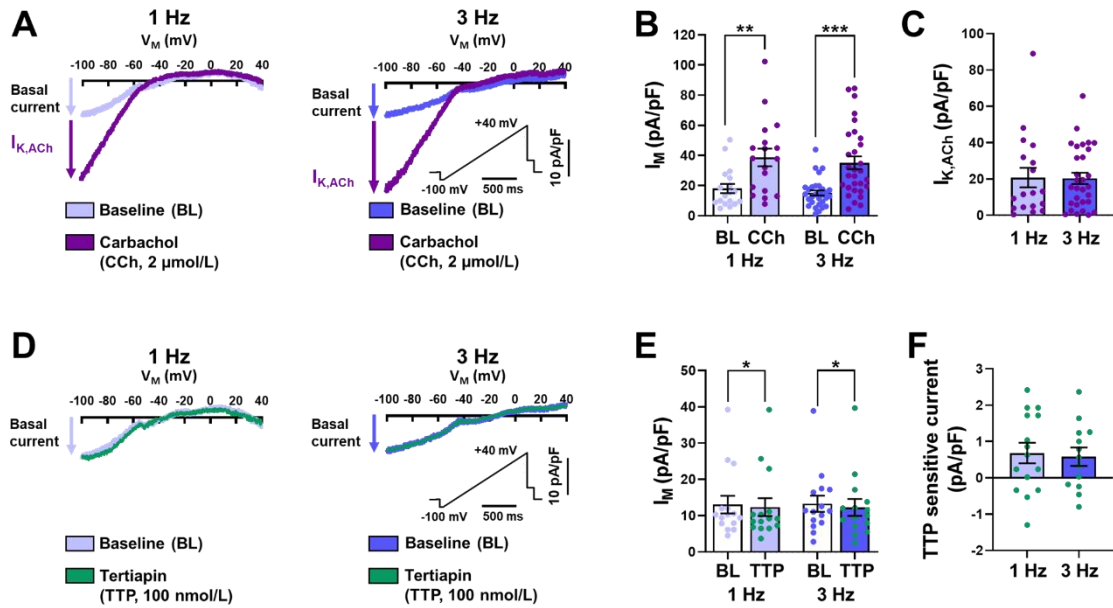


Figure 17: Electrical tachypacing in low- Ca^{2+} medium prevents the electrical tachypacing-induced $I_{K,ACh}$ remodelling and the apparition of a constitutive $I_{K,ACh}$. **A**, Representative recordings of inward-rectifier K^+ currents before (baseline, BL) and after the perfusion of $2\mu\text{mol/L}$ carbachol (CCh) or **(D)** the selective $I_{K,ACh}$ blocker tertiapin (TTP, 100 nmol/L) in atrial cardiomyocytes derived from induced pluripotent stem cells (atrial iPSC) after to 24-hour electrical pacing at 1 Hz (left) or 3 Hz (right) in low- Ca^{2+} medium. Voltage-clamp protocol (inset). **B**, Corresponding quantification of basal inward-rectifier K^+ current (membrane current, I_M) densities at -100 mV in absence and presence of CCh (1 Hz: $n=18/2$, 3 Hz: $n=30/2$) or **(E)** TTP (1 Hz: $n=15/2$, 3 Hz: $n=15/2$). **C**, Corresponding quantification of the $I_{K,ACh}$ or **(F)** the agonist independent constitutive $I_{K,ACh}$ ($I_{K,ACh,c}$) defined as block of basal inward-rectifier K^+ current in response to TTP. Data shown as mean \pm SEM. *** $P<0.001$ using paired Student's t -test. n/N =number (n) of atrial iPSC from N batches. Adapted from the MD thesis of Robin Springer with permission.

Likewise, the measurement of the CCh induced $I_{K,ACh}$ in atrial iPSC paced in low Ca^{2+} medium showed the apparition of a current of similar amplitude in both groups (**Figure 17**; 1 Hz baseline vs 3 Hz baseline respectively: $38.67\pm 5.84\text{ pA/pF}$, $n=15/2$ vs $35.2\pm 4.22\text{ pA/pF}$, $n=15/2$). Furthermore, the perfusion of 100 nmol/L TTP to unravel a constitutively active $I_{K,ACh}$ showed apparition of currents of comparable amplitude in both groups. These currents were in a similar range as the ones observed in the 1 Hz group in normal Ca^{2+} conditions (**Figure 14 F**). This finding did not support the theory of the

development of a constitutively active $I_{K,ACH}$ neither in the 1 Hz nor the 3 Hz electrically paced cells within the low Ca^{2+} medium (1 Hz in normal medium vs 1 Hz in low- Ca^{2+} medium vs 3 Hz in low Ca^{2+} medium: 0.845 ± 0.48 pA/pF vs 0.682 ± 0.28 pA/pF vs 0.58 ± 0.25 pA/pF, all $P > 0.05$ using Multiple t -test).

3.4 Atrial fibrillation in an engineered human myocardium model

3.4.1 Atrial and ventricular engineered human myocardium show distinct atrial and ventricular electrophysiological profiles

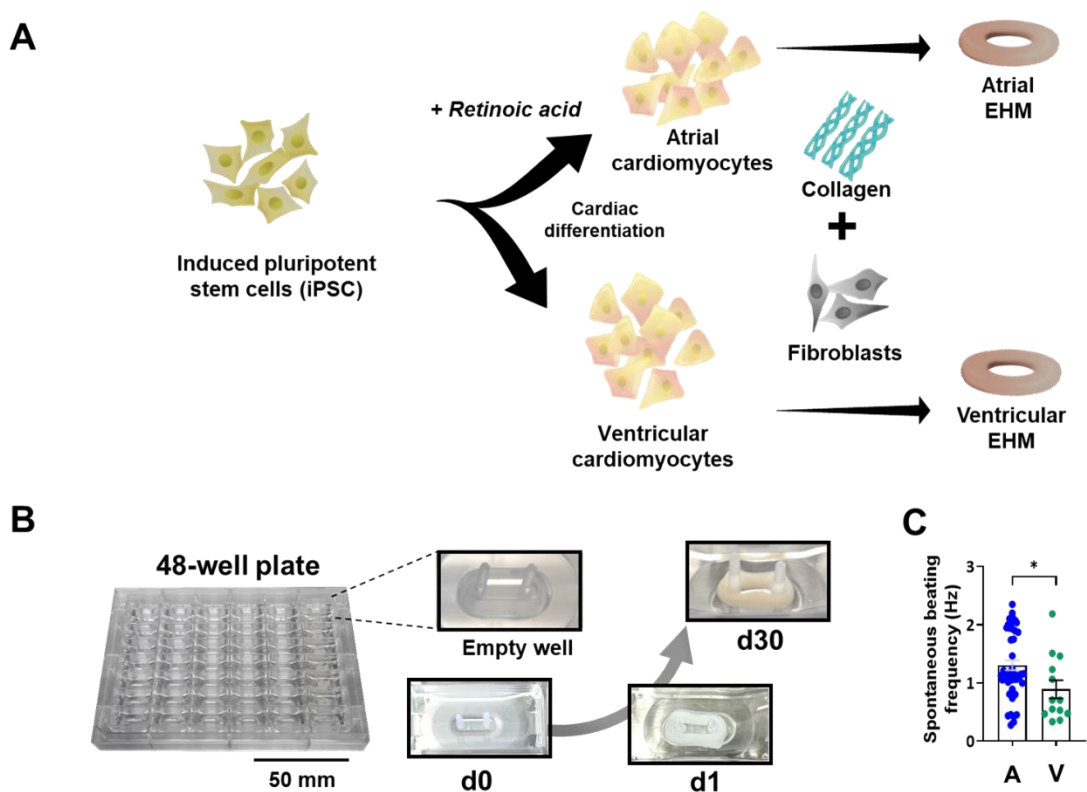


Figure 18: Engineered human myocardium generation protocol. **A**, Schematic representation of the protocol used for the generation of atrial and ventricular engineered human myocardium (EHM). **B**, Pictures of a maturation plate and EHM 1 hour after (d0), 1 day (d1) after and 30 days (d30) after the casting procedure. **C**, Quantification of the spontaneous beating frequency measured in atrial EHM (A, n=46/5) and ventricular EHM (V, n=13/3), 30 days after the casting procedure. Results shown as mean±SEM. * $P < 0.05$ using Mann whitney's test.

To study the effects of the electrical tachypacing in a multicellular environment, we decided to generate engineered human myocardium (EHM) with the previously described iPSC. 30 days after the casting procedure when the tissues were considered mature, electrophysiological investigation was made using the sharp-microelectrode technique to measure their AP. Spontaneous beating frequency analysis showed that atrial EHM had a significantly higher spontaneous beating rate compared to ventricular EHM (atrial vs ventricular respectively: 1.3 ± 0.09 Hz, $n=46/5$ vs 0.89 ± 0.16 Hz, $n=13/3$, $P < 0.05$ using Mann Whitney's test, **Figure 18**). Furthermore, similar to the results obtained in human cells, APD_{50} and APD_{90} were significantly shorter in atrial EHM compared to ventricular EHM (for the APD_{50} , atrial vs ventricular respectively: 60.26 ± 4.33 ms, $n=57/11$ vs 94.9 ± 5.43 ms, $n=27/6$; and for the APD_{90} , atrial vs ventricular respectively: 102.5 ± 3.43 ms vs 205.7 ± 11.49 ms; both $P < 0.001$ using Welch's *t*-test, **Figure 18**). Finally, although non-significant, hyperpolarisation was observed in ventricular EHM compared to atrial EHM (-67.69 ± 1.17 mV vs -66.15 ± 1.5 mV for atrial vs ventricular respectively), significantly higher values were observed in dV/dt_{max} (for atrial vs ventricular respectively: 21.17 ± 1.99 V/s vs 49.16 ± 5.02 V/s, $P < 0.001$ using Welch's *t*-test) and APA (atrial vs ventricular respectively 109.8 ± 3.75 mV vs 82.77 ± 2.25 mV, $P < 0.001$ using Welch's *t*-test) in ventricular tissues.

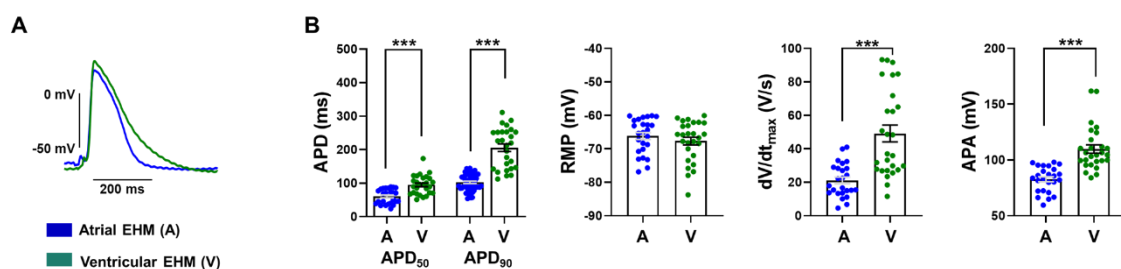


Figure 19: Electrophysiological characterisation of atrial and ventricular engineered human myocardium. **A**, Representative action potential elicited at 1 Hz in atrial (A, blue, $n=57/11$) or ventricular (V, green, $n=27/6$) EHM and (**B**) the quantification of the action potential parameters resting membrane potential (RMP), action potential amplitude (APA), maximum upstroke velocity (dV/dt_{max}) and action potential durations at 50 and 90% repolarisation (respectively APD_{50} and APD_{90}). Data shown as mean \pm SEM. ** $P < 0.01$ and *** $P < 0.001$ using Welch's *t*-test. n/N =number of recording (n) from N tissues.

The atrial-specific drug CCh was then perfused to the tissues. It resulted in an APD₉₀ reduction in atrial EHM (control vs CCh respectively: 94.13±4.09 ms vs 83.44±3.25 ms, n=6/6, P<0.05 using paired Student's *t*-test) and a hyperpolarisation of the RMP (control vs CCh respectively: -66.61±3.80 mV vs -71.72±3.12 mV, n=6/6, P<0.05 using paired Student's *t*-test). No effects were observed in ventricular EHM, neither for the RMP (-62.91±2.33 mV vs -62.86±2.93 mV, n=10/10, for control vs CCh respectively) nor the APD₉₀ (159.8±17.04 mV vs 169.6±20.15 mV, control vs CCh condition respectively, both P>0.05 using paired Student's *t*-test).

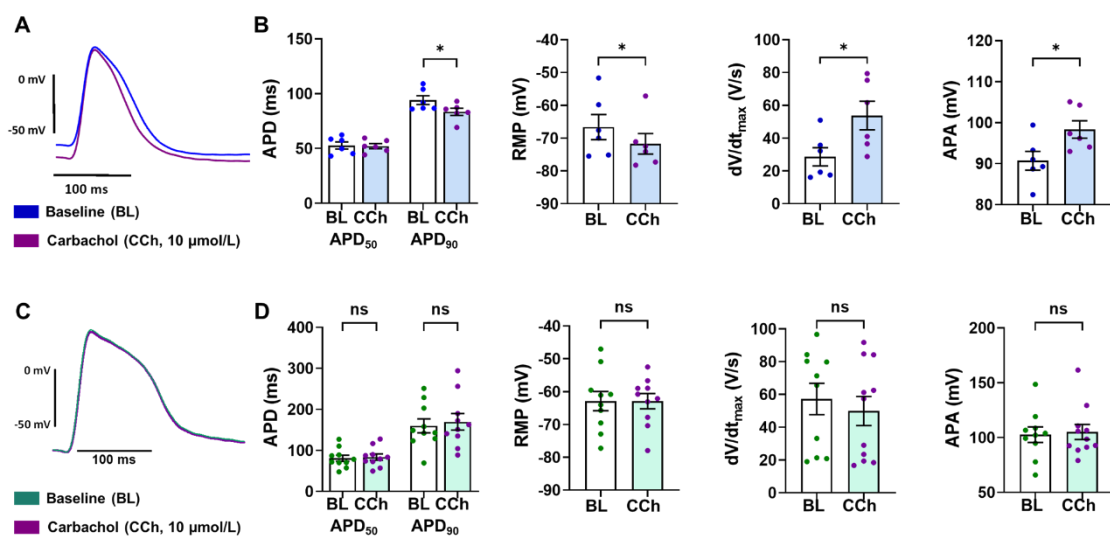


Figure 20: Action potential measurements in response to vagal agonist carbachol in atrial and ventricular engineered human myocardium. **A,C** Representative recordings of action potentials elicited at 1 Hz before (baseline, BL) and after application of the M2-receptor agonist carbachol (CCh, 10 µmol/L) in atrial (**A**, n=6/6) and ventricular (**C**, n=11/11) engineered human myocardium (EHM). **(B,D)** Corresponding quantification of the action potential duration at 50 and 90% repolarisation (APD₅₀ and APD₉₀ respectively), resting membrane potential (RMP), upstroke velocity (dV/dt_{max}) and action potential amplitude (APA, n = 11/11). Data shown as mean±SEM. n/N = number (n) of recording from N EHM.

3.4.2 24-hour electrical tachypacing induces electrical remodelling in atrial engineered human myocardium

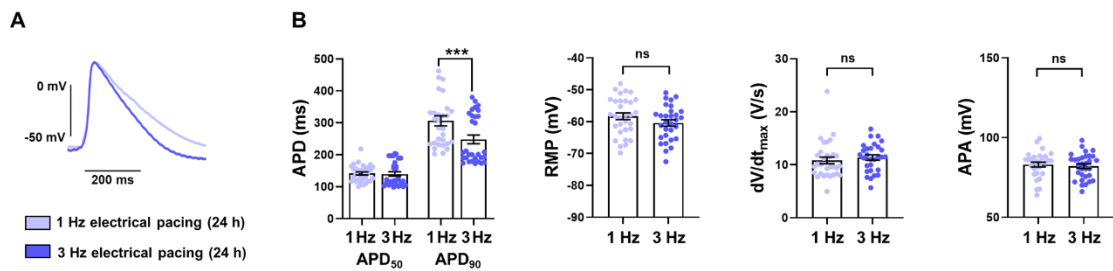


Figure 21: Electrical remodelling of atrial engineered human myocardium induced by 24-hour electrical tachypacing. **A**, Representative action potentials elicited at 1 Hz in atrial engineered human myocardium (EHM) subjected to 24-hour electrical pacing at 1 Hz (light blue, n=30/8) and 3 Hz (dark blue, n=30/8). **B**, Corresponding quantification of the action potential duration at 50 and 90% repolarisation (APD₅₀ and APD₉₀ respectively), resting membrane potential (RMP), maximum upstroke velocity (dV/dt_{max}) and action potential amplitude (APA). Data shown as mean±SEM. **P<0.01 and ***P<0.001 using Welch's *t*-test. n/N=number (n) of recordings from N EHM.

To test the hypothesis that electrical remodelling could be observed in atrial EHM, we subjected them to electrical tachypacing, and measured their AP using the sharp-microelectrode technique (**Figure 21**). Similar results as observed in our cellular model could be observed i.e. abbreviation of the APD₉₀ in the group of EHM paced at 3 Hz in comparison to the group paced at 1 Hz (for 1 Hz vs 3 Hz atrial EHM respectively: 306.4±15.57 ms, n=30/8, vs 248.2±13.68 ms, n=30/8, P<0.001 using Welch's *t*-test) without impairment of the other AP parameters (RMP, dV/dt_{max} and APA).

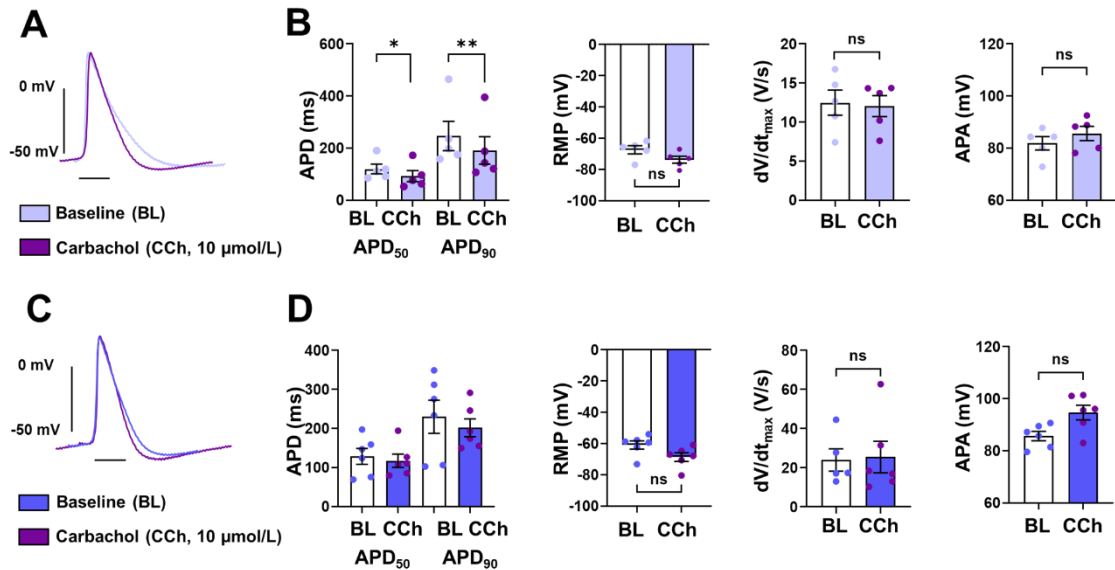


Figure 22: Effects of M2-receptor agonist carbachol on electrically paced atrial engineered human myocardium. **A,C**, Representative recordings of action potentials elicited at 1 Hz before (baseline, BL) and after application of the M2-receptor agonist carbachol (CCh, 10 $\mu\text{mol/L}$, purple) in atrial engineered human myocardium (EHM) subjected to 24-hour electrical pacing at 1 Hz (light blue, A, $n=5/5$) and 3 Hz (dark blue, C, $n=6/6$). **B,D**, Corresponding quantification of the action potential duration at 50 and 90% repolarisation (APD₅₀ and APD₉₀ respectively), resting membrane potential (RMP), maximum upstroke velocity (dV/dt_{max}) and action potential amplitude (APA). Data shown as mean \pm SEM. * $P<0.05$, paired Student's t -test. n/N =number (n) of recordings from N EHM.

To investigate whether 24-hour electrical tachypacing altered the functioning of $I_{K,ACh}$, we perfused 10 $\mu\text{mol/L}$ of the M2-receptor agonist CCh to our tissues. Whereas atrial EHM paced at 1 Hz responded to the perfusion of the drug with a reduction in their APD₉₀ (control vs CCh: 248 ± 55.46 ms vs 184.6 ± 51.84 ms, $n=5/5$, $P<0.05$ using paired t -test), no significant modifications in the AP parameters could be observed in the 3 Hz electrically paced group (**Figure 22**).

Unfortunately, the prolongation of the electrical tachypacing failed and resulted in the death of the atrial EHM and atrial. To investigate whether atrial iPSC model could be used for the investigation of the electrical remodelling associated with long-term tachypacing, we had to find an alternative to circumvent this problematic.

3.5 Optogenetic tools to study long-term atrial tachypacing in atrial engineered human myocardium: the adeno-associated-virus-channelrhodopsin-2 approach

An optogenetic approach seemed to be fitting very well with our purpose. The major limitation associated with the electrical tachypacing appeared to not be of concern with this approach as the cell contraction is triggered by light pulses and not electrical pulses anymore, thus preventing the faradaic reactions, suspected to be at the origin of our EHM death during the long-term electrical pacing protocols.

Created with SnapGene®

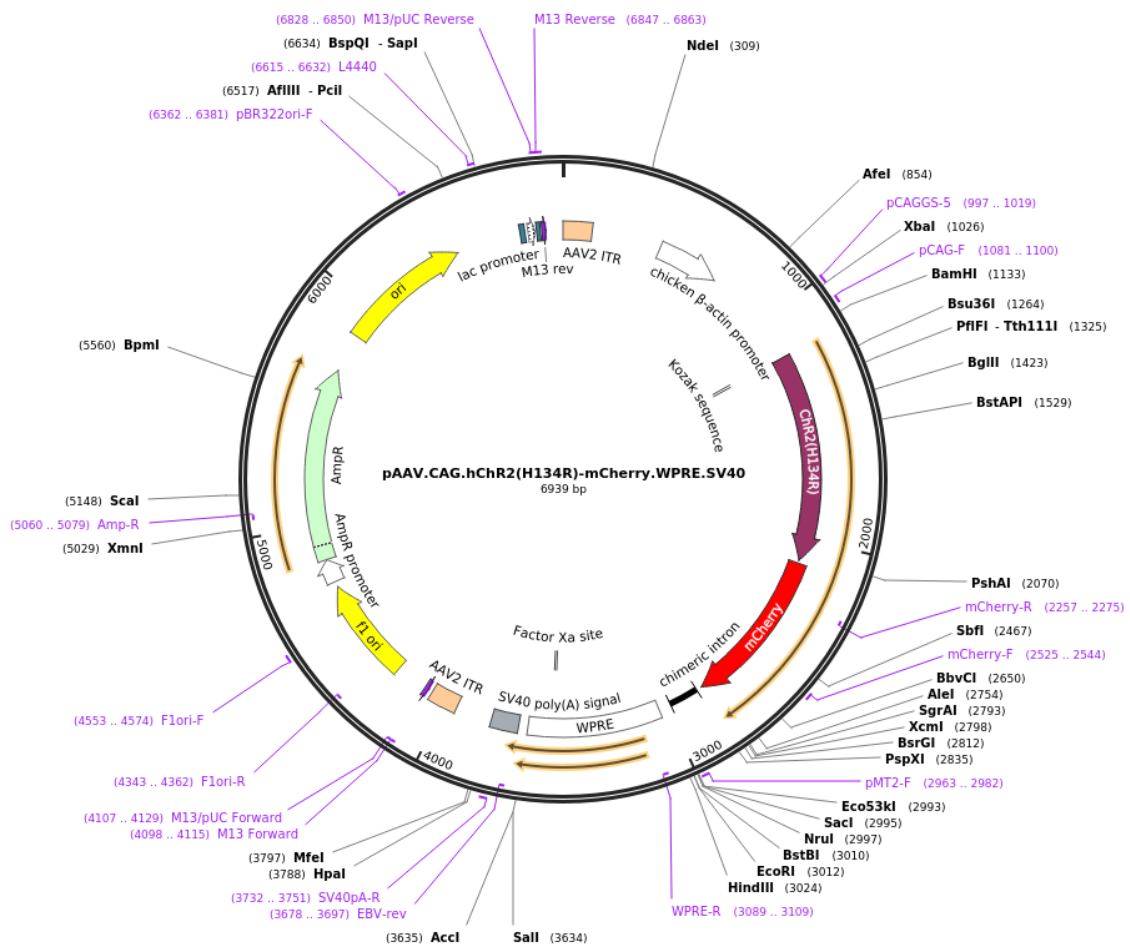


Figure 23: Plasmid construction of the adeno-associated-virus carrying the channelrhodopsin-2.

The first approach decided was designed around the utilisation of an AAV-2 vector to bring a channelrhodopsin-2 (ChR2) to the atrial iPSC and confer them light sensitivity.

This approach had already been successful in a cellular model (Bruegmann et al. 2010), and this particular virus also has the advantage of carrying a reporter gene (mCherry) that would allow us to quantify the expression of the virus in our cell line.

3.5.1 Successful introduction of channelrhodopsin-2 into atrial cardiomyocytes derived from induced pluripotent stem cells using an adeno-associated-virus-2 vector

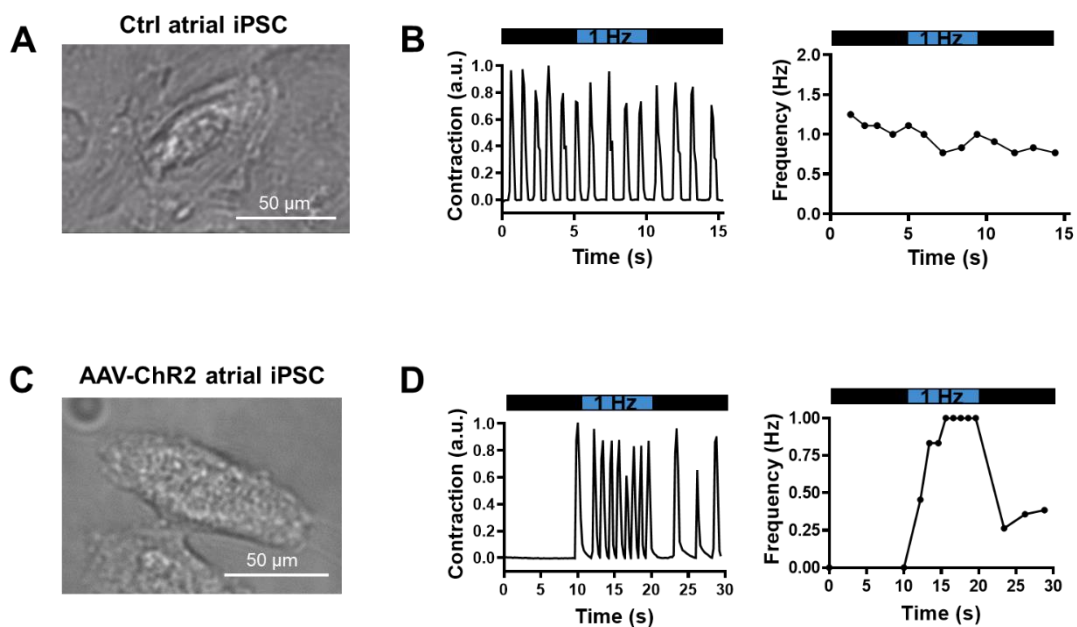


Figure 24: Functional assessment of light sensitivity in atrial cardiomyocytes derived from induced pluripotent stem cells transfected with an adeno-associated-virus-2 carrying a channelrhodopsin-2. A, Representative picture of a control and (C) of a virus transfected atrial cardiomyocyte derived from induced pluripotent stem cells. (B, D, left figure) Live imaging analysis of cell contraction in absence (black) or presence of 1 Hz light pulses (blue rectangles) and (B,D, right figure) analysis of the beating frequency over the time period.

First, we transfected the atrial iPSC with a viral charge concentration of 10^5 gene copies/cell and plated them on small glass coverslip 3 days later to subject them to the illumination protocols using 450 nm LED light pulses. Hence, we applied

trains of 1 Hz light pulses (3 ms square light pulses) to both control and atrial iPSC that received the virus and observed that only the cells carrying the virus were responding to the light pulses (**Figure 24**).

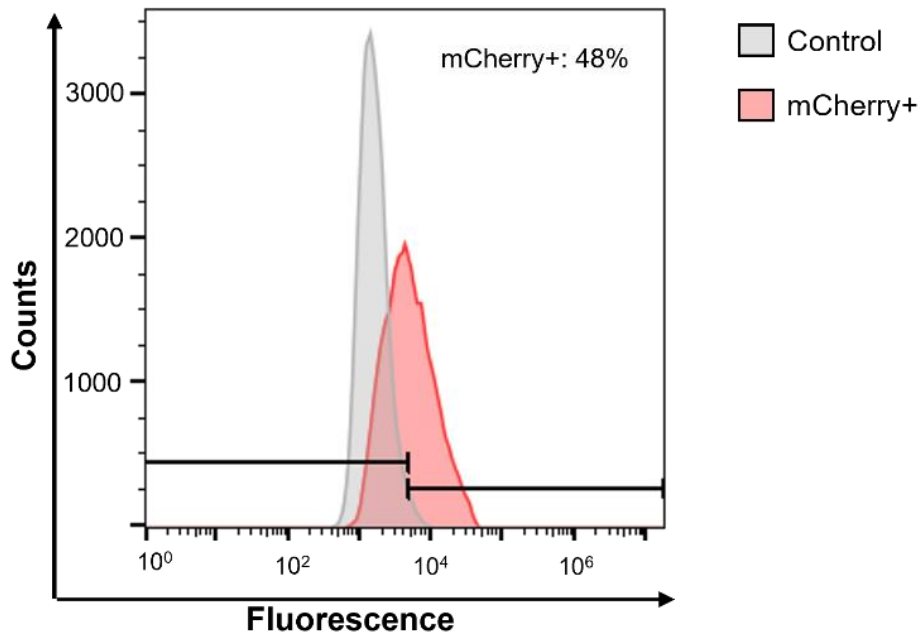


Figure 25: Flow cytometry analysis of atrial derived pluripotent stem cells transfected with an adeno-associated-virus-2 carrying channelrhodopsin-2. Flow cytometry analysis of living (7-AAD negative) non-transfected atrial cardiomyocytes derived from induced pluripotent stem cells (atrial iPSC, grey) and atrial iPSC transfected with an adeno-associated-virus-2 carrying a channelrhodopsin-2 (red). Adapted from the MD thesis of Fiona Popp with permission.

To assess the transfection rate, we performed a flow cytometry cell sorting assay, and the results showed that about 48% of the cell population was positive to mCherry (**Figure 25**).

3.5.2 Atrial engineered human myocardium generated with atrial cardiomyocytes derived from pluripotent stem cells transfected with an adeno-associated-virus-2 carrying a channelrhodopsin-2 are light sensitive, but long-term introduction of the virus impairs electrophysiology of the tissues

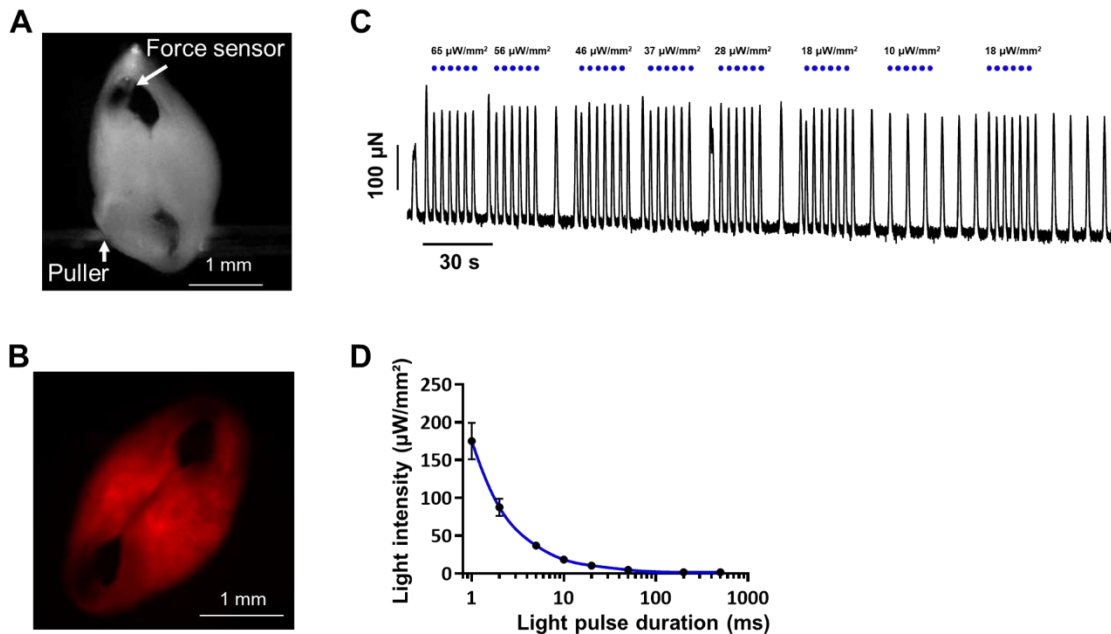


Figure 26: Functional assessment of light sensitivity in atrial engineered human myocardium generated using atrial cardiomyocytes derived from induced pluripotent stem cells transfected with an adeno-associated-virus-2 carrying a channelrhodopsin-2. **A**, Picture of an atrial engineered human myocardium prepared with atrial cardiomyocytes derived from induced pluripotent stem cells transfected with an adeno-associated-virus-2 carrying a channelrhodopsin-2 (AAV2-ChR2 atrial EHM) mounted on the illumination set-up. **B**, Picture of the 620 nm mCherry emission from a AAV2-ChR2 atrial EHM. **C**, Representative recording of an illumination protocol and **(D)** quantification of the results. $n=3/1$. Data shown as mean \pm SEM. n/N : number of EHM (n) from N batches.

Because it has never been investigated whether the light sensitivity of the cells would be kept after such a long-time post-transfection, we first had to ensure the light sensitivity would remain in the tissues. Therefore, we ran illumination protocols at 450 nm and assessed the responsiveness of the tissues to the light pulses (**Figure 26**). Analysis of the chronaxie (66.26 ± 0.01 ms) and a rheobase ($1.74 \mu\text{W}/\text{mm}^2$) demonstrated the light sensitivity of the constructs. The

acquisition of these functional values also was particularly interesting for us as it would serve us as base for the design and the technical requirements of our light pacing device, and the design of our optical pacing protocols.

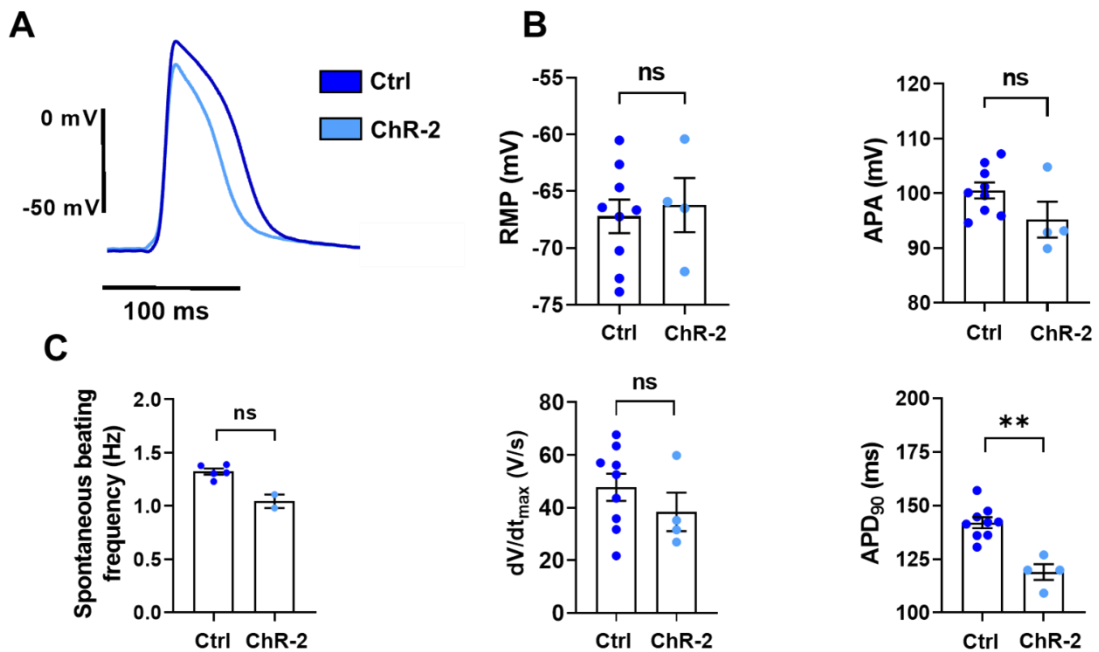


Figure 27: Long-term electrophysiological effects of the introduction of a channelrhodopsin-2 using an adeno-associated-virus-2 vector. **A**, Representative action potential elicited at 1 Hz measured in a control atrial engineered human myocardium (EHM, Ctrl, n=9/1) or in an atrial EHM prepared with atrial cardiomyocytes derived from induced pluripotent stem cells transfected with an adeno-associated-virus-2 carrying a channelrhodopsin-2 (ChR-2, n=4/1) EHM and **(B)** quantification of the resting membrane potential (RMP), action potential amplitude (APA), maximum upstroke velocity (dV/dt_{max}) and action potential duration at 90% repolarisation (APD_{90}). **C**, Quantification of the spontaneous beating frequency. Data shown as mean \pm SEM. ** $P < 0.01$, using Welch's t -test. n/N=number (n) of recordings from N EHM.

Another important aspect of the long-term introduction of the virus into the cells was to ensure it has no effects on the normal electrophysiology of the cells. To assess this point, we prepared atrial EHM with and without virus-transfected cells and measured their AP using the sharp-microelectrode method. Results showed that although the introduction of the virus did not alter the RMP, APA, dV/dt_{max} or the spontaneous beating frequency, it had an effect on the APD, especially on the APD_{90} , which was significantly reduced in the AAV2-ChR2 atrial EHM (control

vs AAV2-ChR2 atrial EHM respectively: 142 ± 2.53 ms, $n=9/1$, vs 119 ± 3.67 ms, $n=4/1$, $p < 0.01$ using Mann-Whitney's test).

3.5.3 Optical tachypacing of atrial engineered human myocardium generated with atrial induced pluripotent stem cells transfected with an adeno-associated-virus-2 carrying a channelrhodopsin-2 induces electrical remodelling

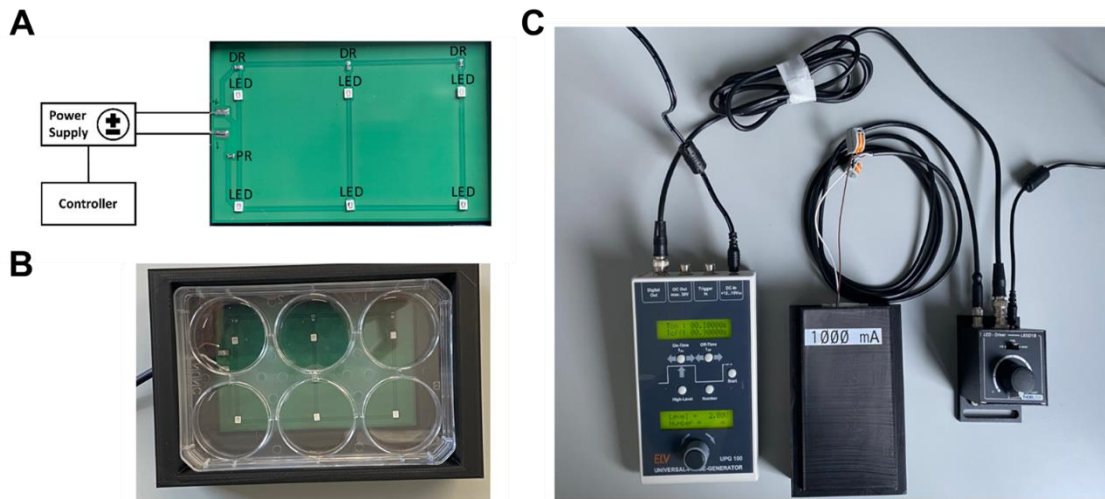


Figure 28: Self-constructed pacer for the optical pacing of atrial engineered human myocardium expressing the channelrhodopsin-2. **A**, Schematic circuit diagram of the custom-made LED-plate used to stimulate atrial engineered human myocardium prepared with atrial cardiomyocytes derived from induced pluripotent stem cells expressing a channelrhodopsin-2. DR, dropping resistor, PR, parallel resistor. **B**, Bottom view of LED-plate and housing covering a standard six-well plate. **C**, Picture of the whole system including from left to right: the stimulation controller, the pacing plate and current controller.

Although it seemed that long-term introduction of the channelrhodopsin into the cells had a deleterious effect on their electrophysiology, we still decided to run the optical pacing protocol using our self-constructed optical pacing device, to observe whether we could measure any remodelling in these tissues. Results showed that after 24 hours of optical pacing, tissues paced at 3 Hz recapitulated the electrical remodelling already observed in atrial iPSC, but also using the electrical tachypacing on non AAV-2-transfected atrial EHM. Hence, we observed no impairment on the RMP or the APA, but a significantly reduced APD₉₀ in the

3 Hz optically paced group (1 Hz vs 3 Hz respectively: 515.9 ± 5.66 ms, $n=11/2$ vs 410 ± 12.65 ms, $n=10/2$, $p < 0.001$ using Mann-Whitney's test).

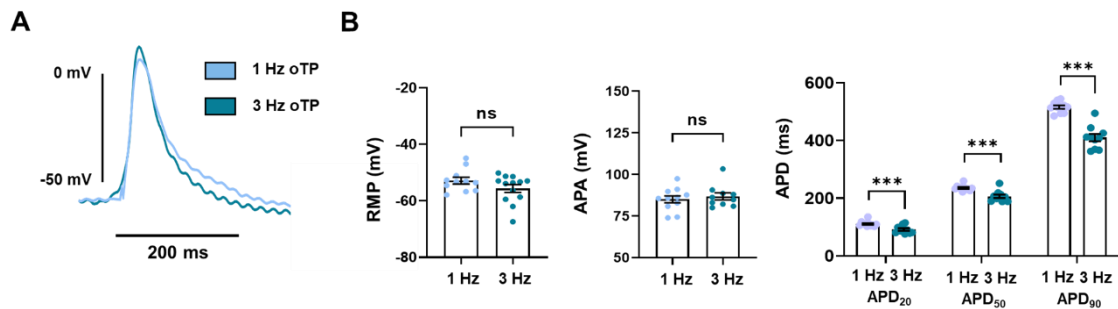


Figure 29: Electrical remodelling of atrial engineered human myocardium generated with atrial induced pluripotent stem cells transfected with an adeno-associated-virus-2 carrying a channelrhodopsin-2 induced by 24-hour electrical tachypacing. **A**, Representative action potentials elicited at 1 Hz in atrial engineered human myocardium (EHM) subjected to 24-hour electrical pacing at 1 Hz (light blue, $n=11/2$) and 3 Hz (dark blue, $n=10/2$). **B**, Corresponding quantification of action potential duration at 50 and 90% repolarisation (APD₅₀ and APD₉₀ respectively), resting membrane potential (RMP), maximum upstroke velocity (dV/dt_{max}) and action potential amplitude (APA). Data shown as mean \pm SEM. ** $P < 0.01$ and *** $P < 0.001$ using Welch's t -test. n/N =number (n) of recordings from N EHM.

3.6 Optogenetic tools to study long-term atrial tachypacing in atrial engineered human myocardium: the chromson approach

To circumvent the difficulties associated with the long-term introduction of the ChR2 using an AAV-2, we decided to change our strategy and used CRISPR-Cas modified stem cell line expressing a fast variant of the light-gated channelrhodopsin chromson.

3.6.1 Chromson atrial engineered human myocardium show distinct atrial electrophysiological specificity

Because we acquired the cell line as stem cell, we first had to ensure our differentiation protocol would work and reliably provide us with atrial specific iPSC. Therefore, we differentiated atrial and ventricular chromson iPSC using our standard differentiation protocol described in **Figure 8**, generated atrial and ventricular chromson EHM and assessed their electrophysiology using the sharp-microelectrode technique (**Figure 30**).

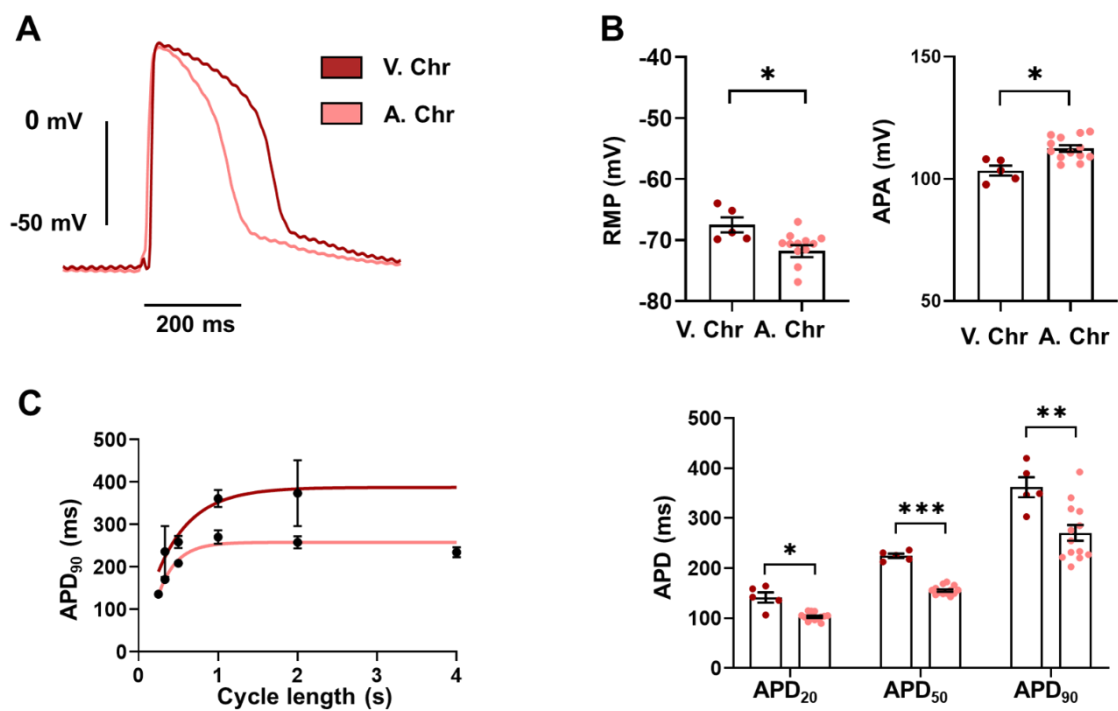


Figure 30: Electrophysiological characterisation of atrial and ventricular chromson engineered human myocardium. **A**, Representative recordings of action potentials elicited at 1 Hz in atrial (A. Chr, n=12/3) and ventricular (V. Chr, n = 5/2) chromson engineered human myocardium (EHM). **(B)** Corresponding quantification of the action potential duration at 50 and 90% repolarisation (APD₅₀ and APD₉₀ respectively), resting membrane potential (RMP) and action potential amplitude (APA). **(C)**, Restitution curves. Data shown as mean±SEM. *P<0.05, **P<0.01 and ***P<0.001 using Welch's *t*-test. n/N = number (n) of recording from N EHM. Adapted from the MD thesis of Fiona Popp with permission.

Results showed longer APD at 20, 50 and 90% repolarisation in ventricular chrimson EHM compared to the atrial chrimson EHM (respectively for atrial vs ventricular EHM; $n=12/3$ and $n=5/2$; APD_{20} : 102.8 ± 2.19 ms vs 141.4 ± 10.19 ms, $p < 0.01$; APD_{50} : 144.6 ± 2.49 ms vs 224.6 ± 4.25 ms, $p < 0.001$; APD_{90} : 270.6 ± 15.73 ms vs 361.6 ± 20 ms, $p < 0.01$ using Mann-Whitney's test). This finding was independent of the stimulation frequency applied. Furthermore, results showed a hyperpolarised RMP (atrial vs ventricular chrimson EHM respectively: -71.8 ± 0.98 mV vs -67.49 ± 1.22 mV, $p < 0.05$ using Mann-Whitney's test) and a higher APA (for atrial vs ventricular chrimson EHM respectively: 103.4 ± 2.04 mV vs 112.4 ± 1.3 mV, $p < 0.05$ using Mann-Whitney's test) in atrial chrimson EHM compared to ventricular chrimson EHM).

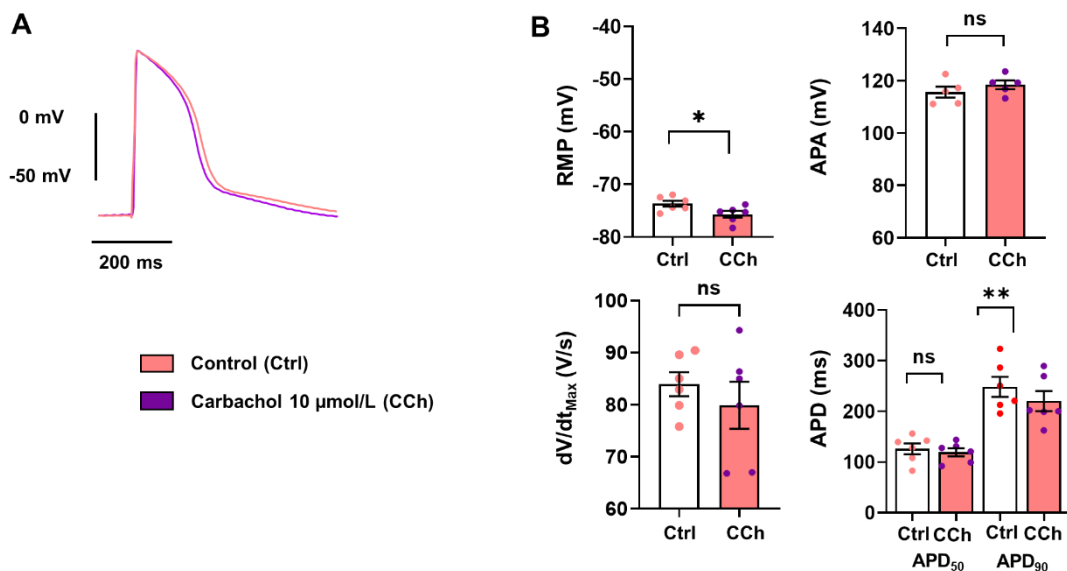


Figure 31: Action potential measurements in response to M2-receptor agonist carbachol in atrial chrimson engineered human myocardium. **A**, Representative recordings of action potentials elicited at 1 Hz before (Control, Ctrl) and after perfusion of the M2-receptor agonist carbachol (CCh, 10 µmol/L). **(B)** Corresponding quantification of the action potential duration at 50 and 90% repolarisation (APD_{50} and APD_{90} respectively), resting membrane potential (RMP), upstroke velocity (dV/dt_{max}) and action potential amplitude (APA). $n = 6/5$. Data shown as mean \pm SEM. * $P < 0.05$, ** $P < 0.01$, *** $P < 0.001$ using paired Student's t -test. $n/N =$ number (n) of recording from N EHM. Adapted from the MD thesis of Fiona Popp with permission.

Finally, we perfused CCh to the atrial chrimson EHM (**Figure 31**), and it led to a reduction of the APD₉₀ (control vs CCh respectively: 220.4±19.78 ms, n=6/6 vs 248.3±19.92 ms, p<0.01 using Student's paired *t*-test), and a hyperpolarisation of the RMP (control vs CCh respectively: -73.67±0.56 mV vs -75.67±0.63 mV, p<0.05 using Student's paired *t*-test).

3.6.2 Chrimson atrial engineered human myocardium is light sensitive

Next, we prepared our tissues to perform illumination protocols, and measured the response of the tissues to light stimulation. In order to optimise the future optical pacing conditions and adequately choose the LEDs to use on our optical light pacer, we decided to run the protocol using different light wavelengths and investigate the maximum responsiveness of the tissues (**Figure 32**).

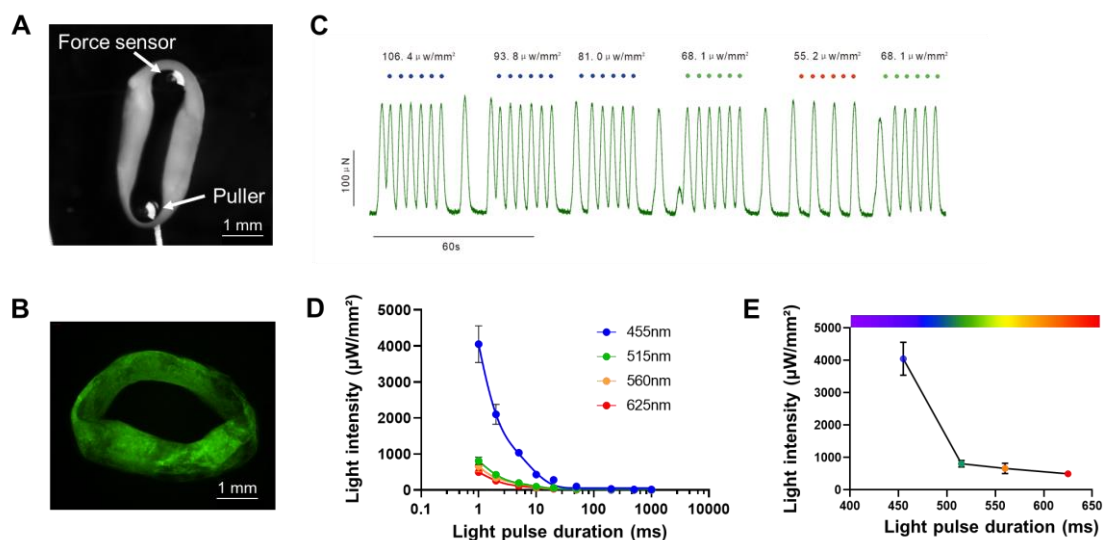


Figure 32: Functional assessment of light sensitivity in chrimson atrial engineered human myocardium. **A**, Picture of an atrial chrimson engineered human myocardium (EHM) mounted on the illumination set-up. **B**, Picture of the 515 nm eGFP emission from a chrimson atrial EHM. **C**, Representative recording of an illumination protocol run at 625 nm and (**D**) quantification of the results at the different light wavelengths. **E**, Result of the illumination protocol at 1 ms. n=7/2. Data shown as mean±SEM. n/N: number of EHM (n) from N batches.

The analysis of the rheobase showed a higher response to red shifted wavelengths, with a maximum sensitivity observed at 625 nm (455 nm vs 515 nm

vs 560 vs 625 nm: 22.96 ± 16.40 vs 13.10 ± 3.25 vs 10.66 ± 4.115 vs $6.48 \pm 1.78 \mu\text{W}/\text{mm}^2$).

3.6.3 24-hour optical pacing induces electrical remodelling in atrial chrimson engineered human myocardium

Finally, we optically paced our atrial chrimson EHM for 24 hours using 625 nm LEDs and measured their AP using sharp-microelectrode technique (**Figure 33**). The results showed no modifications in RMP, APA or dV/dt_{max} , but a significantly reduced APD_{50} (1 Hz vs 3 Hz respectively: 125 ± 4.9 ms, $n=48/14$ vs 141.9 ± 6.17 ms, $n=61/15$, $p < 0.05$ using Student's *t*-test) and APD_{90} (1 Hz vs 3 Hz respectively: 239.7 ± 6.17 ms vs 215.7 ± 4.87 ms, $p < 0.01$ using Student's *t*-test) in atrial chrimson EHM paced at 3 Hz compared to the 1 Hz optically paced group.

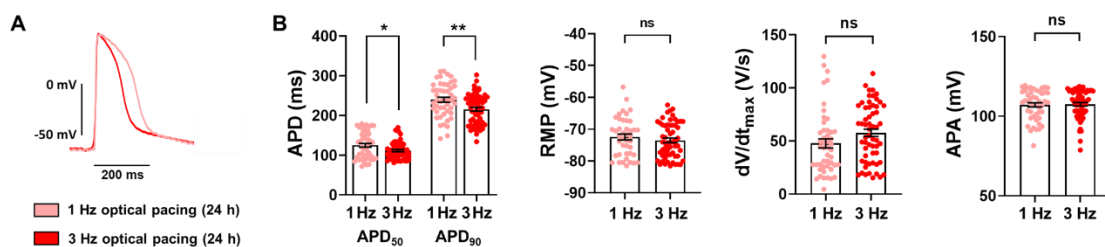


Figure 33: Electrical remodelling of atrial chrimson engineered human myocardium induced by 24-hour optical tachypacing. **A**, Representative action potentials elicited at 1 Hz in atrial engineered human myocardium (EHM) after 24-hour optical pacing at 1 Hz (light red) and 3 Hz (dark red). **B**, Corresponding quantification of the action potential duration at 50 and 90% repolarisation (APD_{50} and APD_{90} respectively) resting membrane potential (RMP), upstroke velocity (dV/dt_{max}) and action potential amplitude (APA; 1 Hz: $n=49/14$, 3 Hz: $n=61/15$). Data shown as mean \pm SEM. * $P < 0.05$, ** $P < 0.01$, using Welch's *t*-test. n/N =number (n) of recordings from N EHM. Adapted from the MD thesis of Fiona Popp with permission.

Furthermore, we perfused CCh on both 1 Hz and 3 Hz optically paced EHM and observed that only the atrial chrimson EHM paced at 1 Hz reacted to the drug perfusion (**Figure 34**). This response was characterised by a significant reduction in APD_{90} (control vs CCh condition respectively: 217.7 ± 20.7 ms, $n=8/8$ vs 170.6 ± 17.71 ms, $p < 0.05$ using Student's paired *t*-test).

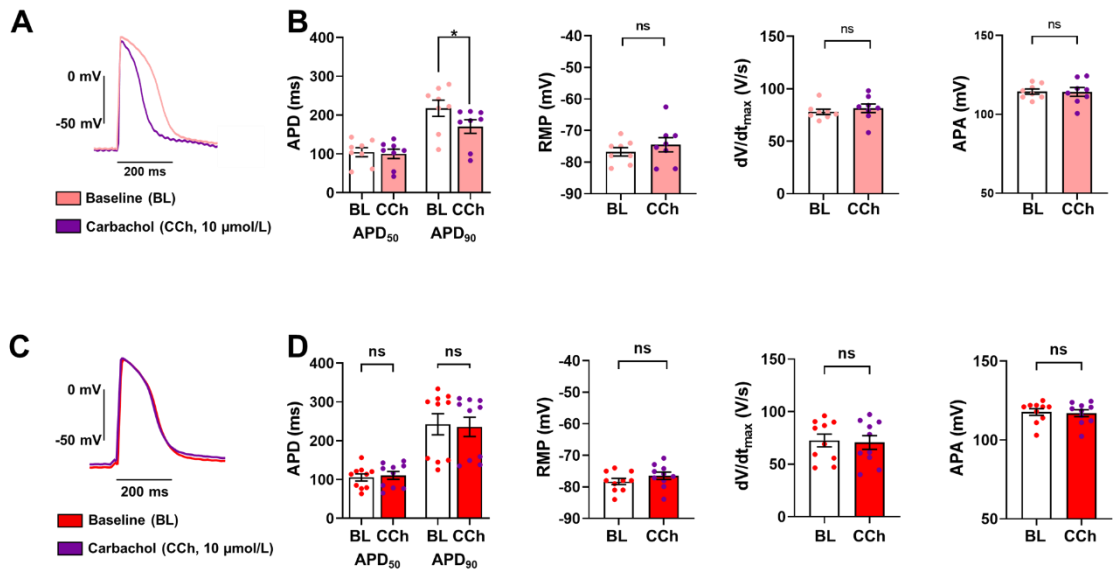


Figure 34: Effects of M2-receptor agonist carbachol on 24-hour optically paced atrial engineered human myocardium. **A,C**, Representative recordings of action potentials elicited at 1 Hz before (baseline, BL) and after application of the M2-receptor agonist carbachol (CCh, 10 $\mu\text{mol/L}$) in atrial chrimson engineered human myocardium (EHM) subjected to 24-hour optical pacing at 1 Hz (A) and 3 Hz (C). **B,D**, Corresponding quantification of action potential duration at 50 and 90% repolarisation (APD₅₀ and APD₉₀ respectively), resting membrane potential (RMP), maximum upstroke velocity (dV/dt_{max}) and action potential amplitude (APA; 1 Hz: $n=8/5$, 3 Hz: $n=10/5$). Data shown as mean \pm SEM. * $P<0.05$, paired Student's t -test. n/N =number (n) of recordings from N EHM. Adapted from the MD thesis of Fiona Popp with permission.

Interestingly, mRNA level measurements in atrial chrimson EHM showed that the expression of the KCNJ5 gene coding for the inward rectifier K⁺ channel was significantly lowered in the 3 Hz paced group. However, CACNA1C ($I_{\text{Ca,L}}$), KCNJ2 (I_{K1}), KCNJ3 ($I_{\text{K,ACH}}$), CHRM2 (M2-R) and ADORA1 (A1-R) mRNA levels were unchanged after 24 hours of optical pacing (**Figure 35**).

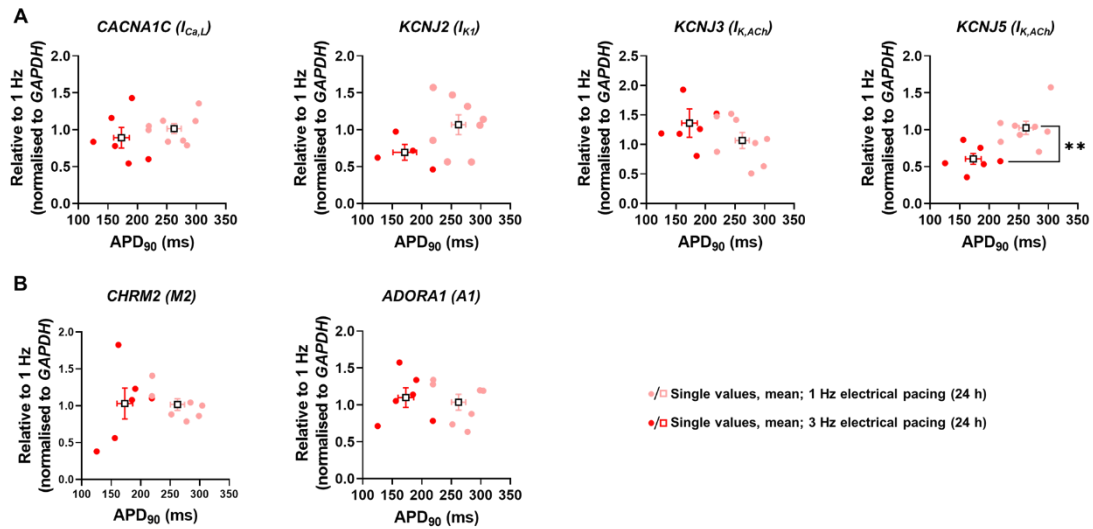


Figure 35: mRNA levels of L-Type Ca^{2+} channels, inward-rectifier K^{+} channels, muscarinic receptors and adenosine receptors in atrial engineered human myocardium subjected to 24-hour optical tachypacing. mRNA levels of *CACNA1C*, *KCNJ2*, *KCNJ3* and *KCNJ5* (A), as well as *CHRM2* and *ADORA1* (B) were plotted as single values against the corresponding APD_{90} . Squares indicate mean \pm SEM. ** $P < 0.01$ using Mann-Whitney-U test.

3.6.4 7-day optical pacing extends the spectrum of electrical remodelling in atrial chrimson engineered human myocardium

Following the acute (24 hours) experiments, we aimed to increase the pacing duration to one week to assess whether we could use our EHM model for the study of electrical remodelling after long-term optical tachypacing.

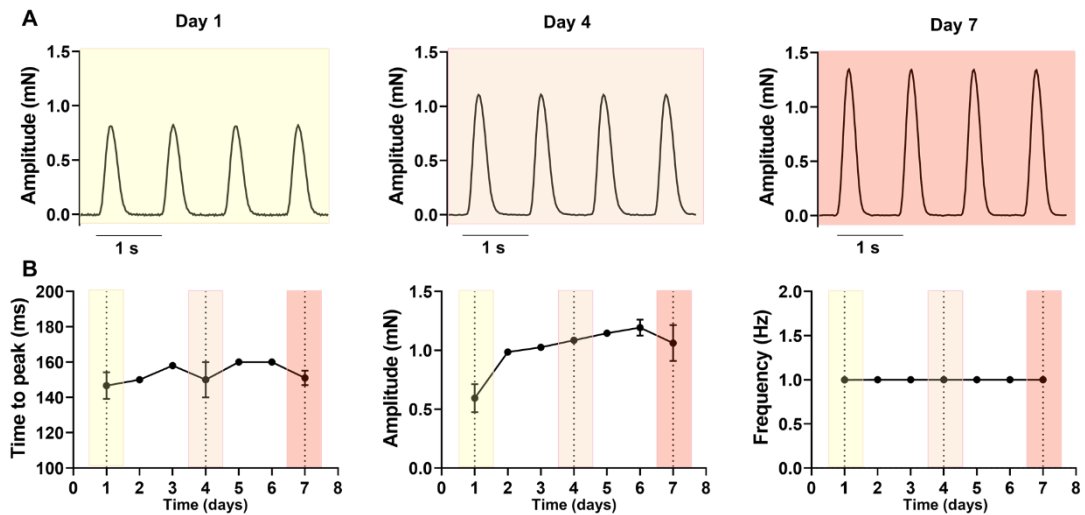


Figure 36: Continuous optical long-term pacing for 7 days at 1 Hz. A, Representative recordings of force of contraction of atrial EHM on day 1, day 4 and day 7. **B,** Timecourse of corresponding time-to-peak, amplitude and frequency values based on measurements in 1-4 atrial engineered human myocardium. Data shown as mean \pm SEM.

An important aspect of the long-term pacing protocol is ensuring that the tissues respond to the optical stimuli throughout the experimental protocol. Therefore, we mounted our chromson atrial tissues on a force measurement chamber and observed their responses to light stimuli for one week (**Figure 36**). Pictures of the experimental set-up can be found in the **Supplemental figure 5**. The experiments showed that the light capture remained perfect over time, with a 1 Hz response after the seventh day of pacing. Interestingly, the results showed an increase of the force amplitude after one week, although time to peak remained the same.

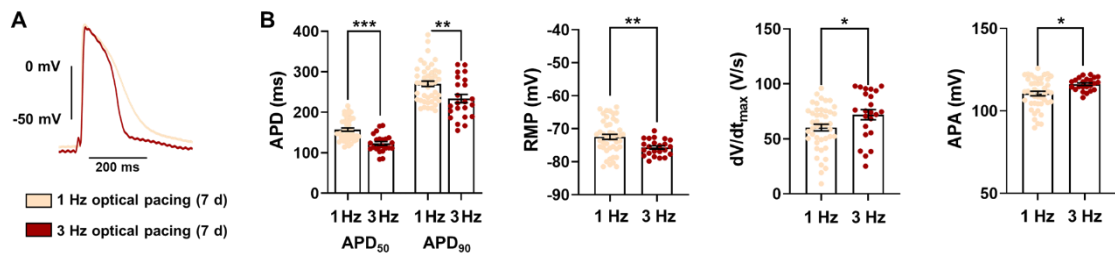


Figure 37: Electrical remodelling of atrial engineered human myocardium induced by 7-day optical tachypacing. **A**, Representative action potentials elicited at 1 Hz in atrial chrimson engineered human myocardium (EHM) subjected to 7-day (7 d) optical pacing at 1 Hz (light red) and 3 Hz (dark red). **B**, Corresponding quantification of the action potential duration at 50 and 90% repolarisation (APD₅₀ and APD₉₀ respectively), resting membrane potential (RMP), maximum upstroke velocity (dV/dt_{max}) and action potential amplitude (APA; 1 Hz: n=45/8, 3 Hz: n=23/9). Data shown as mean±SEM. *P<0.05, **P<0.01, ***P<0.001 using Welch's *t*-test. n/N=number (n) of recordings from N EHM. Adapted from the MD thesis of Fiona Popp with permission.

We then repeated the pacing protocol using the 1 Hz and 3 Hz pacing frequencies on freshly matured atrial chrimson EHM and measured their AP using the sharp-microelectrode set-up after one week of optical pacing (**Figure 37**). The results showed that tissues paced at 3 Hz did not only have a significantly shortened APD₅₀ and APD₉₀ (for APD₅₀: 1 Hz vs 3 Hz respectively, 157.2±4.08 ms, n=45/8 vs 123.1±4.57 ms, n=23/9, p<0.001 using Welch's *t*-test; for APD₉₀: 1 Hz vs 3 Hz respectively, 270.5±6.77 ms vs 233.8±10.33 ms, p<0.01 using Welch's *t*-test), but the RMP was also significantly hyperpolarised in tissues paced at 3 Hz (1 Hz vs 3 Hz respectively: -72.47±0.77 mV vs -75.69±0.51 mV, p<0.01 using Welch's *t*-test). Interestingly, dV/dt_{max} and APA values were significantly higher in 3 Hz paced tissues as well (for dV/dt_{max}, 1 Hz vs 3 Hz; 60.36±3.07 V/s vs 72.11±4.63 V/s, p<0.05 using Welch's *t*-test; for APA, 1 Hz vs 3 Hz respectively: 110.6±1.38 mV vs 116.2±0.79 mV, p<0.05 using Welch's *t*-test).

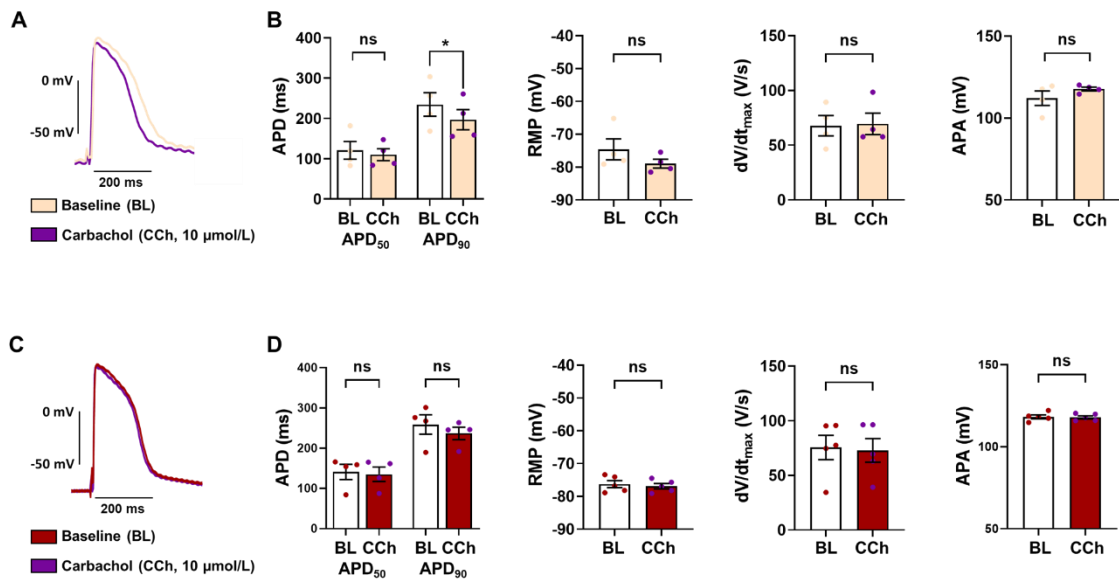


Figure 38: Effects of M2-receptor agonist carbachol on atrial engineered human myocardium optically paced for 7 days. **A,C**, Representative recordings of action potentials elicited at 1 Hz before (baseline, BL) and after application of the M2-receptor agonist carbachol (CCh, 10 $\mu\text{mol/L}$, purple traces) in atrial chrimson engineered human myocardium (EHM) subjected to 1-week optical pacing at 1 Hz (light red, **A**, $n=4/4$) and 3 Hz (dark red, **C**, $n=5/4$). **B,D**, Corresponding quantification of the action potential duration at 50 and 90% repolarisation (APD_{50} and APD_{90} respectively), resting membrane potential (RMP), maximum upstroke velocity (dV/dt_{max}) and action potential amplitude (APA). Data shown as mean \pm SEM. * $P<0.05$ using paired Student's t -test. n/N =number (n) of recordings from N EHM. Adapted from the MD thesis of Fiona Popp with permission.

To conclude, we measured the effects of the perfusion of the M2-receptor agonist CCh on the tissues optically paced for one week (**Figure 38**). The measurement of their AP before and after the perfusion of CCh showed that the tissues paced at 1 Hz still showed a response to the drug characterised by a significant reduction in the APD_{90} (control vs CCh condition respectively, 234.6 ± 29.12 ms vs 197 ± 24.98 ms, $n=4/4$, $p<0.05$ using Student's paired t -test), whereas it was blunted in the 3 Hz paced group and no effects could be observed neither on the APD_{50} or APD_{90} , nor on the other AP parameters.

4 Discussion

4.1 Induced pluripotent stem cells serve as a model to study electrical remodelling associated with atrial fibrillation

In the first part of this thesis, we showed that we could generate atrial cardiomyocytes derived from induced pluripotent stem cells (atrial iPSC) that exhibit atrial specific electrophysiological characteristics and use them to generate atrial engineered human myocardium (EHM). The atrial iPSC showed a higher spontaneous beating frequency compared to ventricular iPSC but also a shorter optical action potential (AP). At the current level, smaller current densities for the L-type calcium (Ca^{2+})-current ($I_{\text{Ca,L}}$) and the inward rectifier potassium current (I_{K1}) were observed. Also, a response to the atrial specific muscarinic 2 (M2)-receptor agonist carbachol (CCh) was only observed in the atrial cell population and was characterised by a shortening of the AP, and at the current level by the presence of an $I_{\text{K,ACh}}$ current in the atrial cell population only. Finally, the mRNA level expression compared with human native tissues showed similar expression profiles in iPSC and native tissues, namely a significantly reduced expression of KCJN2 (coding for I_{K1}) in atrial cells and a significantly higher level of KCJN3 (coding for $I_{\text{K,ACh}}$). The same trend was observed for KCNJ5 (coding for $I_{\text{K,ACh}}$).

Next, we generated and electrophysiologically characterised our atrial EHM, to ensure that they conserved their atrial specificity after the long-term integration into 3D organoid structures. We therefore generated ventricular and atrial EHM and compared their AP in the absence and in presence of the atrial specific drug CCh using the sharp-microelectrode technique. We were able to show that atrial EHM AP were significantly shorter than ventricular EHM AP. Furthermore, we observed a resting membrane potential (RMP) hyperpolarisation in ventricular EHM compared to atrial EHM, and that the maximum upstroke velocity (dV/dt_{max}) and the action potential amplitude (APA) were significantly higher in ventricular EHM. Finally, we demonstrated that only atrial EHM were sensitive to the M2-receptor agonist CCh.

4.1.1 Addition of retinoic acid during induced pluripotent stem cell differentiation promotes atrial differentiation

To promote atrial differentiation in our iPSC line, we used retinoic acid during the differentiation protocol. The importance of retinoic acid in the atrial differentiation mechanism was rapidly understood and studies showed that its inhibition in mouse or chicken embryos resulted in larger ventricles and smaller or even non-existing atria (Xavier-Neto et al. 1999; Hochgreb et al. 2003). Following this observation, the pioneer work of Gassanov et al. on iPSC set the base of what would become a standard protocol for atrial iPSC differentiation, while showing that the addition of retinoic acid to embryonic bodies during early differentiation stage led them towards an atrial phenotype (Gassanov et al. 2008). Our results aligned to the findings of these essential works and we demonstrated molecularly, the efficacy of our differentiation protocol, showing that principal AP actors were expressed in a similar way as in native human tissue (**Figure 9**).

4.1.2 Atrial cardiomyocytes derived from induced pluripotent stem cells show distinct electrophysiological profile compared to ventricular cardiomyocytes derived from induced pluripotent stem cells

To continue, we functionally demonstrated the atrial specificity of our cell population. As expected, the measurement of optical AP showed a significantly reduced APD in the atrial cell type (**Figure 10**). In human tissue, the shorter AP in the atrial compartment can be explained by the different expression of ion currents: repolarising currents such as I_{Kur} and $I_{K,ACh}$ are absent in ventricular cells (Wettwer et al. 2004; Voigt N. et al. 2007), and the current density of $I_{Ca,L}$ is larger in the ventricular cells (Voigt et al. 2012).

The absence of the functional expression of $I_{K,ACh}$ in the ventricular compartment is of particular interest because it is an interesting choice for assessing atrial specificity, as shown by our results as well. The M2-receptor agonist CCh was perfused to the cells and an $I_{K,ACh}$ current in response to the drug could not be observed in ventricular cells, whereas it was responsible for the generation of an $I_{K,ACh}$ current in atrial cells (**Figure 12**). Finally, automated voltage-clamp measurements showed a significantly larger $I_{Ca,L}$ current density in ventricular cells, as already described in the literature (Voigt et al. 2012).

Altogether, our results clearly demonstrated that we were able to generate an atrial specific iPSC line, exerting a similar electrophysiological profile as native human cardiomyocytes.

4.1.3 Atrial engineered human myocardium shows distinct atrial electrophysiological phenotype

In order to use the EHM model as a model to investigate electrical remodelling associated with AF, we first had to ensure that the previously described cells would handle their long-term integration into the organoid model and that it would not be associated with an impairment of their normal electrophysiology.

Using the sharp-microelectrode technique, the electrophysiological characterisation of the atrial and ventricular EHM showed a clear atrial specificity of the atrial EHM tissues. The shorter APD observed in atrial EHM in comparison to ventricular EHM (**Figure 19**), coupled with the absence of a response to the atrial specific agonist CCh in ventricular EHM but present in the atrial EHM (**Figure 20**) clearly demonstrated the atrial and ventricular specificities of our constructs. However, we were expecting to observe a hyperpolarised RMP in our ventricular EHM in comparison to atrial EHM (Wang et al. 1998). The voltage-clamp results clearly showed that ventricular iPSC had a larger I_{K1} current density and it is believed that this is responsible for the presence of a more negative RMP in ventricular cells. Because the measurements in cells and in tissues were performed at separate times and using different batches, it is possible that unchanged RMP results from longer maturation times of cardiomyocytes embedded into EHM.

4.2 Hallmarks of electrical remodelling associated with atrial fibrillation

In this second part, we assessed the electrophysiological characteristics of the electrical remodelling associated with the development of AF in human tissue. Using the sharp-microelectrode method, we showed that electrical remodelling in patients suffering from AF is characterised by a hyperpolarisation of the RMP, a significant shortening of the AP and the effective refractory period (ERP) and an impairment to response to the M2-receptor agonist CCh.

4.2.1 Action potential shortening and resting membrane potential hyperpolarisation are classical hallmarks of electrical remodelling

To have a great overview of the atrial electrophysiological remodelling associated with AF in human tissue, sharp-microelectrode measurements of AP in tissues obtained from patients in SR or AF were made (**Figure 6**). As previously described (Wettwer et al. 2004; Grandi et al. 2011), our first observation was that the AP was shorter in AF tissues. AP shortening is the consequence of an impairment in the balance between inward depolarising and outward repolarising currents. Amongst them, it is known that AF is associated with a decreased current density of $I_{Ca,L}$, a depolarising current (Heijman et al. 2014), but also the development of a constitutively active $I_{K,ACh}$, an atrial specific repolarising current (Dobrev et al. 2005).

The second observation was that the RMP was significantly hyperpolarised in the AF group. It fits to previous studies reporting this observation and was attributed to an upregulation of I_{K1} (Bosch et al. 1999; Workman et al. 2001). Finally, the effective refractory period (ERP) was shown to be reduced. This observation is commonly described in the context of AF (Yu et al. 1998; Wiedmann et al. 2020; Guichard et al. 2021) where it can act as a pro-arrhythmic substrate that can lead to the maintenance of AF while promoting re-entries (Kumagai et al. 2004).

4.2.2 Impaired response to an M2-receptor agonist is another hallmark of atrial fibrillation

To conclude the characterisation, we investigated the electrophysiological response to the M2-receptor agonist carbachol in native cardiomyocytes from patients suffering from AF. As expected, we observed that the response to the M2-receptor agonist CCh was blunted in the AF group, as the perfusion of the drug failed to significantly reduce the APD in the AF group. In the normal cardiac physiology, $I_{K,ACh}$ is a current placed under the control of the activation of the M2-receptor, a G_i -protein whose activation by ACh upon parasympathetic activation leads to the opening of an atrial specific potassium channel responsible for the $I_{K,ACh}$ current, and has been shown to be constitutively active in AF (Dobrev et al. 2005). The development of a constitutively active $I_{K,ACh}$ has been attributed to its greatly increased opening probability promoted by the reduced inhibition of

its opening (Voigt N. et al. 2007), which is a consequence of a disbalance in the phosphorylation activity of protein kinases (for example PKA ϵ and PKC δ , Makary et al., 2011).

4.3 Electrical tachypacing induces electrical remodelling in atrial induced pluripotent stem cells

In this third part, we explored the electrical remodelling induced by acute electrical tachypacing on the atrial iPSC model and the EHM model. First, we showed that 24-hour electrical pacing of atrial iPSC induced electrical remodelling like the one described in human AF. At the AP level, we demonstrated that it was associated with a significant reduction of the APD and at the current level, that 24-hour electrical pacing was sufficient to significantly impair the $I_{Ca,L}$ and $I_{K,ACh}$ currents. Furthermore, we showed that the impairment of the CCh-induced $I_{K,ACh}$ current was associated with the development of a constitutively active TTP-sensitive $I_{K,ACh}$ current in atrial iPSC electrically paced at 3 Hz. Finally, we showed that the remodelling observed after 24-hour electrical tachypacing could be prevented by pacing the cells in low Ca^{2+} medium, highlighting the crucial role of Ca^{2+} in the apparition of tachypacing-induced electrical remodelling. Next, we investigated the effects of 24-hour electrical tachypacing on atrial EHM. We showed that, as observed in cells, 24-hour electrical tachypacing of atrial EHM resulted in an AF-like electrophysiological remodelling characterised by an APD reduction with no impairment on the other AP parameters, and an alteration of the response to M2-receptor agonist CCh.

4.3.1 Electrical tachypacing induces atrial fibrillation-like electrical remodelling

On the long journey to recreate AF and electrical remodelling experimentally, many protocols have been described. The most used *in vivo* are the congenital heart failure model, the mitral valve regurgitation model and the electrical tachypacing model (Rankin et al. 1975; Wijffels et al. 1995; Gaspo 1999; Wakimoto et al. 2001; Bauer et al. 2004; Sun et al. 2008; Yeh et al. 2008; Tsujino et al. 2019; Bouwmeester et al. 2022). The last has the great advantage to be declinable in many study models, including *in vitro* in 2D and 3D models.

Electrical tachypacing has first been described *in vivo* in a goat model by Wijffels et al. in 1995 in his pioneer study demonstrating the self-maintenance and worsening characteristics of atrial fibrillation (Wijffels et al. 1995).

For these reasons, we utilised the electrical tachypacing method to promote electrical remodelling in our atrial iPSC and atrial EHM.

At the cellular level, we first observed that electrical remodelling was associated with a shortening of the optical AP (**Figure 13**) after electrical tachypacing. This finding confirmed the utilisation of the electrical tachypacing method to promote electrical remodelling in our atrial iPSC, and recapitulated AP shortening classically described in human AF (Bosch et al. 1999). To decorticate the ion channel alterations responsible for this shortening, we performed voltage-clamp measurements on atrial iPSC and measured key ion channels involved in the AP generation.

We first started with the measurement of K⁺ currents (**Figure 14**) and showed that the electrical tachypacing of the cells impaired their response to the M2-agonist CCh. On top of this observation, the application of the I_{K,ACh} specific blocker tertiapin (TTP) unravelled the presence of an agonist-independent constitutively active I_{K,ACh}. The development of the constitutively active I_{K,ACh} is a classical observation associated with electrical remodelling associated with AF (Dobrev et al. 2005; Voigt et al. 2007) and it could at least partially explain the shortening of the optical AP observed. Similar to other studies, we could not observe any significant alteration of the basal current measured at -100 mV, suggesting that I_{K1} was not significantly altered by the acute electrical pacing (Qi et al. 2008).

I_{Ca,L} is another key player of the AP generation in human, and has also been shown to be a target of the electrical remodelling in AF. Also, the measurement of I_{Ca,L} after 24-hour electrical tachypacing showed a significant reduction of the I_{Ca,L} current density (**Figure 15**). This is a common observation in human AF (Heijman et al., 2014). An explanation for the mechanisms underlying the reduction of the I_{Ca,L} is the decreased mRNA expression of its α_{1C} subunit (Yue

et al. 1997; Brundel et al. 1999), mediated by the activation of the calcineurin activated pathway, in particular NFATc3 and NFATc4 (Qi et al. 2008). Interestingly, Qi et al. showed that in dog, the activation of NFAT pathways could be prevented using Ca^{2+} chelators, suggesting the key role of Ca^{2+} in electrical remodelling induced by electrical tachypacing.

4.3.2 Calcium is a major key player of electrical remodelling

To challenge the hypothesis of Ca^{2+} mediated electrical remodelling in response to electrical tachypacing, we repeated the electrical pacing experiments in low Ca^{2+} conditions. Consistently with the literature (Qi et al. 2008), we also could observe that acute electrical tachypacing failed to induce electrical remodelling in atrial iPSC paced in low Ca^{2+} concentration medium. This was characterised by an absence of AP shortening in response to electrical tachypacing (**Figure 16**), and also the prevention of the apparition of a constitutively active $I_{K,ACH}$ in response to electrical tachypacing (**Figure 17**).

Altogether, these observations demonstrated that our atrial iPSC showed electrical remodelling comparable to what is observed in human AF in response to electrical tachypacing, and that it is mediated by Ca^{2+} .

4.3.3 Electrical tachypacing on atrial engineered human myocardium induces atrial fibrillation-like electrical remodelling

To observe whether our atrial EHM could reproduce the cellular observations, we generated atrial EHM and subjected them to acute electrical tachypacing.

Interestingly, the AP recordings in atrial EHM paced for 24 hours showed the same signs of electrical remodelling as observed in our 2D iPSC model, i.e. a significant reduction of the APD with no alterations of the other AP parameters (**Figure 21**). The observation made regarding the measurement of the K^+ currents that indicated no alteration of the basal current, echoed with the absence of significant changes on the RMP parameter and the literature (Qi et al. 2008), suggesting that RMP hyperpolarisation is not happening in the early remodelling stages.

Moreover, a response to the M2-receptor agonist CCh could only be observed in the 1 Hz electrically paced group (**Figure 22**), suggesting an impairment of the $I_{K,ACh}$ in the electrically tachypaced group, and also confirming that 24-hour electrical tachypacing was sufficient to induce $I_{K,ACh}$ remodelling in atrial iPSC.

Unfortunately, the prolongation of the pacing protocol failed using this model and caused the death of the tissues. This phenomenon could be explained by the apparition of Faradaic reactions related to the utilisation of carbon electrodes for the electrical tachypacing (Zhang et al. 2018). Their long-term utilisation could result in their oxidation and the generation of chlorine, hydroxyl radicals and the generation of hypochlorous and hypochlorine, which are particularly toxic and deleterious for the cells (Lemme et al. 2020).

4.4 Acute optical tachypacing induces electrical remodelling in atrial engineered human myocardium

In this part, we investigated the possibilities of using an adeno-associated-virus-2 carrying a channelrhodopsin-2 (AAV2-ChR2) vector and to transfect atrial iPSC to confer them light sensitivity and use them in our atrial EHM construct to replace the electrical tachypacing method by an optical pacing approach. First, we transfected atrial iPSC with the described virus. After plating them onto small glass coverslips, we observed that the virus introduction conferred them light sensitivity, as the cells were responding to light pulses. Next, we used cell sorting assays to measure the transfection success rate, based on the expression of mCherry in cells, and observed that our transfection rate was in the range of the usually described range in literature. To continue, we used these cells to generate atrial EHM, and after their maturation period we assessed the functional expression of the virus using illumination protocols that demonstrated the high light sensitivity of the tissues. Next, we measured AP of transfected and non AAV2-ChR2-transfected atrial EHM using the sharp-microelectrode technique and compared their electrophysiological characteristics. The results showed that the introduction of the ChR2 impaired the electrophysiology of the cells, resulting in a shorter AP and a lower spontaneous beating frequency. Finally, we built up our own optical pacing device, subjected our light sensitive tissues to 24 hours of

optical tachypacing and measured their AP. Results showed electrical remodelling in response to optical tachypacing, characterised by a significant reduction of the APD with no modification of the other AP parameters.

4.4.1 Atrial cardiomyocytes derived from induced pluripotent stem cells transfected with an adeno-associated-virus-2 carrying a channelrhodopsin-2 show light sensitivity

Thanks to the pioneer works of Deisseroth and Nagel in the characterisation of channelrhodopsins and the definition of optogenetics, optogenetic tools became widely used and extensively developed over the two last decades (Nagel et al. 2002; Nagel et al. 2003; Adamantidis et al. 2015). Thanks to this discovery, Brügmann and Arrenberg used this technology in cardiac tissues, as a tool to control the membrane potential (Arrenberg et al. 2010; Bruegmann et al. 2010). Following this idea of using light to control the membrane potential of our cardiomyocytes, we decided to utilise optogenetic tools to replace electrical stimulation pulses. Furthermore, based on Brügmann's work, we decided to use an AAV2-ChR-2 vector to transfect our cell population. Functional and molecular investigation showed light sensitivity in our cells, characterised by contractions in response to light pulses (**Figure 24**). Moreover, the cell sorting assays showed that 48% of the cell population was positive to mCherry (**Figure 25**), which is comparable with published literature (Vogt et al. 2015; Bruegmann et al. 2018). Aiming for a higher percentage would have necessarily implied a greater viral charge, and the potential effects on cell viability would not have been guaranteed. Also, previous work demonstrated that even a very small change of the percentage of transfected cells could lead to a physiological response *in vivo* (Lagali et al. 2008).

4.4.2 Atrial cardiomyocytes derived from induced pluripotent stem cells transfected with an adeno-associated-virus-2 carrying a channelrhodopsin-2 can be used for generating light sensitive tissues but long-term introduction of the virus impairs the normal electrophysiology of the cells

It was important to ensure that the introduction of the virus would not alter the electrophysiology of the cells, otherwise we could not certify whether the possible electrical remodelling observed, following an optical tachypacing protocol, could be attributed to the pacing protocol or the virus itself. Also, long-term effects associated with the long-term introduction of the AAV2-ChR2 in atrial iPSC were unknown. Therefore, we generated atrial EHM using transfected cells, and after 30 days of maturation, tissues were mounted onto the illumination set-up to measure their light sensitivity. The experiments showed that the tissues were still responding to light pulses and the chronaxie and rheobase measurements clearly demonstrated a great light sensitivity in the constructs (**Figure 26**). Furthermore, the fluorescence measurements at 620 nm using fluorescent microscopy showed a clear mCherry signal, homogeneously distributed in the tissue. The high fluorescence observed was consistent with the high transfection rate measured in the cells.

However, the measurement of the electrophysiology of the virus-transfected tissues showed that the introduction of the virus significantly impaired the APD, without altering the other parameters.

All these observations pointed towards toxicity associated with the long-term introduction of the virus. The ChR2 is activated by blue light wavelengths, and blue light phototoxicity could be one of the reasons of the cell toxicity observed. Tyssowski and Gray showed that the exposure of a neuronal cultures to long-term blue light flashlights without the introduction of a channelrhodopsin resulted in an alteration of gene activity, characterised by an overexpression of Fos mRNA (Tyssowski and Gray 2019). Interestingly, these observations could not be repeated with other light wavelengths (green and red). The same observation was made in specific microglial cells, where the authors showed an alteration of

the basal inflammatory and neurotrophic genes, and the reduced expression of pro-inflammatory genes (Cheng et al. 2016). Finally, studies on epithelial cells showed that the long time (6 hours) blue light illumination was responsible for a decrease of cell viability, associated with mitochondrial DNA lesions, associated with lipofuscin mediated production of reactive oxygen species (ROS; Godley et al., 2005; Sparrow et al., 2000).

The utilisation of an AAV-2 vector could also be one reason for the cell function impairment. It has been shown that the utilisation of a lentiviral vector to express doxorubicin-induced ChR2 in neonatal rat ventricular myocytes was associated with cytotoxic effects, when a high multiplicity of infection was used (Li et al. 2017). However, high ChR2 expression level was reported in this study, and we used a viral charge lower than normally used in literature (Vogt et al. 2015). Furthermore, no similar observations of direct cytotoxicity were reported with the utilisation of an AAV-2 vector.

4.4.3 24-hour optical tachypacing of atrial engineered human myocardium generated with atrial cardiomyocytes derived from induced pluripotent stem cells transfected with an adeno-associated-virus-2 carrying a channelrhodopsin-2 induces atrial fibrillation-like electrical remodelling

To validate our approach and assess whether an alternative to the virus could be interesting to search for, we ran a 24-hour optical tachypacing protocol on our atrial light sensitive tissues (**Figure 29**). Using the sharp-microelectrode technique, we measured their AP and observed that 24 hours of optical tachypacing resulted in a significant reduction of the APD₉₀ with no impairment on the other AP parameters.

However, because of the previously observed effects on the cell electrophysiology, a definitive conclusion was difficult to draw at this moment. Furthermore, the utilisation of this approach to investigate long-term effects of optical tachypacing was compromised as the lone introduction of the ChR2 seemed to have altered the normal electrophysiology of the atrial EHM.

Altogether, this set of experiments allowed us to confirm the possibilities of an optogenetic-based approach but showed that the AAV-2-based approach was not adequate for a long-term introduction of the virus, as it was associated with alterations in the normal electrophysiology of the tissues. Another point to mention is that although we used much lower viral charge than described in the literature, morphological changes could be observed in our tissues and all of them, without exception, turned pink only a few days after the casting procedure and kept their pink colour until utilisation (**Supplemental figure 4**). Furthermore, sharp-microelectrode measurements turned out to be particularly difficult with the optically paced tissues: the contraction of the tissues appeared weakened after the pacing protocol, no spontaneous beating activity could be observed and eliciting AP required stimulation pulses of much higher intensity than with control tissues.

All taken together, we decided to reconsider the viral approach to one that can be less harmful for the cells. Long-term introduction of a channelrhodopsin is not often investigated because they are often used acutely or over a brief period, and this limitation is major as the tissues must mature for at least 30 days before being used for electrophysiological measurements when being integrated in EHM.

4.5 Long-term optical tachypacing extends the electrical remodelling observed after acute optical tachypacing

In this final part, we investigated the possibilities of using an iPSC line modified to express the fast variant of the channelrhodopsin chrimson, to generate light sensitive atrial EHM suitable for long-term optical pacing. In the first part, we ensured the robustness of our differentiation protocol and generated ventricular and atrial chrimson EHM to assess their normal electrophysiological properties. We demonstrated atrial specificity of our atrial chrimson EHM model, showing that our atrial EHM had atrial specific electrophysiological properties characterised by a shorter AP compared to ventricular chrimson EHM, and an electrophysiological response to M2-receptor agonist CCh of our atrial constructs. Next, we ensured the light sensitivity of our model, and searched for the optimal wavelength for the optical stimulation of our tissues. Results of the

chronaxie and rheobase data did not only demonstrate the high light sensitivity of our model, but also showed that 625 nm was the optimal wavelength for the stimulation of the tissues. To continue, we investigated the effects of 24-hour optical pacing and showed that it resulted in the same electrical remodelling observed in all the previous models (AP shortening and no impairment of the other parameters). The perfusion of CCh demonstrated that acute optical tachypacing led to a loss of response to the agonist, which could be explained by the reduced mRNA KCNJ5 measured in the optically tachypaced group. Finally, after ensuring the chrimson EHM could endure a 7-day optical pacing protocol, we measured AP in 1-week paced tissues and observed that long-term optical tachypacing was responsible for an extension of the electrical remodelling in our atrial chrimson EHM, characterised by a hyperpolarisation of the RMP on top of the previously described features (AP shortening and alteration in the response to CCh).

4.5.1 Atrial chrimson engineered human myocardium show atrial electrophysiological specificity and are light sensitive

A classical drawback with the utilisation of optogenetic tools for long-term applications is the phototoxicity associated with the chronic channelrhodopsin activation. Furthermore, some channelrhodopsins (particularly channelrhodopsin-2, ChR2) are prone to desensitisation (Lin et al. 2009), mitigating their potential. To overcome these two major points, the scientific community developed chimeric or mutant variants of classical channelrhodopsins to enhance their properties (Lin et al. 2009; Lin et al. 2013; Jun and Cardin 2020). One variant of the chrimson channelrhodopsin developed by Mager et al. was particularly of interest because of its red shifted activation wavelength, and its rapid activation and deactivation kinetics (Mager et al. 2018). This variant was achieved by introducing two specific mutations (Y261F/S267M) in chrimson channelrhodopsin's helix F, speeding up on/off kinetics. Also, they showed that this new variant could be stimulated at remarkably high frequency (up to 60 Hz), and no phototoxicity could be observed even after several months post viral-introduction of the channelrhodopsin in mouse interneurons. Therefore, we used this recent technology coupled with the CRISPR/Cas recombination

technology to generate an iPSC line carrying the f-chrimson variant and repeated our approach.

The first point to ensure was the good functioning of our cell differentiation protocol. Because the chrimson cell line was different from the one previously used, it was important to ensure that we could obtain atrial cardiomyocytes of comparable phenotype and electrophysiological properties. As expected, the measurement of AP in atrial and ventricular chrimson EHM showed atrial specific differences including shorter AP (**Figure 30**) and response to the atrial specific drug CCh in our atrial tissues (**Figure 31**). Interestingly, RMP and APA were significantly hyperpolarised and higher. This could be explained by the small number of recordings and batch number of ventricular chrimson EHM.

Next, we ran the illumination protocol, and the tissues showed great light sensitivity at 625 nm (**Figure 32**). This was expectable because of the previous descriptions of the channelrhodopsin chrimson (Klapoetke et al. 2014; Mager et al. 2018; Jun and Cardin 2020).

Taken together, our results clearly demonstrated that our atrial f-chrimson cell line was atrial specific, and light sensitive.

4.5.2 24-hour optical pacing of atrial chrimson engineered human myocardium results in atrial fibrillation-like electrical remodelling

Next, we decided to optically stimulate our chrimson atrial EHM for 24 hours. We observed that it resulted in the same electrical remodelling as observed in cells and tissues after acute electrical pacing and was characterised by the reduction of the APD with no impairment on the other parameters (**Figure 33**). Interestingly, the application of CCh also resulted in a significant shortening of the AP only in the 1 Hz optically paced group, but did not result in any changes in the 3 Hz paced group (**Figure 34**) suggesting the impairment of the $I_{K,ACh}$ current. This finding could be explained by the down expression of the KCNJ5 gene coding for $I_{K,ACh}$ (**Figure 35**) observed in 24-hour optically paced atrial tissues.

4.5.3 Long-term pacing of atrial chrimson engineered human myocardium unravels time specific character of electrical remodelling

After ensuring that the tissues could follow optical stimulation for 1 whole week (**Figure 36**), we extended the original 24-hour pacing protocol to 7 days and recorded the AP of the tissues using the sharp-microelectrode technique (**Figure 37**). Interestingly, we did not only observe a reduction of the APD and an alteration in the response to CCh (**Figure 38**), but 7-day optical tachypacing also induced a hyperpolarisation of the RMP in the tachypaced group. This is particularly interesting because it was never observable after 24-hour pacing, independently from the stimulation method we used. This observation goes in line with the hypothesis of a time dependant electrical remodelling in which $I_{K,ACH}$ and $I_{Ca,L}$ would be the first currents to be affected and where the I_{K1} alteration would only appear after several days. In human AF, an increase in I_{K1} has been attributed to the increased expression of Kir2.1 mRNA (Dobrev et al. 2005; Gaborit et al. 2005), consecutive to the reduced levels of miR-1 (Girmatsion et al. 2009) or miR-26 (Wang et al. 2011; Luo et al. 2013).

Likewise, the significantly increased maximum upstroke velocity and APA could be explained by a higher availability of I_{Na} channels consecutive to the more negative RMP.

The constant increase in physiological functions of the tissue along the optical pacing protocol characterised by an increased contraction amplitude is particularly interesting (**Figure 36**). Since the beginning of the utilisation of organoid 3D models, attempts to increase their maturity and physiological, structural, and electrophysiological characteristics were made (Lyra-Leite et al. 2022). Interestingly, long-term pacing of the tissues is an approach widely accepted to improve physiological and contractile function of the tissue, via the improvement of myofibril organisation, sarcomere re-arrangement or even T-tubule maturation (Ruan et al. 2016; Ronaldson-Bouchard et al. 2018; Ronaldson-Bouchard et al. 2019).

Altogether, we demonstrated that the atrial chrimson EHM could be a suitable model to study acute and long term tachypacing induced electrical remodelling.

5 Limitations

Because atrial fibrillation (AF) is an evolving disease, and each development stage is associated with its own electrophysiological and structural characteristics, it is important to note that the models described could only be used for the study of acute and short-term remodelling associated with the development of atrial fibrillation.

The utilisation of atrial iPSC and atrial EHM models is associated with a certain number of limitations. It is known that cardiomyocytes derived from induced pluripotent stem cells (iPSC) represent an immature state of development (Goversen et al. 2018). The presence of a depolarising current conferring them a spontaneous beating activity is an obvious example of this. However, techniques have been investigated for the improvement of the maturity of iPSC derived cardiomyocytes and organoid constructs based on the utilisation of cardiomyocytes derived from iPSC during their development (Lyra-Leite et al. 2022) and should therefore be considered in the future for further investigation. Also, the action potential (AP) measurements in the UMGi014-C cell line showed short AP and a depolarised membrane potential in comparison to native human atrial tissue. This observation underlines the differences in ion channel expression and functioning between the two models. This could have potentially masked remodelling or modifications associated with the electrical pacing protocols: the detection of the impairment of an ion channel whose basal activity is already low is particularly challenging. Another iPSC line with more comparable electrophysiological properties to human native atria could be considered.

Susceptibility to develop arrhythmogenic episodes was only poorly investigated. The principal reason was the structure of the tissue itself. Preliminary investigations using the multi electrode array system showed that the measurement of the conduction velocity was not compatible with the apparition of re-entry mechanisms and the self-perpetuation of a depolarising wave, because of the too small size of the tissue.

Another limitation of this work is the lack of mechanism-based evidence for the electrical remodelling observed in our models. Although mRNA level measurements showed that the KCNJ5 mRNA level was reduced, no investigation on the protein levels and phosphorylation status of other key proteins involved in the AP generation was done. Likewise, phosphorylation status and expression levels of calcineurin and other key proteins involved in Ca²⁺ handling were not investigated.

6 Summary and outlook

The work of this thesis was articulated towards the development of two new models for the study of the electrical remodelling associated with atrial fibrillation. The first model was based on the utilisation of atrial cardiomyocytes derived from induced pluripotent stem cells (iPSC), and the second using the engineered human myocardium (EHM) technology. All along the project, the electrophysiological prism was used to investigate the potentials of these models.

This work started with the electrophysiological characterisation of the electrical remodelling in native human atrial tissue. The measurement of action potentials (AP) from patients suffering from chronic atrial fibrillation using the sharp-microelectrode technique helped us characterising hallmarks associated with electrical remodelling which is associated with the development of atrial fibrillation. It was characterised by an action potential shortening, resting membrane potential hyperpolarisation, and an impairment in the response to the atrial specific muscarinic-2 receptor agonist carbachol.

To continue, we installed an iPSC differentiation protocol in our lab, based on the utilisation of retinoic acid during the mesoderm induction to obtain atrial specific iPSC. Using voltage-clamp and optical dye techniques, we demonstrated that our atrial iPSC population showed an atrial specific electrophysiology. At the AP level, it was characterised by a reduced action potential duration (APD) compared to the ventricular population but also by the response to atrial specific carbachol, absent in our ventricular population. Moreover, using voltage-clamp techniques, we demonstrated that our atrial cell population was characterised by a lower $I_{Ca,L}$ and I_{K1} current density.

Next, we investigated whether electrical tachypacing protocols could be used to induce electrical remodelling in our atrial iPSC model. Results demonstrated that the utilisation of electrical tachypacing protocol resulted in the development of an electrical remodelling in atrial iPSC resembling the electrical remodelling observed in patients with persistent atrial fibrillation, characterised by a reduction of the APD, a reduction of $I_{Ca,L}$ and $I_{K,ACh}$ current densities, and the development

of an agonist independent and constitutively active $I_{K,ACh}$. Furthermore, we demonstrated that the electrical remodelling observed was Ca^{2+} -mediated, because the electrical remodelling induced by electrical tachypacing could not be reproduced when electrically tachypacing our atrial iPSC in low- Ca^{2+} concentration pacing medium.

Because the utilisation of a cellular model is associated with a certain number of limitations, we decided to continue exploring the possibilities of using atrial iPSC to investigate the electrical remodelling associated with the development of atrial fibrillation while integrating our cardiomyocytes into an organoid EHM model, and attempted to observe this electrical remodelling in a 3D model. We started with the generation of atrial and ventricular EHM with the cells previously mentioned and confirmed that they kept their electrophysiological properties after the incorporation in the EHM and after the maturation of the tissues. For this purpose, we used the sharp-microelectrode technique to measure AP in atrial and ventricular EHM, and confirmed the results obtained with the measurement of the optical action potential, i.e., a shorter AP in the atrial population. Furthermore, the ventricular model did not react to carbachol, whereas it was associated with a shortening of the AP and a hyperpolarisation of the resting membrane potential (RMP) in atrial tissues.

We continued with the investigation of the effects of 24-hour electrical tachypacing in our atrial EHM and showed that it resulted in an atrial fibrillation like electrophysiological remodelling characterised by a reduction of the APD. However, because of the deleterious effects of the electrical tachypacing, we could not extend the pacing protocol to longer duration and explore its long-term effects.

To address this difficulty, we explored the possibilities conferred by the utilisation of optogenetic tools to confer light sensitivity to our cells, and replace the electrical pulses with light stimulation pulses. Our first approach was based on the utilisation of an adeno-associated-virus-2 vector carrying a channelrhodopsin-2 (ChR2). Promising results were observed at the cellular level but also when integrated into tissues as both showed light sensitivity. However,

long-term introduction of the channelrhodopsin-2 resulted in an impairment of the normal electrophysiology, characterised by an alteration of the AP parameters. Nevertheless, the optical tachypacing of the tissues for 24 hours resulted in the apparition of a similar electrical remodelling as observed using the electrical pacing and characterised by a reduction of the APD. For all these reasons, we decided to change the method to bring light sensitivity to the tissues.

Thanks to the utilisation of a CRISPR/Cas modified iPSC line expressing a fast variant of the channelrhodopsin chrimson, we managed to tackle this difficulty. The fast (f)-chrimson variant is particularly of interest because of its red light shifted maximum response proprieties, and the interesting results in terms of cell viability demonstrated by the original publishing group. Using this new cell line, we first ensured that the utilisation of our differentiation protocol would provide us with cells showing atrial and ventricular phenotypes. We then generated atrial and ventricular chrimson EHM and using the sharp-microelectrode method, we showed that AP measured in atrial chrimson EHM were shorter than the AP measured in ventricular chrimson EHM and specifically responded to the atrial specific drug carbachol whereas this response was absent in the ventricular tissues.

To continue, we repeated the acute optical tachypacing protocol on our chrimson EHM and showed that 24-hour optical tachypacing was sufficient to induce electrical remodelling, characterised by a reduction of the APD. Furthermore, the extension of the protocol to 7 days did not only recapitulate the remodelling observed with the 24-hour protocol, but also induced a hyperpolarisation of the resting membrane potential, another hallmark of the electrical remodelling associated with the development of atrial fibrillation.

A couple of points could not be investigated during the time of this thesis and would be interesting to address in the future.

The susceptibility to arrhythmogenesis is a classical point assessed with the utilisation of pacing protocols. In our model, the generation of re-entrant circuits could not be investigated because of the small size of the tissue that was not compatible with the perpetuation of macro-arrhythmia. A possibility to overcome this difficulty could be to increase the size of the tissue.

Regarding the arrhythmogenicity assessment, we were using a one stimulation electrode method to trigger AP in tissues. Because the tissue is ring-shaped and the depolarisation wave travels simultaneously on opposite directions, the wavefront breaks on the other side of the tissue, making the probability to trigger re-entry extremely low. Using a system with two stimulation electrodes could be a way to improve the situation: a second pulse would be triggered right after the first one to break the depolarisation wavefront on one side and therefore allowing re-entries to happen.

Cellular experiments showed evidence that the electrical remodelling observed after a 24-hour electrical tachypacing was mediated by Ca^{2+} , but we did not clarify the role of Ca^{2+} in the electrical remodelling observed. Ca^{2+} /calcineurin kinase II (CaMKII) is a major protein kinase involved in the phosphorylation of proteins participating in the Ca^{2+} handling and the activity of ion channels involved in the AP. Verifying its activation status could be a potential lead for the explanation of the electrical remodelling observed.

Similarly, experiments showed that electrical remodelling was time dependant, and that RMP hyperpolarisation could only be observed after one week, whereas the impairment of $I_{K,ACH}$ could already be observed after 24 hours, suggesting that two distinct molecular mechanisms are involved. The RMP depends on the activity of the inward rectifier potassium channel responsible for I_{K1} , and its activity has been shown to be increased in the context of atrial fibrillation, because of the overexpression of its α -subunit Kir2.1. However, I_{K1} is also a known phosphorylation target of CaMKII. It would be interesting to investigate the participation of CaMKII in the RMP remodelling, and assess whether the modification of $I_{K,ACH}$, normally placed under the control of the different isoforms of the protein kinase C, is also a consequence of the activity of the CaMKII.

The electrical remodelling was the only aspect of the development of atrial fibrillation investigated along this work, however, *in vivo* studies using tachypacing protocols have demonstrated evidence for the development of a structural remodelling associated with tachypacing methods. Because structural

remodelling takes longer to be initiated, it would be interesting to explore this dimension using long-term optical pacing protocols.

Finally, we stopped the optical tachypacing protocol after 7 days, but Mager et al., at the origin of the the fast variant of the chrimson channelrhodopsin, reported that the activity of the channel was maintained in mouse for several months after the introduction (Mager et al. 2018). Furthermore, they did not report cell death because of the long-term introduction. It would be interesting to know whether the optical pacing protocol could be used for longer optical pacing periods and if so, to investigate the effects.

7 References

- Abriel H (2007): Roles and regulation of the cardiac sodium channel Nav1.5: Recent insights from experimental studies. *Cardiovasc Res* 76, 381–389
- Aguilar M, Nattel S (2016): The pioneering work of George Mines on cardiac arrhythmias: Groundbreaking ideas that remain influential in contemporary cardiac electrophysiology. *Journal of Physiology* 594, 2377–2386
- Airan RD, Thompson KR, Fenno LE, Bernstein H, Deisseroth K (2009): Temporally precise in vivo control of intracellular signalling. *Nature* 458, 1025–1029
- Akar FG, Spragg DD, Tunin RS, Kass DA, Tomaselli GF (2004): Mechanisms underlying conduction slowing and arrhythmogenesis in nonischemic dilated cardiomyopathy. *Circ Res* 95, 717–725
- Akar FG, Nass RD, Hahn S, Cingolani E, Shah M, Hesketh GG, DiSilvestre D, Tunin RS, Kass DA, Tomaselli GF (2007): Dynamic changes in conduction velocity and gap junction properties during development of pacing-induced heart failure. *Am J Physiol Heart Circ Physiol* 293
- Allessie M, Ausma J, Schotten U (2002): Electrical, contractile and structural remodeling during atrial fibrillation. *Cardiovasc Res* 54, 230–246
- Antzelevitch C, Nof E (2008): Brugada syndrome: Recent advances and controversies. *Curr Cardiol Rep* 10, 376–383
- Arrenberg AB, Stainier DYR, Baier H, Huisken J (2010): Optogenetic control of cardiac function. *Science* (1979) 330, 971–974
- Ausma J, Wijffels M, Thoné F, Wouters L, Allessie M, Borgers M (1997): Structural changes of atrial myocardium due to sustained atrial fibrillation in the goat. *Circulation* 96, 3157–3163
- Banyasz T, Koncz R, Fulop L, Szentandrassy N, Magyar J, Nanasi P (2005): Profile of I_{Ks} During the Action Potential Questions the Therapeutic Value of I_{Ks} Blockade. *Curr Med Chem* 11, 45–60
- Baroudi G, Pouliot V, Denjoy I, Guicheney P, Shrier A, Chahine M (2001): Novel Mechanism for Brugada Syndrome. *Circ Res* 88
- Baroudi G, Acharfi S, Larouche C, Chahine M (2002): Expression and Intracellular Localization of an *SCN5A* Double Mutant R1232W/T1620M Implicated in Brugada Syndrome. *Circ Res* 90
- Baruscotti M, Barbuti A, Bucchini A (2010): The cardiac pacemaker current. *J Mol Cell Cardiol* 48, 55–64
- Bauer A, McDonald AD, Donahue JK (2004): Pathophysiological findings in a model of persistent atrial fibrillation and severe congestive heart failure. *Cardiovasc Res* 61, 764–770
- Benito B, Brugada R, Perich RM, Lizotte E, Cinca J, Mont L, Berruezo A, Tolosana JM, Freixa X, Brugada P, Brugada J (2008): A mutation in the sodium channel is responsible for the association of long QT syndrome and familial atrial fibrillation. *Heart Rhythm* 5, 1434–1440

- Berger T, Senn W, Lüscher HR (2003): Hyperpolarization-activated current Ih disconnects somatic and dendritic spike initiation zones in layer V pyramidal neurons. *J Neurophysiol* 90, 2428–2437
- Bers DM (2002): Cardiac excitation-contraction coupling. *Nature* 415, 198–205
- Borrego J, Feher A, Jost N, Panyi G, Varga Z, Papp F (2021): Peptide inhibitors of kv1.5: An option for the treatment of atrial fibrillation. *Pharmaceuticals* 14, 1303
- Bosch RF, Gaspo R, Busch AE, Lang HJ, Li GR, Nattel S (1998): Effects of the chromanol 293B, a selective blocker of the slow, component of the delayed rectifier K⁺ current, on repolarization in human and guinea pig ventricular myocytes. *Cardiovasc Res* 38, 441–450
- Bosch RF, Zeng X, Grammer JB, Popovic K, Mewis C, Köhlkamp V (1999): Ionic mechanisms of electrical remodeling in human atrial fibrillation. *Cardiovasc Res* 44, 121–131
- Bouwmeester S, van Loon T, Ploeg M, Mast TP, Verzaal NJ, van Middendorp LB, Strik M, van Nieuwenhoven FA, Dekker LR, Prinzen FW, et al. (2022): Left atrial remodeling in mitral regurgitation: A combined experimental-computational study. *PLoS One* 17, e0271588
- Bruegmann T, Malan D, Hesse M, Beiert T, Fuegeman CJ, Fleischmann BK, Sasse P (2010): Optogenetic control of heart muscle in vitro and in vivo. *Nat Methods* 7, 897–900
- Bruegmann T, Beiert T, Vogt CC, Schrickel JW, Sasse P (2018): Optogenetic termination of atrial fibrillation in mice. *Cardiovasc Res* 114, 713–723
- Brundel BJM, van Gelder IC, Henning RH, Tuinenburg AE, Deelman LE, Tieleman RG, Grandjean JG, van Gilst WH, Crijns HJGM (1999): Gene expression of proteins influencing the calcium homeostasis in patients with persistent and paroxysmal atrial fibrillation. *Cardiovasc Res* 42, 443–454
- Bryant SM, Wan X, Shipsey SJ, Hart G (1998): Regional differences in the delayed rectifier current (I(Kr) and I(Ks)) contribute to the differences in action potential duration in basal left ventricular myocytes in guinea-pig. *Cardiovasc Res* 40, 322–331
- Burashnikov A (2017): Late I_{Na} Inhibition as an Antiarrhythmic Strategy. *J Cardiovasc Pharmacol* 70, 159–167
- Calderone V, Testai L, Martinotti E, del Tacca M, Breschi MC (2010): Drug-induced block of cardiac HERG potassium channels and development of torsade de pointes arrhythmias: the case of antipsychotics. *Journal of Pharmacy and Pharmacology* 57, 151–161
- Calloe K, Nof E, Jespersen T, di Diego JM, Chlus N, Olesen SØP, Antzelevitch C, Cordeiro JM (2011): Comparison of the effects of a transient outward potassium channel activator on currents recorded from atrial and ventricular cardiomyocytes. *J Cardiovasc Electrophysiol* 22, 1057–1066
- Cheng KP, Kiernan EA, Eliceiri KW, Williams JC, Watters JJ (2016): Blue Light Modulates Murine Microglial Gene Expression in the Absence of Optogenetic Protein Expression. *Sci Rep* 6

- Christ T, Wettwer E, Voigt N, Hála O, Radicke S, Matschke K, Várro A, Dobrev D, Ravens U (2008): Pathology-specific effects of the $I_{Kur}/I_{to}/I_{K,ACh}$ blocker AVE0118 on ion channels in human chronic atrial fibrillation. *Br J Pharmacol* 154, 1619–1630
- Christophersen IE, Olesen MS, Liang B, Andersen MN, Larsen AP, Nielsen JB, Haunsø S, Olesen S-P, Tveit A, Svendsen JH, Schmitt N (2013): Genetic variation in KCNA5: impact on the atrial-specific potassium current I_{Kur} in patients with lone atrial fibrillation. *Eur Heart J* 34, 1517–1525
- Chu Y, Yang Q, Ren L, Yu S, Liu Z, Chen Y, Wei X, Huang S, Song L, Zhang P, et al. (2020): Late Sodium Current in Atrial Cardiomyocytes Contributes to the Induced and Spontaneous Atrial Fibrillation in Rabbit Hearts. *J Cardiovasc Pharmacol* 76, 437–444
- Citerni C, Kirchhoff J, Olsen LH, Sattler SM, Gentilini F, Forni M, Zannoni A, Grunnet M, Edvardsson N, Bentzen BH, Diness JG (2020): Characterization of Atrial and Ventricular Structural Remodeling in a Porcine Model of Atrial Fibrillation Induced by Atrial Tachypacing. *Front Vet Sci* 7, 179
- Clauss S, Bleyer C, Schüttler D, Tomsits P, Renner S, Klymiuk N, Wakili R, Massberg S, Wolf E, Kääh S (2019): Animal models of arrhythmia: classic electrophysiology to genetically modified large animals. *Nat Rev Cardiol* 16, 457–475
- Colman MA, Saxena P, Kettlewell S, Workman AJ (2018): Description of the Human Atrial Action Potential Derived From a Single, Congruent Data Source: Novel Computational Models for Integrated Experimental-Numerical Study of Atrial Arrhythmia Mechanisms. *Front Physiol* 9, 1211
- Corey S, Krapivinsky G, Krapivinsky L, Clapham DE (1998): Number and stoichiometry of subunits in the native atrial G-protein-gated K^+ channel, $I(K_{ACh})$. *Journal of Biological Chemistry* 273, 5271–5278
- Cyganek L, Tiburcy M, Sekeres K, Gerstenberg K, Bohnenberger H, Lenz C, Henze S, Stauske M, Salinas G, Zimmermann WH, et al. (2018): Deep phenotyping of human induced pluripotent stem cell-derived atrial and ventricular cardiomyocytes. *JCI Insight* 3
- Darbar D, Kannankeril PJ, Donahue BS, Kucera G, Stubblefield T, Haines JL, George AL, Roden DM (2008): Cardiac sodium channel (SCN5A) variants associated with atrial fibrillation. *Circulation* 117, 1927–1935
- Deisseroth K, Feng G, Majewska AK, Miesenböck G, Ting A, Schnitzer MJ: Next-generation optical technologies for illuminating genetically targeted brain circuits. In: *Journal of Neuroscience*. Band 26; Society for Neuroscience 2006, 10380–10386
- DiFrancesco D (1981): A study of the ionic nature of the pace-maker current in calf Purkinje fibres. *J Physiol* 314, 377–393
- Dobrev D, Wettwer E, Kortner A, Knaut M, Schüler S, Ravens U (2002): Human inward rectifier potassium channels in chronic and postoperative atrial fibrillation. *Cardiovasc Res* 54, 397–404

- Dobrev D, Friedrich A, Voigt N, Jost N, Wettwer E, Christ T, Knaut M, Ravens U (2005): The G protein-gated potassium current $I_{K,ACh}$ is constitutively active in patients with chronic atrial fibrillation. *Circulation* 112, 3697–3706
- El-Kholy W, MacDonald PE, Fox JM, Bhattacharjee A, Xue T, Gao X, Zhang Y, Stieber J, Li RA, Tsushima RG, Wheeler MB (2007): Hyperpolarization-activated cyclic nucleotide-gated channels in pancreatic β -cell. *Molecular Endocrinology* 21, 753–764
- Ellinor PT, Nam EG, Shea MA, Milan DJ, Ruskin JN, MacRae CA (2008): Cardiac sodium channel mutation in atrial fibrillation. *Heart Rhythm* 5, 99–105
- Entcheva E (2013): Cardiac optogenetics. *Am J Physiol Heart Circ Physiol* 304
- Ernst OP, Lodowski DT, Elstner M, Hegemann P, Brown LS, Kandori H (2014): Microbial and animal rhodopsins: Structures, functions, and molecular mechanisms. *Chem Rev* 114, 126–163
- Everett IV TH, Li H, Mangrum JM, McRury ID, Mitchell MA, Redick JA, Haines DE (2000): Electrical, morphological, and ultrastructural remodeling and reverse remodeling in a canine model of chronic atrial fibrillation. *Circulation* 102, 1454–1460
- Fakuade FE, Steckmeister V, Seibertz F, Gronwald J, Kestel S, Menzel J, Pronto JRD, Taha K, Haghighi F, Kensah G, et al. (2021): Altered atrial cytosolic calcium handling contributes to the development of postoperative atrial fibrillation. *Cardiovasc Res* 117, 1790–1801
- Freeman J v., Simon DN, Go AS, Spertus J, Fonarow GC, Gersh BJ, Hylek EM, Kowey PR, Mahaffey KW, Thomas LE, et al. (2015): Association Between Atrial Fibrillation Symptoms, Quality of Life, and Patient Outcomes. *Circ Cardiovasc Qual Outcomes* 8, 393–402
- Fuller CM, Howard MB, Bedwell DM, Frizzell RA, Benos DJ (1992): Antibodies against the cystic fibrosis transmembrane regulator. *Am J Physiol Cell Physiol* 262
- Gaspo R (1999): The tachycardia-induced dog model of atrial fibrillation clinical relevance and comparison with other models. *J Pharmacol Toxicol Methods* 42, 11–20
- Gassanov N, Er F, Zagidullin N, Jankowski M, Gutkowska J, Hoppe UC (2008): Retinoid acid-induced effects on atrial and pacemaker cell differentiation and expression of cardiac ion channels. *Differentiation* 76, 971–980
- Gintant GA (2000): Characterization and functional consequences of delayed rectifier current transient in ventricular repolarization. *Am J Physiol Heart Circ Physiol* 278
- Girmatsion Z, Biliczki P, Bonauer A, Wimmer-Greinecker G, Scherer M, Moritz A, Bukowska A, Goette A, Nattel S, Hohnloser SH, Ehrlich JR (2009): Changes in microRNA-1 expression and I_{K1} up-regulation in human atrial fibrillation. *Heart Rhythm* 6, 1802–1809
- Godley BF, Shamsi FA, Liang FQ, Jarrett SG, Davies S, Boulton M (2005): Blue light induces mitochondrial DNA damage and free radical production in epithelial cells. *Journal of Biological Chemistry* 280, 21061–21066

- Goette A, Honeycutt C, Langberg JJ (1996): Electrical remodeling in atrial fibrillation: Time course and mechanisms. *Circulation* 94, 2968–2974
- Goette A, Staack T, Röcken C, Arndt M, Geller JC, Huth C, Ansorge S, Klein HU, Lendeckel U (2000): Increased expression of extracellular signal-regulated kinase and angiotensin-converting enzyme in human atria during atrial fibrillation. *J Am Coll Cardiol* 35, 1669–1677
- Goldin AL, Barchi RL, Caldwell JH, Hofmann F, Howe JR, Hunter JC, Kallen RG, Mandel G, Meisler MH, Netter YB, et al. (2000): Nomenclature of voltage-gated sodium channels. *Neuron* 28, 365–368
- Goversen B, van der Heyden MAG, van Veen TAB, de Boer TP (2018): The immature electrophysiological phenotype of iPSC-CMs still hampers in vitro drug screening: Special focus on IK1. *Pharmacol Ther* 183, 127–136
- Govorunova EG, Sineshchekov OA, Li H, Spudich JL (2017): Microbial rhodopsins: Diversity, mechanisms, and optogenetic applications. *Annu Rev Biochem* 86, 845–872
- Grandi E, Pandit S v., Voigt N, Workman AJ, Dobrev D, Jalife J, Bers DM (2011): Human atrial action potential and Ca²⁺ model: Sinus rhythm and chronic atrial fibrillation. *Circ Res* 109, 1055–1066
- Greenwood IA, Prestwich SA (2002): Characteristics of hyperpolarization-activated cation currents in portal vein smooth muscle cells. *Am J Physiol Cell Physiol* 282
- Grune T, Ott C, Häseli S, Höhn A, Jung T (2019): The “MYOCYTER” – Convert cellular and cardiac contractions into numbers with ImageJ. *Sci Rep* 9, 1–13
- Gu K, Qian D, Qin H, Cui C, Fernando WCHA, Wang D, Wang J, Cao K, Chen M (2021): A novel mutation in KCNH2 yields loss-of-function of hERG potassium channel in long QT syndrome 2. *Pflugers Arch* 473, 219–229
- Guichard JB, Xiong F, Qi XY, L’Heureux N, Hiram R, Xiao J, Naud P, Tardif JC, da Costa A, Nattel S (2021): Role of atrial arrhythmia and ventricular response in atrial fibrillation induced atrial remodelling. *Cardiovasc Res* 117, 462–471
- Gunaga P, Lloyd J, Mummadi S, Banerjee A, Dhondi NK, Hennan J, Subray V, Jayaram R, Rajugowda N, Umamaheshwar Reddy K, et al. (2017): Selective I_{Kur} Inhibitors for the Potential Treatment of Atrial Fibrillation: Optimization of the Phenyl Quinazoline Series Leading to Clinical Candidate 5-[5-Phenyl-4-(pyridin-2-ylmethylamino)quinazolin-2-yl]pyridine-3-sulfonamide. *J Med Chem* 60, 3795–3803
- Hancox JC, McPate MJ, el Harchi A, Zhang Y hong (2008): The hERG potassium channel and hERG screening for drug-induced torsades de pointes. *Pharmacol Ther* 119, 118–132
- Haraguchi Y, Ohtsuki A, Oka T, Shimizu T (2015): Electrophysiological analysis of mammalian cells expressing hERG using automated 384-well-patch-clamp. *BMC Pharmacol Toxicol* 16

- Hashimoto N, Yamashita T, Tsuruzoe N (2006): Tertiapin, a selective $I_{K_{ACH}}$ blocker, terminates atrial fibrillation with selective atrial effective refractory period prolongation. *Pharmacol Res* 54, 136–141
- Heijman J, Voigt N, Wehrens XHT, Dobrev D (2014): Calcium dysregulation in atrial fibrillation: the role of CaMKII. *Front Pharmacol* 5, 30
- Heijman J, Kirchner D, Kunze F, Chrétien EM, Michel-Reher MB, Voigt N, Knaut M, Michel MC, Ravens U, Dobrev D (2018): Muscarinic type-1 receptors contribute to $I_{K_{ACH}}$ in human atrial cardiomyocytes and are upregulated in patients with chronic atrial fibrillation. *Int J Cardiol* 255, 61–68
- Hindricks G, Potpara T, Dagres N, Arbelo E, Bax JJ, Blomström-Lundqvist C, Boriani G, Castella M, Dan G-A, Dilaveris PE, et al. (2021): 2020 ESC Guidelines for the diagnosis and management of atrial fibrillation developed in collaboration with the European Association for Cardio-Thoracic Surgery (EACTS). *Eur Heart J* 42, 373–498
- Hochgreb T, Linhares VL, Menezes DC, Sampaio AC, Yan CYI, Cardoso W v., Rosenthal N, Xavier-Neto J (2003): A caudorostral wave of RALDH2 conveys anteroposterior information to the cardiac field. *Development* 130, 5363–5374
- Hoeker GS, Skarsfeldt MA, Jespersen T, Poelzing S (2017): Electrophysiologic effects of the I_{K1} inhibitor PA-6 are modulated by extracellular potassium in isolated guinea pig hearts. *Physiol Rep* 5
- Huang W, Zhou Y, Wang J, Jiang C, Zhang Y, Zhou R (2022): Generation of two heterozygous GAA mutation-carrying human induced pluripotent stem cell lines (XACHi005-A, XACHi006-A) from parents of an infant with Pompe disease. *Stem Cell Res* 64
- Imredy JP, Penniman JR, Dech SJ, Irving WD, Salata JJ (2008): Modeling of the adrenergic response of the human I_{Ks} current (hKCNQ1/hKCNE1) stably expressed in HEK-293 cells. *American Journal of Physiology-Heart and Circulatory Physiology* 295, H1867–H1881
- Isom LL, de Jongh KS, Patton DE, Reber BFX, Offord J, Charbonneau H, Walsh K, Goldin AL, Catterall WA (1992): Primary structure and functional expression of the $\beta 1$ subunit of the rat brain sodium channel. *Science* (1979) 256, 839–842
- Isom LL, Ragsdale DS, de Jongh KS, Westenbroek RE, Reber BFX, Scheuer T, Catterall WA (1995): Structure and function of the $\beta 2$ subunit of brain sodium channels, a transmembrane glycoprotein with a CAM motif. *Cell* 83, 433–442
- Jebran AF, Tiburcy M, Biermann D, Balfanz P, Didié M, Karikkineth BC, Schöndube F, Kutschka I, Zimmermann WH (2022): Transmural myocardial repair with engineered heart muscle in a rat model of heterotopic heart transplantation – A proof-of-concept study. *J Mol Cell Cardiol* 168, 3–12
- Jiang D, Shi H, Tonggu L, Gamal El-Din TM, Lenaeus MJ, Zhao Y, Yoshioka C, Zheng N, Catterall WA (2020): Structure of the Cardiac Sodium Channel. *Cell* 180, 122-134.e10

- Jing R, Scarfo I, Najia MA, Lummertz da Rocha E, Han A, Sanborn M, Bingham T, Kubaczka C, Jha DK, Falchetti M, et al. (2022): EZH1 repression generates mature iPSC-derived CAR T cells with enhanced antitumor activity. *Cell Stem Cell* 29, 1181-1196.e6
- Jost N, Virág L, Bitay M, Takács J, Lengyel C, Biliczki P, Nagy Z, Bogáts G, Lathrop DA, Papp JG, Varró A (2005): Restricting excessive cardiac action potential and QT prolongation: A vital role for I_{Ks} in human ventricular muscle. *Circulation* 112, 1392–1399
- Jun NY, Cardin JA (2020): Activation of distinct channelrhodopsin variants engages different patterns of network activity. *eNeuro* 7
- Kaneko S (2022): Successful organoid-mediated generation of iPSC-derived CAR-T cells. *Cell Stem Cell* 29, 493–495
- Kang C, Qiao Y, Li G, Baechle K, Camelliti P, Rentschler S, Efimov IR (2016): Human Organotypic Cultured Cardiac Slices: New Platform For High Throughput Preclinical Human Trials. *Sci Rep* 6
- Kato HE, Zhang F, Yizhar O, Ramakrishnan C, Nishizawa T, Hirata K, Ito J, Aita Y, Tsukazaki T, Hayashi S, et al. (2012): Crystal structure of the channelrhodopsin light-gated cation channel. *Nature* 482, 369–374
- Kensah G, Gruh I, Viering J, Schumann H, Dahlmann J, Meyer H, Skvorc D, Bär A, Akhyari P, Heisterkamp A, et al. (2011): A novel miniaturized multimodal bioreactor for continuous in situ assessment of bioartificial cardiac tissue during stimulation and maturation. *Tissue Eng Part C Methods* 17, 463–473
- Klapoetke NC, Murata Y, Kim SS, Pulver SR, Birdsey-Benson A, Cho YK, Morimoto TK, Chuong AS, Carpenter EJ, Tian Z, et al. (2014): Independent optical excitation of distinct neural populations. *Nat Methods* 11, 338–346
- Klapper-Goldstein H, Murninkas M, Gillis R, Mulla W, Levanon E, Elyagon S, Schuster R, Danan D, Cohen H, Etzion Y (2020): An implantable system for long-term assessment of atrial fibrillation substrate in unanesthetized rats exposed to underlying pathological conditions. *Sci Rep* 10, 1–12
- Koncz I, Verkerk AO, Nicastro M, Wilders R, Árpádfy-Lovas T, Magyar T, Tóth N, Nagy N, Madrid M, Lin Z, Efimov IR (2022): Acetylcholine Reduces I_{Kr} and Prolongs Action Potentials in Human Ventricular Cardiomyocytes. *Biomedicines* 10
- Kostin S, Klein G, Szalay Z, Hein S, Bauer EP, Schaper J (2002): Structural correlate of atrial fibrillation in human patients. *Cardiovasc Res* 54, 361–379
- Kovoor P, Wickman K, Maguire CT, Pu W, Gehrman J, Berul CI, Clapham DE (2001): Evaluation of the role of I_{KACH} in atrial fibrillation using a mouse knockout model. *J Am Coll Cardiol* 37, 2136–2143
- Krapivinsky G, Gordon EA, Wickman K, Velimirović B, Krapivinsky L, Clapham DE (1995): The G-protein-gated atrial K^+ channel I_{KACH} is a heteromultimer of two inwardly rectifying K^+ -channel proteins. *Nature* 374, 135–141
- Krummen DE, Swarup V, Narayan SM (2015): The role of rotors in atrial fibrillation. *J Thorac Dis* 7, 142–151

- Kumagai K, Ogawa M, Noguchi H, Yasuda T, Nakashima H, Saku K (2004): Electrophysiologic properties of pulmonary veins assessed using a multielectrode basket catheter. *J Am Coll Cardiol* 43, 2281–2289
- Lagali PS, Balya D, Awatramani GB, Münch TA, Kim DS, Buszkamp V, Cepko CL, Roska B (2008): Light-activated channels targeted to ON bipolar cells restore visual function in retinal degeneration. *Nat Neurosci* 11, 667–675
- Lane JD, Tinker A (2017): Have the findings from clinical risk prediction and trials any key messages for safety pharmacology? *Front Physiol* 8, 890
- Lemme M, Braren I, Prondzynski M, Aksehirlioglu B, Ulmer BM, Schulze ML, Ismaili D, Meyer C, Hansen A, Christ T, et al. (2020): Chronic intermittent tachypacing by an optogenetic approach induces arrhythmia vulnerability in human engineered heart tissue. *Cardiovasc Res* 116, 1487–1499
- Lemoine MD, Lemme M, Ulmer BM, Braren I, Krasemann S, Hansen A, Kirchhof P, Meyer C, Eschenhagen T, Christ T (2020): Intermittent Optogenetic Tachypacing of Atrial Engineered Heart Tissue Induces Only Limited Electrical Remodelling. *J Cardiovasc Pharmacol* 77, 291–299
- Lemoine MD, Lemme M, Ulmer BM, Braren I, Krasemann S, Hansen A, Kirchhof P, Meyer C, Eschenhagen T, Christ T (2021): Intermittent Optogenetic Tachypacing of Atrial Engineered Heart Tissue Induces Only Limited Electrical Remodelling. *J Cardiovasc Pharmacol* 77, 291–299
- Lengyel C, Iost N, Virág L, Varró A, Lathrop DA, Papp JG (2001): Pharmacological block of the slow component of the outward delayed rectifier current (I_{Ks}) fails to lengthen rabbit ventricular muscle QTc and action potential duration. *Br J Pharmacol* 132, 101–110
- Lévy S, Hartikainen J, Ritz B, Juhlin T, Carbajosa-Dalmau J, Domanovits H (2021): Vernakalant for Rapid Cardioversion of Recent-Onset Atrial Fibrillation: Results from the SPECTRUM Study. *Cardiovasc Drugs Ther* 35, 283–292
- Li D, Fareh S, Leung TK, Nattel S (1999): Promotion of Atrial Fibrillation by Heart Failure in Dogs. *Circulation* 100, 87–95
- Li Q, Ni RR, Hong H, Goh KY, Rossi M, Fast VG, Zhou L (2017): Electrophysiological Properties and Viability of Neonatal Rat Ventricular Myocyte Cultures with Inducible ChR2 Expression. *Sci Rep* 7
- Lin JY, Lin MZ, Steinbach P, Tsien RY (2009): Characterization of engineered channelrhodopsin variants with improved properties and kinetics. *Biophys J* 96, 1803–14
- Lin JY, Knutsen PM, Muller A, Kleinfeld D, Tsien RY (2013): ReaChR: A red-shifted variant of channelrhodopsin enables deep transcranial optogenetic excitation. *Nat Neurosci* 16, 1499–1508
- Liu DW, Antzelevitch C (1995): Characteristics of the delayed rectifier current (I_{Kr} and I_{Ks}) in canine ventricular epicardial, midmyocardial, and endocardial myocytes: A weaker I_{Ks} contributes to the longer action potential of the M cell. *Circ Res* 76, 351–365

- Liu DW, Gintant GA, Antzelevitch C (1993): Ionic bases for electrophysiological distinctions among epicardial, midmyocardial, and endocardial myocytes from the free wall of the canine left ventricle. *Circ Res* 72, 671–687
- Liu Q, Sun J, Dong Y, Li P, Wang J, Wang Y, Xu Y, Tian X, Wu B, He P, et al. (2022): Tetramisole is a new I_{K1} channel agonist and exerts I_{K1} -dependent cardioprotective effects in rats. *Pharmacol Res Perspect* 10, e00992
- Loose S, Mueller J, Wettwer E, Knaut M, Ford J, Milnes J, Ravens U (2014): Effects of I_{Kur} blocker MK-0448 on human right atrial action potentials from patients in sinus rhythm and in permanent atrial fibrillation. *Front Pharmacol* 5 MAR
- Lubitz SA, Benjamin EJ, Ellinor PT (2010): Atrial Fibrillation in Congestive Heart Failure. *Heart Fail Clin* 6, 187–200
- Lundby A, Ravn LS, Svendsen JH, Haunsø S, Olesen SP, Schmitt N (2008): KCNE3 mutation V17M identified in a patient with lone atrial fibrillation. *Cellular Physiology and Biochemistry* 21, 47–54
- Luo X, Pan Z, Shan H, Xiao J, Sun X, Wang N, Lin H, Xiao L, Maguy A, Qi XY, et al. (2013): MicroRNA-26 governs profibrillatory inward-rectifier potassium current changes in atrial fibrillation. *Journal of Clinical Investigation* 123, 1939–1951
- Lyra-Leite DM, Gutiérrez-Gutiérrez Ó, Wang M, Zhou Y, Cyganek L, Burridge PW (2022): A review of protocols for human iPSC culture, cardiac differentiation, subtype-specification, maturation, and direct reprogramming. *STAR Protoc* 3, 101560
- Mager T, Morena DLD Ia, Senn V, Schlotte J, Derrico A, Feldbauer K, Wrobel C, Jung S, Bodensiek K, Rankovic V, et al. (2018): High frequency neural spiking and auditory signaling by ultrafast red-shifted optogenetics. *Nat Commun* 9
- Maier SKG, Westenbroek RE, Yamanushi TT, Dobrzynski H, Boyett MR, Catterall WA, Scheuer T (2003): An unexpected requirement for brain-type sodium channels for control of heart rate in the mouse sinoatrial node. *Proc Natl Acad Sci U S A* 100, 3507–3512
- Makary S, Voigt N, Maguy A, Wakili R, Nishida K, Harada M, Dobrev D, Nattel S (2011): Differential protein kinase c isoform regulation and increased constitutive activity of acetylcholine-regulated potassium channels in atrial remodeling. *Circ Res* 109, 1031–1043
- Makiyama T, Akao M, Shizuta S, Doi T, Nishiyama K, Oka Y, Ohno S, Nishio Y, Tsuji K, Itoh H, et al. (2008): A Novel SCN5A Gain-of-Function Mutation M1875T Associated With Familial Atrial Fibrillation. *J Am Coll Cardiol* 52, 1326–1334
- Marban E, Yamagishi T, Tomaselli GF (1998): Structure and function of voltage-gated sodium channels. *J Physiol* 508, 647–657
- Melillo E, Rago A, Proietti R, Attena E, Carrella M, Golino P, D’Onofrio A, Nigro G, Russo V (2020): Atrial Fibrillation and Mitral Regurgitation: Clinical

- Performance of Direct Oral Anticoagulants in a Real-World Setting. *J Cardiovasc Pharmacol Ther* 25, 564–569
- Mellor GJ, Panwar P, Lee AK, Steinberg C, Hathaway JA, Bartels K, Christian S, Balaji S, Roberts JD, Simpson CS, et al. (2019): Type 8 long QT syndrome: Pathogenic variants in CACNA1C-encoded Cav1.2 cluster in STAC protein binding site. *Europace* 21, 1725–1732
- Mesirca P, Marger L, Toyoda F, Rizzetto R, Audoubert M, Dubel S, Torrente AG, DiFrancesco ML, Muller JC, Leoni AL, et al. (2013): The G-protein-gated K⁺ channel, I_{KACH}, is required for regulation of pacemaker activity and recovery of resting heart rate after sympathetic stimulation. *Journal of General Physiology* 142, 113–126
- Mesubi OO, Rokita AG, Abrol N, Wu Y, Chen B, Wang Q, Granger JM, Tucker-Bartley A, Luczak ED, Murphy KR, et al. (2021): Oxidized CaMKII and O-GlcNAcylation cause increased atrial fibrillation in diabetic mice by distinct mechanisms. *Journal of Clinical Investigation* 131
- Morgan K, Stevens EB, Shah B, Cox PJ, Dixon AK, Lee K, Pinnock RD, Hughes J, Richardson PJ, Mizuguchi K, Jackson AP (2000): $\beta 3$: An additional auxiliary subunit of the voltage-sensitive sodium channel that modulates channel gating with distinct kinetics. *Proc Natl Acad Sci U S A* 97, 2308–2313
- Morillo CA, Klein GJ, Jones DL, Guiraudon CM (1995): Chronic rapid atrial pacing: Structural, functional, and electrophysiological characteristics of a new model of sustained atrial fibrillation. *Circulation* 91, 1588–1595
- Mulla W, Hajaj B, Elyagon S, Mor M, Gillis R, Murninkas M, Klapper-Goldstein H, Plaschkes I, Chalifa-Caspi V, Etzion S, Etzion Y (2019): Rapid Atrial Pacing Promotes Atrial Fibrillation Substrate in Unanesthetized Instrumented Rats. *Front Physiol* 10, 1218
- Müller M, Bamann C, Bamberg E, Kühlbrandt W (2011): Projection structure of channelrhodopsin-2 at 6 Å resolution by electron crystallography. *J Mol Biol* 414, 86–95
- Murphy MB, Kim K, Kannankeril PJ, Subati T, van Amburg JC, Barnett J v., Murray KT (2022): Optimizing transesophageal atrial pacing in mice to detect atrial fibrillation. *Am J Physiol Heart Circ Physiol* 322, H36–H43
- Nagel G, Ollig D, Fuhrmann M, Kateriya S, Musti AM, Bamberg E, Hegemann P (2002): Channelrhodopsin-1: A light-gated proton channel in green algae. *Science* (1979) 296, 2395–2398
- Nagel G, Szellas T, Huhn W, Kateriya S, Adeishvili N, Berthold P, Ollig D, Hegemann P, Bamberg E (2003): Channelrhodopsin-2, a directly light-gated cation-selective membrane channel. *Proc Natl Acad Sci U S A* 100, 13940–13945
- Nánási PP, Horváth B, Tar F, Almássy J, Szentandrassy N, Jost N, Baczkó I, Bányász T, Varró A (2021): Canine myocytes represent a good model for human ventricular cells regarding their electrophysiological properties. *Pharmaceuticals* 14

- Nattel S, Burstein B, Dobrev D (2008): Atrial remodeling and atrial fibrillation: mechanisms and implications. *Circ Arrhythm Electrophysiol* 1, 62–73
- Nattel S, Xiong F, Aguilar M (2017): Demystifying rotors and their place in clinical translation of atrial fibrillation mechanisms. *Nat Rev Cardiol* 14, 509–520
- Ni H, Zhang H, Grandi E, Narayan SM, Giles WR (2019): Transient outward K⁺ current can strongly modulate action potential duration and initiate alternans in the human atrium. *Am J Physiol Heart Circ Physiol* 316, H527–H542
- Nielsen MW, Olesen MS, Refsgaard L, Haunsø S, Svendsen JH (2013): Screening of the I_{to} regulatory subunit Klf15 in patients with early-onset lone atrial fibrillation. *Front Genet* 4
- Nyns ECA, Jin T, Fontes MS, van den Heuvel T, Portero V, Ramsey C, Bart CI, Zeppenfeld K, Schalij MJ, van Brakel TJ, et al. (2022): Optical ventricular cardioversion by local optogenetic targeting and LED implantation in a cardiomyopathic rat model. *Cardiovasc Res* 118, 2293–2303
- Olesen MS, Yuan L, Liang B, Hols AG, Nielsen N, Nielsen JB, Hedley PL, Christiansen M, Olesen SP, Haunsø S, et al. (2012): High prevalence of long QT syndrome-associated SCN5A variants in patients with early-onset lone atrial fibrillation. *Circ Cardiovasc Genet* 5, 450–459
- Olesen MS, Refsgaard L, Holst AG, Larsen AP, Grubb S, Haunsø S, Svendsen JH, Olesen S-P, Schmitt N, Calloe K (2013): A novel KCND3 gain-of-function mutation associated with early-onset of persistent lone atrial fibrillation. *Cardiovasc Res* 98, 488–495
- Olson TM, Alekseev AE, Liu XK, Park S, Zingman L v., Bienengraeber M, Sattiraju S, Ballew JD, Jahangir A, Terzic A (2006): Kv1.5 channelopathy due to KCNA5 loss-of-function mutation causes human atrial fibrillation. *Hum Mol Genet* 15, 2185–2191
- Opačić D, van Hunnik A, Zeemering S, Dhalla A, Belardinelli L, Schotten U, Verheule S (2021): Electrophysiological effects of ranolazine in a goat model of lone atrial fibrillation. *Heart Rhythm* 18, 615–622
- Ortner NJ, Striessnig J (2016): L-type calcium channels as drug targets in CNS disorders. *Channels* 10, 7–13
- Oudit GY, Kassiri Z, Sah R, Ramirez RJ, Zobel C, Backx PH (2001): The molecular physiology of the cardiac transient outward potassium current (I_{to}) in normal and diseased myocardium. *J Mol Cell Cardiol* 33, 851–872
- Pan CH, Lin JL, Lai LP, Chen CL, Stephen Huang SK, Lin CS (2007): Downregulation of angiotensin converting enzyme II is associated with pacing-induced sustained atrial fibrillation. *FEBS Lett* 581, 526–534
- Pandit L, Malli C, D’Cunha A, Sudhir A (2021): Overcoming the challenges in diagnosis of AQP4-IgG positive neuromyelitis optica spectrum disorders in resource poor settings using an indigenized and cost effective cell based assay. *J Neuroimmunol* 360
- Parikh J, Gurev V, Rice JJ (2017): Novel Two-Step Classifier for Torsades de Pointes Risk Stratification from Direct Features. *Front Pharmacol* 8, 816

- Parvez B, Darbar D (2010): Lone AF – Etiologic Factors and Genetic Insights into Pathophysiology. *J Atr Fibrillation* 3
- Pelliccia F, Cecchi F, Olivotto I, Camici PG (2022): Microvascular Dysfunction in Hypertrophic Cardiomyopathy. *J Clin Med* 11, 6560
- Peper J, Kownatzki-Danger D, Weninger G, Seibertz F, Pronto JRD, Sutanto H, Pacheu-Grau D, Hindmarsh R, Brandenburg S, Kohl T, et al. (2021): Caveolin3 Stabilizes McT1-Mediated Lactate/Proton Transport in Cardiomyocytes. *Circ Res* 128, e102–e120
- Pond AL, Scheve BK, Benedict AT, Petrecca K, van Wagoner DR, Shrier A, Nerbonne JM (2000): Expression of distinct ERG proteins in rat, mouse, and human heart. Relation to functional I(Kr) channels. *Journal of Biological Chemistry* 275, 5997–6006
- Power JM, Beacom GA, Alferness CA, Raman J, Wijffels M, Farish SJ, Burrell LM, Tonkin AM (1998): Susceptibility to atrial fibrillation: A study in an ovine model of pacing-induced early heart failure. *J Cardiovasc Electrophysiol* 9, 423–435
- Printemps R, Salvétat C, Faivre J, Grand M le, Bois P, Moha ou Maati H (2019): Role of Cardiac I_{Ks} Current in Repolarization Reserve Process During Late Sodium Current (I_{NaL}) Activation. *Cardiol Cardiovasc Med* 03
- Qi XY, Yeh YH, Xiao L, Burstein B, Maguy A, Chartier D, Villeneuve LR, Brundel BJM, Dobrev D, Nattel S (2008): Cellular signaling underlying atrial tachycardia remodeling of L-type calcium current. *Circ Res* 103, 845–854
- Qiao Y, Wu L, Hou B, Sun W, Zheng L, Ding L, Chen G, Zhang S, Yao Y (2016): Functional mitral regurgitation: Predictor for atrial substrate remodeling and poor ablation outcome in paroxysmal atrial fibrillation. *Medicine (United States)* 95
- Rankin JS, Nicholas LM, Kouchoukos NT (1975): Experimental mitral regurgitation: effects on left ventricular function before and after elimination of chronic regurgitation in the dog. *Journal of Thoracic and Cardiovascular Surgery* 70, 478–488
- Ravn LS, Aizawa Y, Pollevick GD, Hofman-Bang J, Cordeiro JM, Dixen U, Jensen G, Wu Y, Burashnikov E, Haunso S, et al. (2008): Gain of function in I_{Ks} secondary to a mutation in KCNE5 associated with atrial fibrillation. *Heart Rhythm* 5, 427–435
- Reilly L, Eckhardt LL (2021): Cardiac potassium inward rectifier Kir2: Review of structure, regulation, pharmacology, and arrhythmogenesis. *Heart Rhythm* 18, 1423–1434
- Richter C, Bruegmann T (2020): No light without the dark: Perspectives and hindrances for translation of cardiac optogenetics. *Prog Biophys Mol Biol* 154, 39–50
- Rivard L, Sinno H, Shiroshita-Takeshita A, Schram G, Leung TK, Nattel S (2007): The pharmacological response of ischemia-related atrial fibrillation in dogs: Evidence for substrate-specific efficacy. *Cardiovasc Res* 74, 104–113

- Ronaldson-Bouchard K, Ma SP, Yeager K, Chen T, Song LJ, Sirabella D, Morikawa K, Teles D, Yazawa M, Vunjak-Novakovic G (2018): Advanced maturation of human cardiac tissue grown from pluripotent stem cells. *Nature* 556, 239–243
- Ronaldson-Bouchard K, Yeager K, Teles D, Chen T, Ma S, Song LJ, Morikawa K, Wobma HM, Vasciaveo A, Ruiz EC, et al. (2019): Engineering of human cardiac muscle electromechanically matured to an adult-like phenotype. *Nat Protoc* 14, 2781–2817
- Ruan JL, Tulloch NL, Razumova M v., Saiget M, Muskheli V, Pabon L, Reinecke H, Regnier M, Murry CE (2016): Mechanical Stress Conditioning and Electrical Stimulation Promote Contractility and Force Maturation of Induced Pluripotent Stem Cell-Derived Human Cardiac Tissue. *Circulation* 134, 1557–1567
- Salata JJ, Jurkiewicz NK, Wang J, Evans BE, Orme HT, Sanguinetti MC (1998): A novel benzodiazepine that activates cardiac slow delayed rectifier K⁺ currents. *Mol Pharmacol* 54, 220–230
- Sasse P, Funken M, Beiert T, Bruegmann T (2019): Optogenetic termination of cardiac arrhythmia: Mechanistic enlightenment and therapeutic application? *Front Physiol* 10
- Satin J, Schroder EA, Crump SM (2011): L-type calcium channel auto-regulation of transcription. *Cell Calcium* 49, 306–313
- Satoh T, Zipes DP (1996): Unequal atrial stretch in dogs increases dispersion of refractoriness conducive to developing atrial fibrillation. *J Cardiovasc Electrophysiol* 7, 833–842
- Schüttler D, Bapat A, Kääb S, Lee K, Tomsits P, Clauss S, Hucker WJ (2020): Animal Models of Atrial Fibrillation. *Circ Res* 127, 91–110
- Schwartz PJ, Moreno C, Kotta M-C, Pedrazzini M, Crotti L, Dagradi F, Castelletti S, Haugaa KH, Denjoy I, Shkolnikova MA, et al. (2021): Mutation location and *I*_{Ks} regulation in the arrhythmic risk of long QT syndrome type 1: the importance of the KCNQ1 S6 region. *Eur Heart J* 42, 4743–4755
- Seibertz F, Reynolds M, Voigt N (2020): Single-cell optical action potential measurement in human induced pluripotent stem cell-derived cardiomyocytes. *Journal of Visualized Experiments* 2020, e61890
- Seibertz F, Rapedius M, Fakuade FE, Tomsits P, Liutkute A, Cyganek L, Becker N, Majumder R, Clauß S, Fertig N, Voigt N (2022): A modern automated patch-clamp approach for high throughput electrophysiology recordings in native cardiomyocytes. *Commun Biol* 5
- Senst B, Zeltser R: Reentry Arrhythmia. StatPearls Publishing 2019
- Sharifi M, Buzatu D, Harris S, Wilkes J (2017): Development of models for predicting Torsade de Pointes cardiac arrhythmias using perceptron neural networks. *BMC Bioinformatics* 18, 497
- Sossalla S, Wagner S, Rasenack ECL, Ruff H, Weber SL, Schöndube FA, Tirilomis T, Tenderich G, Hasenfuss G, Belardinelli L, Maier LS (2008): Ranolazine improves diastolic dysfunction in isolated myocardium from

- failing human hearts - Role of late sodium current and intracellular ion accumulation. *J Mol Cell Cardiol* 45, 32–43
- Sossalla S, Kallmeyer B, Wagner S, Mazur M, Maurer U, Toischer K, Schmitto JD, Seipelt R, Schöndube FA, Hasenfuss G, et al. (2010): Altered Na⁺ Currents in Atrial Fibrillation. Effects of Ranolazine on Arrhythmias and Contractility in Human Atrial Myocardium. *J Am Coll Cardiol* 55, 2330–2342
- Sparrow JR, Nakanishi K, Parish CA (2000): The lipofuscin fluorophore A2E mediates blue light-induced damage to retinal pigmented epithelial cells. *Invest Ophthalmol Vis Sci* 41, 1981–1989
- Sun Q, Tang M, Pu J, Zhang S (2008): Pulmonary venous structural remodelling in a canine model of chronic atrial dilation due to mitral regurgitation. *Canadian Journal of Cardiology* 24, 305–308
- Suresh A, Martens P, Tang WHW (2022): Biomarkers for Myocarditis and Inflammatory Cardiomyopathy. *Curr Heart Fail Rep* 19, 346–355
- Tiburcy M, Hudson JE, Balfanz P, Schlick S, Meyer T, Liao MLC, Levent E, Raad F, Zeidler S, Wingender E, et al. (2017): Defined engineered human myocardium with advanced maturation for applications in heart failure modeling and repair. *Circulation* 135, 1832–1847
- Tiburcy M, Meyer T, Liaw NY, Zimmermann WH (2020): Generation of Engineered Human Myocardium in a Multi-well Format. *STAR Protoc* 1, 100032
- Timmermann V, Dejgaard LA, Haugaa KH, Edwards AG, Sundnes J, McCulloch AD, Wall ST (2017): An integrative appraisal of mechano-electric feedback mechanisms in the heart. *Prog Biophys Mol Biol* 130, 404–417
- Ton AT, Nguyen W, Sweat K, Miron Y, Hernandez E, Wong T, Geft V, Macias A, Espinoza A, Truong K, et al. (2021): Arrhythmogenic and antiarrhythmic actions of late sustained sodium current in the adult human heart. *Sci Rep* 11, 1–16
- Tsujino Y, Sakamoto T, Kinoshita K, Nakatani Y, Yamaguchi Y, Kataoka N, Nishida K, Kinugawa K (2019): Edoxaban suppresses the progression of atrial fibrosis and atrial fibrillation in a canine congestive heart failure model. *Heart Vessels* 34, 1381–1388
- Tyssowski KM, Gray JM (2019): Blue light increases neuronal activity-regulated gene expression in the absence of optogenetic proteins. *eNeuro* 6
- van Wagoner DR, Pond AL, McCarthy PM, Trimmer JS, Nerbonne JM (1997): Outward K⁺ current densities and Kv1.5 expression are reduced in chronic human atrial fibrillation. *Circ Res* 80, 772–781
- van Wagoner DR, Pond AL, Lamorgese M, Rossie SS, McCarthy PM, Nerbonne JM (1999): Atrial L-type Ca²⁺ currents and human atrial fibrillation. *Circ Res* 85, 428–436
- Varró A, Baláti B, Iost N, Takács J, Virág L, Lathrop DA, Csaba L, Tálosi L, Papp JG (2000): The role of the delayed rectifier component I(Ks) in dog ventricular muscle and Purkinje fibre repolarization. *Journal of Physiology* 523, 67–81

- Veerman CC, Verkerk AO, Blom MT, Klemens CA, Langendijk PNJ, van Ginneken ACG, Wilders R, Tan HL (2013): Slow delayed rectifier potassium current blockade contributes importantly to drug-induced long QT syndrome. *Circ Arrhythm Electrophysiol* 6, 1002–1009
- Verheule S, Wilson E, Everett IV T, Shanbhag S, Golden C, Olgin J (2003): Alterations in atrial electrophysiology and tissue structure in a canine model of chronic atrial dilatation due to Mitral Regurgitation. *Circulation* 107, 2615–2622
- Verkerk AO, van Ginneken ACG, Wilders R (2009): Pacemaker activity of the human sinoatrial node: Role of the hyperpolarization-activated current, *I_f*. *Int J Cardiol* 132, 318–336
- Vogt CC, Bruegmann T, Malan D, Ottersbach A, Roell W, Fleischmann BK, Sasse P (2015): Systemic gene transfer enables optogenetic pacing of mouse hearts. *Cardiovasc Res* 106, 338–343
- Voigt N., Maguy A, Yeh Y-H, Qi X, Ravens U, Dobrev D, Nattel S (2007): Changes in *I_{K,ACH}* single-channel activity with atrial tachycardia remodelling in canine atrial cardiomyocytes. *Cardiovasc Res* 77, 35–43
- Voigt Niels, Friedrich A, Bock M, Wettwer E, Christ T, Knaut M, Strasser RH, Ravens U, Dobrev D (2007): Differential phosphorylation-dependent regulation of constitutively active and muscarinic receptor-activated *I_{K,ACH}* channels in patients with chronic atrial fibrillation. *Cardiovasc Res* 74, 426–437
- Voigt N, Li N, Wang Q, Wang W, Trafford AW, Abu-Taha I, Sun Q, Wieland T, Ravens U, Nattel S, et al. (2012): Enhanced sarcoplasmic reticulum Ca^{2+} Leak and increased Na^{+} - Ca^{2+} exchanger function underlie delayed afterdepolarizations in patients with chronic atrial fibrillation. *Circulation* 125, 2059–2070
- Voigt N, Heijman J, Trausch A, Mintert-Jancke E, Pott L, Ravens U, Dobrev D (2013): Impaired Na^{+} -dependent regulation of acetylcholine-activated inward-rectifier K^{+} current modulates action potential rate dependence in patients with chronic atrial fibrillation. *J Mol Cell Cardiol* 61, 142–152
- Vonck J (2000): Structure of the bacteriorhodopsin mutant F219L N intermediate revealed by electron crystallography. *EMBO Journal* 19, 2152–2160
- Wagner S, Dybkova N, Rasenack ECL, Jacobshagen C, Fabritz L, Kirchhof P, Maier SKG, Zhang T, Hasenfuss G, Brown JH, et al. (2006): Ca^{2+} /calmodulin-dependent protein kinase II regulates cardiac Na^{+} channels. *Journal of Clinical Investigation* 116, 3127–3138
- Wakimoto H, Maguire CT, Kover P, Hammer PE, Gehrman J, Triedman JK, Berul CI (2001): Induction of atrial tachycardia and fibrillation in the mouse heart. *Cardiovasc Res* 50, 463–473
- Wang YP, Sun BY, Li Q, Dong L, Zhang GH, Grundy D, Rong WF (2012): Hyperpolarization-activated cyclic nucleotide-gated cation channel subtypes differentially modulate the excitability of murine small intestinal afferents. *World J Gastroenterol* 18, 522–531

- Wang Z, Yue L, White M, Pelletier G, Nattel S (1998): Differential distribution of inward rectifier potassium channel transcripts in human atrium versus ventricle. *Circulation* 98, 2422–2428
- Wang Z, Lu Y, Yang B (2011): MicroRNAs and atrial fibrillation: New fundamentals. *Cardiovasc Res* 89, 710–721
- Weisbrod D, Khun SH, Bueno H, Peretz A, Attali B (2016): Mechanisms underlying the cardiac pacemaker: The role of SK4 calcium-activated potassium channels. *Acta Pharmacol Sin* 37, 82–97
- Wemhöner K, Friedrich C, Stallmeyer B, Coffey AJ, Grace A, Zumhagen S, Seebohm G, Ortiz-Bonnin B, Rinné S, Sachse FB, et al. (2015): Gain-of-function mutations in the calcium channel CACNA1C (Cav1.2) cause non-syndromic long-QT but not Timothy syndrome. *J Mol Cell Cardiol* 80, 186–195
- Wettwer E, Hála O, Christ T, Heubach JF, Dobrev D, Knaut M, Varró A, Ravens U (2004): Role of I_{Kur} in controlling action potential shape and contractility in the human atrium: Influence of chronic atrial fibrillation. *Circulation* 110, 2299–2306
- Wiedmann F, Beyersdorf C, Zhou X, Büscher A, Kraft M, Nietfeld J, Walz TP, Unger LA, Loewe A, Schmack B, et al. (2020): Pharmacologic twik-related acid-sensitive K^+ channel (Task-1) potassium channel inhibitor a293 facilitates acute cardioversion of paroxysmal atrial fibrillation in a porcine large animal model. *J Am Heart Assoc* 9
- Wijffels MCEF, Kirchhof CJHJ, Dorland R, Allessie MA (1995): Atrial fibrillation begets atrial fibrillation: A study in awake chronically instrumented goats. *Circulation* 92, 1954–1968
- Wilde AAM, Amin AS (2018): Clinical Spectrum of SCN5A Mutations: Long QT Syndrome, Brugada Syndrome, and Cardiomyopathy. *JACC Clin Electrophysiol* 4, 569–579
- Wit AL, Cranefield PF (1978): Reentrant excitation as a cause of cardiac arrhythmias. *Am J Physiol Heart Circ Physiol* 4
- Witchel HJ (2011): Drug-induced hERG block and long QT syndrome. *Cardiovasc Ther* 29, 251–259
- Wong CX, John B, Brooks AG, Chandy ST, Kuklik P, Lau DH, Sullivan T, Roberts-Thomson KC, Sanders P (2012): Direction-dependent conduction abnormalities in the chronically stretched atria. *Europace* 14, 954–961
- Workman AJ, Kane KA, Rankin AC (2001): The contribution of ionic currents to changes in refractoriness of human atrial myocytes associated with chronic atrial fibrillation. *Cardiovasc Res* 52, 226–235
- Wu J, Wang X, Chung YY, Koh CH, Liu Z, Guo H, Yuan Q, Wang C, Su S, Wei H (2017): L-type calcium channel inhibition contributes to the proarrhythmic effects of aconitine in human cardiomyocytes. *PLoS One* 12
- Xavier-Neto J, Neville CM, Shapiro MD, Houghton L, Wang GF, Nikovits W, Stockdale FE, Rosenthal N (1999): A retinoic acid-inducible transgenic

- marker of sino-atrial development in the mouse heart. *Development* 126, 2677–2687
- Xi Y, Wu G, Yang L, Han K, Du Y, Wang T, Lei X, Bai X, Ma A (2009): Increased late sodium currents are related to transcription of neuronal isoforms in a pressure-overload model. *Eur J Heart Fail* 11, 749–757
- Yang T, Smith JA, Leake BF, Sanders CR, Meiler J, Roden DM (2013): An allosteric mechanism for drug block of the human cardiac potassium channel KCNQ1. *Mol Pharmacol* 83, 481–489
- Yang Y, Xia M, Jin Q, Bendahhou S, Shi J, Chen Yiping, Liang B, Lin J, Liu Y, Liu B, et al. (2004): Identification of a KCNE2 gain-of-function mutation in patients with familial atrial fibrillation. *Am J Hum Genet* 75, 899–905
- Ye D, Zhou W, Hamrick SK, Tester DJ, Kim CSJ, Barajas-Martinez H, Hu D, Giudicessi JR, Antzelevitch C, Ackerman MJ (2022): Acacetin, a Potent Transient Outward Current Blocker, May Be a Novel Therapeutic for KCND3-Encoded Kv4.3 Gain-of-Function-Associated. *Circ Genom Precis Med*
- Yeh YH, Wakili R, Qi XY, Chartier D, Boknik P, Käab S, Ravens U, Coutu P, Dobrev D, Nattel S (2008): Calcium-handling abnormalities underlying atrial arrhythmogenesis and contractile dysfunction in dogs with congestive heart failure. *Circ Arrhythm Electrophysiol* 1, 93–102
- Yu H, Wu J, Potapova I, Wymore RT, Holmes B, Zuckerman J, Pan Z, Wang H, Shi W, Robinson RB, et al. (2001): MinK-Related Peptide 1. *Circ Res* 88
- Yu W-C, Chen S-A, Lee S-H, Tai C-T, Feng A-N, Kuo BI-T, Ding Y-A, Chang M-S (1998): Tachycardia-Induced Change of Atrial Refractory Period in Humans. *Circulation* 97, 2331–2337
- Yue L, Feng J, Gaspo R, Li GR, Wang Z, Nattel S (1997): Ionic remodeling underlying action potential changes in a canine model of atrial fibrillation. *Circ Res* 81, 512–525
- Yue L, Melnyk P, Gaspo R, Wang Z, Nattel S (1999): Molecular mechanisms underlying ionic remodeling in a dog model of atrial fibrillation. *Circ Res* 84, 776–784
- Zhang C, He D, Ma J, Tang W, Waite TD (2018): Faradaic reactions in capacitive deionization (CDI) - problems and possibilities: A review. *Water Res* 128, 314–330
- Zhang H, Garratt CJ, Zhu J, Holden A v. (2005): Role of up-regulation of I_{K1} in action potential shortening associated with atrial fibrillation in humans. *Cardiovasc Res* 66, 493–502
- Zhang H, Ren L, Shivnaraine RV (2022): Targeting GPCRs to treat cardiac fibrosis. *Front Cardiovasc Med* 9
- Zhang X, Cao H, Bai S, Huo W, Ma Y (2017): Differentiation and characterization of rhesus monkey atrial and ventricular cardiomyocytes from induced pluripotent stem cells. *Stem Cell Res* 20, 21–29
- Zhao Z, Xie Y, Wen H, Xiao D, Allen C, Fefelova N, Dun W, Boyden PA, Qu Z, Xie L-H (2012): Role of the transient outward potassium current in the

- genesis of early afterdepolarizations in cardiac cells. *Cardiovasc Res* 95, 308–316
- Zhou Y, Jiang C, Wang J, Huang W, Zhang Y, Zhou R (2022): Generation of one human induced pluripotent stem cell line (XACHi004-A) with heterozygous mutation of RYR2 gene from an atrial fibrillation patient. *Stem Cell Res* 65, 102955
- Zimmer T, Surber R (2008): SCN5A channelopathies - An update on mutations and mechanisms. *Prog Biophys Mol Biol* 98, 120–136
- Zimmermann WH, Fink C, Kralisch D, Remmers U, Weil J, Eschenhagen T (2000): Three-dimensional engineered heart tissue from neonatal rat cardiac myocytes. *Biotechnol Bioeng* 68, 106–114
- Zöller B, Ohlsson H, Sundquist J, Sundquist K (2013): High familial risk of atrial fibrillation/atrial flutter in multiplex families: a nationwide family study in Sweden. *J Am Heart Assoc* 2

Supplements

Table of supplemental contents

1	Introduction to electrophysiology	137
1.1	Biophysical basis of electrogenesis	137
1.1.1	Conventions and definitions	137
1.1.2	Equilibrium potential and driving force	137
1.1.3	Membrane potential	138
1.2	Ion channels and ion currents	140
1.2.1	Ion currents	140
1.2.2	Structure function	141
1.2.3	Structure and function of voltage gated ion channels	142
2	Calcium handling remodelling associated with the development of atrial fibrillation	145
3	Treatments for atrial fibrillation	148
3.1	Anticoagulation strategy – Stroke prevention	148
3.2	Rate and rhythm control – Symptom management	148
3.3	Identification and management of concomitant diseases	150
4	Other models used for the study of atrial fibrillation	151
4.1	Murine models	151
4.2	Large mammalian models	152
4.2.1	Dog models	152
4.2.2	Goat models	153
4.2.3	Swine models	154
4.3	In silico models	155
4.4	Small non mammalian models	157
5	Other techniques to initiate atrial fibrillation in vivo	160
5.1	Congestive heart failure	160
5.2	Mitral regurgitation	161
6	Investigation of the cardiac electrophysiology	163
6.1	<i>In vivo</i> approaches	163
6.1.1	Electrocardiogram	163
6.1.2	Electrographic imaging techniques	164
6.2	<i>In vitro</i> and <i>ex vivo</i> approaches	164
6.2.1	Tissular	164
6.2.2	Multi-cellular	165
6.2.3	Cellular	165
7	Adeno-associated-virus-2 genome sequence	168

8	Engineered human myocardium generated with induced pluripotent stem cells transfected with an adeno-associated virus-2 carrying a channelrhodopsin-2	173
9	Long-term optical tachypacing experimental set-up	174
10	Supplemental references	175

Table of supplemental figures

Supplemental figure 1: Schematic representation of ion channel gating configurations.	142
Supplemental figure 2: Schematic representation of the structure of voltage-gated Na ⁺ , Ca ²⁺ and K ⁺ channels.	144
Supplemental figure 3: The different patch-clamp configurations.	167
Supplemental figure 4: Pictures of atrial engineered human myocardium generated with induced pluripotent stem cells transfected with an adeno-associated virus-2 carrying a channelrhodopsin-2, 30 days after the tissue preparation.	173
Supplemental figure 5: Pictures of the experimental set-up used for the optical tachypacing of the chrimson-engineered human myocardium.	174

Table of supplemental tables

Supplemental table 1: Advantages and disadvantages of the utilisation of the mouse model for the study of atrial fibrillation.	152
Supplemental table 2: Advantages and disadvantages of the utilisation of the canine model for the study of atrial fibrillation.	153
Supplemental table 3: Advantages and disadvantages of the utilisation of the goat model for the study of atrial fibrillation.	154
Supplemental table 4: Advantages and disadvantages of the utilisation of the swine model for the study of atrial fibrillation.	155
Supplemental table 5: Advantages and disadvantages of the utilisation of <i>in silico</i> models for the study of atrial fibrillation.	157
Supplemental table 6: Advantages and disadvantages of the utilisation of non-mammalian models for the study of atrial fibrillation.	159

1 Introduction to electrophysiology

In this part, we will briefly define the biophysical concepts underlying the functioning of classic ion channels and the ionic movements through a biological membrane.

1.1 Biophysical basis of electrogenesis

1.1.1 Conventions and definitions

A biological membrane is defined as a non-permeable lipidic bilayer electrically chargeable (Bruce et al. 2002). The comparison of two compartments (intra- and extracellular) shows the apparition of ionic gradients maintained by the presence of permeable pores in the membrane (ion channels for example). The resulting charged ionic flux crossing the membrane is responsible for an ionic current, experimentally measurable. Furthermore, experiments showed that at steady state, the inside of the membrane is negatively charged.

The term hyperpolarisation is used to describe the evolution of a potential towards a more negative state. Oppositely, the term depolarisation is used to describe the evolution of a potential towards a more positive state. Finally, the term repolarisation is used to describe the evolution of the potential towards a more negative state, consecutively to a depolarisation.

By convention, the terminology used to describe the behaviour of an ion channel is given accordingly to the transfer of a positive charge (cation). Hence, an inward current refers to the entrance of cations (Na^+ , Ca^{2+} , K^+) or an exit of anions (Cl^-). Therefore, because the inside of a cell is negatively charged, an inward current will be depolarising, and an outward current hyperpolarising.

1.1.2 Equilibrium potential and driving force

An ion present in two compartments A and B (or external and internal) separated by a membrane specifically permeable for this ion is subjected to two forces: a concentration gradient force and an electrical gradient force. These two forces can either be directed towards the same direction or be opposed. In such

condition exists a membrane potential, where concentration and electrical gradients are exactly opposite. This state is called equilibrium potential (E_{ion}) and can be calculated using Nernst's equation.

$$E_m = E_A - E_B = \frac{RT}{zF} \ln \frac{[I]_{ext}}{[I]_{int}}$$

Where R is the ideal gas constant, T is the temperature in Kelvin, z is the charge of the ion, F is the Faraday's constant and $[I]_{ext}$ and $[I]_{int}$ are the ion concentrations in the external and internal compartment, respectively.

We can also define the driving force as follows:

$$E_{DF} = E_m - E_{ion}$$

It corresponds in the difference between the membrane potential (E_m) and the equilibrium potential of an ion (E_{ion}). The higher the driving force is, the more ions cross the membrane (if they have the possibility to pass through an ion channel).

1.1.3 Membrane potential

Because of the presence in the membrane of ion channels selective for an ion and the presence of an ionic gradient, we can observe a difference of potential across the membrane, which can be calculated using the Goldman-Hodgkin-Katz's (GHK) equation.

$$E_m = \frac{RT}{zF} \ln \left(\frac{\sum_{cations} P_i [i]_{ext} + \sum_{anions} P_i [i]_{ext}}{\sum_{cations} P_i [i]_{int} + \sum_{anions} P_i [i]_{int}} \right)$$

Where R is the ideal gas constant, T is the temperature in Kelvin, z is the charge of the ion, F is the Faraday's constant, P_i is the ion permeability, and $[I]_{ext}$ and $[I]_{int}$ are the ion concentrations in the external and internal compartment, respectively.

In a biological system permeable for K^+ , Na^+ , Cl^- and Ca^{2+} , we can develop the GHK's equation as follows:

$$E_m = -\frac{RT}{zF} \ln \left(\frac{P_{Na^+}[Na^+]_{ext} + P_{K^+}[K^+]_{ext} + P_{Ca^{2+}}[Ca^{2+}]_{ext} + P_{Cl^-}[Cl^-]_{ext}}{P_{Na^+}[Na^+]_{int} + P_{K^+}[K^+]_{int} + P_{Ca^{2+}}[Ca^{2+}]_{int} + P_{Cl^-}[Cl^-]_{int}} \right)$$

This equation includes the channel permeabilities for the different ions, and the ion concentrations.

Another way to present this equation consists in using the ionic conductances instead:

$$E_m = \sum \left(\frac{G_i E_i}{G_i} \right)$$

In the same conditions of a biological membrane permeable to K^+ , Na^+ , Ca^{2+} and Cl^- , we can develop the equation as follows:

$$E_m = \frac{G_{K^+} E_{K^+} + G_{Na^+} E_{Na^+} + G_{Ca^{2+}} E_{Ca^{2+}} + G_{Cl^-} E_{Cl^-}}{G_{K^+} + G_{Na^+} + G_{Ca^{2+}} + G_{Cl^-}}$$

In a cardiomyocyte, at resting state, permeabilities (and therefore conductances) for Na^+ , Ca^{2+} and Cl^- are neglected and we can simplify the equation as follows:

$$E_m = G_{K^+} \cdot E_{K^+}$$

For this reason, in a resting cardiomyocyte we classically assimilate the resting potential to the potassium equilibrium potential (E_{K^+}).

1.2 Ion channels and ion currents

1.2.1 Ion currents

For a single ion channel, the passage of an ion is accompanied with the generation of an ionic current following the Ohm's law.

$$V = R \cdot I$$

Where V is the voltage, I is the intensity and R the resistance.

$$i_{ion} = \gamma_{ion}(E_m - E_{ion})$$

Where i_{ion} and γ_{ion} are respectively the ionic current and the conductance of the channel, and $E_m - E_{ion}$ is the driving force (E_{DF}).

At the unitary scale, the relation between ion current and membrane potential is linear, and the Ohm's law directly applies.

By convention, an outward current is signed positively (+), whereas an inward current negatively (-).

For this reason, when a membrane potential is more negative than the equilibrium potential of the ion, E_{DF} becomes negative, and the resulting current will necessarily be an inward current.

Furthermore, during the application of a train of potentials, an ion channel is not constantly opened, but it is oscillating between an opened and a closed configuration. The probability of opening (P_o) for an ion channel can then be defined as the opening time over the closed time during a recorded period. P_o can vary over time (for example, a sodium [Na^+] channel has its opening probability close to 1 at the beginning of an AP, but close to 0 towards the end), or even be artificially modified (for example while using an agonist or an antagonist drug for this channel). Finally, some ion channels are dependent on external stimuli to trigger their opening. These stimuli can be of extremely various

natures (e.g. voltage-dependant ion channels, light-gated ion channels, thermoreceptors, chemoreceptors, baroreceptors).

If we are extrapolating the unitary conductance to N channels on a membrane, membrane conductance can be calculated as follows:

$$G_{ion} = N_{ion} \cdot \gamma_{ion} \cdot P_0$$

Where G_{ion} is the membrane conductance for the ion and N_{ion} is the number of ion channels present on the membrane.

It is important to note that unlike γ_{ion} , G_{ion} does not vary linearly over time with E_m , because P_0 depends on voltage and time.

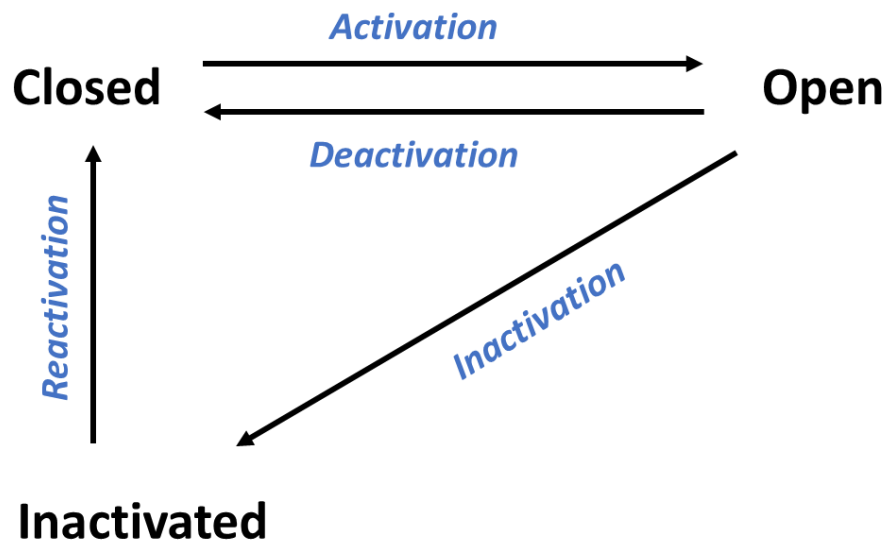
1.2.2 Structure function

Membrane conductance can be visualised as a gate whose open widening depends on voltage and time, and where the doors of the gate can take an infinity of intermediate positions between two extreme states: a completely closed state (0) and a completely opened one (1). To be functional, an ion channel must be able to navigate between at least two opening states (opened and closed). In reality, many ion channels have at least two distinct closed states: closed and inactivated. Likewise, it is not rare that ion channels have several inactivated and/or closed states cohabiting, and more complex modelling aims to describe their interactions more precisely, Markov models for example (Siekmann et al. 2011; Lampert and Korngreen 2014). For clarity purposes, we will here stick to a standard model.

From these three states we can define several kinetics:

- Activation: from closed to opened state;
- Deactivation: from opened to closed state;
- Inactivation: from opened to inactivated state;
- Reactivation: from inactivated to closed state.

Furthermore, an inactivated ion channel can only be activated again if it transits by the closed state (reactivation). Transition from the different states is placed under the control of the voltage and varies over time. Additionally, the different states and their transitions are influenced by numerous factors including phosphorylation, temperature, or pharmacological substances.



Supplemental figure 1: Schematic representation of ion channel gating configurations.

1.2.3 Structure and function of voltage gated ion channels

Voltage-gated ion channels are a class of transmembrane proteins activated by membrane potential changes. Although many differences exist between the different ion channel families (with respect to ion selectivity, kinetics of activation and inactivation), structural and functional similarities can be found. Na⁺ and

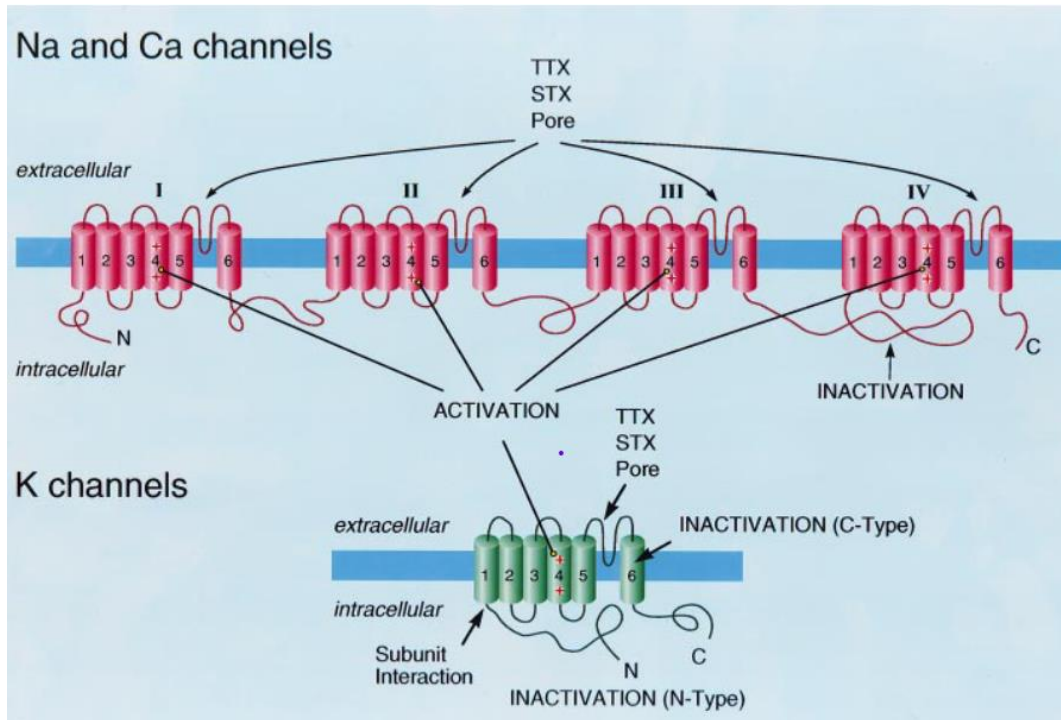
calcium (Ca^{2+}) channels are very comparable in their structures. Potassium (K^+) channels have their own structure.

Na^+ and Ca^{2+} channels are formed of only one main subunit called α -subunit composed of four homologous domains (named I to IV), each of them constituted by six transmembrane segments (named S1-S6). Each segment carries specific biophysiological properties. Moreover, the final channel is associated with auxiliary proteins (or regulatory subunits) involved in the modulation of the ion channel kinetics. The Na^+ α -subunit is classically associated with two regulatory subunits (called $\beta 1$ and $\beta 2$), and the Ca^{2+} α -subunit with four regulatory subunits (called $\alpha 2$, β , γ and δ ; Marban et al. 1998; Jiang et al. 2020).

The voltage sensing ability of the Ca^{2+} and Na^+ channels is located on the S4 segment (called the voltage sensing domain, VSD), and is permitted thanks to the repetition of charged motifs Arg/Lys-X-X. The pore region (called P) is located between S5 and S6 segments. It is constituted of two segments (called SS1 and SS2), diving in and out of the membrane (Marban et al. 1998; Jiang et al. 2020).

K^+ voltage-gated channels are constituted by the assembly of four α -subunits. Modulatory subunits also exist in K^+ voltage-gated ion channels and are associated in a 1:1 stoichiometry with the α -subunits. A fully assembled K^+ voltage-gated ion channel is a protein complex formed by four α -subunits and four β -modulatory subunits. The voltage sensing domain is also located on the S4 segment in voltage-gated K^+ channels. However, it is not compulsory for voltage sensitivity, as two-domain K^+ channels (K2P) do not have one but still show voltage sensitive behaviour (Schewe et al. 2016).

Activation and deactivation kinetics depend on the channel's type and are modulated by various factors including phosphorylation state, pH, temperature, ionic concentration, but also by the action of the regulatory subunits composing the ion channel complex.



Supplemental figure 2: Schematic representation of the structure of voltage-gated Na^+ , Ca^{2+} and K^+ channels. From Terlau and Stühmer, *Naturwissenschaften*, 1998, with permission.

2 Calcium handling remodelling associated with the development of atrial fibrillation

The term Ca^{2+} handling recapitulates the molecular mechanisms involved in Ca^{2+} buffering, storage, and utilisation. Many proteins are involved in these mechanisms, and alterations of parts of these systems can have consequences on the initiation and the maintenance of arrhythmogenic events, but also on the contractile function of the cardiac muscle.

Ca^{2+} handling remodelling in the context of AF is characterised by a series of events leading to an impairment of the normal property of the cell to efficiently handle the Ca^{2+} cycling. It is characterised by a chronic increase in intracellular Ca^{2+} concentration, the chronic activation of Ca^{2+} dependant kinases and phosphatases, the apparition of spontaneous Ca^{2+} releases from the sarcoplasmic reticulum (SRet) and the alteration in functioning in Ca^{2+} channels.

The chronic increase of the intracellular Ca^{2+} concentration will have direct effects on the cell functioning, mainly because of the consequent chronic activation of the Ca^{2+} /Calmodulin kinase II δ (CAMKII δ). The CAMKII δ is a protein kinase and has its activity placed under the control of Ca^{2+} : as the Ca^{2+} concentration rises, Ca^{2+} binds to the Ca^{2+} binding site and induces a conformational change, allowing the protein to bind to its target (Swulius and Waxham 2008). The targets of the CAMKII δ are multiple, and most of them play a crucial role in Ca^{2+} handling remodelling.

The first targets are proteins involved in Ca^{2+} reuptake: the ryanodine receptor 2 (RyR2), phospholamban and sarcolipin.

The RyR2 is the major sarcoplasmic reticulum Ca^{2+} -release channel involved in EC-coupling, and its activity is highly regulated by its regulatory subunits including the FKBP12.6 proteins, but also the calmodulin, calsequestrin-2, junctin, triadin and junctophilin-2. All its regulatory units are involved in the control of the gating of the channel and the control of its opening probability. On the ryanodine receptor itself, several phosphorylation sites exist for the CAMKII δ , and the phosphorylation of the RyR2 on the S2808 and/or S2814 site has shown to

increase susceptibility to leaks. Such phosphorylation status is observed in the context of AF. Interestingly, although Ca^{2+} leaks and spontaneous Ca^{2+} events are also present in paroxysmal AF, the phosphorylation of these sites is not systematic, suggesting the involvement of different molecular pathways (Voigt et al. 2014).

Phospholamban is another protein involved in the CICR and is participating in intracellular Ca^{2+} concentration regulation. The phospholamban activity is regulated by its phosphorylation status. In a resting cell, phospholamban is dephosphorylated and has an inhibitory role on the SERCA pump activity, preventing Ca^{2+} reuptake. However, activation by phosphorylation (either on Ser16 by PKA, or Thr17 by CAMKII) alleviates the inhibitory function and promotes Ca^{2+} reuptake via the SERCA. This phosphorylation mechanism is particularly useful in physiological conditions and plays the role of an adaptative mechanism to stress or exercise via the activity of the PKA upon β -adrenergic stimulation. The mRNA expression levels of phospholamban were shown unchanged in AF patients (Lai et al. 1999). However, in the context of AF with an already existing phosphorylated RyR2, this adaptative mechanism can act in disfavour of the cell, promoting the cycling of the Ca^{2+} leaking from the RyR2, and acting in favour of the development of arrhythmogenic events such as delayed afterdepolarisations (DAD; Mattiazzi & Kranias, 2014).

The role of sarcolipin is not fully understood in the atria. However, it has been shown that sarcolipin acts as a regulator of SERCA and has an inhibitory role on its functioning. Interestingly, sarcolipin mRNA levels have been shown to be significantly reduced in AF patients (Lai et al. 1999; Shanmugam et al. 2011). Furthermore, studies on sarcolipin $\text{KO}^{-/-}$ mice showed that prolongation of an enhanced SERCA activity was associated with atrial remodelling characterised by an increased SR Ca^{2+} load and occurrence of spontaneous Ca^{2+} events, but also an increased APD_{90} due to the increased L-type Ca^{2+} channel and the activation of the forward mode of the NCX (Xie et al. 2012). Altogether, these observations were in line with a pro-arrhythmogenic role, via the promotion of the apparition of DADs (Voigt et al. 2012).

Another set of targets of the activation of the CAMKII δ are ion channels, in particular channels involved in AP generation including repolarising currents (I_{to} , I_{Kur} , and I_{K1}) but also depolarising currents ($I_{Ca,L}$, I_{Na} , but also I_{NCX}).

Regarding the repolarising reserve, studies showed that CAMKII acute and chronic activity was responsible for an increase in the $I_{to,s}$ amplitude and expression, and $I_{to,f}$ in a chronic way (Wagner et al. 2009). The same study showed that acute overexpression of CaMKII was also associated in an increase of I_{K1} . Finally, CaMKII has been shown to also modulate positively the activity or I_{Kur} (Tessier et al. 1999). Altogether, CAMKII activation has been shown to participate in the abbreviation of the APD via the enhancement of the repolarisation reserve.

On the depolarisation side, it has also been shown that CaMKII plays a modulatory role. CAMKII has a positive effect on the $I_{Ca,L}$ (Swaminathan et al. 2012) but also promotes the $I_{Na,late}$ (Wagner et al. 2011). Finally, studies have shown that CAMKII has enhancing effects on the I_{NCX} functioning (Voigt et al. 2012).

To conclude, besides the phosphorylation activity led by the CaMKII promoted by an increased intracellular Ca^{2+} concentration, long-term effects are also promoted, via the activation of the nuclear factor of activated T-cells (NFAT) leading to cell hypertrophy (Molkentin et al. 1998; Sussman et al. 1998; Lim et al. 2000). Interestingly, in a mouse model of progressive AF, it has been shown that knockout of the NFAT2 gene prevented the evolution of AF (Ni et al. 2021). For this reason, NFAT as a possible therapeutic target presents large interests. Recently, the utilisation of sacubitril/valsartan, a drug used for heart failure therapy, has shown interesting results in a rabbit model of AF, mitigating electrical and structural remodelling induced by atrial tachypacing (Li et al. 2020).

3 Treatments for atrial fibrillation

According to the last ESC guidelines (Hindricks et al. 2021), treatments for AF is oriented around 3 problematics: prevent the apparition of stroke, control the symptoms of the disease, and detect and manage the cardiovascular risk factors and the concomitant disease of atrial fibrillation.

3.1 Anticoagulation strategy – Stroke prevention

The first panel is oriented around the establishment of a proper anticoagulation strategy for the patient to avoid the development of thrombi whose exit from the heart to the systemic or pulmonary circulation could lead to thromboembolic incidents, amongst them strokes.

A stroke is the most dangerous thromboembolic event for the patient's prognosis, and therefore risk assessment scores have been developed and are frequently used prior to the treatment decision making and the use of an active anti-thrombotic therapy. The most commonly used is the CHA₂DS₂-VASc score. It includes several criteria: the presence of heart failure, hypertension, age ≥ 75 or from 65 to 74 years old, diabetes mellitus, stroke, vascular disease, and sex category. A score from 0 to 9 is then calculated (where the minimum is 0 for male and 1 for female patients, and 9 the maximum), and decision making is made from this point on. When a patient's score is 0 for male, and 1 for female, an active oral anticoagulation therapy is not considered. However, a higher score is always raising the consideration of the use of an active anticoagulation therapy (Hindricks et al. 2021).

3.2 Rate and rhythm control – Symptom management

The second panel is quite large and englobes all the considerations around the management of the symptoms associated with the disease. It includes two major points namely rate control (ventricular considerations) and rhythm control (supraventricular considerations).

Rate control is an important aspect of the patient's disease management and aims to mitigate the symptoms associated with AF and enable the patient to

exercise, improve the haemodynamic profile, and prevent the development of heart failure. During an episode of AF, systolic output from the atria is reduced (because of faster beat rate and/or uncoordinated contraction) and can be further reduced at the exit of the ventricle because of the impaired precharge (also because of faster beat rate, but also possibly associated comorbidities such as heart failure with non-preserved ejection fraction). For these reasons, the first line treatments aim to control the ventricular depolarisation rate, using drugs such as β -blockers, non-dihydropyridine Ca^{2+} -channel antagonists or blockers. The addition of other inhibitors such as amiodarone to further reduce ventricular rate or digoxin when the contractile function also needs to be restored, are considered as second line treatments. Finally, if none of the pharmacological approaches manages to control the ventricular rate, catheter ablation of the atrioventricular node and/or implantation of a pacemaker is considered (van Gelder et al. 2016).

Rhythm control is the second aspect and is focused on the control of the atrial depolarisation rate and the restoration of a normal sinus rhythm. Rhythm control is usually considered in accordance with the severity of the symptoms, but also for the treatment of acute AF episodes. Rhythm control strategies include cardioversion, antiarrhythmic medication, and catheter ablation, all of them most of the time associated with oral anticoagulation medication.

Cardioversion can either be electrical or pharmacological. Electrical cardioversion is usually preferred for acute intervention when the haemodynamic status of the patient is compromised because of its instantaneous results. Electrical cardioversion consists in applying a controlled amount of energy through the atria to disrupt an episode of AF and restore sinus rhythm. Pharmacological cardioversion, however, is indicated in haemodynamically stable patients, and consists in intra venous perfusion of anti-arrhythmic drugs (for example flecainide, amiodarone or vernakalant depending on the patient's electrophysiological profile).

Besides the cardioversion, antiarrhythmic drugs can be proposed to help maintaining SR in patients. Oral antiarrhythmic treatment aims to treat symptoms and increase the patient's quality of life. Strategies are articulated around utilisation of different drugs all aiming to reduce the pacemaker cell's depolarisation rate. Different inhibitors exist and the selection of the appropriate

antiarrhythmic drug is carefully guided by the patient's specific profile to avoid toxicity or even worsening the already existing condition.

Finally, catheter ablation can be proposed to the patient as an alternative to antiarrhythmic drug treatment, or when the pharmacological approach failed. Catheter ablation is a mini-invasive surgery that consists in the isolation or the destruction of arrhythmogenic areas in the atria (e.g. around the pulmonary veins) with a catheter brought to the heart via the femoral vein and using high energy radiofrequencies or low temperature (cryoablation). Catheter ablation has been shown to efficiently reduce symptoms in patients with paroxysmal or persistent AF (Andrade et al. 2022; Lo et al. 2022; Mannakkara et al. 2022).

3.3 Identification and management of concomitant diseases

The last panel of the treatment proposed by the ESC draws the attention to the identification and the management of concomitant diseases, cardiometabolic risk factors and the prevention of unhealthy lifestyle factors.

Many lifestyle interventions can be proposed to the patient to involve him/her in the disease management. They include actions on nicotine abuse management, body weight and weight loss, but also on alcohol and caffeine consumption and physical activity.

Finally, several risk factors and comorbidities are associated with the development of AF, and their identification/handling must be of concern during patient's disease management. It includes hypertension, heart failure, coronary artery disease, diabetes mellitus or even sleep apnoea.

4 Other models used for the study of atrial fibrillation

4.1 Murine models

The mouse model remains an interesting model to study AF. Although physiological parameters in mouse tissue are quite different from the human one (heart rhythm for instance). The mouse myocardium has the advantage to express most of the currents responsible for the generation of an AP in human (Xu et al. 1999; Kovoor et al. 2001). Furthermore, the induction of AF has been shown to be possible, and most of the protocols to induce AF in large mammals (such as rapid atrial tachypacing or congestive heart failure protocols) are also applicable in the mouse model (Murphy et al. 2022).

One of the biggest advantages of using mouse as a model to study AF is that mouse has been genetically modified early, and today a diverse collection of genetically modified mouse lines is available on the market (Riley et al. 2012; Schüttler et al. 2020). Moreover, with the recent progresses in gene targeting and gene edition technologies, the generation of a new mouse line is not as laborious and expensive as it was before, allowing access to the research teams. For all these reasons, the utilisation of the mouse model is precious to unravel molecular pathways underlying remodelling mechanisms, and the model remains largely used.

Finally, costs for maintenance are reasonable in comparison with large animal models.

On the other hand, some limitations are associated with the utilisation of the murine model. The major issue is that the normal physiology of the mice is different from human. Mouse heart weights from 0.2 to 0.3 g, and its beating rate oscillates between 600 and 800 beats per minute, far from the normal range of human. Furthermore, AF does not occur spontaneously in mouse without genetic manipulation (Ozcan et al. 2015; Fu et al. 2022), and the episodes are sustained only for a few seconds (Wakimoto et al. 2001), whereas fibrillatory events in human can last for days. At the AP level, the atrial mouse AP is much shorter than human AP (from 40 to 80 ms) and pacing rate adaptation is not very marked.

The rat model does not significantly outline the mouse model as it shares many of the possibilities and incapacities that the mouse model does. However, some specific models have been developed in the context of AF including hypertensive rats (Doris 2017), long-term intensive training models (Benito et al. 2011), sleep apnoea and obesity models (Iwasaki et al. 2012) or a myocardial infarction model (Liu et al. 2019). However, unlike the mouse model, the rat model does not have the same genetic modified bibliotheca associated with it and is therefore only rarely used for the study of AF.

Advantages	Disadvantages
Genetic intervention (extensive mouse KO collection)	Translationalability
<i>In vivo</i> experiments	
Maintenance costs	

Supplemental table 1: Advantages and disadvantages of the utilisation of the mouse model for the study of atrial fibrillation.

4.2 Large mammalian models

4.2.1 Dog models

The dog model is a common model for the study of AF. Because of its small size, a lot of equipment used for human paediatrics can be used, and surgical procedures have been shown reliable results with only few complications.

Although dogs have a higher natural heart rate than humans, the heart mass is quite comparable with the human heart, and their electrophysiology is comparable.

Similarly as for other large mammalian models, the use of the pacing method became a gold standard for the study of AF in this model and resulted in the production of a large amount of scientific knowledge, which is still increasing.

Dog atrial electrophysiology is comparable with human electrophysiology, and the AP shape and duration are comparable. For these reasons, electrical remodelling is investigated using dog models, and results are often applicable to human (Li et al. 1999; Yue et al. 1999; Sinno et al. 2003; Voigt et al. 2007). Besides the rapid pacing protocols, congestive heart failure models (Sato and

Zipes 1996) and mitral regurgitation models (Mitchell et al. 1998) were also developed in dogs. Finally, atrial ischemia models have also been established (Sinno et al. 2003; Rivard et al. 2007).

However, some limitations are associated with the utilisation of the dog model. The first one is ECG differences including shorter P waves, QRS complexes and QT intervals (Clauss et al. 2019). Furthermore, the comparability of research performed on dogs are sometimes challenging because of the genetic background of breeds used for research, and the lack of standardised breeds. Finally, the dog is not widely accepted as a model for research, and ethic committees in many countries are not always in favour of their utilisation for research purposes.

Advantages	Disadvantages
Many models exist	No genetic breed
Translationability	Ethical acceptance
Long-term protocol feasible	
Utilisation of many already existing equipment possible	

Supplemental table 2: Advantages and disadvantages of the utilisation of the canine model for the study of atrial fibrillation.

4.2.2 Goat models

The goat model was one of the first models to be used for the study of AF, and many discoveries have been attributed to the use of the goat model, including the famous “AF begets AF” from Wijffels *et al* (1995).

Many protocols have been initiated using the goat as a study model, including the rapid atrial pacing protocol now widely accepted by the scientific community for the investigation of the different types of remodelling associated with AF.

Utilisation of the goat model has many advantages. The first one is that AF and pacing protocols can be maintained for a very long time (up to several months), allowing long pacing protocols, and both acute (paroxysmal) and long-term (persistent) effects of atrial remodelling to be studied. Furthermore, AF episodes can last for a very long time (up to two weeks), recapitulating human pathology

well. Because of the great resilience of the animal to pacing protocols, structural remodelling is also commonly studied in the goat model (Verheule et al. 2003). Furthermore, left atrial dilatation (a common risk factor for atrial fibrillation, Power et al. 1998), or chronic atrial inflammation models have also been developed (Zhang et al. 2015).

However, a couple of difficulties can occur with the use of the goat as a study model. First, to date, only one transgenic model of AF exists in goat (Polejaeva et al. 2016). Furthermore, goats have a lower respiratory rate in comparison to humans. This is associated with a maximum heart rate laying within the lower range of humans. Electrophysiologically, the AP is shorter, and only few cellular electrophysiological data is available. Furthermore, because goats are ruminants, their unique anatomy and physiology can cause a certain amount of risk with the anaesthesia and can lead to peri-operative complications. For this reason, it is often necessary to plan extra animals. Finally, goat housing and maintenance costs can be elevated.

Advantages	Disadvantages
<i>In vivo</i> AF begets	Availability
Solid model for long-term protocols and remodelling	No or only a few genetic models available
Translationalability	Perioperative stress needs to carefully be managed

Supplemental table 3: Advantages and disadvantages of the utilisation of the goat model for the study of atrial fibrillation.

4.2.3 Swine models

The swine model is now a largely accepted model for the study of AF. As swine body mass, heart size, metabolism and heart rate are comparable to human, the translationalability of the results obtained in the swine model are often applicable to human research.

Rapid atrial pacing protocols work well on swine, and AF can occur quickly (one to seven days) after the beginning of the pacing protocol (Bauer et al. 2004;

Lugenbiel et al. 2015). Other methods have also been developed to study AF, including during its acute phase (Lee et al. 2016).

Also, the swine model has the big advantage to show a remarkably similar electrophysiological profile as human, when comparing ECG, or AP. This can be explained because of swine express most human ion channel except for I_{to} (Mow et al. 2008).

The swine model also has been used as a model to study sleep apnoea induced AF and explore the role of carotid baroreceptors (Linz et al. 2016). Because of the similar anatomy and physiology of their heart, swine are also very often used in clinics for the development of catheter ablation procedures, or surgical approaches. Swine models are also a more accepted large model in modern societies (in comparison with dogs).

Amongst the limitations, we can cite the poor availability of genetic breed. The small collateralisation of coronaries that can lead to high risks of uncontrolled infection or even the development of ventricular fibrillation or coronary occlusion, thus being a risk for an increased number of animals (and expenses) for study completion. Maintenance costs associated with housekeeping of large mammals are also to be considered.

Advantages	Disadvantages
Translationalability	Availability
Good model for long-term pacing protocols	Genetic interventions
	Risks of high number required

Supplemental table 4: Advantages and disadvantages of the utilisation of the swine model for the study of atrial fibrillation.

4.3 In sillico models

In sillico models are remarkably interesting for the study of AF. Briefly, they aim to use computer simulations to recapitulate a physiological or electrophysiological phenomenon.

The greatest advantage associated with the utilisation of *in sillico* models, is that they do not require the utilisation of human or any biological material. Therefore, the legal/ethical requirements are less demanding. For these reasons, computer simulations can be accessible at any times under the only condition to be able to access and execute the programme. Another advantage of the *in sillico* model is that because each parameter enriching the simulation is coded, it is possible to individually study the participation of each factor in a biological process.

Adding to the versatility of the model, a wide variety of *in sillico* has been developed since the first computational model proposed by Nobel prize winners Hodgkin and Huxley in 1952 (Hodgkin and Huxley 1952), the first modelling of a cardiac AP in 1960 by Denis Noble (Noble 1960), and the first model for atrial fibrillation in 1964 developed by Gordon Moe (Moe et al. 1964).

Nowadays we have a large variety of possibilities for the modelling of the human AP (Courtemanche et al. 1998; Scholz et al. 2013), but also for the modelling of other species including swine (Peris-Yagüe et al. 2022), or mouse AP (Bondarenko et al. 2004; Asfaw et al. 2020).

Finally, computational modelling has largely evolved since its initial conception, compared to how it is now, in the context of AF, not only able to simulate AP changes, or 2D propagation, but also to simulate complex phenomena such as rotor or spiral waves propagation behaviour (Elliott et al. 2022; Rappel 2022), and also with the implementation of complex mathematical systems such as machine learning to also help clinicians refining their diagnoses and predict ablation or therapeutic outcomes (Roney et al. 2022).

The major disadvantage of the *in sillico* models are their precisions. Because they are “handmade” simulations, the precision of the result will mostly depend on the number of parameters that have been included in the programme. Electrophysiological behaviour is a phenomenon that requires the integration of many interconnected parameters and simplifying them for modelling purposes can be contra intuitive with regards to the results obtained and the interpretations that can be ended up made. Additionally, data sets used for the modelling are

often incomplete, mainly because of the practical possibilities to acquire the data in the first place (the human material used to perform electrophysiological investigation mainly comes from patients undergoing open heart surgery and is mostly originating from the right atrial appendage). Finally, the patient specific aspect of the current models remains limited, and personalisation (in terms of genetic background and/or environmental risk factors) remains limited as well, but also with regards to patient specific anatomical specificities (including orientation of the cardiac fibres) is often complicated to assess (Heijman et al. 2021).

Advantages	Disadvantages
Availability	Translationalability depends on the precision of the model
++ development at the moment	

Supplemental table 5: Advantages and disadvantages of the utilisation of *in sillico* models for the study of atrial fibrillation.

4.4 Small non mammalian models

The utilisation of non-mammalian models has been associated with the initial development of the experimental research in electrophysiology (ringer, frog), and has also led to the development of the modern comprehension of electrophysiology and their experimental approaches (Hodgkin and Huxley 1939).

However, they are not commonly used anymore, except for drosophila and fish models.

The drosophila model remains an extensively used model for genetic studies not only in cardiac research but also in the other research fields. It has the advantage to have an exceedingly high offspring number (2000 eggs per female), short life cycle (about 10 days at 25°C), conservation of genes and molecular pathways and relatively cheap maintenance costs. The drosophila model is largely used for studying congenital heart diseases because of the good overview and cartography of the model's genome, as it has been one of the first ones entirely

sequenced in March 2000 (Adams et al. 2000). Moreover, the development of recent techniques for genome editing allowed an increased precision on gene targeting. Interestingly, AF induction methods can be applied to drosophila, the most common one being the tachypacing, that can be done electrically (Li et al. 2022), or thanks to the use of optogenetic tools (Men et al. 2020).

From a physiological point of view, the zebrafish model is remarkably interesting as its electrophysiological behaviour is like the one observed in humans. Moreover, most of the genes involved in cardiac ion channels and regulatory subunits have an equivalent in the zebrafish genome. Physiologically, the heart rate is, with an average beating rate comprised between 120 and 180 bpm (Sampurna et al. 2018), in the high range of large mammals. Furthermore, its ECG presents similar waves as human, and its AP is also chamber specific (Brette et al., 2008; Nemtsas et al., 2010). Regarding the AP, although shorter in zebrafish because of faster beating rate, the AP presents the same characteristics as described in human, and although a prominent phase one cannot be observed, a plateau, and a slow repolarisation phase due to the presence of an orthologue of I_{Kr} (Nemtsas et al., 2010). The orthologue of I_{Kr} is already expressed 48 h after fertilisation (Echeazarra et al. 2021). Also, because of regenerative properties of the cardiac myocardium of the zebrafish, the model is extremely resilient and is also classically used in the context of cardiac regeneration and the molecular pathways involved (Milan and MacRae 2008; Jopling et al. 2010; Wilkinson et al. 2014; Rolland et al. 2021). From a technical point of view, the zebrafish model can also be very convenient: high fecundity, small size and easy handling are arguments for the utilisation of this model. Furthermore, because of its high fecundity and the fact that whole animals or whole organs, but also isolated cell experiments can easily be done, the model can fit to a variety of purposes. Finally, the utilisation of genome editing techniques is possible, bringing the possibilities to generate “humanised” cell lines, expressing human orthologs, and giving the model an interesting position in terms of pharmacological investigation and drug testing.

Advantages	Disadvantages
<i>In vivo</i> experiments	Translationalability
Genetic interventions	
Owing to its small size, short gestation period, rapid maturation	

Supplemental table 6: Advantages and disadvantages of the utilisation of non-mammalian models for the study of atrial fibrillation.

5 Other techniques to initiate atrial fibrillation *in vivo*

5.1 Congestive heart failure

Congestive heart failure (HF) is a common cause for AF (Lubitz et al. 2010). From a pathophysiological point of view, the development of HF is an adaptive and long process that results in the inability of the heart to maintain the contractile function of the heart (Malik et al. 2022), hence promoting atrial dilatation and apparition of fibrosis, a powerful substrate for the development of AF.

From an experimental point of view, the congestive heart failure model is achieved thanks to the implantation of a defibrillating pacemaker in the ventricle, followed by high frequency stimulation over a prolonged period (usually several weeks).

Results show that four weeks pacing resulted in a dramatic decrease of the ejection fraction, the enlargement of left atrial volumes, and the apparition of fibrosis (Knackstedt et al. 2008).

Similarly, the work of Li *et al.* in a dog model showed that five weeks of rapid ventricular pacing was associated with an increase of fibrosis, associated with an increase in susceptibility to AF induction after burst pacing, but no impairment in ERP and conduction velocity and wavelength size (Li et al. 1999).

Interestingly, this model has also allowed, in complement with a computational model, to investigate electrical remodelling in fibroblasts subjected to the CHF protocol. Patch-clamp investigation showed that CHF induced a downregulation of the tetraethylammonium-sensitive voltage-gated fibroblast current ($I_{Kv,fb}$), upregulation of the Ba^{2+} -sensitive inward rectifier current ($I_{Kir,fb}$), and a significant increase in cell capacitance. The implementation of these results to a computational model including cardiomyocyte-fibroblast electrical coupling showed that $I_{Kir,fb}$ had a profibrillatory effect on the cardiomyocytes, through AP shortening and RMP hyperpolarisation. Oppositely, they showed that $I_{Kv,fb}$ carried an antifibrillatory effect (Aguilar et al. 2014).

An increase in cAMP and cytosolic Ca²⁺ in the myocyte leads to an increased myocardial contractility and further prevents myocardial relaxation.

A decrease in cardiac output also stimulates the renin angiotensin aldosterone system that has been shown to increase myocardial cellular hypertrophy and interstitial fibrosis ("Effects of Enalapril on Mortality in Severe Congestive Heart Failure," 1987).

5.2 Mitral regurgitation

AF is frequently associated with mitral valve regurgitation (Melillo et al. 2020) and its presence is associated with an elevated risk of recidivism post-ablation (Qiao et al. 2016).

Therefore, it was thought that it could be used as a model to induce AF in an *in vivo* experimental model. On this base, the experimental model was first developed in dogs and rapidly exported to other animals as it had shown great results in developing an AF substrate (Spratt et al., 1983).

The mitral valve regurgitation model consists in surgically impairing the mitral valve function to cause blood reflux in the atria leading to atrial dilatation to generate a substrate for the inducibility of AF (Rankin et al. 1975).

This model was able to recapitulate a certain amount of remodelling associated with AF.

Regarding the structural remodelling, Verheule *et al.* showed that in dogs, six weeks of mitral valve regurgitation was associated with atrial dilatation with no impairment of the fractional shortening in right atria. Furthermore, chronic inflammation signs were observed in left atria, characterised by the infiltration of inflammatory cells while it was absent in right atria (Verheule et al. 2003). Interestingly, in another dog model, Bouwmeester *et al.* showed that mitral valve regurgitation was associated with a progressive atrial strain decrease after four weeks, and decompensated after 20 weeks, as the atrial dilatation progressed (Bouwmeester et al. 2022).

Interestingly, Sun *et al.* also showed that mitral valve regurgitation was associated with a decrease in connexin 40 and connexin 43, and the apparition of interstitial fibrosis in the pulmonary veins (Sun et al. 2008).

For the electrical remodelling, it was shown that the mitral valve regurgitation model in dogs, was associated with an increased susceptibility of AF induction of sustained episodes (<1 hour), and a prolongation of ERP in both atria at 300 ms cycle length (Verheule et al., 2003).

6 Investigation of the cardiac electrophysiology

6.1 *In vivo* approaches

6.1.1 Electrocardiogram

Initially named Einthoven's galvanometer, the electrocardiogram (ECG) was first introduced to the clinical world in 1901 by Nobel prize winner Willem Einthoven and first used by physicians MacNalty, Oxon and Lewis in 1908 for diagnostic purposes. Since then, the technique has been improved to make it more sensitive, and easier to install (it was originally weighting over 300 kg), thus leading to its rapid spread and worldwide use, however, the principle remains the same.

ECG is a technique used to measure the electrical potential of the heart during a systole-diastole cycle, thanks to the utilisation of surface electrodes placed on the skin. The resulting traces are called ECG and are composed of five different waves and complexes, all referring to specific cardiac events: the P wave corresponding in the depolarisation of the atria, followed by the QRS complex representing the depolarisation of the ventricles and the repolarisation of the atria, and finally, the T wave for the repolarisation of the ventricles. Originally, three electrodes were used to measure the ECG, but due to the evolution of the technique and the better understanding of the cardiac electrophysiology, 12 electrodes ECG is now the classic in clinical diagnostics as standard measure. Each trace taken from each derivation gives a very precise time and spatial overview of the heart electrical situation.

The utilisation of the ECG in clinic and research remains one of the gold standards in cardiac electrophysiology as it is now extremely easy to install and very versatile in the range of information it can allow to measure in a short amount of time. Furthermore, the development of the technology now allows portable devices to install on the patient's chest for long time recording.

6.1.2 Electrographic imaging techniques

Following decades of research on the optimisation of the ECG, a new non-invasive technique has been developed, the electrographic imaging techniques (ECGI). The torso is part of this group and consists in the utilisation of a vest with 252 unipolar surface electrodes connected to a non-invasive imaging system (computer tomography) that aims to reconstruct a structural and electrophysiological 3D map of the heart. ECGI techniques give extremely precise information thanks to the possibility of generating activation map, voltage map, isopotential maps or phase maps (Intini et al. 2005; Cluitmans et al. 2018; Pereira et al. 2020).

These techniques are extremely useful in the context of AF, as they can give unprecedented insight and whole tissue representation of complex mechanisms (for example the initiation and the maintenance of rotor or re-entry processes), so far only observable in explanted heart conditions.

They are also widely used in clinics together with the catheter ablation procedures to guide and orientate the movements and ensure the complete ablation of arrhythmogenic areas.

6.2 *In vitro* and *ex vivo* approaches

6.2.1 Tissular

At the tissular level, two major techniques are used for *ex vivo* investigations: the optical mapping technique and the sharp-microelectrode technique.

The optical mapping is a method that consists in the measurement of voltage and Ca^{2+} cellular changes in a tissue over time. Optical mapping techniques utilise properties of Ca^{2+} and voltage sensitive dyes in order to visualise and quantify their changes over time.

Using the same principle, voltage dyes were created for cellular or multicellular measurements (Kulkarni & Miller, 2017).

Since its first development by Hodgkin and Huxley and their experiments on giant squid axons, the sharp-microelectrode technique rapidly became inevitable for cardiac and neuronal electrophysiology research because of its versatility and its precision that constantly improved as the electronics and the amplifier

components quality improved over the last decades. The sharp-microelectrode technique allows the measurement of membrane potentials or currents in a cell using a high resistance glass microelectrode to access the inner side of the cell membrane. The principal advantage of this technique precisely resides in the utilisation of a high resistance pipette with very sharp and thin opening that allows measurement in living/beating organs or cells, without the need to break open the membrane to get electrical access. For this reason, it is also widely used for the measurement of currents and potentials in expression systems (especially oocytes).

6.2.2 Multi-cellular

The multi electrode array (or MEA) technique is a method used for the measurement of field potentials in multi-cellular preparations. Thanks to the spatial arrangement of the electrodes around the recording plate, and fixed distances separating the recording electrodes, this technique also allows the measurement of integrated parameters such as conduction velocity or the identification of depolarisation waves.

Furthermore, because the recording plates are detachable from the recording hardware, cell culture (and co-cultures) directly on the recording plates are also possible.

6.2.3 Cellular

The patch-clamp technique and its different configurations is the gold standard of examining cellular electrophysiology. Developed by Bert Sakmann and Erwin Neher in the middle of the years 1980 (Sakmann and Neher 1984), the patch-clamp is a technique used to measure membrane potentials or transmembrane currents in a single cell using a glass pipette. The recording is achieved by forming a close - high resistance - contact with the cell with the recording pipette (the pipette is “attached”, “patched” to the cell). Direct consequence of the Ohm’s Law, the measurement of either voltage or current must be associated with the control of the other parameter that is said “clamped”.

The classical patch-clamp experiment is decomposed in several steps: first, a glass recording pipette is approached to the vicinity of the cell, and a gentle

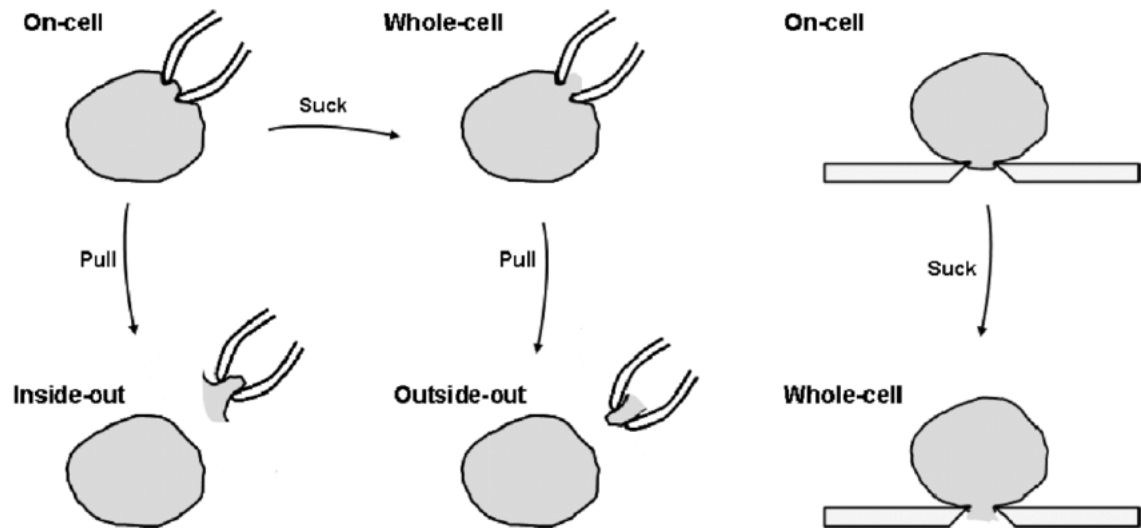
negative pressure is applied to the cell to form a close contact (so called giga-seal) between the cell and the recording pipette: this is the cell attached configuration. When breaking up the membrane while applying a stronger negative pressure, an opening to the inside of the cell is made, this is the whole-cell configuration. From the whole cell configuration, the experimenter can reach the outside-out configuration while pulling on the cell. Another configuration can be reached from the cell-attached configuration while pulling the cell membrane out: this is the inside-out configuration. Finally, it can be decided that the cell opening will not be done using physical approach but using chemical reagents such as antifungal (typically amphotericin). In this condition, electrical access is gained gradually through the generation of small permeability pores connecting the inside of the cell and the pipette solution: this is the perforated patch-clamp configuration. Perforated patch-clamp is made from the cell-attached configuration (Linley 2013).

After reaching any of these configurations, the experimenter chooses whether voltage or current is investigated. Measuring the voltage and clamping (controlling) the current defines the current-clamp mode. Clamping the voltage and measuring the current defines the voltage-clamp mode of the patch-clamp.

Planar patch-clamp also exists and is the base of some automated patch-clamp technologies. The principle resides in replacing the recording pipette with a perforated platform, from where the cell attaches (Vanoye et al. 2021).

Pipette-Based Patch Clamp

Planar Patch Clamp



Supplemental figure 3: The different patch-clamp configurations. From, Brueggemann et. al., Springer Nature books, 2009, with permissions.

7 Adeno-associated-virus-2 genome sequence

CTGCGCGCTCGCTCGCTCACTGAGGCCGCCCGGGCAAAGCCCGGGCGTC
GGGCGACCTTTGGTCGCCCGGCCTCAGTGAGCGAGCGAGCGCGCAGAGA
GGGAGTGGCCAACTCCATCACTAGGGGTTCCCTTGATGTTAATGATTAACCC
GCCATGCTACTTATCTACGTAGCCATGCTCTAGGAAGAGTACCATTGACGT
CAATAATGACGTATGTTCCCATAGTAACGCCAATAGGGACTTTCCATTGAC
GTCAATGGGTGGAGTATTTACGGTAAACTGCCCACTTGGCAGTACATCAAG
TGTATCATATGCCAAGTACGCCCCCTATTGACGTCAATGACGGTAAATGGC
CCGCCTGGCATTATGCCCAGTACATGACCTTATGGGACTTTCCCTACTTGGC
AGTACATCTACGTATTAGTCATCGCTATTACCATGGTTCGAGGTGAGCCCA
CGTTCTGCTTCACTCTCCCCATCTCCCCCCCCCTCCCCACCCCAATTTTGT
ATTTATTTATTTTTTAATTATTTTGTGCAGCGATGGGGGCGGGGGGGGGGG
GGGGGCGCGCGCCAGGCGGGGCGGGGCGGGGCGAGGGGCGGGGCGG
GGCGAGGCGGAGAGGTGCGGCGGCAGCCAATCAGAGCGGCGCGCTCCG
AAAGTTTCCTTTTATGGCGAGGCGGCGGGCGGCGGCCCTATAAAAAGC
GAAGCGCGCGGCGGGCGGGAGTCGCTGCGCGCTGCCTTCGCCCCGTGC
CCCGCTCCGCCGCCGCTCGCGCCGCCCGCCCCGGCTCTGACTGACCG
CGTTACTCCACAGGTGAGCGGGCGGGACGGCCCTTCTCCTCCGGGCTG
TAATTAGCGCTTGGTTTAATGACGGCTTGTTTCTTTTCTGTGGCTGCGTGA
AAGCCTTGAGGGGCTCCGGGAGGGCCCTTTGTGCGGGGGGAGCGGCTC
GGGGCTGTCCGCGGGGGGACGGCTGCCTTCGGGGGGGACGGGGCAGG
GCGGGGTTCCGGCTTCTGGCGTGTGACCGGCGGCTCTAGAGCCTCTGCTA
ACCATGTTTCATGCCTTCTTCTTTTCTACAGCTCCTGGGCAACGTGCTGG
TTATTGTGCTGTCTCATCATTTTGGCAAAGAATTGGATCGGGATCCACTAG
TCCAGTGTGGTGAATTGCCCTTGCTGCCACCATGGACTATGGCGGCGCT
TTGTCTGCCGTCGGACGCGAACTTTTGTTCGTTACTAATCCTGTGGTGGTG
AACGGGTCCGTCCTGGTCCCTGAGGATCAATGTTACTGTGCCGGATGGAT
TGAATCTCGCGGCACGAACGGCGCTCAGACCGCGTCAAATGTCCTGCAGT
GGCTTGCAGCAGGATTCAGCATTTTGTCTGCTGATGTTCTATGCCTACCAA
CCTGGAAATCTACATGCGGCTGGGAGGAGATCTATGTGTGCGCCATTGAA
ATGGTTAAGGTGATTCTCGAGTTCTTTTTTGTGTTAAGAATCCCTCTATGC
TCTACCTTGCCACAGGACACCGGGTGCAGTGGCTGCGCTATGCAGAGTG
GCTGCTCACTTGTCTGTGCATCCTTATCCGCCTGAGCAACCTCACCGGCCT

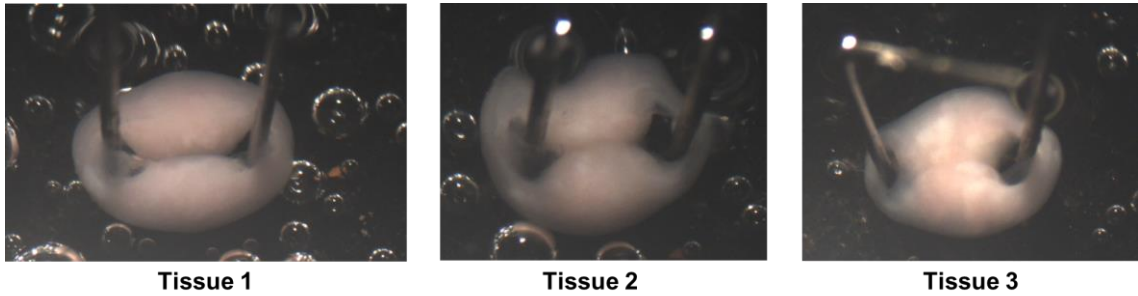
GAGCAACGACTACAGCAGGAGAACCATGGGACTCCTTGTCTCAGACATCG
GGACTATCGTGTGGGGGGCTACCAGCGCCATGGCAACCGGCTATGTTAAA
GTCATCTTCTTTTGTCTTGGATTGTGCTATGGCGCGAACACATTTTTTCACG
CCGCCAAAGCATATATCGAGGGTTATCATACTGTGCCAAAGGGTCGGTGC
CGCCAGGTCGTGACCGGCATGGCATGGCTGTTTTTCGTGAGCTGGGGTAT
GTTCCCAATTCTCTTCATTTTGGGGCCCGAAGGTTTTGGCGTCCTGAGCGT
CTATGGCTCCACCGTAGGTCACACGATTATTGATCTGATGAGTAAAAATTG
TTGGGGGTTGTTGGGACACTACCTGCGCGTCCTGATCCACGAGCACATAT
TGATTCACGGAGATATCCGCAAACCACCAAACCTGAACATCGGCGGAACG
GAGATCGAGGTCGAGACTCTCGTCTGAAGACGAAGCCGAGGCCGGAGCCG
TGCCAGCGGCCCGCGTGAGCAAGGGCGAGGAGGATAACATGGCCATCAT
CAAGGAGTTCATGCGCTTCAAGGTGCACATGGAGGGCTCCGTGAACGGC
CACGAGTTCGAGATCGAGGGCGAGGGCGAGGGCCGCCCTACGAGGGC
ACCCAGACCGCCAAGCTGAAGGTGACCAAGGGTGGCCCCCTGCCCTTCG
CCTGGGACATCCTGTCCCCTCAGTTCATGTACGGCTCCAAGGCCTACGTG
AAGCACCCCGCCGACATCCCCGACTACTTGAAGCTGTCCTTCCCCGAGGG
CTTCAAGTGGGAGCGCGTGATGAACTTCGAGGACGGCGGCGTGTTGACC
GTGACCCAGGACTCCTCCCTGCAGGACGGCGAGTTCATCTACAAGGTGAA
GCTGCGCGGCACCAACTTCCCCTCCGACGGCCCCGTAATGCAGAAGAAG
ACCATGGGCTGGGAGGCCTCCTCCGAGCGGATGTACCCCGAGGACGGCG
CCCTGAAGGGCGAGATCAAGCAGAGGCTGAAGCTGAAGGACGGCGGCCA
CTACGACGCTGAGGTCAAGACCACCTACAAGGCCAAGAAGCCCGTGCAG
CTGCCCGGGCGCCTACAACGTCAACATCAAGTTGGACATCACCTCCCACAA
CGAGGACTACACCATCGTGGAACAGTACGAACGCGCCGAGGGCCGCCAC
TCCACCGGCGGCATGGACGAGCTGTACAAGTAAAGCGGCCCCCGGACTCG
AGGCCGCGAGGTAAGTATCAAGGTTACAAGACAGGTTTAAGGAGACCAATA
GAACTGGGCTTGTGCGAGACAGAGAAGACTCTTGCGTTTTCTGATAGGCAC
CTATTGGTCTTACTGACATCCACTTTGCCTTTCTCTCCACAGGTGTCGAGT
GGAGCTCGCGACTAGTCGATTCGAATTCGATATCAAGCTTATCGATAATCA
ACCTCTGGATTACAAAATTTGTGAAAGATTGACTGGTATTCTTA ACTATGTT
GCTCCTTTTACGCTATGTGGATACGCTGCTTTAATGCCTTTGTATCATGCTA
TTGCTTCCCGTATGGCTTTTCATTTTCTCCTCCTTGTATAAATCCTGGTTGCT
GTCTCTTTATGAGGAGTTGTGGCCCGTTGTCAGGCAACGTGGCGTGTTGT
GCACTGTGTTTGCTGACGCAACCCCCACTGGTTGGGGCATTGCCACCACC

TGTCAGCTCCTTTCCGGGACTTTTCGCTTTCCCCCTCCCTATTGCCACGGCG
GAACTCATCGCCGCCTGCCTTGCCCGCTGCTGGACAGGGGCTCGGCTGT
TGGGCACTGACAATTCCGTGGTGTGTCGGGGAAATCATCGTCCTTTCTT
GGCTGCTCGCCTGTGTTGCCACCTGGATTCTGCGCGGGACGTCCTTCTGC
TACGTCCCTTCGGCCCTCAATCCAGCGGACCTTCCTTCCCGCGGCCTGCT
GCCGGCTCTGCGGCCTCTTCCGCGTCTTCGCCTTCGCCCTCAGACGAGTC
GGATCTCCCTTTGGGCCGCCTCCCCGCATCGATAACCGTCGACCCGGGCG
GCCGCTTCGAGCAGACATGATAAGATAATTGATGAGTTTGGACAAACCAC
AACTAGAATGCAGTGAAAAAATGCTTTATTTGTGAAATTTGTGATGCTATT
GCTTTATTTGTAACCATTATAAGCTGCAATAACAAGTTAACAACAACAATT
GCATTCATTTTATGTTTCAGGTTTCAGGGGGAGATGTGGGAGGTTTTTTAAA
GCAAGTAAAACCTCTACAAATGTGGTAAAATCGATAAGGATCTTCCTAGAG
CATGGCTACGTAGATAAGTAGCATGGCGGGTTAATCATTAACTACAAGGAA
CCCCTAGTGATGGAGTTGGCCACTCCCTCTCTGCGCGCTCGCTCGCTCAC
TGAGGCCGGGCGACCAAAGGTCGCCCGACGCCCGGGCTTTGCCCGGGC
GGCCTCAGTGAGCGAGCGAGCGCGCAGCCTTAATTAACCTAATCACTGG
CCGTCGTTTTACAACGTCGTGACTGGGAAAACCCTGGCGTTACCCAACTTA
ATCGCCTTGCAGCACATCCCCCTTTCGCCAGCTGGCGTAATAGCGAAGAG
GCCCGCACCGATCGCCCTTCCCAACAGTTGCGCAGCCTGAATGGCGAATG
GGACGCGCCCTGTAGCGGCGCATTAAAGCGCGGGCGGGTGTGGTGGTTACG
CGCAGCGTGACCGCTACACTTGCCAGCGCCCTAGCGCCCGCTCCTTTTCG
CTTTCTTCCCTTCCTTTCTCGCCACGTTGCGCCGGCTTTCCCGTCAAGCTC
TAAATCGGGGGCTCCCTTTAGGGTTCCGATTTAGTGCTTTACGGCACCTCG
ACCCCAAAAACTTGATTAGGGTGATGGTTCACGTAGTGGGCCATCGCCC
TGATAGACGGTTTTTTCGCCCTTTGACGTTGGAGTCCACGTTCTTTAATAGT
GGACTCTTGTTCCAAACTGGAACAACACTCAACCCTATCTCGGTCTATTCT
TGATTTAACAAAAATTTAACGCGAATTTAACAAAATATTAACGCTTACAATT
TAGGTGGCACTTTTCGGGGAAATGTGCGCGGAACCCCTATTTGTTTATTT
TCTAAATACATTCAAATATGTATCCGCTCATGAGACAATAACCCTGATAAAT
GCTTCAATAATATTGAAAAAGGAAGAGTATGAGTATTCAACATTTCCGTGTC
GCCCTTATTCCCTTTTTTTCGGGCATTTTGCCTTCCTGTTTTTGTCAACCCAG
AAACGCTGGTGAAAGTAAAAGATGCTGAAGATCAGTTGGGTGCACGAGTG
GGTTACATCGAACTGGATCTCAACAGCGGTAAGATCCTTGAGAGTTTTTCG
CCGAAGAACGTTTTCCAATGATGAGCACTTTTAAAGTTCTGCTATGTGGC

GCGGTATTATCCCGTATTGACGCCGGGCAAGAGCAACTCGGTGCGCCGCAT
ACACTATTCTCAGAATGACTTGGTTGAGTACTCACCAGTCACAGAAAAGCA
TCTTACGGATGGCATGACAGTAAGAGAATTATGCAGTGCTGCCATAACCAT
GAGTGATAACACTGCGGCCAACTTACTTCTGACAACGATCGGAGGACCGA
AGGAGCTAACCGCTTTTTTGCACAACATGGGGGATCATGTAACCTGCTTG
ATCGTTGGGAACCGGAGCTGAATGAAGCCATACCAAACGACGAGCGTGAC
ACCACGATGCCTGTAGCAATGGCAACAACGTTGCGCAAACCTATTAACCTGG
CGAACTACTTACTCTAGCTTCCCGGCCAACAATTAATAGACTGGATGGAGGC
GGATAAAGTTGCAGGACCACTTCTGCGCTCGGCCCTTCCGGCTGGCTGGT
TTATTGCTGATAAATCTGGAGCCGGTGAGCGTGGGTCTCGCGGTATCATT
GCAGCACTGGGGCCAGATGGTAAGCCCTCCCGTATCGTAGTTATCTACAC
GACGGGGAGTCAGGCAACTATGGATGAACGAAATAGACAGATCGCTGAGA
TAGGTGCCTCACTGATTAAGCATTGGTAACTGTCAGACCAAGTTTACTCAT
ATATACTTTAGATTGATTTAAACTTCATTTTTAATTTAAAGGATCTAGGTG
AAGATCCTTTTTGATAATCTCATGACCAAATCCCTTAACGTGAGTTTTCGT
TCCACTGAGCGTCAGACCCCGTAGAAAAGATCAAAGGATCTTCTTGAGATC
CTTTTTTCTGCGCGTAATCTGCTGCTTGCAAACAAAAAACCACCGCTAC
CAGCGGTGGTTTGTGGCCGGATCAAGAGCTACCAACTCTTTTTCCGAAGG
TAACTGGCTTCAGCAGAGCGCAGATACCAAATACTGTTCTTCTAGTGTAGC
CGTAGTTAGGCCACCACTTCAAGAACTCTGTAGCACCGCCTACATACCTCG
CTCTGCTAATCCTGTTACCAGTGGCTGCTGCCAGTGGCGATAAGTCGTGT
CTTACCGGGTTGGACTCAAGACGATAGTTACCGGATAAGGCGCAGCGGTC
GGGCTGAACGGGGGGTTCGTGCACACAGCCCAGCTTGGAGCGAACGACC
TACACCGAACTGAGATACCTACAGCGTGAGCTATGAGAAAGCGCCACGCT
TCCCGAAGGGAGAAAGGCGGACAGGTATCCGGTAAGCGGCAGGGTCGGA
ACAGGAGAGCGCACGAGGGAGCTTCCAGGGGGAAACGCCTGGTATCTTT
ATAGTCCTGTCGGGTTTCGCCACCTCTGACTTGAGCGTCGATTTTTGTGAT
GCTCGTCAGGGGGGCGGAGCCTATGGAAAACGCCAGCAACGCGGCCTT
TTTACGGTTCCTGGCCTTTTGCTGGCCTTTTGCTCACATGTTCTTTCCTGC
GTTATCCCCTGATTCTGTGGATAACCGTATTACCGCCTTTGAGTGAGCTGA
TACCGCTCGCCGCAGCCGAACGACCGAGCGCAGCGAGTCAGTGAGCGAG
GAAGCGGAAGAGCGCCCAATACGCAAACCGCCTCTCCCCGCGCGTTGGC
CGATTCATTAATGCAGCTGGCACGACAGGTTTCCCGACTGGAAAGCGGGC
AGTGAGCGCAACGCAATTAATGTGAGTTAGCTCACTCATTAGGCACCCCA

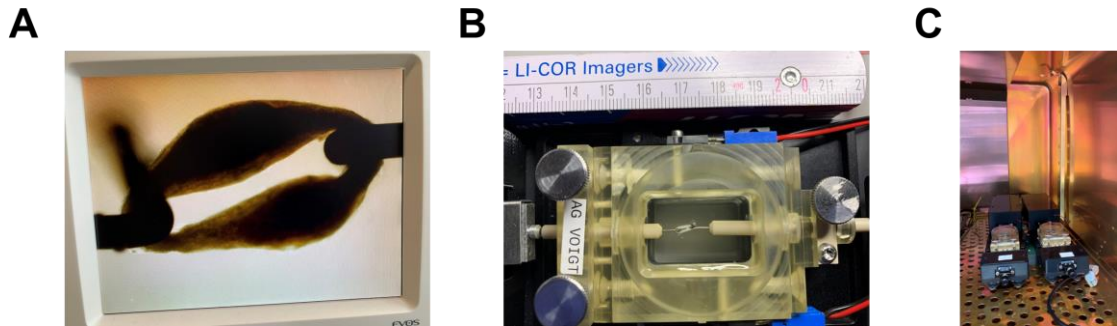
GGCTTTACACTTTATGCTTCCGGCTCGTATGTTGTGTGGAATTGTGAGCGG
ATAACAATTTACACAGGAAACAGCTATGACCATGATTACGCCAGATTTAAT
TAAGGGCAACTGTTGGGAAGGGCGATCGGTGCGGGCCTCTTCGCTATTAC
GCCAG

8 Engineered human myocardium generated with induced pluripotent stem cells transfected with an adeno-associated virus-2 carrying a channelrhodopsin-2



Supplemental figure 4: Pictures of atrial engineered human myocardium generated with induced pluripotent stem cells transfected with an adeno-associated virus-2 carrying a channelrhodopsin-2, 30 days after the tissue preparation.

9 Long-term optical tachypacing experimental set-up



Supplemental figure 5: Pictures of the experimental set-up used for the optical tachypacing of the chromson-engineered human myocardium. A, Picture of a chromson EHM mounted on the force recording set-up to measure its contraction during the 7 day optical tachypacing protocol and **B,** picture of the cultivation chamber containing an EHM. **C,** Picture of the experimental set-up placed in the incubator for temperature and oxygen control.

10 Supplemental references

- Adams MD, Celniker SE, Holt RA, Evans CA, Gocayne JD, Amanatides PG, Scherer SE, Li PW, Hoskins RA, Galle RF, et al. (2000): The genome sequence of *Drosophila melanogaster*. *Science* (1979) 287, 2185–2195
- Aguilar M, Qi XY, Huang H, Nattel S (2014): Fibroblast electrical remodeling in heart failure and potential effects on atrial fibrillation. *Biophys J* 107, 2444–2455
- Andrade JG, Deyell MW, Macle L, Wells GA, Bennett M, Essebag V, Champagne J, Roux J-F, Yung D, Skanes A, et al. (2022): Progression of Atrial Fibrillation after Cryoablation or Drug Therapy. *New England Journal of Medicine*
- Asfaw TN, Tyan L, Glukhov A v., Bondarenko VE (2020): A compartmentalized mathematical model of mouse atrial myocytes. *Am J Physiol Heart Circ Physiol* 318, H485–H507
- Bauer A, McDonald AD, Donahue JK (2004): Pathophysiological findings in a model of persistent atrial fibrillation and severe congestive heart failure. *Cardiovasc Res* 61, 764–770
- Benito B, Gay-Jordi G, Serrano-Mollar A, Guasch E, Shi Y, Tardif JC, Brugada J, Nattel S, Mont L (2011): Cardiac arrhythmogenic remodeling in a rat model of long-term intensive exercise training. *Circulation* 123, 13–22
- Bondarenko VE, Szigetzi GP, Bett GCL, Kim S-J, Rasmusson RL (2004): Computer model of action potential of mouse ventricular myocytes. *American Journal of Physiology-Heart and Circulatory Physiology* 287, H1378–H1403
- Bouwmeester S, van Loon T, Ploeg M, Mast TP, Verzaal NJ, van Middendorp LB, Strik M, van Nieuwenhoven FA, Dekker LR, Prinzen FW, et al. (2022): Left atrial remodeling in mitral regurgitation: A combined experimental-computational study. *PLoS One* 17, e0271588
- Brette F, Luxan G, Cros C, Dixey H, Wilson C, Shiels HA (2008): Characterization of isolated ventricular myocytes from adult zebrafish (*Danio rerio*). *Biochem Biophys Res Commun* 374, 143–146
- Bruce A, Alexander J, Julian L, Martin R, Keith R, Peter W: *Molecular Biology of the Cell - Books - NCBI*. Garland Science; 2002
- Clauss S, Bleyer C, Schüttler D, Tomsits P, Renner S, Klymiuk N, Wakili R, Massberg S, Wolf E, Käab S (2019): Animal models of arrhythmia: classic electrophysiology to genetically modified large animals. *Nat Rev Cardiol* 16, 457–475
- Cluitmans M, Brooks DH, MacLeod R, Dössel O, Guillem MS, van Dam PM, Svehlikova J, He B, Sapp J, Wang L, Bear L (2018): Validation and opportunities of electrocardiographic imaging: From technical achievements to clinical applications. *Front Physiol* 9, 1305
- Courtemanche M, Ramirez RJ, Nattel S (1998): Ionic mechanisms underlying human atrial action potential properties: Insights from a mathematical model. *Am J Physiol Heart Circ Physiol* 275

- Doris PA (2017): Genetics of hypertension: An assessment of progress in the spontaneously hypertensive rat. *Physiol Genomics* 49, 601–617
- Echeazarra L, Hortigón-Vinagre MP, Casis O, Gallego M (2021): Adult and Developing Zebrafish as Suitable Models for Cardiac Electrophysiology and Pathology in Research and Industry. *Front Physiol* 11, 1692
- Effects of Enalapril on Mortality in Severe Congestive Heart Failure (1987) *New England Journal of Medicine* 316, 1429–1435
- Elliott J, Mainardi L, Rodriguez Matas JF (2022): Cellular heterogeneity and repolarisation across the atria: an in silico study. *Med Biol Eng Comput* 60, 3153–3168
- Fu F, Pietropaolo M, Cui L, Pandit S, Li W, Tarnavski O, Shetty SS, Liu J, Lussier JM, Murakami Y, et al. (2022): Lack of authentic atrial fibrillation in commonly used murine atrial fibrillation models. *PLoS One* 17, e0256512
- Heijman J, Sutanto H, Crijns HJGM, Nattel S, Trayanova NA (2021): Computational models of atrial fibrillation: Achievements, challenges, and perspectives for improving clinical care. *Cardiovasc Res* 117, 1682–1699
- Hindricks G, Potpara T, Dagres N, Arbelo E, Bax JJ, Blomström-Lundqvist C, Boriani G, Castella M, Dan G-A, Dilaveris PE, et al. (2021): 2020 ESC Guidelines for the diagnosis and management of atrial fibrillation developed in collaboration with the European Association for Cardio-Thoracic Surgery (EACTS). *Eur Heart J* 42, 373–498
- Hodgkin AL, Huxley AF (1939): Action potentials recorded from inside a nerve fibre. *Nature* 144, 710–711
- Hodgkin AL, Huxley AF (1952): A quantitative description of membrane current and its application to conduction and excitation in nerve. *J Physiol* 117, 500–544
- Intini A, Goldstein RN, Jia P, Ramanathan C, Ryu K, Giannattasio B, Gilkeson R, Stambler BS, Brugada P, Stevenson WG, et al. (2005): Electrocardiographic imaging (ECGI), a novel diagnostic modality used for mapping of focal left ventricular tachycardia in a young athlete. *Heart Rhythm* 2, 1250–1252
- Iwasaki YK, Shi Y, Benito B, Gillis MA, Mizuno K, Tardif JC, Nattel S (2012): Determinants of atrial fibrillation in an animal model of obesity and acute obstructive sleep apnea. *Heart Rhythm* 9, 1409-1416.e1
- Jiang D, Shi H, Tonggu L, Gamal El-Din TM, Lenaeus MJ, Zhao Y, Yoshioka C, Zheng N, Catterall WA (2020): Structure of the Cardiac Sodium Channel. *Cell* 180, 122-134.e10
- Jopling C, Sleep E, Raya M, Martí M, Raya A, Belmonte JCI (2010): Zebrafish heart regeneration occurs by cardiomyocyte dedifferentiation and proliferation. *Nature* 464, 606–609
- Knackstedt C, Gramley F, Schimpf T, Mischke K, Zarse M, Plisiene J, Schmid M, Lorenzen J, Frechen D, Neef P, et al. (2008): Association of echocardiographic atrial size and atrial fibrosis in a sequential model of congestive heart failure and atrial fibrillation. *Cardiovascular Pathology* 17, 318–324

- Kovoor P, Wickman K, Maguire CT, Pu W, Gehrman J, Berul CI, Clapham DE (2001): Evaluation of the role of $I_{K_{ACH}}$ in atrial fibrillation using a mouse knockout model. *J Am Coll Cardiol* 37, 2136–2143
- Kulkarni RU, Miller EW (2017): Voltage Imaging: Pitfalls and Potential. *Biochemistry* 56, 5171–5177
- Lai LP, Su MJ, Lin JL, Lin FY, Tsai CH, Chen YS, Huang SKS, Tseng YZ, Lien WP (1999): Down-regulation of L-type calcium channel and sarcoplasmic reticular Ca^{2+} -ATPase mRNA in human atrial fibrillation without significant change in the mRNA of ryanodine receptor, calsequestrin and phospholamban: An insight into the mechanism of atrial electrical remodeling. *J Am Coll Cardiol* 33, 1231–1237
- Lampert A, Korngreen A: Markov Modeling of Ion Channels. In: Progress in molecular biology and translational science. Band 123; Prog Mol Biol Transl Sci 2014, 1–21
- Lee AM, Miller JR, Voeller RK, Zierer A, Lall SC, Schuessler RB, Damiano RJ, Melby SJ (2016): A Simple Porcine Model of Inducible Sustained Atrial Fibrillation. *Innovations: Technology and Techniques in Cardiothoracic and Vascular Surgery* 11, 76–78
- Li D, Fareh S, Leung TK, Nattel S (1999): Promotion of Atrial Fibrillation by Heart Failure in Dogs. *Circulation* 100, 87–95
- Li J, Qi X, Ramos KS, Lanters E, Keijer J, de Groot N, Brundel B, Zhang D (2022): Disruption of Sarcoplasmic Reticulum-Mitochondrial Contacts Underlies Contractile Dysfunction in Experimental and Human Atrial Fibrillation: A Key Role of Mitofusin 2. *J Am Heart Assoc*
- Li L yi fei, Lou Q, Liu G zhong, Lv J chen, Yun F xiang, Li T kai, Yang W, Zhao H yan, Zhang L, Bai N, et al. (2020): Sacubitril/valsartan attenuates atrial electrical and structural remodelling in a rabbit model of atrial fibrillation. *Eur J Pharmacol* 881, 173120
- Lim HW, de Windt LJ, Mante J, Kimball TR, Witt SA, Sussman MA, Molkenin JD (2000): Reversal of cardiac hypertrophy in transgenic disease models by calcineurin inhibition. *J Mol Cell Cardiol* 32, 697–709
- Linley JE (2013): Perforated whole-cell patch-clamp recording. *Methods in Molecular Biology* 998, 149–157
- Linz D, Hohl M, Khoshkish S, Mahfoud F, Ukena C, Neuburger HR, Wirth K, BÖHM M (2016): Low-Level But Not High-Level Baroreceptor Stimulation Inhibits Atrial Fibrillation in a Pig Model of Sleep Apnea. *J Cardiovasc Electrophysiol* 27, 1086–1092
- Liu M, Li W, Wang H, Yin L, Ye B, Tang Y, Huang C (2019): CTRP9 Ameliorates Atrial Inflammation, Fibrosis, and Vulnerability to Atrial Fibrillation in Post-Myocardial Infarction Rats. *J Am Heart Assoc* 8
- Lo M, Nair D, Mansour M, Calkins H, Reddy VY, Colley BJ, Tanaka-Esposito C, Sundaram S, DeLurgio DB, Sanders P, et al. (2022): Contact force catheter ablation for the treatment of Persistent Atrial Fibrillation: Results from the Persist-End Study. *J Cardiovasc Electrophysiol*

- Lubitz SA, Benjamin EJ, Ellinor PT (2010): Atrial Fibrillation in Congestive Heart Failure. *Heart Fail Clin* 6, 187–200
- Lugenbiel P, Wenz F, Govorov K, Schweizer PA, Katus HA, Thomas D (2015): Atrial fibrillation complicated by heart failure induces distinct remodeling of calcium cycling proteins. *PLoS One* 10
- Malik A, Brito D, Vaqar S, Chhabra L, Doerr C: Congestive Heart Failure (Nursing). 2022
- Mannakkara NN, Porter B, Child N, Sidhu BS, Mehta VS, Elliott MK, Gould J, Ahmed S, Razavi R, Rinaldi CA, et al. (2022): Convergent Ablation for Persistent Atrial Fibrillation: Outcomes from a Single-Center Real-world Experience. *European Journal of Cardio-Thoracic Surgery*
- Marban E, Yamagishi T, Tomaselli GF (1998): Structure and function of voltage-gated sodium channels. *J Physiol* 508, 647–657
- Mattiazzi A, Kranias EG (2014): The role of CaMKII regulation of phospholamban activity in heart disease. *Front Pharmacol* 5 JAN, 5
- Melillo E, Rago A, Proietti R, Attena E, Carrella M, Golino P, D'Onofrio A, Nigro G, Russo V (2020): Atrial Fibrillation and Mitral Regurgitation: Clinical Performance of Direct Oral Anticoagulants in a Real-World Setting. *J Cardiovasc Pharmacol Ther* 25, 564–569
- Men J, Li A, Jerwick J, Li Z, Tanzi RE, Zhou C (2020): Non-invasive red-light optogenetic control of *Drosophila* cardiac function. *bioRxiv* 2020.01.26.920132
- Milan DJ, MacRae CA (2008): Zebrafish genetic models for arrhythmia. *Prog Biophys Mol Biol* 98, 301–308
- Mitchell MA, McRury ID, Haines DE (1998): Linear Atrial Ablations in a Canine Model of Chronic Atrial Fibrillation. *Circulation* 97, 1176–1185
- Moe GK, Rheinboldt WC, Abildskov JA (1964): A computer model of atrial fibrillation. *Am Heart J* 67, 200–220
- Molkentin JD, Lu JR, Antos CL, Markham B, Richardson J, Robbins J, Grant SR, Olson EN (1998): A calcineurin-dependent transcriptional pathway for cardiac hypertrophy. *Cell* 93, 215–228
- Mow T, Arlock P, Laursen M, Ganderup N-C (2008): Major ion currents except ito are present in the ventricle of the Göttingen minipig heart. *J Pharmacol Toxicol Methods* 58, 165
- Murphy MB, Kim K, Kannankeril PJ, Subati T, van Amburg JC, Barnett J v., Murray KT (2022): Optimizing transesophageal atrial pacing in mice to detect atrial fibrillation. *Am J Physiol Heart Circ Physiol* 322, H36–H43
- Nemtsas P, Wettwer E, Christ T, Weidinger G, Ravens U (2010a): Adult zebrafish heart as a model for human heart? An electrophysiological study. *J Mol Cell Cardiol* 48, 161–171
- Nemtsas P, Wettwer E, Christ T, Weidinger G, Ravens U (2010b): Adult zebrafish heart as a model for human heart? An electrophysiological study. *J Mol Cell Cardiol* 48, 161–171

- Ni L, Lahiri SK, Nie J, Pan X, Abu-Taha I, Reynolds JO, Campbell HM, Wang H, Kamler M, Schmitz W, et al. (2021): Genetic inhibition of nuclear factor of activated T-cell c2 prevents atrial fibrillation in CREM transgenic mice. *Cardiovasc Res*
- Noble D (1960): Cardiac action and pacemaker potentials based on the Hodgkin-Huxley equations. *Nature* 188, 495–497
- Ozcan C, Battaglia E, Young R, Suzuki G (2015): Lkb1 knockout mouse develops spontaneous atrial fibrillation and provides mechanistic insights into human disease process. *J Am Heart Assoc* 4
- Pereira H, Niederer S, Rinaldi CA (2020): Electrocardiographic imaging for cardiac arrhythmias and resynchronization therapy. *Europace* 22, 1447–1462
- Peris-Yagüe V, Rubio T, Fakuade FE, Voigt N, Luther S, Majumder R (2022): A Mathematical Model for Electrical Activity in Pig Atrial Tissue. *Front Physiol* 13, 250
- Polejaeva IA, Ranjan R, Davies CJ, Regouski M, Hall J, Olsen AL, Meng Q, Rutigliano HM, Dossdall DJ, Angel NA, et al. (2016): Increased Susceptibility to Atrial Fibrillation Secondary to Atrial Fibrosis in Transgenic Goats Expressing Transforming Growth Factor- β 1. *J Cardiovasc Electrophysiol* 27, 1220–1229
- Power JM, Beacom GA, Alferness CA, Raman J, Wijffels M, Farish SJ, Burrell LM, Tonkin AM (1998): Susceptibility to atrial fibrillation: A study in an ovine model of pacing-induced early heart failure. *J Cardiovasc Electrophysiol* 9, 423–435
- Qiao Y, Wu L, Hou B, Sun W, Zheng L, Ding L, Chen G, Zhang S, Yao Y (2016): Functional mitral regurgitation: Predictor for atrial substrate remodeling and poor ablation outcome in paroxysmal atrial fibrillation. *Medicine (United States)* 95
- Rankin JS, Nicholas LM, Kouchoukos NT (1975): Experimental mitral regurgitation: effects on left ventricular function before and after elimination of chronic regurgitation in the dog. *Journal of Thoracic and Cardiovascular Surgery* 70, 478–488
- Rappel WJ (2022): Intermittent trapping of spiral waves in a cardiac model. *Phys Rev E* 105, 014404
- Riley G, Syeda F, Kirchhof P, Fabritz L (2012): An introduction to murine models of atrial fibrillation. *Front Physiol* 3 AUG, 296
- Rivard L, Sinno H, Shiroshita-Takeshita A, Schram G, Leung TK, Nattel S (2007): The pharmacological response of ischemia-related atrial fibrillation in dogs: Evidence for substrate-specific efficacy. *Cardiovasc Res* 74, 104–113
- Rolland L, Harrington A, Faucherre A, Gangatharan G, Gamba L, Severac D, Pratlong M, Moore-Morris T, Jopling C (2021): The regenerative response of cardiac interstitial cells. *bioRxiv* 2021.10.25.465720
- Roney CH, Sim I, Yu J, Beach M, Mehta A, Alonso Solis-Lemus J, Kotadia I, Whitaker J, Corrado C, Razeghi O, et al. (2022): Predicting Atrial Fibrillation

- Recurrence by Combining Population Data and Virtual Cohorts of Patient-Specific Left Atrial Models. *Circ Arrhythm Electrophysiol* 15, e010253
- Sakmann B, Neher E (1984): Patch clamp techniques for studying ionic channels in excitable membranes. *Annu Rev Physiol* VOL. 46, 455–472
- Sampurna B, Audira G, Juniardi S, Lai Y-H, Hsiao C-D (2018): A Simple ImageJ-Based Method to Measure Cardiac Rhythm in Zebrafish Embryos. *Inventions* 3, 21
- Satoh T, Zipes DP (1996): Unequal atrial stretch in dogs increases dispersion of refractoriness conducive to developing atrial fibrillation. *J Cardiovasc Electrophysiol* 7, 833–842
- Schewe M, Nematian-Ardestani E, Sun H, Musinszki M, Cordeiro S, Bucci G, de Groot BL, Tucker SJ, Rapedius M, Baukrowitz T (2016): A Non-canonical Voltage-Sensing Mechanism Controls Gating in K2P K⁺ Channels. *Cell* 164, 937–949
- Scholz EP, Carrillo-Bustamante P, Fischer F, Wilhelms M, Zitron E, Dössel O, Katus HA, Seemann G (2013): Rotor termination is critically dependent on kinetic properties of I_{Kur} inhibitors in an In Silico model of chronic atrial fibrillation. *PLoS One* 8
- Schüttler D, Bapat A, Kääb S, Lee K, Tomsits P, Clauss S, Hucker WJ (2020): Animal Models of Atrial Fibrillation. *Circ Res* 127, 91–110
- Shanmugam M, Molina CE, Gao S, Severac-Bastide R, Fischmeister R, Babu GJ (2011): Decreased sarcolipin protein expression and enhanced sarco(endo)plasmic reticulum Ca²⁺ uptake in human atrial fibrillation. *Biochem Biophys Res Commun* 410, 97–101
- Siekman I, Wagner LE, Yule D, Fox C, Bryant D, Crampin EJ, Sneyd J (2011): MCMC estimation of Markov models for ion channels. *Biophys J* 100, 1919–1929
- Sinno H, Derakhchan K, Libersan D, Merhi Y, Leung TK, Nattel S (2003): Atrial ischemia promotes atrial fibrillation in dogs. *Circulation* 107, 1930–1936
- Spratt J, Olsen C, Jr GT, ... DGJ-TJ of T, 1983 undefined Experimental mitral regurgitation: physiological effects of correction on left ventricular dynamics. Elsevier
- Sun Q, Tang M, Pu J, Zhang S (2008): Pulmonary venous structural remodelling in a canine model of chronic atrial dilation due to mitral regurgitation. *Canadian Journal of Cardiology* 24, 305–308
- Sussman MA, Lim HW, Gude N, Taigen T, Olson EN, Robbins J, Colbert MC, Gualberto A, Wiczorek DF, Molkentin JD (1998): Prevention of cardiac hypertrophy in mice by calcineurin inhibition. *Science* (1979) 281, 1690–1693
- Swaminathan PD, Purohit A, Hund TJ, Anderson ME (2012): Calmodulin-dependent protein kinase II: Linking heart failure and arrhythmias. *Circ Res* 110, 1661–1677
- Swilius MT, Waxham MN (2008): Ca²⁺/calmodulin-dependent protein kinases. *Cellular and Molecular Life Sciences* 65, 2637–2657

- Tessier S, Karczewski P, Krause EG, Pansard Y, Acar C, Lang-Lazdunski M, Mercadier JJ, Hatem SN (1999): Regulation of the transient outward K⁺ current by Ca²⁺/calmodulin-dependent protein kinases II in human atrial myocytes. *Circ Res* 85, 810–819
- van Gelder IC, Rienstra M, Crijns HJGM, Olshansky B (2016): Rate control in atrial fibrillation. *The Lancet* 388, 818–828
- Vanoye CG, Thompson CH, Desai RR, DeKeyser JM, Chen L, Rasmussen-Torvik LJ, Welty LJ, George AL: Functional evaluation of human ion channel variants using automated electrophysiology. In: *Methods in Enzymology*. Band 654; Academic Press Inc. 2021, 383–405
- Verheule S, Wilson E, Everett IV T, Shanbhag S, Golden C, Olgin J (2003): Alterations in atrial electrophysiology and tissue structure in a canine model of chronic atrial dilatation due to Mitral Regurgitation. *Circulation* 107, 2615–2622
- Voigt N, Maguy A, Yeh Y-H, Qi X, Ravens U, Dobrev D, Nattel S (2007): Changes in I_{K,ACh} single-channel activity with atrial tachycardia remodelling in canine atrial cardiomyocytes. *Cardiovasc Res* 77, 35–43
- Voigt N, Li N, Wang Q, Wang W, Trafford AW, Abu-Taha I, Sun Q, Wieland T, Ravens U, Nattel S, et al. (2012): Enhanced sarcoplasmic reticulum Ca²⁺ Leak and increased Na⁺-Ca²⁺ exchanger function underlie delayed afterdepolarizations in patients with chronic atrial fibrillation. *Circulation* 125, 2059–2070
- Voigt N, Heijman J, Wang Q, Chiang DY, Li N, Karck M, Wehrens XHT, Nattel S, Dobrev D (2014): Cellular and molecular mechanisms of atrial arrhythmogenesis in patients with paroxysmal atrial fibrillation. *Circulation* 129, 145–156
- Wagner S, Hacker E, Grandi E, Weber SL, Dybkova N, Sossalla S, Sowa T, Fabritz L, Kirchhof P, Bers DM, Maier LS (2009): Ca/calmodulin kinase II differentially modulates potassium currents. *Circ Arrhythm Electrophysiol* 2, 285–294
- Wagner S, Ruff HM, Weber SL, Bellmann S, Sowa T, Schulte T, Anderson ME, Grandi E, Bers DM, Backs J, et al. (2011): Reactive oxygen species-activated Ca/calmodulin kinase II δ is required for late I_{Na} augmentation leading to cellular Na and Ca overload. *Circ Res* 108, 555–565
- Wakimoto H, Maguire CT, Kover P, Hammer PE, Gehrman J, Tiedman JK, Berul CI (2001): Induction of atrial tachycardia and fibrillation in the mouse heart. *Cardiovasc Res* 50, 463–473
- Wilkinson RN, Jopling C, van Eeden FJM: Zebrafish as a model of cardiac disease. In: *Progress in Molecular Biology and Translational Science*. Band 124; Elsevier B.V. 2014, 65–91
- Xie LH, Shanmugam M, Park JY, Zhao Z, Wen H, Tian B, Periasamy M, Babu GJ (2012): Ablation of sarcolipin results in atrial remodeling. *Am J Physiol Cell Physiol* 302

- Xu H, Guo W, Nerbonne JM (1999): Four kinetically distinct depolarization-activated K⁺ currents in adult mouse ventricular myocytes. *Journal of General Physiology* 113, 661–677
- Yue L, Melnyk P, Gaspo R, Wang Z, Nattel S (1999): Molecular mechanisms underlying ionic remodeling in a dog model of atrial fibrillation. *Circ Res* 84, 776–784
- Zhang Y, Wang YT, Shan ZL, Guo HY, Guan Y, Yuan HT (2015): Role of inflammation in the initiation and maintenance of atrial fibrillation and the protective effect of atorvastatin in a goat model of aseptic pericarditis. *Mol Med Rep* 11, 2615–2623